U.S.NRC
United States Nuclear Regulatory Commission
Protecting People and the Environment

NUREG/CR-7207
PNNL-23708

Spent Fuel Transportation Package Response to the Newhall Pass Tunnel Fire Scenario

Final Report

Office of Nuclear Material Safety and Safeguards

AVAILABILITY OF REFERENCE MATERIALS IN NRC PUBLICATIONS

NRC Reference Material

As of November 1999, you may electronically access NUREG-series publications and other NRC records at NRC's Library at www.nrc.gov/reading-rm.html. Publicly released records include, to name a few, NUREG-series publications; *Federal Register* notices; applicant, licensee, and vendor documents and correspondence; NRC correspondence and internal memoranda; bulletins and information notices; inspection and investigative reports; licensee event reports; and Commission papers and their attachments.

NRC publications in the NUREG series, NRC regulations, and Title 10, "Energy," in the *Code of Federal Regulations* may also be purchased from one of these two sources.

1. **The Superintendent of Documents**
   U.S. Government Publishing Office
   Mail Stop IDCC
   Washington, DC 20402-0001
   Internet: bookstore.gpo.gov
   Telephone: (202) 512-1800
   Fax: (202) 512-2104

2. **The National Technical Information Service**
   5301 Shawnee Rd., Alexandria, VA 22312-0002
   www.ntis.gov
   1-800-553-6847 or, locally, (703) 605-6000

A single copy of each NRC draft report for comment is available free, to the extent of supply, upon written request as follows:

Address: **U.S. Nuclear Regulatory Commission**
Office of Administration
Publications Branch
Washington, DC 20555-0001
E-mail: distribution.resource@nrc.gov
Facsimile: (301) 415-2289

Some publications in the NUREG series that are posted at NRC's Web site address www.nrc.gov/reading-rm/doc-collections/nuregs are updated periodically and may differ from the last printed version. Although references to material found on a Web site bear the date the material was accessed, the material available on the date cited may subsequently be removed from the site.

Non-NRC Reference Material

Documents available from public and special technical libraries include all open literature items, such as books, journal articles, transactions, *Federal Register* notices, Federal and State legislation, and congressional reports. Such documents as theses, dissertations, foreign reports and translations, and non-NRC conference proceedings may be purchased from their sponsoring organization.

Copies of industry codes and standards used in a substantive manner in the NRC regulatory process are maintained at—

The NRC Technical Library
Two White Flint North
11545 Rockville Pike
Rockville, MD 20852-2738

These standards are available in the library for reference use by the public. Codes and standards are usually copyrighted and may be purchased from the originating organization or, if they are American National Standards, from—

American National Standards Institute
11 West 42nd Street
New York, NY 10036-8002
www.ansi.org
(212) 642-4900

Legally binding regulatory requirements are stated only in laws; NRC regulations; licenses, including technical specifications; or orders, not in NUREG-series publications. The views expressed in contractorprepared publications in this series are not necessarily those of the NRC.

The NUREG series comprises (1) technical and administrative reports and books prepared by the staff (NUREG–XXXX) or agency contractors (NUREG/CR–XXXX), (2) proceedings of conferences (NUREG/CP–XXXX), (3) reports resulting from international agreements (NUREG/IA–XXXX), (4) brochures (NUREG/BR–XXXX), and (5) compilations of legal decisions and orders of the Commission and Atomic and Safety Licensing Boards and of Directors' decisions under Section 2.206 of NRC's regulations (NUREG–0750).

U.S.NRC
United States Nuclear Regulatory Commission
Protecting People and the Environment

NUREG/CR-7207
PNNL-23708

Spent Fuel Transportation Package Response to the Newhall Pass Tunnel Fire Scenario

Final Report

Manuscript Completed: July 2016
Date Published: October 2016

Prepared by:
H. E. Adkins, Jr.[1], J. M. Cuta[1], N. A. Klymyshyn[1],
S. R. Suffield[1], K. B. McGrattan[2], and C. S. Bajwa[3],
C. E. Beyer[1], and A. Sotomayor-Rivera[4]

[1]Pacific Northwest National Laboratory
P. O. Box 999
Richland, WA 99352

[2]National Institute of Standards and Technology
Engineering Laboratory
100 Bureau Drive, Stop 8600
Gaithersburg, MD 20899-8600

[3]International Atomic Energy Agency
Vienna International Centre
P.O. Box 100
A-1400 Vienna, Austria

[4]U.S. Nuclear Regulatory Commission

J. Piotter, NRC Project Manager

NRC Job Code J5701

Office of Nuclear Material Safety and Safeguards

ABSTRACT

The U.S. Nuclear Regulatory Commission has established requirements for packaging and transportation of spent nuclear fuel assemblies under normal conditions of transport and for hypothetical accident conditions. Real-world accidents of greater severity are possible, but are of much lower probability, and the probability of such an accident involving a spent nuclear fuel (SNF) package is even lower. However, because of the potential consequences, the U.S. Nuclear Regulatory Commission has undertaken the examination of specific accidents to determine the potential consequences to an SNF package. The Newhall Pass tunnel accident of October 2007, which did not involve SNF, was selected for evaluation because of the length of the fire and the wide range of potential fire exposure scenarios.

The General Atomics GA-4 Legal Weight Truck transportation package was selected for this investigation. Based on fire modeling with the Fire Dynamics Simulator code, and physical examination of material samples obtained onsite, a bounding fire scenario was defined for this accident. Due to uncertainties in the overall fire timeline and incomplete information on the actual cargo of some of the trucks, five specific fire modeling cases were defined to bound the possible range of fire conditions.

Detailed thermal models of the GA-4 package were constructed for the ANSYS and COBRA-SFS codes, and transient evaluations were performed to determine the response of the package to bounding cases defining the fire scenario. The peak fire temperatures obtained in the Fire Dynamics Simulator modeling for vehicles at the hottest fire location and longest fire location were used to define the fully engulfing fire conditions for the GA-4 package. These evaluations also included the post-fire cooldown transient. The ANSYS model predicted higher fuel temperatures, due mainly to the simplified representation of the fuel region. In three of the five cases, this model predicts that the peak cladding temperature at the hottest fire location would exceed the short-term limit of 1058°F (570°C), shortly after the end of the vehicle fire at that location. The more realistic predictions from the COBRA-SFS model show that this limit would not be exceeded in any of these cases. At the location with the longest fire duration, both models show peak temperatures that are under this limit.

Fuel cladding performance was evaluated using the FRAPTRAN-1.4 code. For the fuel region temperature histories from the ANSYS modeling, burst rupture is predicted to occur at 1038°F (559°C). For the ANSYS model thermal analysis results, this indicates fuel failure for three of the five cases at the hottest fire location. For the fuel cladding temperatures predicted with COBRA-SFS, fuel rod cladding would not fail by burst rupture in this fire scenario in any of the cases evaluated. Both models predict that seal temperature limits will be exceeded for several hours of the post-fire cooldown transient.

The potential release from this fire scenario is bounded by that from the more severe MacArthur Maze fire scenario, where no more than approximately one-fourth of the mixture A2 quantity is predicted to be released. Since the regulatory limit is specified as an A2 quantity per week for accident conditions, the estimated release is below the prescribed limit for safety. This very conservative estimate indicates that the potential release from this package, were it to be involved in a fire accident as severe as the Newhall Pass Tunnel fire scenario, would not pose a risk to public health and safety.

TABLE OF CONTENTS

LIST OF FIGURES

LIST OF TABLES

EXECUTIVE SUMMARY

The U.S. Nuclear Regulatory Commission (NRC) has established requirements for packaging and transportation of spent nuclear fuel (SNF) assemblies under normal conditions of transport and for hypothetical accident conditions (HAC). These requirements (10 CFR 71) conservatively bound conditions that an SNF package might be subjected to in the course of its service life. However, real-world accidents of greater severity are certainly possible, and rare as they may be, the NRC has proactively undertaken the examination of such accidents, to determine what the potential consequences might be, were such an accident ever to involve an SNF package.

Three previous studies of transportation accidents, one resulting in a fire in a railroad tunnel (NUREG/CR-6886 2009), one in a highway tunnel (NUREG/CR-6894 2007), and one on a highway interchange (NUREG/CR-7206 2015) were undertaken with four different SNF package designs. Based on conservative scenarios constructed from these real-world fire conditions, the results of these studies have shown that the design basis for SNF packages is sufficiently robust for them to survive such beyond-design-basis conditions without adverse consequences to public safety. In all cases evaluated, the modeling results showed that the various SNF packages would be expected to maintain required shielding for ionizing radiation, and also would maintain the integrity of the containment boundary sufficiently to limit potential release of radioactive material from the packages to within regulatory bounds for accident conditions.

The Newhall Pass Tunnel accident of October 12, 2007 was selected as a fourth study in this series of evaluations of real-world accidents because of the long duration of the fire and the wide range of potential fire exposure scenarios, due to the large number of vehicles involved in the accident and fire. Since this was a highway accident, the only type of SNF package that could potentially be involved would be a legal weight truck (LWT) package. The General Atomics GA-4 LWT transportation package was selected for this investigation, mainly because it can carry a relatively large payload for an over-the-road transportation package, and therefore the potential consequences of package failure could be more severe than for packages with smaller payload capacities. The GA-4 package is designed to transport up to four intact pressurized water reactor spent fuel assemblies, with a maximum total package decay heat load of 2.5 kW. (This is the same package that was evaluated in the MacArthur Maze highway interchange fire and roadway collapse [NUREG/CR-7206 2015].)

The Newhall Pass Tunnel accident consisted of a chain reaction traffic collision and fire involving 33 commercial tractor-trailer rigs and one passenger vehicle, on a section of the southbound Interstate 5 truck route where it passes under the main north-south lanes of Interstate 5. A fire started within the close pile-up of vehicles near the tunnel exit and spread rapidly into the tunnel, eventually filling the entire tunnel and destroying the twenty-four tractor-trailer rigs that were trapped within it. The cargoes of the trucks consisted mainly of foodstuffs, and none were carrying hazardous flammable material (i.e., no gasoline tankers, such as in the Caldecott Tunnel fire (NUREG/CR-6894 2007) and the MacArthur Maze fire (NUREG/CR-7206 2015). The severe tunnel-filling fire is estimated to have lasted more than 2 hours, and possibly as long as 5 hours. Figure S.1 shows an image of the tunnel entrance, one of many photographs obtained by first-responders on the scene (CHP 2007). Figure S.2 shows a sonar image of the configuration of the destroyed vehicles within the tunnel after the end of the fire, obtained prior to the beginning of salvage operations, and a diagram of the inferred locations of the trucks trapped within the tunnel prior to the start of the fire.

Figure S.1. Newhall Pass Tunnel Entrance at 10/13/2007 2:47 a.m. (photo from MAIT Report, CHP 2007, reprinted with permission.)

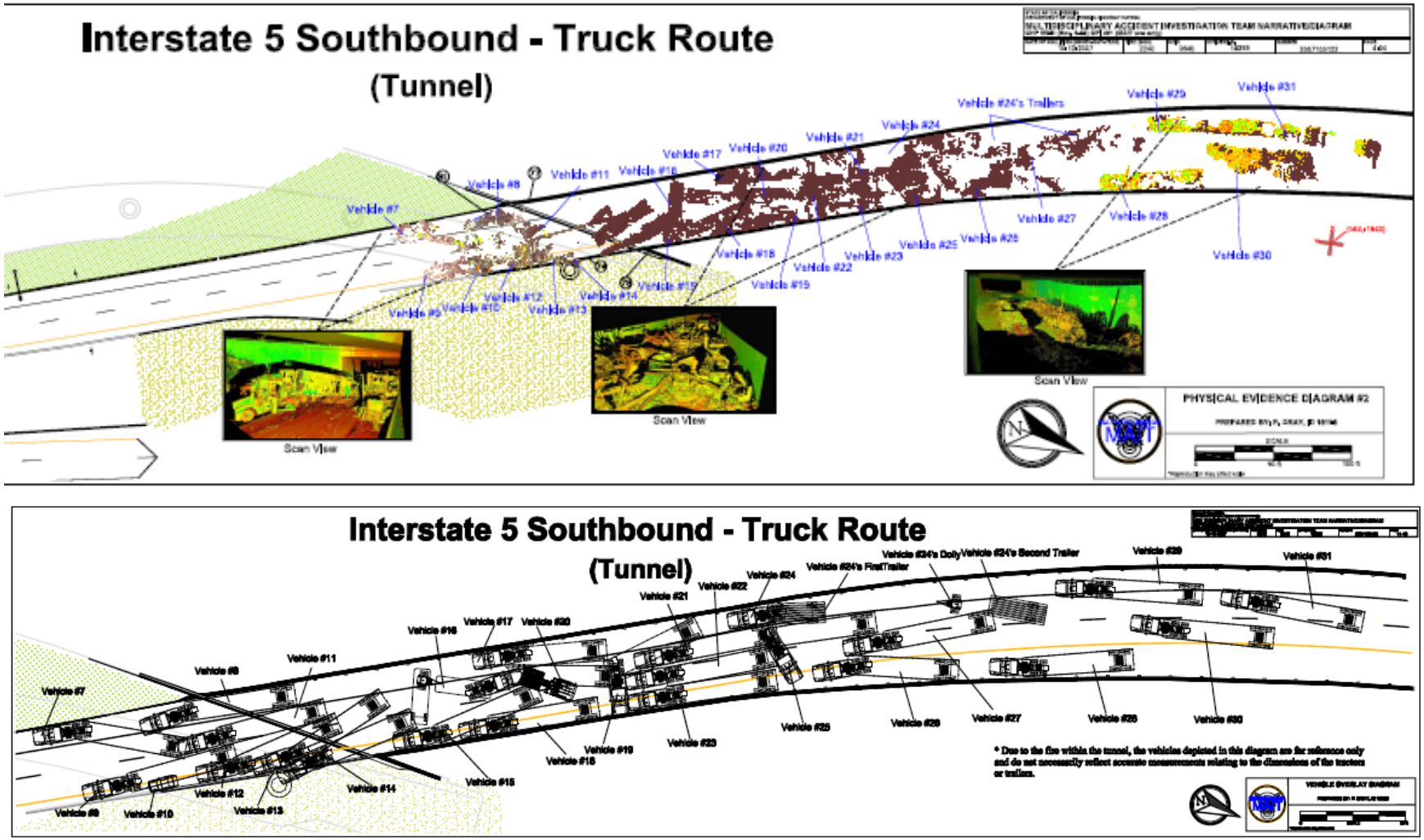

Figure S.2. Sonar Map and Diagram of Inferred Locations of Vehicles Involved in Accident and Fire within Newhall Pass Tunnel (image and diagram from MAIT Report, CHP 2007, reprinted with permission.)

Based on fire modeling with the FDS code, and physical examination of material samples obtained from the remnants of the vehicles removed from the tunnel, a bounding fire scenario was defined for thermal evaluations of the potential effects of this fire on an SNF package. Due to uncertainties in the overall fire timeline and incomplete information on the actual cargo of some of the trucks, five specific fire modeling cases were defined to bound the possible range of fire conditions. The fire modeling approach utilized a feature in FDS that allows the fire behavior to be defined with a total mass of fuel and a specified burn time. Based on the available information, a bounding "fuel budget" was developed for a typical vehicle within the tunnel, consisting of the combustible components of the vehicle, plus an estimated combustible mass for a typical cargo.

Cases were developed for assumed fire spread rates that spanned the range of uncertainty in the actual duration of the intense fire within the tunnel, estimated as ranging from 2 hours to 5 hours. Figure S.3 shows the peak fire temperatures predicted for each vehicle assuming a "slow" spread rate, matching the maximum estimated fire duration of approximately five hours. Figures S.4 and S.5 show the peak fire temperatures predicted for each vehicle assuming a "moderate" and "fast" spread rate, respectively. The results with the fast spread rate yield a total fire duration matching the shortest possible duration of the actual fire.

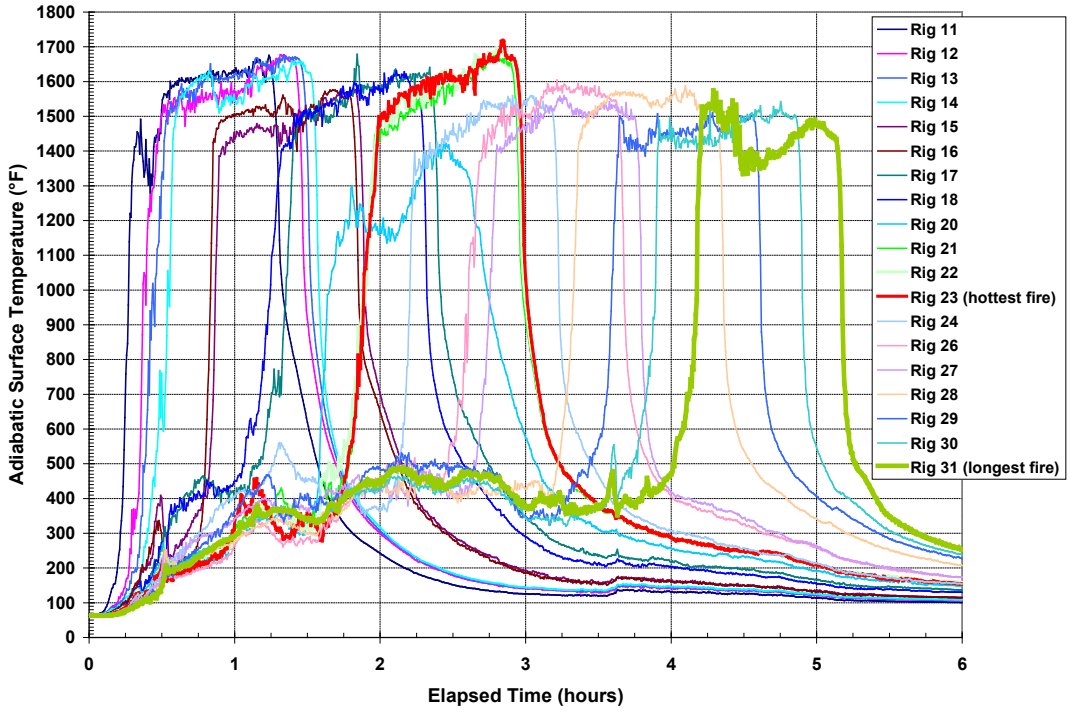

Figure S.3. Peak Fire Temperatures at Each Vehicle Location for Assumed "Slow" Spread Rate, Yielding Fire Duration of approximately 5 Hours (Case NIST-01)

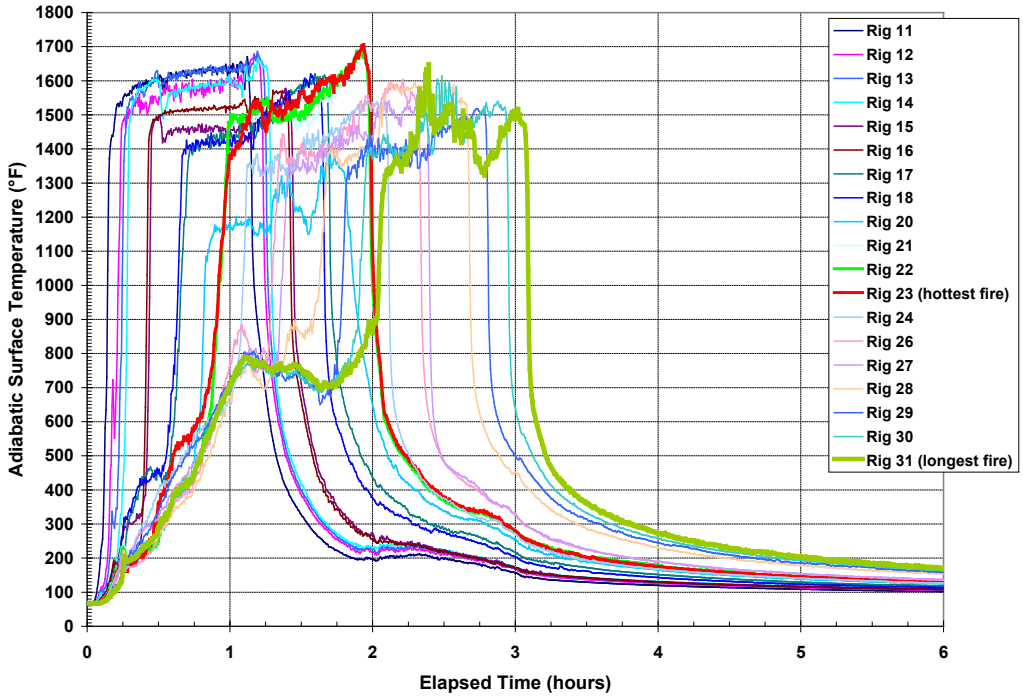

Figure S.4. Peak Fire Temperatures at Each Vehicle Location for Assumed "Moderate" Spread Rate, Yielding Fire Duration of approximately 3 Hours (Case NIST-02)

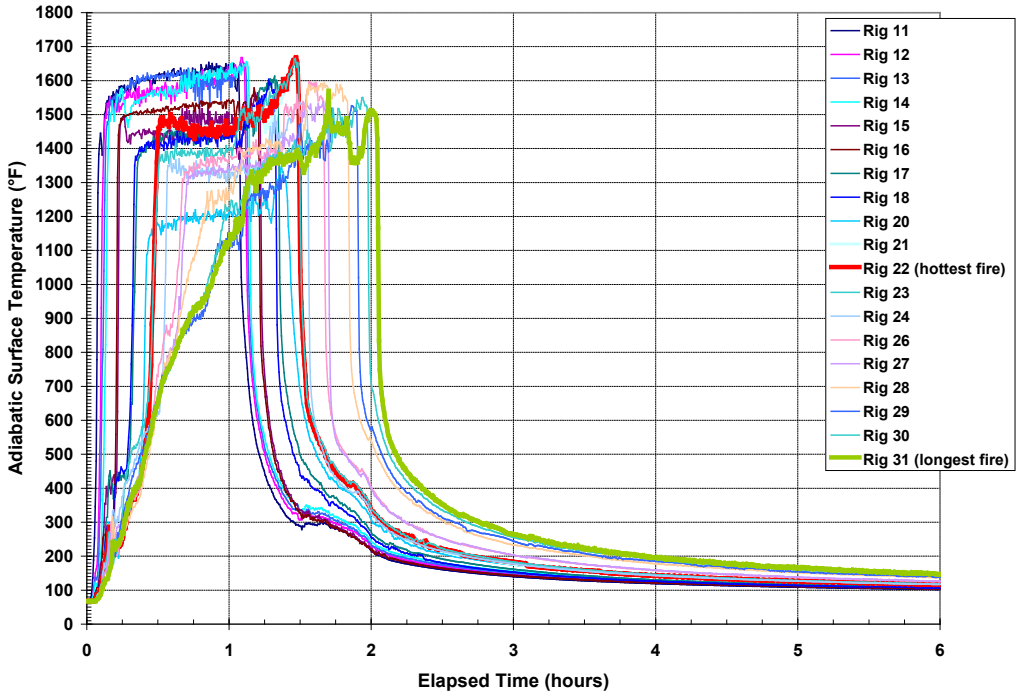

Figure S.5. Peak Fire Temperatures at Each Vehicle Location for Assumed "Fast" Spread Rate, Yielding Fire Duration of approximately 2 Hours (Case NIST-03)

To verify the conservatism of the "typical" fuel budget, with respect to the actual fuel load available on each vehicle, combustible mass of the actual cargo for each of the vehicles in the tunnel was estimated, based on information extracted from the Multi-Discipline Accident Investigation Team (MAIT) report (CHP 2007). Figure S.6 shows the peak fire temperatures predicted for this case. The temperatures obtained with these modeling assumptions represent conservative bounding values for the fire that destroyed the vehicles and their cargoes in this accident.

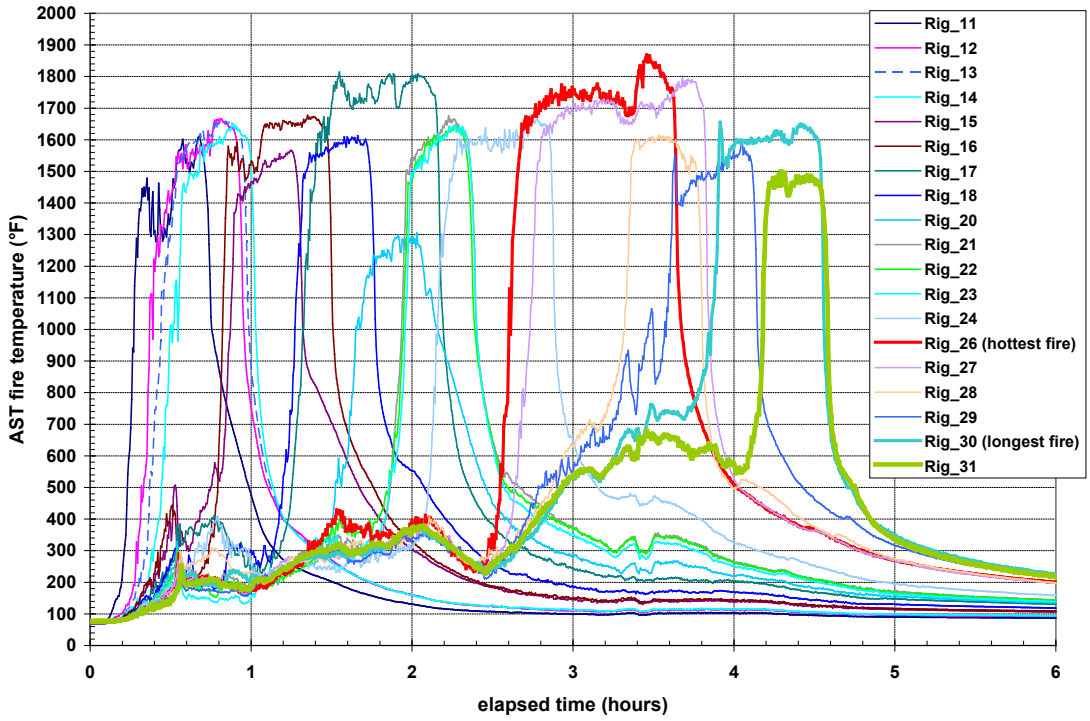

Figure S.6. Peak Fire Temperatures at Each Vehicle Location with Fuel Load Defined by Estimated Combustible Mass of Actual Cargo (Case NIST-06)

Thermal Modeling Approach and Summary of Results

Detailed thermal models of the GA-4 package were constructed for the ANSYS and COBRA-SFS codes, for transient evaluations to determine the temperature response of the package to bounding cases defining the fire scenario. Figure S.7 shows an exploded view of the GA-4 package, illustrating its main design features. Figure S.8 shows an axial cross-sectional diagram of the ANSYS model of the package, and Figure S.9 shows a diagram of the COBRA-SFS model. These evaluations also included the post-fire cooldown transient, and all evaluations were run out to approximately 10 hours. This is not long enough for the package to have returned to steady-state, but in this fire scenario, this relatively short cooldown time is sufficient for all component temperatures in the package to be trending downward. (For fires of greater severity than the Newhall Pass Tunnel fire, the time to this turn-around is generally many hours longer, resulting in peak component temperatures [including peak fuel cladding temperatures] occurring long after the end of the fire, as noted in documentation of the previous studies mentioned above.)

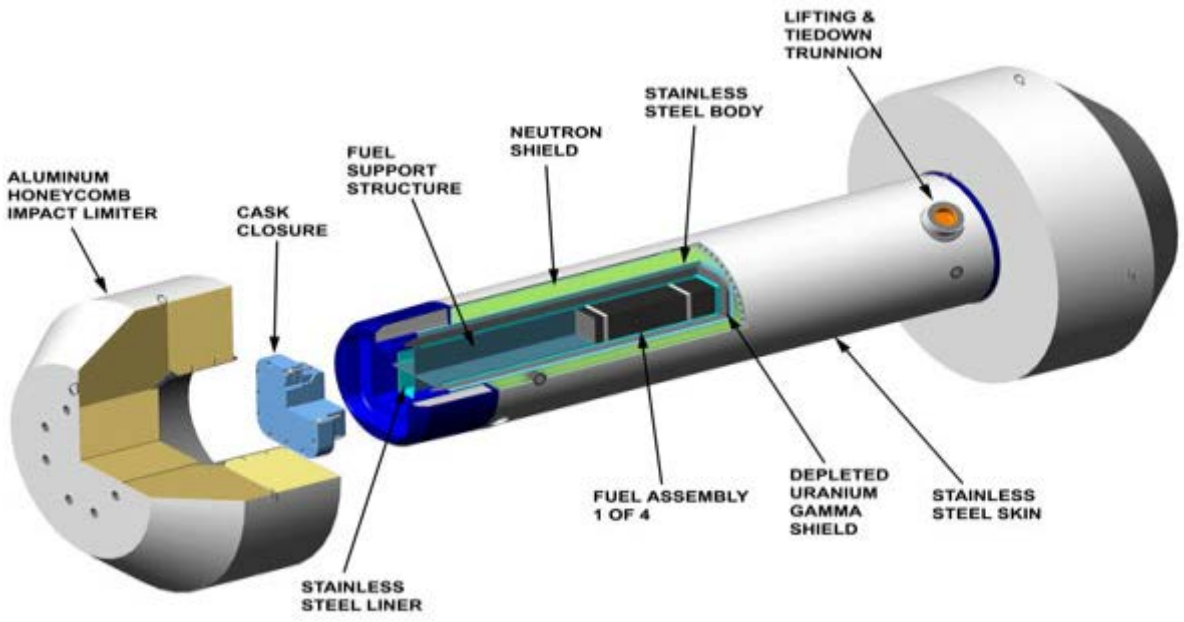

Figure S.7. GA-4 Package: Exploded View (General Atomics 1998)

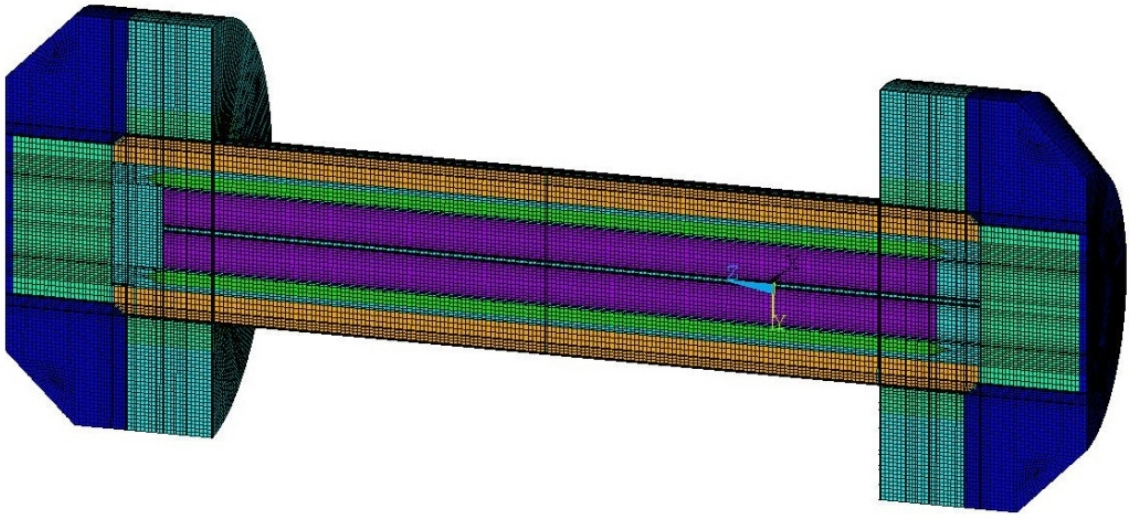

Figure S.8. Axial Cross-Section of ANSYS Model of GA-4 Package

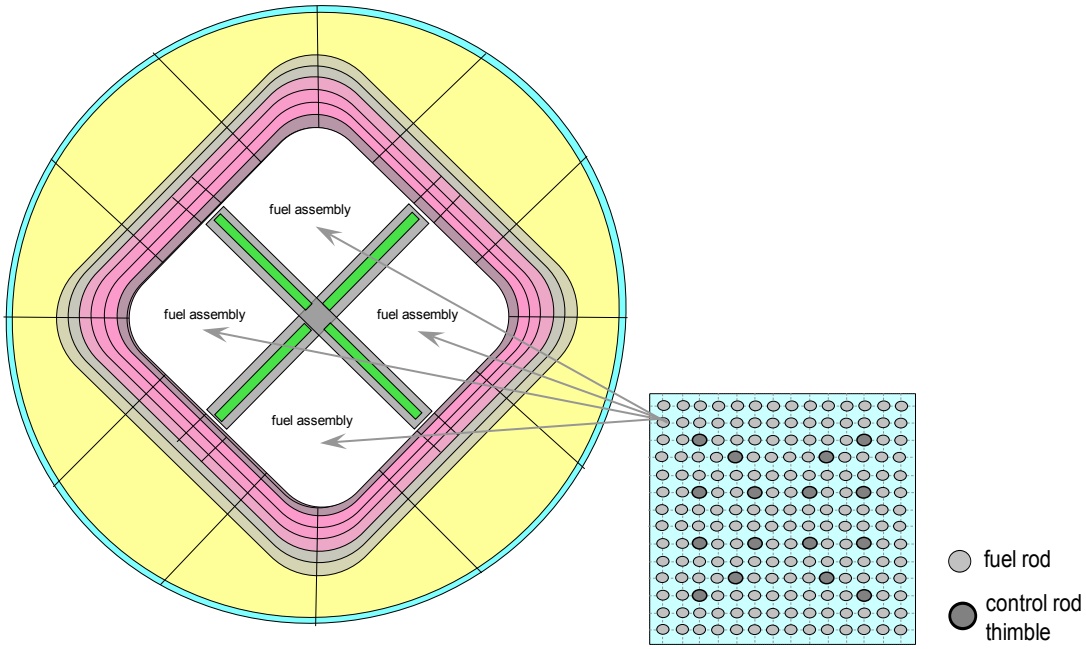

Figure S.9. Cross-Section of COBRA-SFS Model of GA-4 Package

The initial condition of the package at the start of the fire scenario in each case was defined as steady-state normal conditions of transport. The tunnel fire consisted of a series of fires on the individual vehicles, as the fire spread through the tunnel, with the “overlap” of vehicle fires in a given case determined by the specified spread rate. The results of the FDS modeling were used to identify the vehicle with the hottest fire in a given case, to define the most adverse location for the SNF package within the tunnel, with respect to peak fire temperature exposure. Because of the length of the fire, these results were also used to identify the location with the longest exposure to elevated temperatures during the fire in a given case. In all cases, the “hottest fire location” corresponded to a vehicle near the center of the tunnel, and the longest fire location corresponded to the last vehicle to be consumed by the fire (i.e., the vehicle closest to the tunnel entrance). The complex and dynamic fire conditions predicted with FDS for the vehicle at the hottest fire location and the vehicle at the longest fire location were represented for the GA-4 package as a fully engulfing pool fire in the thermal analyses for each case.

Thermal evaluations of the package response to the various bounding cases developed to represent the Newhall Pass Tunnel fire scenario show that the peak temperatures would be expected to be higher for the fire at the hottest fire location, compared to the longest fire location in all cases. Figure S.10 summarizes the predicted fire temperatures from the FDS modeling and peak fuel cladding temperatures from the thermal models of the GA-4 for all cases at the hottest fire location. Figure S.11 presents a similar summary for these cases, for the package at the longest fire location. The results obtained with the ANSYS model are conservative (that is, higher temperatures are predicted) with respect to the COBRA-SFS model, due mainly to the simplifications in the representation of the fuel region in the ANSYS model.

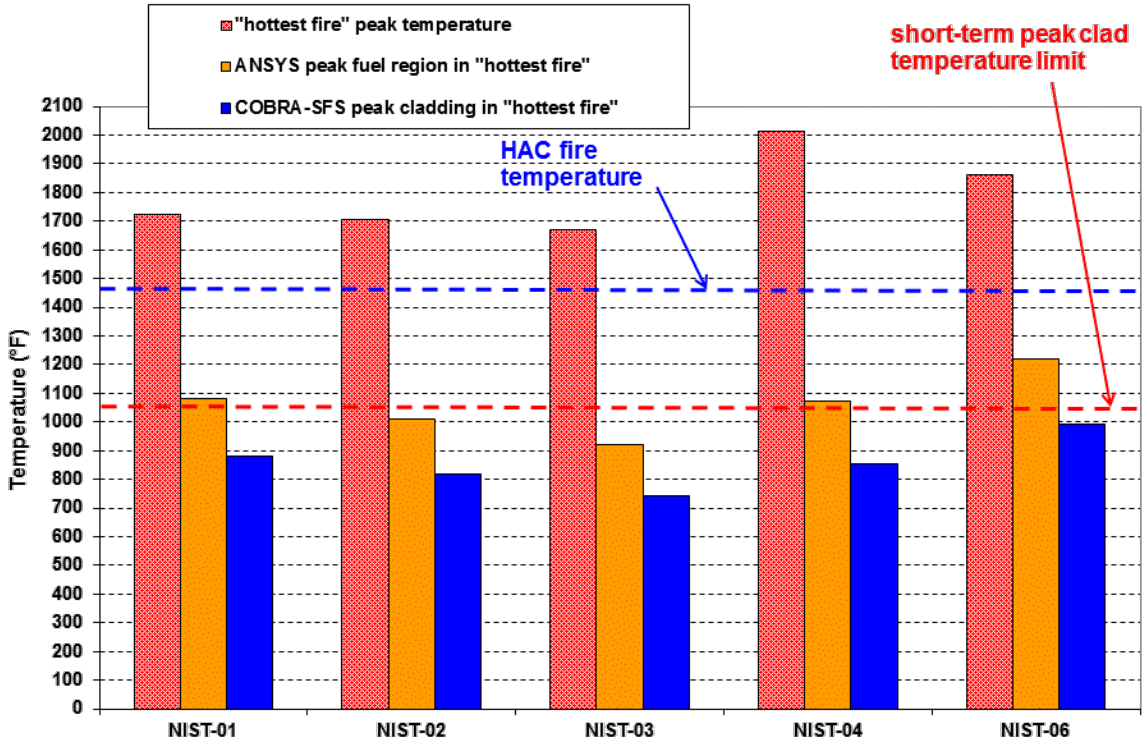

Figure S.10. Maximum Predicted Temperatures in All Cases for the Hottest Fire Location

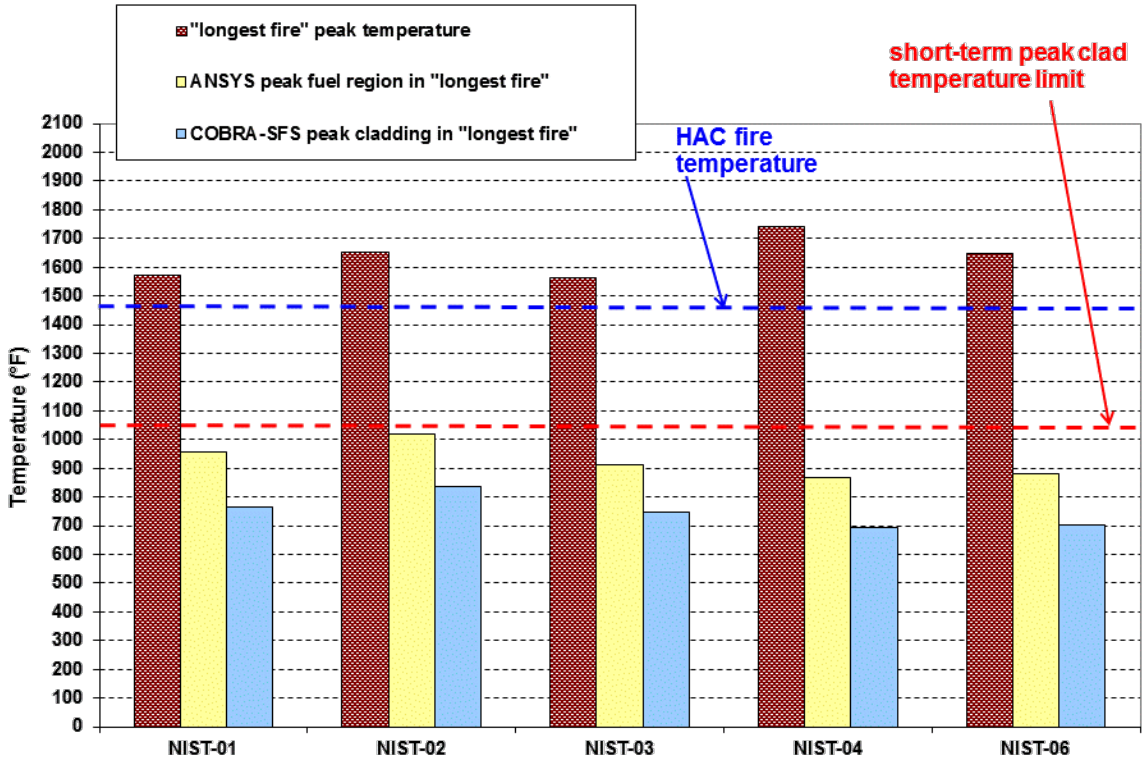

Figure S.11. Maximum Predicted Temperatures in All Cases for the Longest Fire Location

In three of the five cases, the ANSYS model predicts that the peak cladding temperature in response to the fire at the hottest fire location would be expected to exceed the short-term limit of 1058°F (570°C) for zircaloy cladding, shortly after the end of the vehicle fire at that location. The corresponding results from the COBRA-SFS model show that this limit would not be exceeded in any of these cases. Both models predict that the peak cladding temperature would remain below this limit in all cases for the local vehicle fire at the "longest fire" location.

The maximum peak cladding temperature in the transient is predicted with the ANSYS model to be 1217°F (659°C) for case NIST-06, compared to 994°F (534°C) predicted with the COBRA-SFS model for the same bounding case. Both models predict temperatures in the regions of the package seals that are within the seal material operating temperature limits during the fire portion of the transient for each case evaluated. However, in all cases, both models predict that the seal temperature limits will be exceeded for several hours during the post-fire cooldown transient, due to the thermal inertia of the package and the insulating effect of the impact limiters attached to the ends of the package.

Fuel Rod Performance Evaluation

Based on the predicted fuel cladding temperatures from the ANSYS and COBRA-SFS modeling, fuel performance was evaluated using the burst rupture model in the FRAPTRAN-1.4 code (NUREG/CR-7023 2011). For the fuel region temperature histories predicted for the five cases evaluated in this fire scenario with the ANSYS model, the FRAPTRAN analysis predicts clad ballooning at 924°F (497°C) and cladding burst rupture at 1038°F (559°C). For the fuel cladding temperature histories predicted with the COBRA-SFS model for these five cases, the FRAPTRAN analysis predicts that although some rods may experience ballooning in the most severe case (NIST-06, for the hottest fire location), rod burst rupture would not be expected to occur in any of these cases. Based on the predicted burst rupture temperature, fuel failure is predicted with the ANSYS model results for three of the five cases considered with the GA-4 package at the hottest fire location in the tunnel. For the more realistic fuel modeling with COBRA-SFS, however, fuel failure by burst rupture is not predicted in any of the cases evaluated.

These results suggest that although fuel failure is possible as a result of the conditions of the Newhall Pass Tunnel fire, it is likely that a realistic assessment of the fire conditions and realistic thermal modeling would show that fuel would not be expected to fail. However, as a bounding evaluation the potential release from the GA-4 package in the Newhall Pass Tunnel fire scenario is assumed to be potentially the same as that predicted for the MacArthur Maze fire scenario. In the MacArthur Maze fire scenario, the potential consequences are evaluated assuming that all rods in the package fail.

Potential Radiological Consequences

Neutron and gamma radiation dose rates from the GA-4 package as a result of the postulated conditions of the Newhall Pass Tunnel fire scenario will not exceed the design basis of the package, which is well within the regulatory limits for HAC. The neutron shielding is lost early in the transient in all cases, but loss of the neutron shield tank is a design-basis assumption for this package in all HAC analyses. The conditions of the Newhall Pass Tunnel fire can do no more damage to the GA-4 package neutron shield than is assumed *a priori* in the HAC analyses. The gamma shielding for the GA-4 is provided by a layer of depleted uranium (DU) within the stainless steel package body. The shielding function of this material is not affected by the temperatures it is predicted to reach in the Newhall Pass Tunnel fire scenario. There is no

credible scenario in this fire accident that could result in neutron and gamma dose rates from the design-basis GA-4 package exceeding the regulatory limits for accident conditions.

Loss of the package seals due to exceeding seal material thermal limits means that there is the potential for radioactive material to escape from the package. Rupture of all rods in the package is assumed as a bounding limit, even though conservative estimates of maximum fuel temperature histories from the ANSYS modeling for the various cases indicate that only a relatively small percentage of rods would be expected to exceed the burst rupture temperature in this scenario. Conservative evaluations with more physically realistic thermal modeling of fuel behavior in the COBRA-SFS model indicate that no fuel failures would occur in the Newhall Pass Tunnel fire scenario. For evaluations of potential release from the package, 100% spalling of CRUD from the external surfaces of the fuel rods is assumed, per NRC guidance.

With these extremely conservative assumptions, the package release evaluations for the GA-4 in the MacArthur Maze fire scenario (NUREG/CR-7206 2015) are by definition bounding on the potential release from the package in the Newhall Pass Tunnel fire. Detailed evaluations for the severe conditions of the MacArthur Maze fire scenario show that the total possible release from the package, as a mixture of fission gases, fuel particulate, and CRUD particles could be no more than approximately one-fourth of the mixture A_2 quantity for the release. Since the regulatory limit is specified as an A_2 quantity per week for accident conditions, the estimated release is below the prescribed limit for safety. This very conservative estimate indicates that the potential release from this package, were it to be involved in a fire accident as severe as the MacArthur Maze or Newhall Pass fire scenarios, would not pose a risk to public health and safety.

ACKNOWLEDGMENTS

Evaluations of the potential thermal consequences of severe fire accidents, should such an event ever involve a spent nuclear fuel (SNF) package has been the work of many contributors over several years. The successful completion of this work has been due in large measure to Chris Bajwa, the U.S. Nuclear Regulatory Commission (NRC) Project Manager initially guiding this effort, in the evaluation of the potential effects of MacArthur Maze fire and highway collapse on an SNF package. As a follow-on study with the same SNF package, this work has been extended to evaluation of the potential effects of the Newhall Pass Tunnel fire, another severe and complicated real-world fire accident. He has supported and encouraged the continuation of this evaluation after leaving NRC to work with the International Atomic Energy Agency. As with the fire modeling in the MacArthur Maze evaluations, the work of Kevin McGrattan (NIST) was an invaluable contribution, providing realistic assessment of the behavior of the fire itself in the unusual tunnel environment, and defining the bounding fire scenario used in the analysis. The California Highway Patrol (CHP), in particular the members of the Multi-Disciplinary Accident Investigation Team for this fire, provided invaluable assistance and detailed information, through personal communications and also in the detailed and comprehensive Multi-Disciplinary Accident Investigation Team Report published by CHP describing the accident. CHP officers personally assisted the NRC in obtaining physical samples from the wreckage of vehicles removed from the tunnel, providing direct evidence to determine estimates of temperatures reached in the fire. The work of Carl Beyer and Kenneth Geelhood of Pacific Northwest National Laboratory, and their expertise related to nuclear fuel and cladding behavior under severe thermal and mechanical stresses that could lead to burst rupture was vital to the assessment of the potential consequences of exposing SNF to an accident of the severity of the Newhall Pass tunnel fire scenario. The efforts of technical editors Colleen Winters and Susan Tackett were invaluable in making the details of this complex fire scenario and the evaluation results understandable to the wide audience for which it has been prepared.

ABBREVIATIONS AND ACRONYMS

ASME	American Society of Mechanical Engineers
AST	adiabatic surface temperature
CFD	computational fluid dynamics
CHP	California Highway Patrol
CNWRA	Center for Nuclear Waste Regulatory Analyses
CRUD	Chalk River Unknown Deposit, a generic term for corrosion and wear products (rust particles, etc.) that become radioactive (i.e., activated) when exposed to radiation.
DU	depleted uranium
FDS	Fire Dynamics Simulator
FSS	fuel support structure
HAC	Hypothetical accident conditions
ILSS	impact limiter support structure
LACoFD	Los Angeles County Fire Department
LWT	legal weight truck
MAIT	Multi-Discipline Accident Investigation Team
NCT	normal conditions of transport
NIST	National Institute of Standards and Technology
NRC	U.S. Nuclear Regulatory Commission
PWR	pressurized water reactor
SAR	safety analysis report
SNF	spent nuclear fuel
TBq	Terabecquerel (SI unit for radioactivity; equal to 27 Curies (Ci))

1.0 INTRODUCTION

Current U.S. Nuclear Regulatory Commission (NRC) regulations specify that spent nuclear fuel (SNF) transportation packages must be designed to survive exposure to a fully engulfing fire accident lasting no less than 30 minutes with an average flame temperature of no less than "1475°F (800°C)" (10 CFR 71 2003). The package must maintain containment, shielding, and criticality functions throughout the fire and post-fire cool down in order to meet regulations. (The term "package" refers to both the contents, in this case spent nuclear fuel, and the protective enclosure in which the contents are placed.) The intent of the regulations is to ensure that SNF transportation packages survive real-world accidents, including those involving severe fires.

The performance of spent fuel packages in severe accidents has been examined in previous studies by the NRC, as documented in NUREG-0170 (*Final Environmental Statement on the Transportation of Radioactive Material by Air and Other Modes*[1]), NUREG/CR-4829 (*Shipping Container Response to Severe Highway and Railway Accident Conditions*[2], also known as the "Modal Study"), and NUREG/CR-6672 (*Re-examination of Spent Fuel Shipment Risk Estimates*[3]). However, these studies did not specifically examine the effects of an actual transportation accident consisting of a severe tunnel fire involving a large number of vehicles.

NRC has undertaken the examination of real-world accidents of greater severity than postulated in the hypothetical accident conditions (HAC) fire, to determine what the potential consequences might be, were such an accident ever to involve an SNF package. Based on conservative scenarios constructed from these real-world fire conditions, the results of these studies have shown that the design basis for SNF packages is sufficiently robust for them to survive such beyond-design-basis conditions without adverse consequences to public safety. In all cases evaluated, the modeling results showed that the various SNF packages would be expected to maintain required shielding for ionizing radiation, and also would maintain the integrity of the containment boundary sufficiently to limit potential release of radioactive material from the packages to within regulatory bounds for accident conditions.

Three previous studies of transportation accidents have been performed; the first was of the 2001 fire in the Howard Street railroad tunnel in Baltimore, Maryland (NUREG/CR-6886 2009). The second was of the 1982 fire in the Caldecott Tunnel on California State Route 24 near Oakland, California (NUREG/CR-6894 2007). The third was of the long-duration gasoline fire and roadway collapse on the Interstate 880 connector of the MacArthur Maze interchange near Oakland, California (NUREG/CR-7206 2015). The current study reported here is of a highway tunnel fire on the Interstate 5 truck route known as the Newhall Pass, in Los Angeles County, California.

The Newhall Pass Tunnel accident occurred on October 12, 2007 at approximately 11:40 p.m. (PDT), and consisted of a chain reaction traffic collision and fire involving 33 commercial tractor-trailer rigs and one passenger vehicle, on a section of the southbound Interstate 5 truck route where it passes under the main north-south lanes of Interstate 5. Figure 1.1 shows an aerial view of the roadway configuration, with the tunnel location marked by a red oval. (This image was extracted from the California Highway Patrol [CHP] Multi-Discipline Accident Investigation Team [MAIT] report [CHP 2007].)

[1] NUREG-0170, U.S. Nuclear Regulatory Commission, Washington, D.C., December 1977.
[2] NUREG/CR-4829, U.S. Nuclear Regulatory Commission, Washington, D.C., February 1987.
[3] NUREG/CR-6672, U.S. Nuclear Regulatory Commission, Washington, D.C., March 2000.

The accident began when a tractor-trailer rig went out of control after exiting the tunnel and collided with the concrete median barrier, eventually coming to rest blocking both southbound lanes. The resulting pile-up of on-coming vehicles was reconstructed in the CHP MAIT report (CHP 2007) as thirteen separate collision sequences consisting of a total of 51 distinct impacts, with 24 of the 33 tractor-trailer rigs trapped within the Newhall Pass Tunnel. A fire started within the close pile-up of vehicles near the tunnel exit and spread rapidly into the tunnel, spreading from vehicle to vehicle and eventually filling the entire tunnel. Figure 1.2 shows a sonar image taken of the tunnel after the fire and before salvage operations began. For clarity, Figure 1.2 also includes a diagram of the reconstructed positions of the 24 vehicles within the tunnel. (Both images in Figure 1.2 are from the MAIT report [CHP 2007].)

The vehicles involved in the accident are identified by numbers 1 through 33 in the MAIT report, as shown on the diagram in Figure 1.2. Vehicles #1 through #6, #32, and #33 were not involved in the tunnel fire (and do not appear on this diagram). Vehicles #7 and #9, and the single passenger car involved in the accident (vehicle #10) were outside the tunnel exit. Vehicle #8 and vehicles #11 through #14 were at the tunnel exit, only partially within the tunnel. Vehicles #15 through #31 were distributed within the tunnel as shown in the diagram.

Figure 1.1. Aerial View of Roadway Configuration Showing Location of Newhall Pass Tunnel (photo from MAIT Report, CHP 2007, reprinted with permission.)

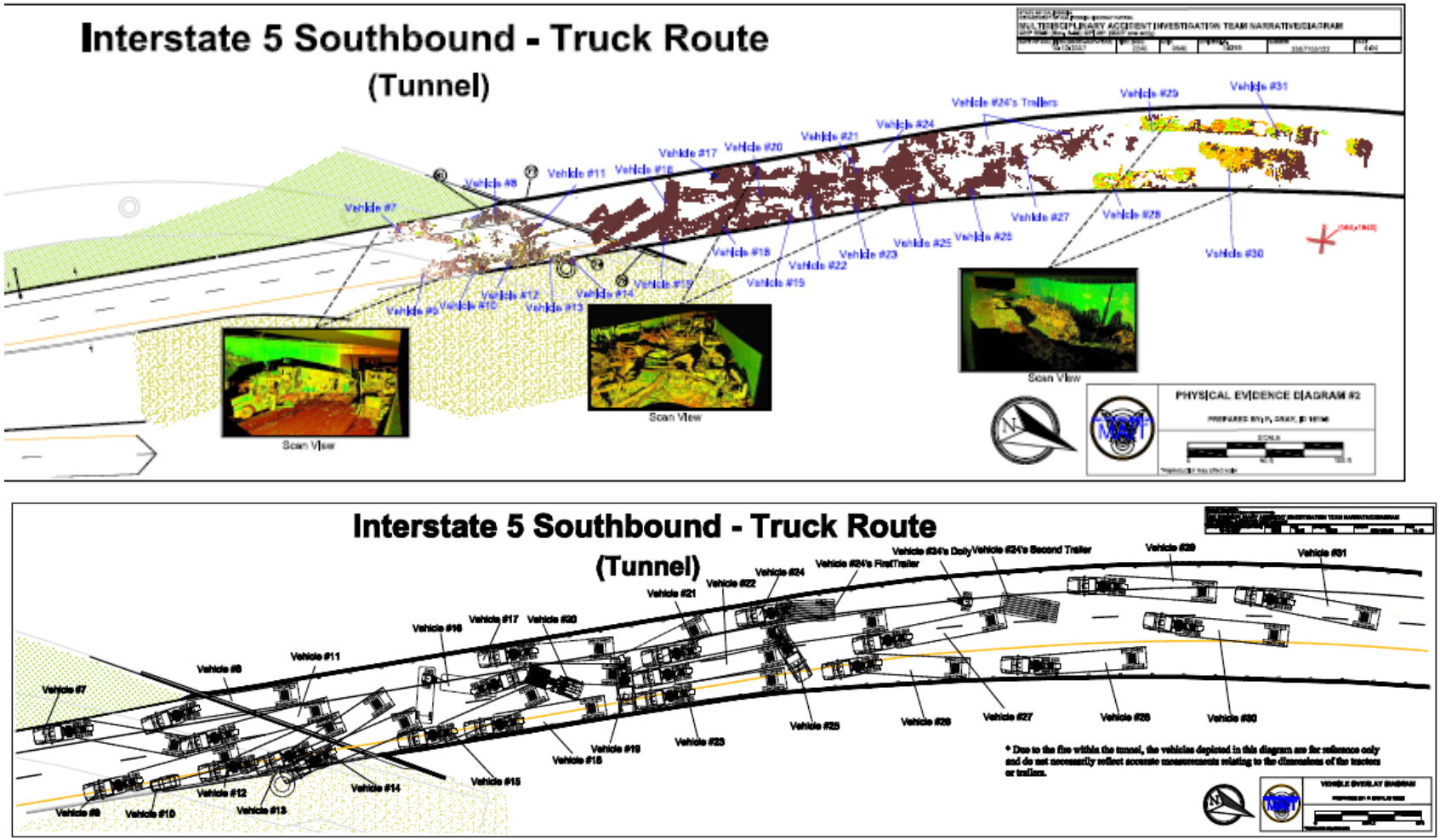

Figure 1.2. Sonar Map and Diagram of Inferred Locations of Vehicles Involved in Accident and Fire within Newhall Pass Tunnel (image and diagram from MAIT Report, CHP 2007, reprinted with permission.)

The staff of the NRC Division of Spent Fuel Storage and Transportation undertook an investigation of the fire to determine what impact this event might have on the risk associated with SNF transportation on public roadways. This evaluation included an assessment of the fire exposure temperatures within the tunnel (NUREG/CR-7101 2011), computational fluid dynamics (CFD) modeling of the tunnel fire, and an analytical evaluation of the response of a representative NRC Certified SNF transportation package to boundary conditions simulating exposure temperatures predicted for the Newhall Pass Tunnel fire.

This report presents the results of these analyses. Section 2.0 contains a description of the Newhall Pass Tunnel fire scenario and summarizes the results of material temperature estimates based on samples obtained from vehicles involved in the fire. Section 3.0 describes the numerical modeling of the Newhall Pass fire and development of boundary conditions for analysis of the effect of the fire on an SNF package. Section 4.0 describes the fire scenario developed for this evaluation, based on the known accident conditions and numerical modeling of the fire. Section 5.0 presents the analytical models developed for evaluation of the effect of the Newhall Pass fire scenario on an SNF package. Section 6.0 describes the analysis method, including assumptions and boundary conditions. Section 7.0 summarizes the thermal performance of the GA-4 package in this fire scenario, as predicted with the analytical models. The potential consequences of the Newhall Pass Tunnel fire scenario for the GA-4 package are summarized in Section 8.0. Results and conclusions of this study are summarized in Section 9.0, and references are listed in Section 10.0.

2.0 THE NEWHALL PASS TUNNEL FIRE

This section presents a description of the fire and summarizes the results of analyses of material samples obtained to characterize temperatures reached by structures in or near the fire. Section 2.1 contains the fire description. Section 2.2 summarizes the analyses to determine the material exposure temperatures due to the fire.

2.1 Description of the Fire

Detailed documentation of the Newhall Pass Tunnel fire is provided in the CHP MAIT report (CHP 2007) on this accident, including photographs and video footage taken by CHP officers and Los Angeles County Fire Department (LACoFD) personnel on the scene. The total duration of the fire is estimated as approximately 25 hours, but this includes the time required to clear debris from the tunnel so that fire fighters could reach localized hot spots within the tunnel, long after the intense fully engulfing fire had ended. The period when intense fire filled the tunnel is estimated as no more than 5 hours, based on photographs and timeline information in the MAIT report.

Figure 2.1 shows vehicles #7 and #9 early in the fire. This photo was taken from the roadway, which is angled sharply to the tunnel exit. A more direct view of the exit of the tunnel, which is filled with flame, is shown in Figure 2.2, with a photo taken from above the wreckage of vehicle #8.

Figure 2.1. Newhall Pass Fire at Tunnel Exit; from Roadway (LACoFD photo from MAIT Report, CHP 2007, reprinted with permission.)

Figure 2.2. Newhall Pass Fire at Tunnel Exit; Looking Directly into Tunnel (LACoFD photo from MAIT Report, CHP 2007, reprinted with permission.)

The time-stamps for the photos in Figure 2.1 and 2.2 have been lost, but based on the reported fire conditions and the timeline in the MAIT report (CHP 2007), they were probably taken within an hour of the start of the fire. The earliest time-stamp available for images of the fire at the tunnel exit is the photo in Figure 2.3, which shows the tunnel exit at 2:47 a.m. on 10/13/2007. This photo shows that the fire at the tunnel exit and for some distance inside was essentially extinguished within 4 hours after the start of the fire.

Figure 2.3. Newhall Pass Tunnel Exit at 10/13/2007 2:47 a.m. (photo from MAIT Report, CHP 2007, reprinted with permission.)

An image of the fire at the tunnel entrance is shown in Figure 2.4. CHP officers at the scene and other eye-witnesses reported that thick black smoke began pouring from the tunnel entrance within 20-30 minutes after the start of the fire. The photo in Figure 2.4 is from a group of similar photos taken by LACoFD personnel. All of these photos lack time-stamps, but the number of photos and their numerical sequencing of filenames suggest that this inferno-like state persisted for some time at the tunnel entrance, possibly several hours.

Figure 2.4. Newhall Pass Tunnel Entrance at 10/13/2007 2:47 a.m. (photo from MAIT Report, CHP 2007, reprinted with permission.)

Although the total duration of this intense fire is uncertain, the end of it is bounded by the time-stamp on the photo shown in Figure 2.5. This photo, taken from the tunnel entrance at 4:04 a.m., shows the charred remains of the last vehicle to enter the tunnel (vehicle #31). At this time, there is no fire within the tunnel that can be detected by the camera's optics. Figure 2.6 shows a photo taken from essentially the same vantage point later that morning in full daylight, at 7:58 a.m. Smoke is still issuing from the tunnel, indicating that localized fires on some vehicles are still smoldering inside the tunnel. Smoke may also have been present in the earlier photo, but is not visible due to darkness. In sum, the photographs show that the intense heat-producing portion of the fire had ended less than 5 hours after the known start time of the fire.

Figure 2.5. Newhall Pass Tunnel Entrance at 10/13/2007 4:04 a.m. (photo from MAIT Report, CHP 2007, reprinted with permission.)[1]

Figure 2.6. Newhall Pass Tunnel Entrance at 10/13/2007 7:58 a.m. (photo from MAIT Report, CHP 2007, reprinted with permission.)

[1] NOTE: image has been brightened by 50% for clarity; original photo was taken in nearly full darkness.

Based on the photographic evidence and the timeline in the MAIT report (CHP 2007), the active, intense fire that destroyed the trucks and their cargoes could have lasted no more than about 5 hours. During this time, fire fully engulfed each of the 24 tractor-trailer rigs within the tunnel, consuming all or most of their respective cargoes, and destroying the vehicles down to their steel frames and engine blocks. Nearly all of the sheet aluminum on the trailer boxes completely vanished, primarily by oxidization rather than melting. Other more substantial aluminum alloy components (such as truck wheels and fuel tank support frames) showed evidence of local melting. Figure 2.7 shows a representative photo of the remnants of vehicles near the middle of the tunnel (identified as vehicles #22 and #23 in the MAIT report[2]). Figure 2.8 shows a post-fire photo of a vehicle near the tunnel exit.

Figure 2.7. Vehicles Near Middle of Tunnel, View Toward Tunnel Entrance (photo from MAIT Report, CHP 2007, reprinted with permission.)

[2] The numbers in orange spray paint which appear in many photographs of the wreckage were applied on-scene, to identify specific vehicles before removal from the tunnel. This numbering accounts only for vehicles actually within the tunnel, and as a result, it is offset from the final vehicle count and numbering scheme used in the MAIT report to identify *all* vehicles involved in the accident.

Figure 2.8. Vehicle Near Tunnel Exit (photo from MAIT Report, CHP 2007, reprinted with permission.)

These photos and the detailed timeline of the fire given in the MAIT report indicate that the fire burned intensely on each tractor-trailer rig for some specific period of time, but could not have burned for the entire 4-5 hours at any one location, simply due to the limited supply of combustible material on or in any one vehicle. This suggests that the fire moved progressively through the tunnel from exit to entrance, burning intensely on each rig for a time, then dying down to smolder through the less combustible elements of the vehicle and cargo.

The temperature distributions and durations needed for analytical evaluations of potential consequences of the fire are not simple to obtain in this type of fire. It requires careful definition of the fire scenario for fire modeling evaluations, and comparison to physical evidence left in the remains of the fire. The following section discusses the results of evaluations to determine material temperatures obtained in the Newhall Pass Tunnel fire.

2.2 Maximum Material Temperatures

An investigation to collect and examine samples from the vehicles involved in the Newhall Pass Tunnel fire was undertaken for the NRC by the Center for Nuclear Waste Regulatory Analyses (CNWRA) (NUREG/CR-7101 2011). Samples recovered from four of the incinerated vehicles were analyzed in detail to estimate temperatures these materials reached during the fire. Because of the timeframe of the investigation, samples were obtained from only four of the 24 vehicles involved in the tunnel fire. Damaged tunnel material had already been removed and disposed of, and was therefore unavailable for sampling.

Table 2.1 lists the samples obtained from vehicles within the tunnel. The first number in the Sample Identification number corresponds to the vehicle number from the MAIT report (see Figure 1.2). Melted aluminum samples indicated that temperatures reached at least 1040°F (560°C) at some locations in the tunnel. Studies of hardness changes in graded bolts recovered from destroyed vehicles within the tunnel indicate that these components reached temperatures no higher than about 1382°F (750°C). A single sample of brass material indicated a local temperature of at least 1620°F (880°C) near the middle of the tunnel during the fire. Evaluation of the severe scaling of the carbon steel vehicle frames indicates that these components were exposed to temperatures exceeding 900°F (482°C).

Table 2.1. Material Samples Obtained from Vehicles for Thermal Evaluation

Sample ID	Description
14-01	aluminum bracket holding steel cable
14-02	copper wire from rear lighting of trailer, with some melted aluminum adhering
14-03	brass clamp holding copper wire, from engine compartment (driver's side)
14-04	melted aluminum and Grade 5 bolt from rear wheel of trailer (driver's side)
14-05	melted aluminum flooring with imbedded steel screw
14-06	melted aluminum from grill of tractor
17-01	partially melted rear brake brass compression fitting
18-01	brass clip containing copper electrical wire
18-02	melted aluminum and Grade 5 bolt from wheel
27-01	melted aluminum and Grade 5 bolt from wheel
27-02	melted aluminum and Grade 5 bolt from wheel
27-03	brass ID tag from axle housing

The available material evidence shows temperatures below 1832°F (1000°C) in the tunnel, and all but one of the samples indicate temperatures below "1472°F (800°C)", which is the design-basis fire temperature for SNF transportation packages under HAC (10 CFR 71 2003). However, these temperatures are based on a very limited sampling of the vehicles involved in the tunnel accident, and the known duration of the Newhall Pass Tunnel fire significantly exceeds the 30-minute duration prescribed for the HAC fire. A more detailed evaluation of the fire temperatures throughout the tunnel was obtained with numerical modeling of the fire, as described in Section 3.0.

3.0 NUMERICAL MODELING OF THE NEWHALL PASS TUNNEL FIRE

This section describes numerical simulations of the Newhall Pass fire using the CFD code Fire Dynamics Simulator (FDS), developed specifically to study fire behavior (McGrattan et al. 2008). A preliminary model of this fire was developed for NRC at the CNWRA, Southwest Research Institute, San Antonio, Texas, and provided an initial scoping analysis of the fire. The model was then refined and final calculations were performed at the National Institute of Standards and Technology (NIST).

3.1 FDS Model Geometry

The Newhall Pass tunnel is an open-ended concrete box extending 544.3 ft (166 m) from entrance to exit, with two traffic lanes, each nominally 12-ft (3.6-m) wide. The right shoulder is approximately 12-ft (3.6-m) wide and the left shoulder is 5-ft (1.5-m) wide, for a total nominal roadway width of 41 ft (12.5 m). Actual local horizontal width varies by about 10 ft (~3 m) over the length of the tunnel, due in part to the slight curvature to the left. Vertical clearance within the tunnel varies from 18 ft (5.4 m) at the entrance to 25 ft (7.6 m) at the exit. The tunnel has a downhill grade of approximately 6% from entrance to exit.

The computational domain of the model developed for FDS to represent the tunnel consisted of a rectangular mesh of 0.5 m cells, with the tunnel cross-section represented with approximately average dimensions of 45.9 ft (14 m) wide and 19.7 ft (6 m) high. The lateral curve was neglected, but the modeling included the gravitational effect of the downhill grade. The axial length of the tunnel was modeled as 551.2 ft (168 m), to capture the effect of the angled exit face of the tunnel. The vehicles within the tunnel were modeled as solid obstructions, and arranged to represent the estimated configuration of the vehicles within the tunnel (see Figure 1.2). Each of the vehicle representations were placed as closely as possible to their actual position in the tunnel, within the resolution of the rectangular grid of the model mesh. Vehicles #19 and #25 were not included as solid obstructions, due to the limitations of the relatively coarse mesh of the 0.5 m grid. Figure 3.1 shows the overall geometry of the model, including the locations of the modeled vehicles within the tunnel.

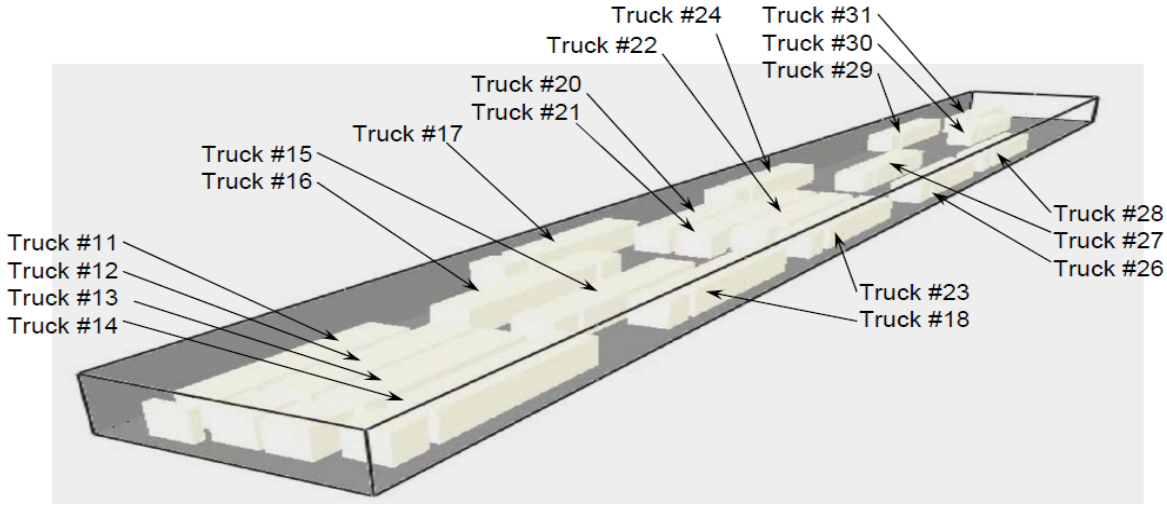

Figure 3.1. Simplified Model Geometry

3.2 FDS Model Fire

The total heat release rate for a fire is a function of the burning rate (i.e., mass loss rate, which is also a function of the availability of oxygen), fuel properties (including heat of combustion and density), and the geometry of the fire. A major difficulty in determining the burning rate and fuel properties for the Newhall Pass fire is that the type of fuel and the total amount available is not completely known. Table 3.1 summarizes the available information on the cargoes carried by the vehicles within the tunnel, as documented in the MAIT report (CHP 2007).

Table 3.1. Summary of Vehicle Cargoes

Vehicle #	Cargo Information	Cargo Weight
11	grapes in cardboard boxes	40,000 lb (~18,000 kg)
12	apples in cardboard boxes	not known
13	oranges in cardboard boxes	not known
14	cantaloupe in cardboard boxes	not known
15	canned olives	not known
16	2 trailers; first trailer carrying cotton; second trailer empty	not known
17	refrigerator truck, carrying frozen bread	42,000 lb (~19,000 kg)
18	melons	40,000 lb (~18,000 kg)
19	empty	N/A
20	empty	N/A
21	tomatoes	not known
22	empty	N/A
23	empty	N/A
24	2 trailers, carrying general freight	not known
25	coffee	20,000 lb (~9,100 kg)
26	empty	N/A
27	sugar on 14 wooden pallets	23,000 lb (~10,400 kg)
28	tile and nails in cardboard boxes	78,000 lb (~35,400 kg)
29	produce	not known
30	baked goods	not known
31	empty	N/A

Photographs of vehicles within the tunnel after the fire, and video of the process of removing the wreckage of vehicles from the tunnel, which are included in the MAIT report (CHP 2007), show that a substantial portion of the cargoes of vehicles #11 through #15 survived the fire, albeit in a somewhat charred condition. The remains of vehicle #18 appear buried in charred melons, and vehicle #21 is surrounded by heaps of small blackened round objects that are probably tomatoes. Photos show the fire-blackened remains of the trailer of vehicle #28 virtually buried under a heap of highly oxidized nails (minus their cardboard packaging boxes), and miscellaneous ceramic dishes were visible in the remains of vehicle #24. There were no identifiable remains associated with the vehicles carrying more readily combustible cargoes, such as #16, #25, #27 and #30. The vehicles running empty (#19, #20, #22, #23, #26, and #31) were reduced to their steel frames covered with ash, with only their exhaust stacks still standing.

In addition to their individual cargoes, the vehicles themselves included combustible material, such as wooden decking under the trailer floors, plastics and upholstery material in the tractor, tires (18 to 36 per vehicle), and diesel fuel in aluminum tanks. Assuming that the fuel tanks were on average about half full, each vehicle can be estimated as having had approximately 200 gallons of diesel on board. An additional source of thermal energy in the fire was the sheet aluminum comprising the trailer walls and ceilings. This material oxidizes rapidly at elevated temperatures, and would have been largely consumed by the fire before reaching the melting temperature of the metal alloy. The large variation in combustible material from vehicle to vehicle means that the burning rate of the fire would have varied significantly with location in the tunnel. In conjunction with the large uncertainty in cargo loads and the wide range in degree of destruction of the individual cargoes, it is impossible to directly calculate the heat release rate for this fire.

The fire modeling approach used in this analysis utilized a feature in FDS that allows the fire behavior to be defined with a total mass of fuel and a specified burn time. Based on the available information, a fuel budget was developed for a typical vehicle within the tunnel, consisting of the combustible components of the vehicle, plus an estimated combustible mass for a typical cargo. Since the majority of the cargoes consisted of material containing a large fraction of non-combustible material (i.e., intrinsic water in the fruits and vegetables, and metal or ceramics in the general cargo), the actual combustible mass is estimated as much less than the gross weight of the cargo.

The fuel budget assumed for a typical vehicle in the fire is shown in Table 3.2. Assuming a burn time of approximately 1 hour (3600 seconds) per vehicle, the heat release rate for each vehicle is estimated as 27 MW, which is typical for a truck or a bus. This approach yields a conservative estimate of the available fuel for the fire within the tunnel, with two significantly conservative assumptions. First, the typical combustible cargo mass of 3000 kg (6614 lb) is applied to all vehicles in the tunnel, including the six vehicles that were known to be running empty. Second, it is assumed that the entire combustible mass of each cargo was fully consumed in the fire, when in fact a substantial portion of the cargo of some vehicles survived the fire.

Table 3.2. Fuel Budget for Typical Vehicle in Newhall Pass Tunnel Fire

Fuel Source	**Combustible Mass**	**Heat of Combustion**
diesel fuel	700 kg (1543 lb)	20,000 kJ/kg
tires	400 kg (882 lb)	
combustible mass of generic cargo	3000 kg (6614 lb)	
aluminum (in thin sheets)	800 kg (1764 lb)	
total estimated typical combustible mass per vehicle	4900 kg (10,803 lb)	

To verify the conservatism of the typical fuel budget, with respect to the actual fuel load available on each vehicle, combustible mass of the actual cargo for each of the vehicles in the tunnel was estimated, based on information extracted from the MAIT report (CHP 2007). Table 3.3 summarizes these estimates for the vehicles within the tunnel, as represented in the FDS model. For vehicles #12, #13, #14, #21, and #29, the cargo weight was assumed to be the same as vehicle #11, based on the similarity of the cargo material (i.e., fruit and vegetables). A

rough fraction of the total percentage of the cargo consumed in the fire was developed based on the amount of unburned cargo shown in photographs and video from the MAIT report. The cargo of vehicle #25, which was not represented in the FDS model, due to mesh resolution, was transferred to the nearby vehicle #26, in order to include this highly combustible cargo in the fire scenario. For vehicles #16, #24, and #30, available data was insufficient to obtain a reasonable estimate of the combustible mass of the cargo, and for these vehicles, the cargo combustible mass estimated for a typical vehicle is assumed.

Table 3.3. Estimated Combustible Mass of Cargo for Vehicles in Newhall Pass Tunnel Fire

Vehicle #	Cargo	Cargo Weight	Estimated Mass of Actual Cargo Consumed in Fire	Compared to Assumed Typical Cargo Combustible Mass
11	grapes in cardboard boxes	18,100 kg (40,000 lb)	345 kg (760 lb)	smaller; ~11%
12	apples in cardboard boxes	not known; assumed same as #11	726 kg (1,600 lb)	smaller; ~24%
13	oranges in cardboard boxes	not known; assumed same as #11	590 kg (1,300 lb)	smaller; ~20%
14	cantaloupe in cardboard boxes	not known; assumed same as #11	454 kg (1,000 lb)	smaller; ~15%
15	canned olives	not known; but mostly not combustible	204 kg (450 lb)	smaller; ~7%
16	2 trailers; first trailer carrying cotton; second trailer empty	not known	typical cargo assumed 3,000 kg (6,641 lb)	same
17	frozen bread	19,000 kg (42,000 lb)	5,000 kg (11,023 lb) assuming 74% water	larger (by factor of 1.7)
18	melons	18,100 kg (40,000 lb)	454 kg (1,000 lb)	smaller; ~15%
19	empty	N/A	0	vehicle #19 omitted from model due to grid-size limitations
20	empty	N/A	0	N/A
21	tomatoes	not known; assumed same as #11	272 kg (600 lb)	smaller; ~9%
22	empty	N/A	0	N/A
23	empty	N/A	0	N/A
24	2 trailers, carrying general freight	not known; but mostly not combustible	typical cargo assumed 3,000 kg (6,641 lb)	same
25	coffee	9,100 kg (20,000 lb)	vehicle #25 omitted from model due to grid-size limitations; cargo modeled in vehicle #26	vehicle #25 omitted from model due to grid-size limitations; cargo modeled in vehicle #26

Table 3.3. (continued)

Vehicle #	Cargo	Cargo Weight	Estimated Mass of Actual Cargo Consumed in Fire	Compared to Assumed Typical Cargo Combustible Mass
26	empty; but modeled as carrying cargo of vehicle #25	9,100 kg (20,000 lb)	7000 kg (15,400 lb) assumed 23% water	larger (by factor of 2.3)
27	sugar on 14 wooden pallets	10,400 kg (23,000 lb)	10,400 kg (23,000 lb)	larger (by factor of 3.5)
28	tile and nails in cardboard boxes	35,400 kg (78,000 lb); but mostly not combustible	354 kg (780 lb) assumed only 1% combustible	smaller; ~12%
29	produce	not known; assumed same as #11	1270 kg (2800 lb)	smaller; ~42%
30	baked goods	not known	typical cargo assumed 3,000 kg (6,641 lb)	same
31	empty	N/A	0	N/A

The estimated combustible mass values for each vehicle, as summarized in Table 3.3, show that the assumed typical cargo mass yields a very conservative estimate of the total fuel load for the fire. The overall tunnel fire modeling is quite conservative, in that the estimated actual combustible cargo mass is only a relatively small fraction of the assumed typical cargo combustible mass. However, the actual combustible cargo mass estimated for three of the vehicles (#17, #26, and #27, as modeled), is significantly larger than the typical assumed cargo mass. This raises the possibility that local fire conditions near these vehicles could be significantly different from local fire conditions with the assumed typical cargo mass. The effect of this more realistic distribution of the combustible fuel load for the fire in the Newhall Pass Tunnel is also investigated in the matrix of cases developed for this evaluation.

3.3 Matrix of Cases for FDS Model of Newhall Pass Tunnel Fire

With the considerations discussed in Section 3.2 regarding the potential fuel load for the Newhall Pass Tunnel fire, and the general approach for defining the fire, a matrix of cases was developed to bound the known fire behavior. This was accomplished by considering bounding variations in the fire spread rate and the local vehicle fire burn time, to encompass the known parameters of the fire scenario. Table 3.4 summarizes these cases. In all cases, the total calculated fire duration is bounded by the uncertainty in the timeline of the fire. The period of intense, fully engulfing fires with the tunnel is known to have been somewhat longer than 2 hours, but less than 5 hours. Table 3.4 also summarizes two sensitivity cases evaluated, to conservatively bound the full range of possible fire behavior. NIST-05 evaluated the effect of the concrete spalling model in FDS on predicted fire temperatures. Case NIST-06 represented a bounding estimate of the actual fuel load for each vehicle, based on available information on the cargo of the various vehicles, as presented in Table 3.3. This case was developed to verify that the assumed typical fuel load for all vehicles (including the empty ones) produced conservative estimates of the possible range of fire temperatures.

Table 3.4. FDS Cases Modeling Newhall Pass Tunnel Fire

Case	Fuel Load	Burn Rate	Fire Spread Rate
NIST 01	typical fuel budget for each modeled vehicle (see Table 3.2)	1.36 kg/s	0.01 m/s (slow)
NIST 02			0.015 m/s (moderate)
NIST 03			0.022 m/s (fast)
NIST 04	typical fuel budget for each modeled vehicle, but with burn rate doubled	2.72 kg/s	0.01 m/s (slow)
NIST 05	same as NIST 01 – sensitivity study on concrete spalling model in FDS		
NIST 06	fuel load based on actual cargo (if known), typical cargo (if not known); no cargo for empty vehicles	1.36 kg/s	0.01 m/s (slow)

The typical fuel budget defined in Table 3.2 was applied to each vehicle in the tunnel, including those known to be running empty, for cases NIST-01 through NIST-05, resulting in a conservative estimate of the total fuel load available within the tunnel. For case NIST-06, the fuel budget defined in Table 3.2 was modified to replace the typical cargo mass with the estimated actual mass, from Table 3.3. For vehicles running empty, case NIST-06 considers only the combustible portions of the vehicle itself (e.g., diesel fuel, tires, aluminum sheeting).

The specified spread rates for the fire, (slow, moderate and fast), produce different total duration times for the intense, fully engulfing portion of the fire, by controlling the length of time required for the fire to reach each vehicle. The slow spread rate (cases NIST-01, NIST-04, and NIST-06) results in a total fire duration of approximately 5 hours, which is slightly longer than the known timeline of this portion of the fire. The moderate spread rate (case NIST-02) results in a total fire duration of slightly over 3 hours. This is within the known timeline, but is a less conservative estimate of the fire duration than obtained in cases NIST-01 and NIST-04. The fast spread rate (case NIST-03) results in a total fire duration of just over 2 hours. This is within the uncertainty in the fire timeline, but results in a fire scenario that is much less conservative than the other two cases. Case NIST-04, with the slow spread rate but increased burn rate, results in an overall fire duration that is approximately the same as in case NIST-01, but with hotter, more intense fires of shorter duration on each vehicle.

Case NIST-05 was developed to investigate the effect of the spalling model in the FDS code on predicted fire temperatures. Spalling of the concrete absorbs energy from the fire, and would therefore be expected to result in reduced fire temperatures for the same fire conditions. This case is identical to NIST-01 (the base case), except that the spalling model was turned off.

3.4 FDS Fire Model Output

The primary purpose of performing the FDS simulations was to determine appropriate temperature boundary conditions for evaluating the potential effect of the Newhall Pass Tunnel fire scenario on an SNF package. A significant output of the fire model for this purpose is the quantity referred to as the *adiabatic surface temperature (AST)*. This is a potentially misleading term, since “surface” in this context is a virtual surface, and not the temperature of an actual surface in the fire. The surface referred to in this term is a hypothetical thermal concept defined in fire temperature measurement calculations to represent a perfect, non-intrusive measurement at a specific location within the fire. An AST defines the temperature at a given location in the fire for radiation and convective heat transfer from flames and hot gases to solid surfaces that see the fire. An AST can be obtained for any point in the fire, and is determined in the manner described below.

The net total heat flux seen by an actual surface exposed to fire is composed of two components; thermal radiation and convection. This can be defined simply as:

$$q''_{tot} = q''_{rad} + q''_{con} \tag{3.1}$$

where

q"tot = net total local heat flux
q"rad = local heat flux due to thermal radiation
q"con = local heat flux due to convection

The thermal radiation term in Eq. (3.1) is the difference between the absorbed incident thermal radiation and that emitted from the surface. The heat transmitted through the surface is neglected, and the absorptivity and emissivity are assumed equal, neglecting any dependence on wavelength. With these simplifications, the net heat received by the surface as thermal radiation can be written as:

$$q''_{rad} = \varepsilon (q''_{inc} - \sigma T_s^4) \tag{3.2}$$

where

q"inc = incident thermal radiation heat flux
ε = emissivity of the surface
σ = Stefan-Boltzmann constant
Ts = local surface temperature

The emissivity (or absorptivity) is a material property of the surface that can be determined by measurement. However, in most cases of structural materials exposed to fire, it can be assumed that the initial emissivity will change rapidly to a very high value due to sooting of the surface. A conservative estimate is 0.9 for highly sooted surfaces. A minimum value of 0.8 for absorptivity of exterior surfaces of an SNF package in the HAC fire is specified in 10 CFR 71.

Because fires are characterized by widely varying temperature distributions in space and time, the incident thermal radiation heat flux should ideally include all contributions from nearby flames, hot gases, and other surfaces. The incident thermal radiation may therefore be written as the sum of the contributions from all of the radiating sources:

$$q''_{inc} = \sum_i \varepsilon_i F_i \sigma T_i^4 \tag{3.3}$$

where

q"inc = total local incident thermal radiation heat flux on a given surface from all sources
εi = emissivity of the *i*th source surface
σ = Stefan-Boltzmann constant
Fi = dimensionless geometric view factor between the local surface and the *i*th source surface
Ti = local surface temperature of the *i*th source

FDS includes an algorithm for calculating the incident thermal radiation heat flux using Eq. (3.3), based on the local surface temperatures and the geometry of the mesh.

The convective heat flux depends on the difference between the surrounding gas temperature and the surface temperature, and on local fluid dynamics. The relationship between heat flux and temperature difference is generally characterized with a heat transfer coefficient, which is determined from an empirical heat transfer correlation, such that:

$$q''_{con} = h(T_g - T_s) \tag{3.4}$$

where

h = local heat transfer coefficient
T_g = gas temperature adjacent to the exposed surface
T_s = local surface temperature

Substituting Eq. (3.2) and Eq. (3.4) into Eq. (3.1), the total net heat flux to a surface can therefore be expressed as

$$q''_{tot} = \varepsilon(q''_{inc} - \sigma T_s^4) + h(T_g - T_s) \tag{3.5}$$

The relationship in Eq. (3.5) can be used to determine the AST at the location of an actual surface in the model. The virtual surface at this (and any other) location is by definition a perfect insulator, and since the total net heat flux to this idealized perfect insulator surface is by definition zero, Eq. (3.5) reduces to

$$\varepsilon(q''_{inc} - \sigma T_{AST}^4) + h(T_g - T_{AST}) = 0 \tag{3.6}$$

Numerically, the adiabatic surface temperature is a very useful quantity because it provides a natural interface between models that represent fire behavior and models that represent thermal and mechanical behavior of structures. A fire model in this context is any calculation method used to predict the temperature and species concentrations of a fire-driven flow. A structural model is any calculation method used to predict temperatures or stress/strain responses in an object exposed to the fire. The fire model may compute the evolving temperature of the bounding surfaces out of necessity, but it does not generally include a detailed representation of the thermal response of solid objects. Even a CFD model may only approximate a bounding solid as an infinitely thick slab for the purpose of estimating its surface temperature.

If the results of the fire model are to be used to perform a more detailed heat transfer calculation of the thermal response of a solid object within or near the fire, then some sort of interface is required to transfer information at the gas-solid interface. The most obvious quantity for this purpose is the heat flux at the surface, but in practice, this leads to major computational difficulties. The net heat flux to a surface computed by the fire model is dependent on the corresponding surface temperature, which is also computed by the fire model. Depending on the model, this surface temperature might not be of the desired accuracy. In addition, it is common in many popular solid phase heat transfer programs to input a prescribed thermal boundary based on external gas temperature and calculated surface temperature (as in Eq. 3.9) rather than as a prescribed heat flux. Both of these problems can be circumvented by using the adiabatic surface temperature T_{AST} as the intermediary between the fire and structural models.

The interface is fairly simple. At every surface point at which the fire model computes an incident thermal radiation heat flux and a corresponding gas temperature adjacent to that surface, the following implicit equation can be solved for the adiabatic surface temperature, assuming that the emissivity and convective heat transfer coefficient are effectively constant at that location.

$$\varepsilon(q''_{inc,FM} - \sigma T_{AST}^4) + h(T_{g,FM} - T_{AST}) = 0 \tag{3.7}$$

where

$q''_{inc,FM}$ = incident thermal radiation heat flux computed by the fire model at the exposed surface
$T_{g,FM}$ = gas temperature computed by the fire model adjacent to the exposed surface
T_{AST} = adiabatic surface temperature computed by the fire model

A key feature of Eq. (3.7) is that the fire model does not require any assumptions to compute the incident thermal radiation heat flux. This equation merely serves as the definition of the adiabatic surface temperature, but it does not imply that the fire model calculates the heat flux in any particular way. Most importantly, it does not imply that the fire model uses a fixed heat transfer coefficient, *h.* The values of T_{AST} for any location in the fire model can be stored in a file according to a user-specified time interval and length increment appropriate for the application.

For the model of a structure in the fire, the heat flux to an object's surface and its temperature due to the fire conditions computed by the fire model can be calculated by the relationship:

$$q''_{tot,SM} = \varepsilon(q''_{inc,FM} - \sigma T_{s,SM}^4) + h(T_{g,FM} - T_{s,SM}) \tag{3.8}$$

Subtracting Eq. (3.8) from Eq. (3.7) yields the total net heat flux to the surface of an object as:

$$q''_{tot,SM} = \varepsilon\sigma(T_{AST}^4 - T_{s,SM}^4) + h(T_{AST} - T_{s,SM}) \tag{3.9}$$

where

$q''_{inc,FM}$ = incident thermal radiation heat flux computed by the structural model at the exposed surface
$T_{g,FM}$ = gas temperature computed by the structural model adjacent to the exposed surface
T_{AST} = adiabatic surface temperature computed by the fire model

The AST is interpreted by the model of a given structure as an effective black body radiation temperature for the purpose of computing the incident thermal radiation at an actual surface in that model, and as a gas temperature for the purpose of computing the convective heat flux at the given surface. The advantage of this approach is that it requires transfer of only one quantity, the AST, from a fire model to a model of a specific structure within the fire, rather than bringing over a heat flux, surface temperature, and convective heat transfer coefficient. A side benefit is that the receiving model need not be reconfigured to accept a heat flux as its boundary condition. It needs only to be modified to accept a temporally and spatially varying exposing temperature (i.e., the AST), which it can use to calculate the heat flux based on that

temperature and the surface temperature calculated in the structural model. Most models of this type are already configured to accept a time-varying exposing temperature curve as an external boundary condition.

3.5 Fire Model Results

The FDS analysis with the model described in Sections 3.1 and 3.2 was used to determine predictions of fire behavior during the intense phase of the fire, when the individual vehicles in the tunnel were successively engulfed in flame. The fire boundary conditions were defined as described in Section 3.2, and the fire emissivity is assumed to be 0.9, as there is ample evidence that this was a sooty, optically dense fire. This portion of the fire is estimated to have lasted for a period ranging from 3 to 5 hours, as discussed above. Evaluation of the predicted temperature distributions in the tunnel during the fire determined that the highest temperatures occurred at locations corresponding to the fully engulfing fires defined on each vehicle. Relatively high temperatures were also obtained near the ceiling above each vehicle location, but the peak temperatures near the ceiling were typically 100-200°C below the peak temperatures lower in the tunnel, within the engulfing fires.

3.5.1 Fire Temperatures for Case NIST-01

The peak temperatures predicted with FDS for case NIST-01 are shown in Figure 3.2 for each vehicle in the tunnel. The FDS simulation runs out to 6 hours, and predicts a total fire duration of slightly over 5 hours, with the intense fully engulfing fire on each vehicle lasting for approximately 1 hour. As the fire progresses through the tunnel, the vehicles downstream experience elevated temperatures prior to the fire actually reaching them, as hot fire gas from the burning vehicles closer to the tunnel exit sweeps past them. The highest temperature in this case is predicted to occur on vehicle #23, near the center of the tunnel, at 1721°F (938°C). The peak fire temperature is predicted to exceed 1472°F (800°C) on all but one vehicle (#20), and in general is above 1400°F (750°C) for about an hour for all vehicles in the tunnel.

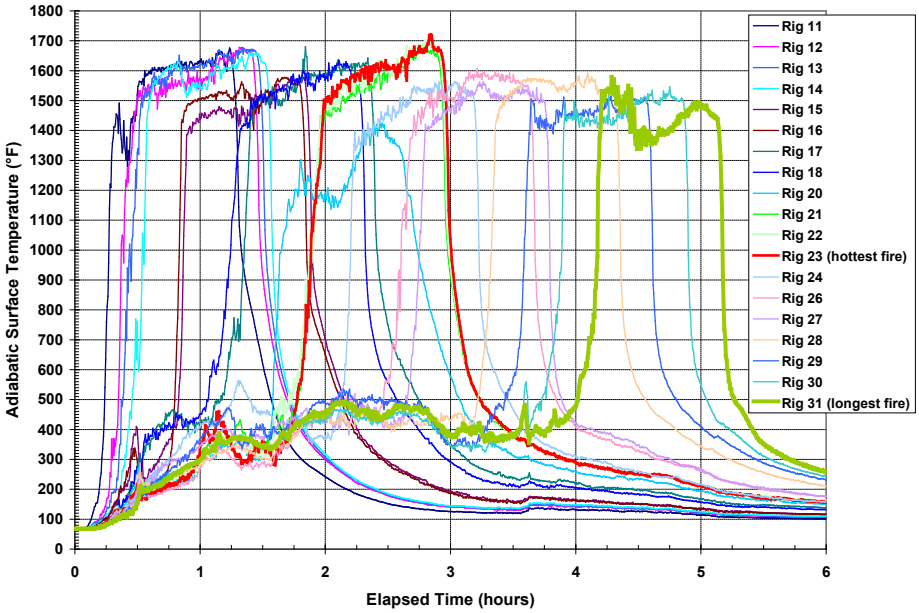

Figure 3.2. Predicted AST Values at Each Vehicle Fire Location for Case NIST-01

3.5.2 Fire Temperatures for Case NIST-02

The predicted peak temperatures for case NIST-02 are shown in Figure 3.3. These temperatures are in essentially the same range as in case NIST-01, as are the fire durations on each rig. The peak temperatures are similar, with the maximum reaching 1708°F (929°C). However, the faster (moderate) spread rate specified for the fire in the NIST-02 calculation results in a shorter total fire duration. In this case, the overall fire has essentially ended in just over 3 hours, which is about 2 hours shorter than the total fire duration predicted in case NIST-01. In case NIST-02, the fire is effectively over at about the time it is predicted to reach the mid-point of the tunnel in case NIST-01. Case NIST-02 may be a more realistic representation of the overall duration of the intense engulfing fire as it spread from rig to rig within the tunnel, based on available evidence of the actual fire timeline. However, it is less conservative for the purpose of determining bounding fire conditions for evaluation of potential effects of this fire on an SNF package.

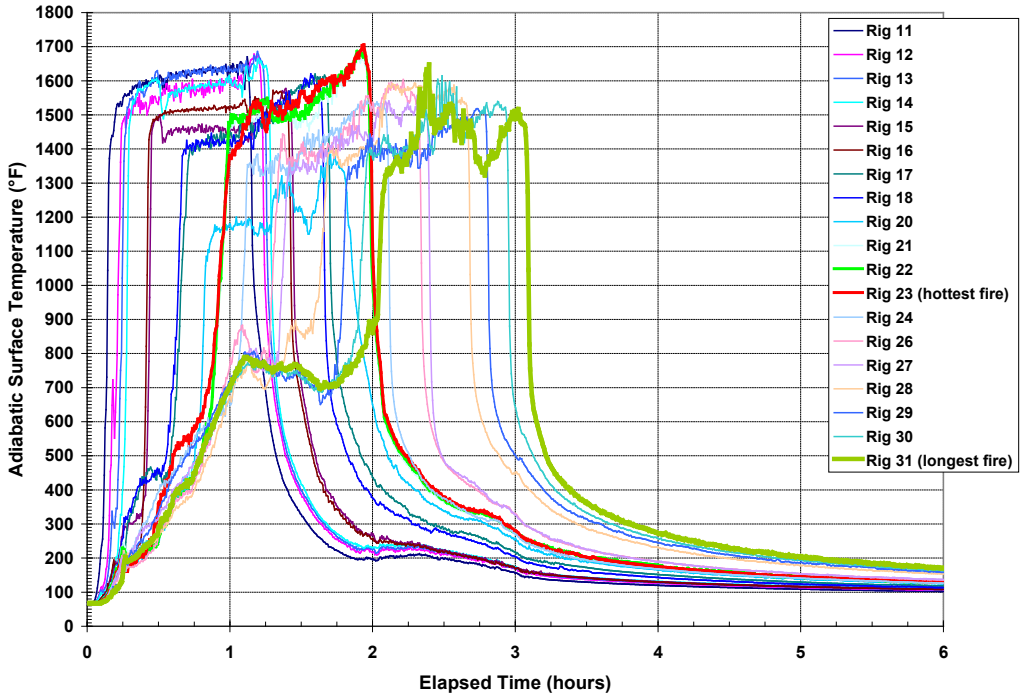

Figure 3.3. Predicted AST Values at Each Vehicle Fire Location for Case NIST-02

3.5.3 Fire Temperatures for Case NIST-03

The predicted peak temperatures for case NIST-03 are shown in Figure 3.4. These temperatures are somewhat lower than those predicted in cases NIST-01 and NIST-02, with the maximum reaching only 1668°F (909°C), even though the local fire durations on each rig are approximately the same as in the other two cases. The fast spread rate compresses the overall duration of the intense fire within the tunnel to approximately 2 hours. The predicted peak temperatures for case NIST-03 have the fire reaching the last vehicle (#31, nearest the tunnel entrance) in less than an hour. This is within the known window of possible overall duration for the fire, but is only just barely credible, based on available information on the fire timeline. This

may be a reasonably accurate simulation of the fire duration, but it is clearly less conservative than cases NIST-01 and NIST-02, and may not be bounding on the actual fire scenario.

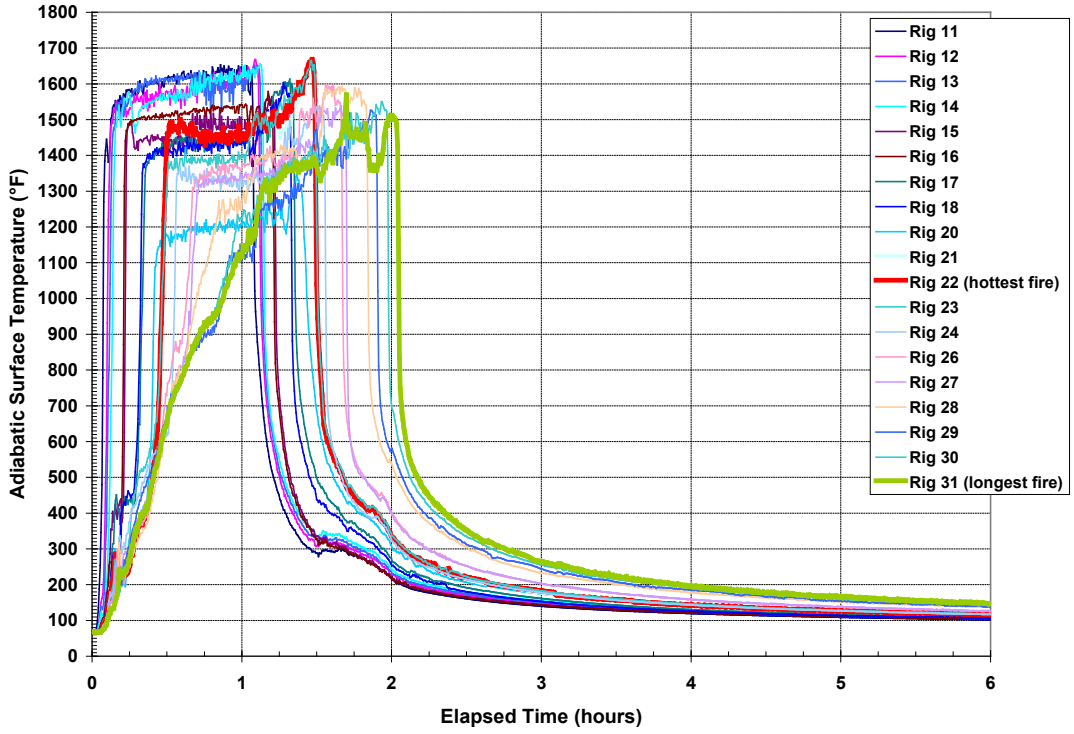

Figure 3.4. Predicted AST Values at Each Vehicle Fire Location for Case NIST-03

3.5.4 Fire Temperatures for Case NIST-04

The highest overall temperatures predicted for case NIST-04 are shown in Figure 3.5. This case is essentially the same as NIST-01 (slow spread rate, identical fuel load assumptions), but with the assumed burn rate doubled. As a result, the fire duration is shorter by approximately 50% (decreasing from about 1 hour per vehicle fire to approximately 30-35 minutes). Burning the same amount of material in approximately half the time results in generally higher peak temperatures, as might be expected. The predicted peak temperature for the hottest vehicle fire (#22, near the center of the tunnel) is 1991°F (1088°C), and the peak temperatures reached in the fires on the other vehicles generally exceed 1700°F (928°C). The overall duration of the tunnel fire in this case is within the conservative estimate of approximately 5 hours, but there is not enough evidence to assess the accuracy of the shorter vehicle fire durations.

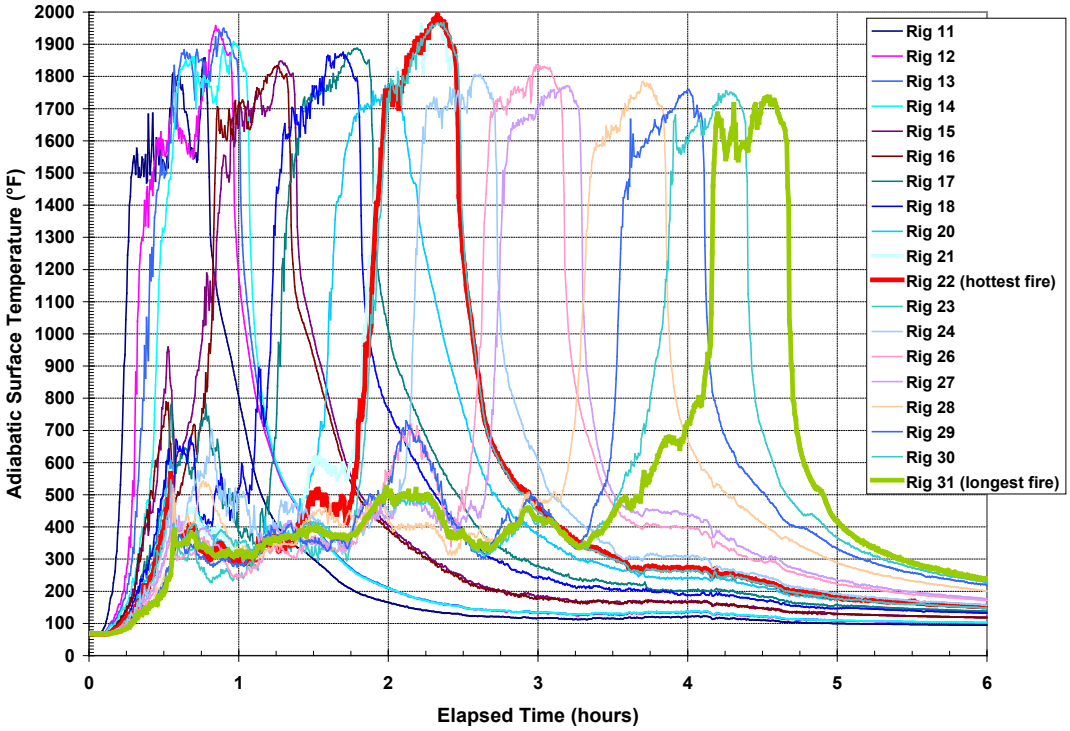

Figure 3.5. Predicted AST Values at Each Vehicle Fire Location for Case NIST-04

3.5.5 Fire Temperatures for Case NIST-05

The predicted peak temperatures for case NIST-05 (with the spalling model turned off) are shown in Figure 3.6. These temperatures are identical to the results obtained for case NIST-01, with the spalling model on. (All other cases were run with the spalling model on.) The spalling model in FDS conservatively assumes spalling can occur only if the temperature near the wall exceeds 1832°F (1000°C). In the fire scenario for case NIST-01, the highest peak fire temperature is below 1742°F (950°C). Peak fire temperatures on the vehicles immediately adjacent to the tunnel wall (#11, #17, #24, and #29 on the right-hand side, and #14, #18, #23, #26, and #28 on the left-hand side), are somewhat lower. The maximum is 1692°F (922°C), and the other peaks are near or below 1652°F (900°C). This is a large, well-ventilated tunnel, and although there is ample evidence of spallation of concrete from the Newhall Pass Tunnel walls due to this fire, the spallation model does not predict that it would occur except at a few locations near the hottest vehicles in the hottest case (NIST-04). This conservatism in the fire modeling results in higher fire temperatures than would be predicted if the assumed threshold for active spalling were to be lowered.

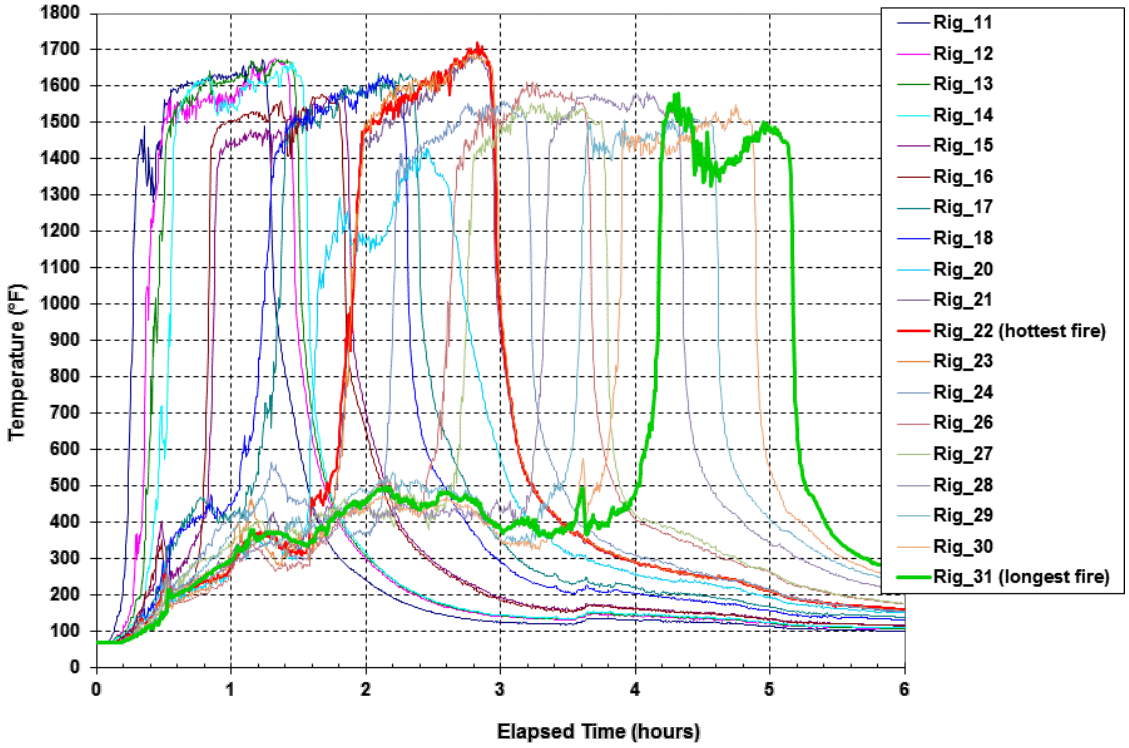

Figure 3.6. Predicted AST Values at Each Vehicle Fire Location for Case NIST-05

3.5.6 Fire Temperatures for Case NIST-06

The predicted peak temperatures for case NIST-06 are shown in Figure 3.7. This case assumes a slow burn rate, but the actual fuel for the individual rig fires is estimated as close as reasonably possible to match the actual combustible cargo mass. As might be expected due to the large variation in fuel load for the individual vehicle fires in this case, these results show greater variation in temperatures and individual vehicle fire duration, compared to the other cases evaluated. In this case, the "hottest fire" occurs on vehicle #26, with its load of coffee (borrowed from vehicle #25, due to meshing considerations, as discussed in Section 3.1). The "longest fire" for this case, on vehicle #31, reaches only about 1489°F (810°C), since this vehicle was not carrying cargo when caught in the Newhall Pass Tunnel fire. The fire on vehicle #30 is treated as the longest fire for case NIST-06 in this analysis. For this vehicle, with its load of baked goods (estimated with typical cargo combustible mass), the local fire is nearly twice as long as the fire on vehicle #30 in this case, and the peak fire temperature is higher, at 1646°F (897°C).

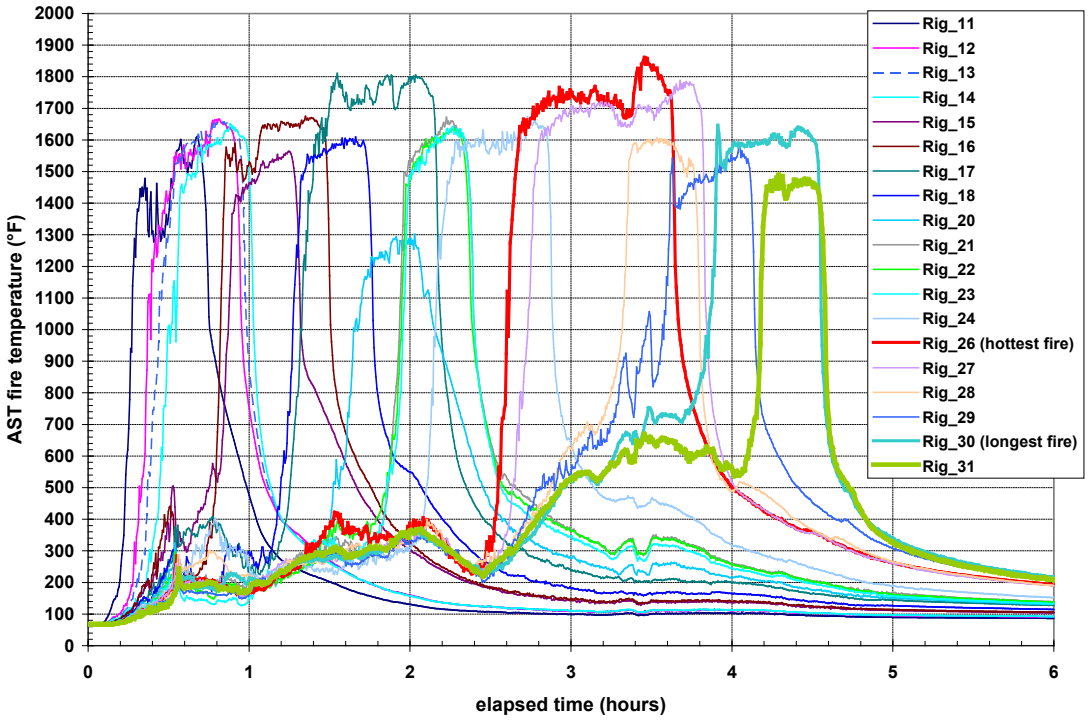

Figure 3.7. Predicted AST Values at Each Vehicle Fire Location for Case NIST-06

The peak fire temperatures on nearly all of the vehicles in case NIST-06 are lower than those obtained in the base case (NIST-01), and are for the most part significantly lower than for the most severe case (NIST-04, with the high burn rate.) Figure 3.8 illustrates this with a comparison of the peak fire temperatures for each vehicle fire in all five cases. For most of the vehicles, the more realistic estimate of actual combustible cargo load in NIST-06 results in essentially the same or slightly lower fire temperatures than were obtained with the typical cargo assumption. The notable exceptions are vehicles #26, and #27, where the peak temperatures are predicted to be substantially higher than in the base case (NIST-01). This is a reasonable result, since the combustible fuel mass for these vehicles is much larger in case NIST-06 than is assumed based on the typical cargo load. However, the difference is quite small, and the general trends shown in Figure 3.8 suggest that case NIST-04 might be the bounding case for this fire scenario, and not necessarily the more realistic modeling in case NIST-06.

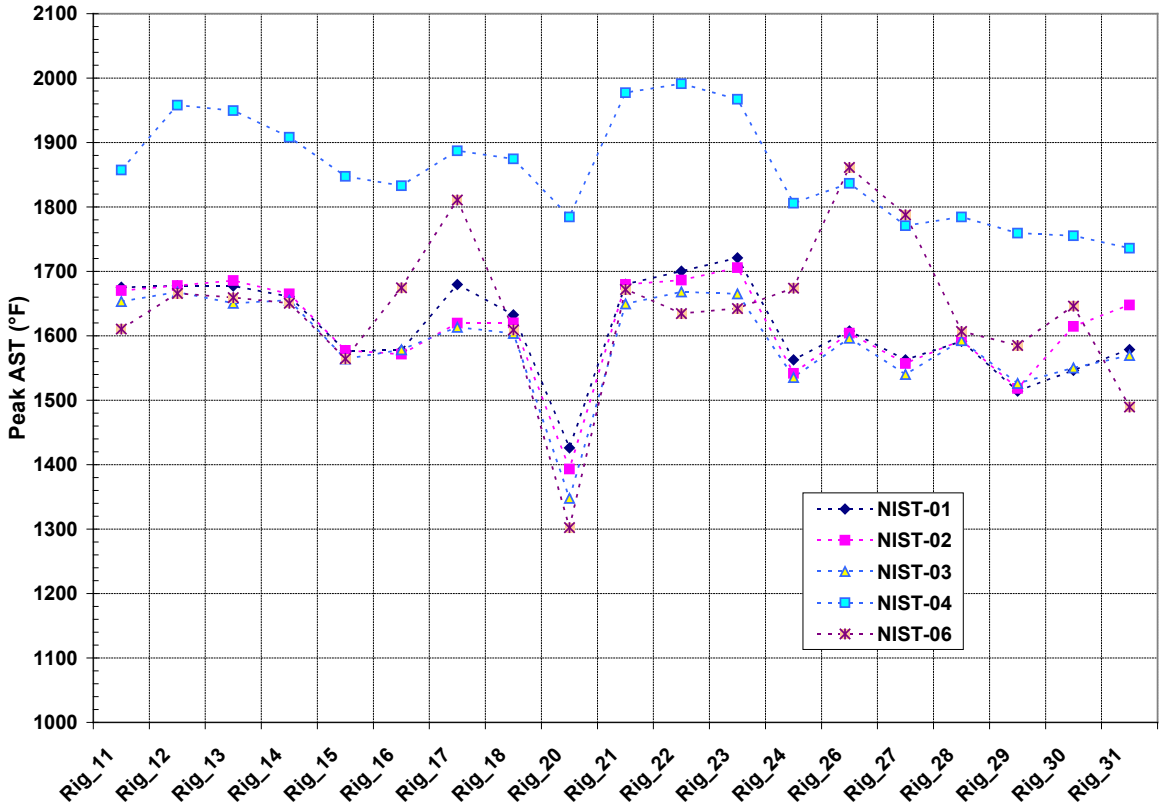

Figure 3.8. Comparison of Peak AST Values at Each Vehicle Fire Location for All Cases

3.5.7 Bounding Scenario for Thermal Response of SNF Package in Newhall Pass Tunnel Fire

The comparison in Figure 3.8 shows that the results obtained for the more intense fires (due to the higher burn rate) in case NIST-04, with typical cargo assumed for each vehicle, effectively bound the results obtained with the more realistic conditions of case NIST-06. The predicted peak temperature for each vehicle fire in case NIST-04 is significantly higher than the value predicted in case NIST-06, with the exception of the fires on vehicles #26 and #27. The peak temperatures for these two vehicle fires are slightly higher than in NIST-04. However, these are two of the three hottest fire temperatures predicted in NIST-06, and are significantly below the hottest fire temperatures predicted in NIST-04. The hottest fire and longest fire locations in NIST-04 clearly bound the equivalent locations in NIST-06.

This comparison shows that the more intense burn rate assumed for NIST-04 has a greater influence on peak fire temperatures than the assumed cargo mass. It also shows that these five cases provide results that reasonably and conservatively bound the known behavior of the Newhall Pass Tunnel fire. The results of these FDS analyses were used to provide boundary conditions for thermal evaluations of the potential performance of a Legal Weight Truck SNF transportation package exposed to this fire scenario. In these evaluations, it was assumed that the SNF package would be fully engulfed by the local fire at the hottest fire location or at the longest fire location for each specific case. No physical mechanism is postulated to explain how this might occur; it is simply assumed as a bounding configuration. If a vehicle carrying an SNF

transportation package had actually been involved in the Newhall Pass Tunnel fire, it would not be expected to experience temperatures higher than obtained with this bounding assumption, and would probably experience considerably lower temperatures.

Based on the results of the FDS analysis, it is clear that the package would experience the hottest fire temperatures if it were exposed to the fire conditions predicted for vehicle #22 or #23 (or #26, in NIST-06), located near the middle of the tunnel. However, the package would be exposed to the longest *duration* of temperatures above design-basis ambient of 100°F (68°C) if it is postulated as being at the location of vehicle #31 (or #30, in NIST-06), a short distance inside the tunnel entrance in this fire scenario. In all cases evaluated, the peak fire exposure temperature would be somewhat lower for the SNF package on a vehicle near the tunnel entrance, in comparison to the temperature exposure on a vehicle near the center of the tunnel, but the package would still experience a fire of greater duration and severity than the regulatory HAC fire. In addition, that exposure would occur after several hours at elevated ambient temperature prior to the local fire.

It is not obvious which of these conditions – exposure to the fire temperatures at the hottest location in the tunnel, or exposure to somewhat lower fire temperatures but with a longer duration at ambient temperatures above design-basis conditions – would provide the most severe thermal challenge to the SNF package. It is therefore necessary to investigate the full range of potential fire conditions, and corresponding locations of the SNF package. This modeling approach is discussed in Section 4.0.

4.0 THE NEWHALL PASS FIRE SCENARIO

There are two main aspects of the Newhall Pass tunnel fire that could expose an SNF package to conditions potentially more severe than the design-basis HAC fire (10CFR71), which is defined as a fully engulfing fire exposure of 30 minutes at “1475°F (800°C).” First, postulating that an SNF package could be exposed to the fire on any one of the individual vehicles involved in this tunnel fire scenario would expose the package to a fully engulfing fire that exceeds the temperature and duration specified for the HAC fire. Second, the overall timeframe of the severe fire portion of the accident, which is estimated to extend as long as 5 hours, would subject the package to a period of preheating at temperatures above design-basis ambient for up to 4 hours prior to being engulfed in fire.

Based on the cases (NIST-01 through NIST-06) described in Section 3.0, which define the bounding scenario for the Newhall Pass tunnel fire, each case contains two potentially most adverse locations for a vehicle carrying a SNF package. The first is the hottest fire location, which is near the center of the tunnel (corresponding to the location of vehicle #22, #23, or #26). This is the location where the SNF package would be exposed to the highest fire temperatures in each case. The second is the longest fire location, which is near the tunnel entrance (on vehicle #30 or #31), where the SNF package would be exposed to temperatures above design-basis ambient for the longest period of time.

The thermal analyses were performed assuming that the SNF package would experience the peak temperatures predicted in the FDS analysis at these most adverse vehicle locations. Table 4.1 lists the boundary conditions for the fire transients representing each case, with peak temperatures and time of peak temperature (relative to the start of the fire on the first vehicle in the tunnel, as modeled with FDS). Case NIST-05 is a sensitivity study on the effect of the concrete spalling model in FDS, assuming the same boundary conditions as NIST-01. Case NIST-05 yielded identical results to case NIST-01, due to the conservative implementation of the spalling model in FDS. Figure 4.1 through Figure 4.5 show the fire boundary temperatures defined for the evaluations of the response of an SNF package, based on the FDS results for the hottest fire and longest fire of each case. In all cases, the boundary conditions are defined to conservatively envelop the dynamic peaks-and-valleys of the FDS model results. The boundary temperatures were defined as steadily increasing or flat during the pre-fire phase for each case, ignoring local dips and intervals of decreasing predicted local fire temperature. A similar convention is used in defining the boundary temperatures for the fire portion of each transient, and in the post-fire cooldown, to ensure conservative boundary conditions for the entire transient.

Table 4.1. Peak Fire Boundary Temperatures at Hottest Fire and Longest Fire Locations

Case	Hottest Fire Location			Longest Fire Location		
	Elapsed Time to Peak (hr)	Local Fire Duration (minutes)	Peak Fire Temperature	Elapsed Time to Peak (hr)	Local Fire Duration (minutes)	Peak Fire Temperature
NIST-01	2.84	~60	1721°F (938°C)	4.29	~60	1579°F (859°C)
NIST-02	1.94	~60	1706°F (930°C)	2.39	~60	1648°F (898°C)
NIST-03	1.47	~60	1668°F (909°C)	1.70	~60	1570°F (854°C)
NIST-04	2.33	~33	1991°F (1088°C)	4.54	~33	1736°F (947°C)
NIST-05	2.84	~60	1721°F (938°C)	4.29	~60	1579°F (859°C)
NIST-06	3.46	~68	1861°F (1016°C)	3.91	~26	1646°F (897°C)

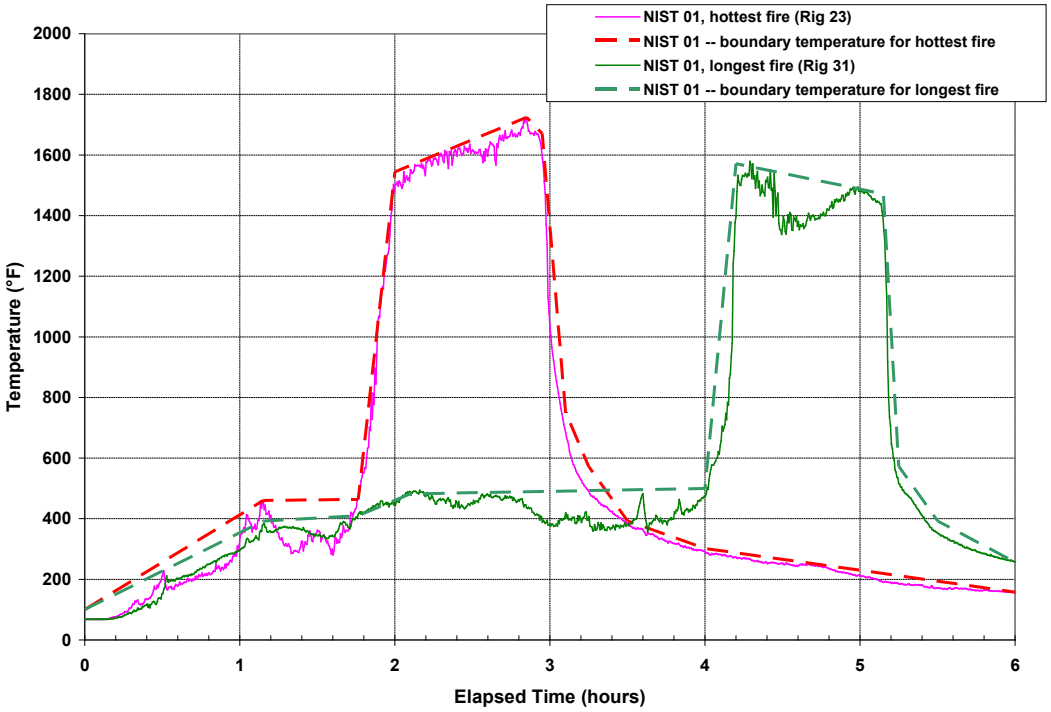

Figure 4.1. Boundary Temperatures for Thermal Analysis of SNF Package in Newhall Pass Fire Scenario at Most Adverse Vehicle Locations for Case NIST-01

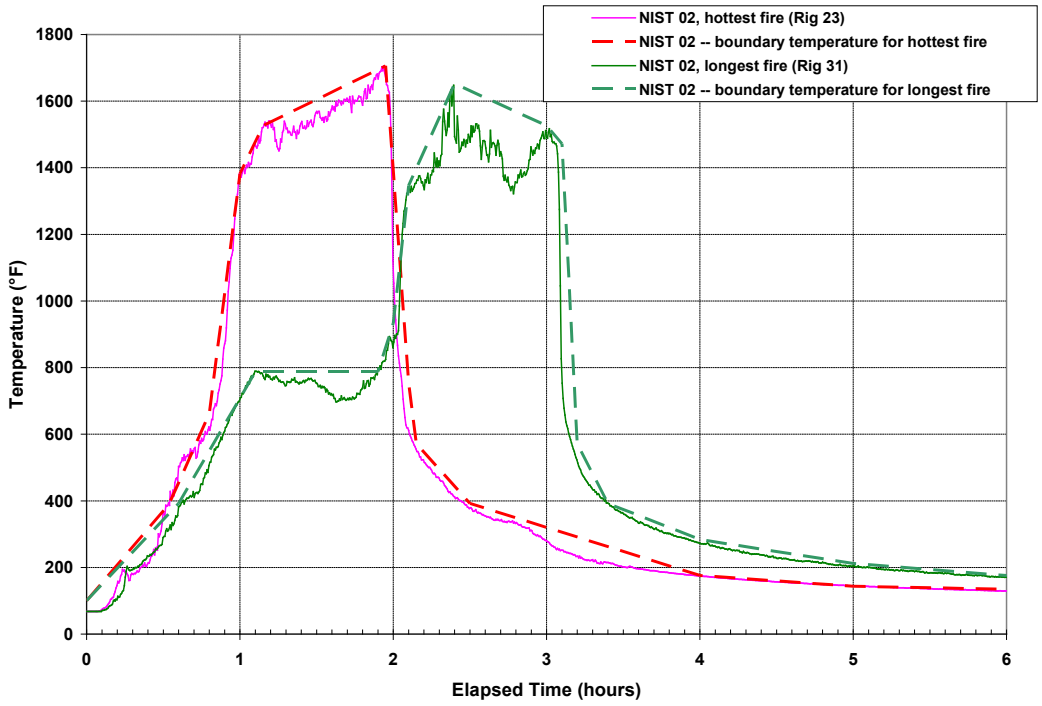

Figure 4.2. Boundary Temperatures for Thermal Analysis of SNF Package in Newhall Pass Fire Scenario at Most Adverse Vehicle Locations for Case NIST-02

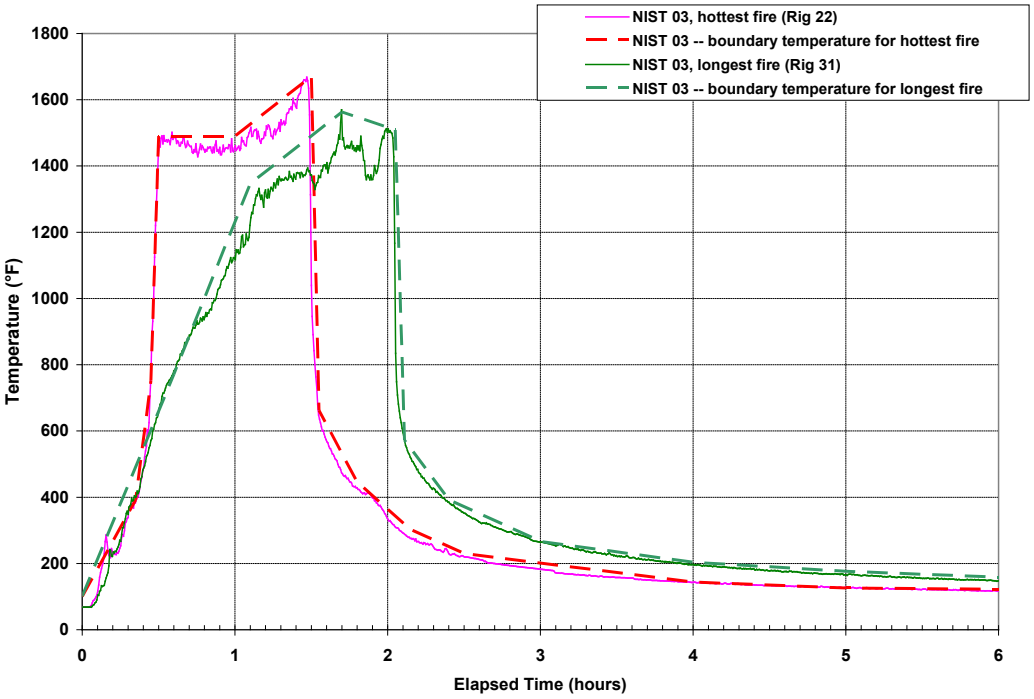

Figure 4.3. Boundary Temperatures for Thermal Analysis of SNF Package in Newhall Pass Fire Scenario at Most Adverse Vehicle Locations for Case NIST-03

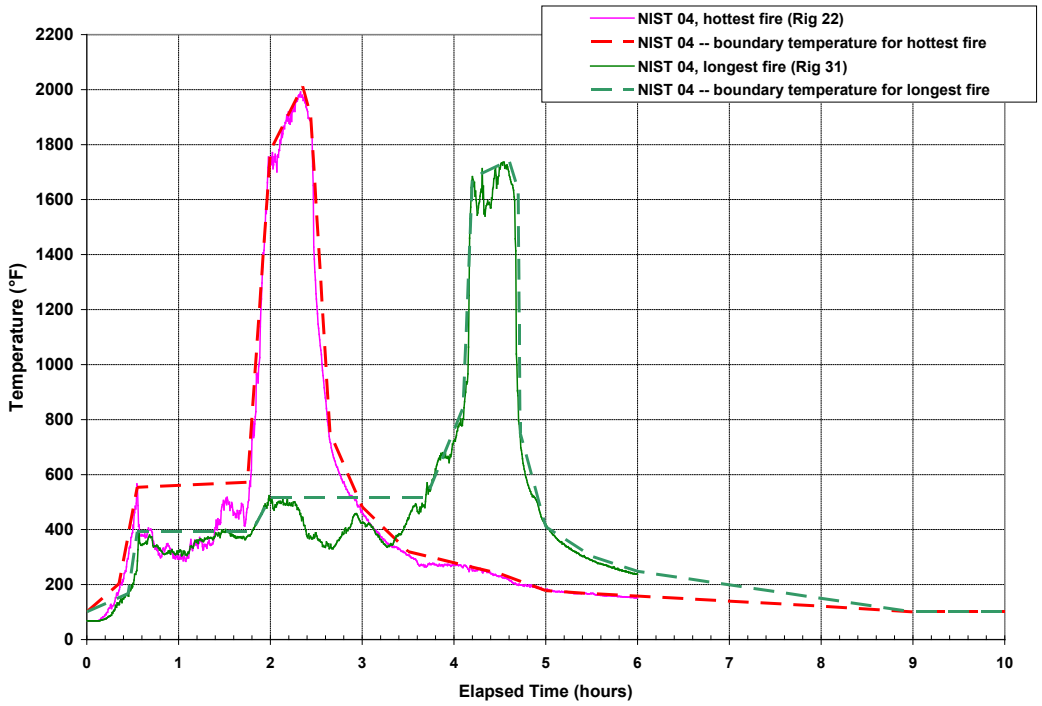

Figure 4.4. Boundary Temperatures for Thermal Analysis of SNF Package in Newhall Pass Fire Scenario at Most Adverse Vehicle Locations for Case NIST-04

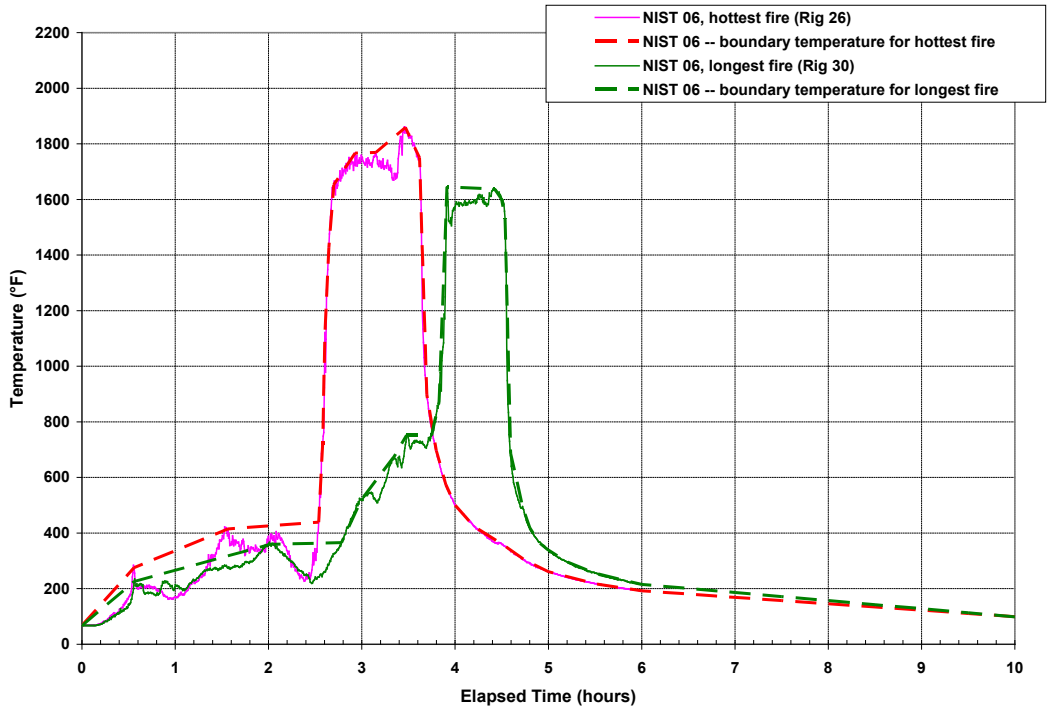

Figure 4.5. Boundary Temperatures for Thermal Analysis of SNF Package in Newhall Pass Fire Scenario at Most Adverse Vehicle Locations for Case NIST-06

5.0 ANALYTICAL MODELS FOR THE NEWHALL PASS FIRE SCENARIO

This section describes the analytical models developed to investigate the potential effects of the Newhall Pass tunnel fire scenario on a typical over-the-road spent fuel transportation package design. This analysis evaluates the transient thermal response of the SNF package from initial steady-state conditions through the various cases defined to characterize the fire scenario, and extends the transient calculation many hours into the post-fire cooldown. The models appropriately capture the thermal inertia of the SNF package, and the transient temperature response of the system in each of the six cases evaluated.

The basic design of the package selected for this analysis is described in Section 5.1. The models representing this package for analysis with the finite element analysis code ANSYS® and the finite-difference COBRA-SFS thermal-hydraulics code are presented in Sections 5.2 and 5.3, respectively. These models were originally developed for evaluations of the MacArthur Maze fire scenario (NUREG/CR-7206 2015). The package representation is essentially the same for analysis in the Newhall Pass Tunnel fire scenario. The model descriptions are repeated here, for completeness.

5.1 GA-4 Legal Weight Truck Spent Fuel Shipping Package

The General Atomics GA-4 legal weight truck (LWT) transportation package was selected for this investigation to evaluate the potential effects of an accident of the magnitude and severity of the Newhall Pass Tunnel fire on an NRC-certified SNF transportation package. This package can carry a relatively large payload for an over-the-road transportation package, and therefore the potential consequences of package failure could be more severe than for packages with smaller payload capacities. The GA-4 package is designed to transport up to four intact pressurized water reactor (PWR) spent fuel assemblies with a maximum decay heat load of 2105.4 Btu/hr (0.617 kW) per assembly, for a total package decay heat load of 8423 Btu/hr (2.468 kW).

The GA-4 can carry zircaloy-clad UO_2 fuel with maximum initial enrichment of 3.15% ^{235}U, in 14x14 assemblies with maximum average burnup of 35 GWd/MTU (minimum cooling time of 10 years), or 15x15 assemblies with maximum average burnup of 45 GWd/MTU (minimum cooling time of 15 years). This package is not licensed to carry high burnup fuel (i.e., fuel with average burnup greater than 45 GWd/MTU). There are packages permitted to carry high burnup fuel pins, but their contents are less than a complete fuel assembly. In addition, transportation of high burnup fuel (>45 GWd/MTU) by road is currently evaluated on a case-by-case basis, pending development of general guidance[1].

For the purpose of this analysis, the package was assumed to contain four WE 14x14 PWR spent nuclear fuel assemblies at the maximum decay heat load. This is the limiting design-basis configuration for thermal analysis of the package. Figure 5.1 shows an exploded view of the package, illustrating the main design features. The payload capacity is 6,648 lb. (3,015 kg),

[1] Transportation of high-burnup fuel is specifically addressed in Revision 2 of NRC Interim Staff Guidance 11 (ISG-11, Rev. 2). A summary of current status of this issue is provided in the Electric Power Research Institute (EPRI) report *Transportation of Commercial Spent Nuclear Fuel, Regulatory Issues Resolution*, EPRI, Palo Alto, CA: 2010. 1016637.

and the fully loaded package weighs approximately 55,000 lb (24,948 kg). The package containment boundary is provided by the following structures:

- stainless steel package body wall
- stainless steel bottom plate
- stainless steel package closure lid secured by Inconel fasteners
- dual O-ring seals for the closure lid, gas sample port, and drain valve.

The stainless steel package body encloses the gamma shield, which consists of an inner shell of depleted uranium (DU). Neutron shielding is provided by a stainless steel neutron shield tank external to the package body, containing a water/propylene glycol mixture. Aluminum honeycomb impact limiters, completely enclosed in a thin stainless steel outer skin and inner housing, are attached to each end of the package. Configuration details, including design drawings, are provided in the safety analysis report (SAR) for this transport package (General Atomics 1998).

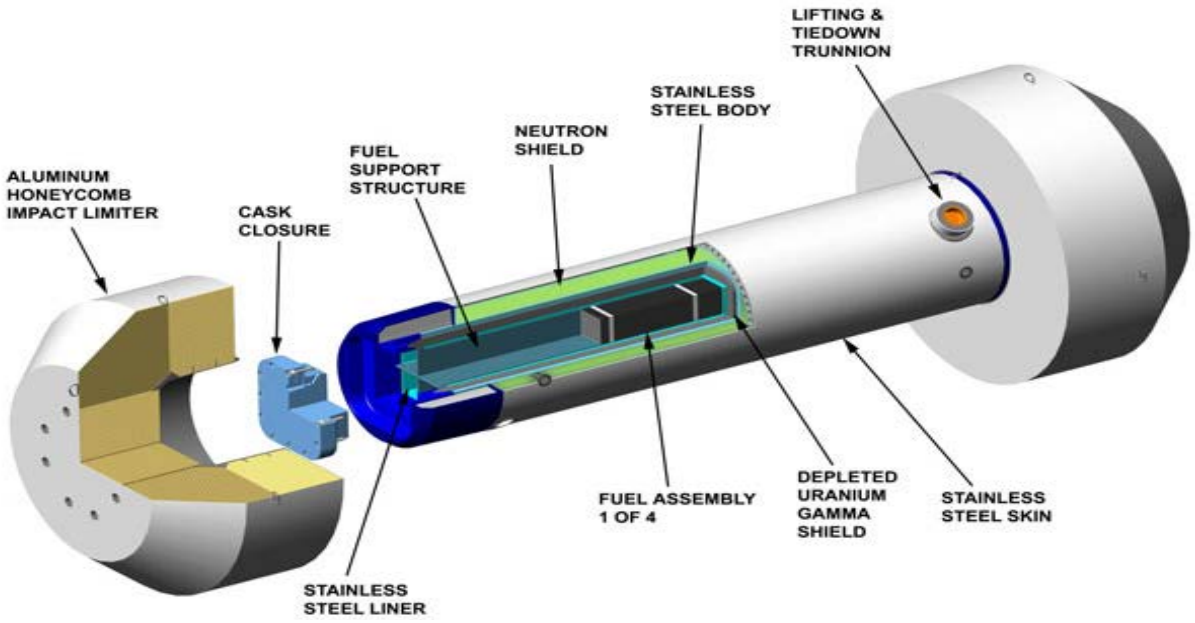

Figure 5.1. GA-4 Package: Exploded View (General Atomics 1998)

5.2 ANSYS Model of GA-4 Package

A detailed three-dimensional representation of the GA-4 package was constructed using ANSYS® (ANSYS 2003). As noted above, this model was developed for the thermal evaluation of the MacArthur Maze fire scenario (NUREG/CR-7206 2015). The detailed description of the model of the GA-4 package presented in the MacArthur Maze report is repeated here, for completeness of the documentation of the evaluations for the Newhall Pass Tunnel fire scenario. Section 5.2.1 describes the detailed ANSYS model of the GA-4 package. Section 5.2.2 presents the material properties used to represent the different elements of the package in the fire and post-fire cooldown transients.

5.2.1 GA-4 Package Representation

The package is assumed to be oriented horizontally throughout the fire scenario, including the actual fire duration, for maximum heat input into the package from the fire. The conveyance carrying the package is omitted from the model as a conservative representation for the thermal modeling of this fire scenario. The fire is treated as fully engulfing, such that the package is subjected to a uniform bounding flame temperature in all directions. In effect, the package is treated as suspended in the fire, and thermal effects of contact with the surface of the conveyance or roadway (e.g., heat conduction losses and potential thermal shielding of portions of the package) are neglected. Including the conveyance in a realistic manner would have the effect of partially shielding the package from the fire. These assumptions constitute a significant conservatism in the overall modeling approach, since the conveyance and the roadway beneath the package could provide substantial limitations on the rate of heat deposition to the package in this fire scenario.

The model geometry was developed from engineering drawings provided in the SAR for the GA-4 package (General Atomics 1998). Table 5.1 summarizes the ANSYS model element types used for the various components of the package and surrounding roadway. The structure of the package is represented in fine detail, including the lifting trunnions and impact limiters. Convection and thermal radiation heat transfer is represented for specific interior and exterior surfaces, including thermal radiation between the outer surfaces of the package and the external environment. During the fire scenario, the package sees the bounding AST temperature from the FDS calculation for the specific case, as described in Section 4.0. The AST values serve as the boundary temperature for thermal radiation exchange between the package and the external environment, and as the sink temperature for forced convection due to the flow of hot fire gases over the package. Surface elements were also generated along the exterior of the package to account for solar insolation loads to calculate the normal conditions of transport (NCT), which defines the initial temperature distribution for the package.

Table 5.1. Summary of Elements in ANSYS Model of GA-4

Number of Elements	Element Type	Modeled Structure(s) or Connections
1,851,067	SOLID70 8-node brick elements	fuel assembly, fuel spacer, FSS inner frame, helium gap, FSS liner, DU gamma shield, steel package body, neutron shield, stiffener ring, ILSS, outer shell, trunnion assembly, closure assembly, and honeycomb structure of the impact limiters
45,240	SHELL57 4-node quadrilateral thermal elements	exterior surface of the impact limiters
761	LINK33 3-D conduction bar elements	package closure bolts, impact limiter attachment bolts
25,331	CONTA173 contact elements	connecting impact limiters, closure assembly, and lifting trunnions to appropriate package assembly surfaces
27,893	TARGE170 contact elements	
232,980	SURF152 elements	convective heat transfer and solar insolation loads at the outer surfaces of the package
218	MATRIX50 elements	radiative heat exchange between internal package surfaces, and between the external surfaces of the package and the environment

A cross-sectional view of the ANSYS model is shown in Figure 5.2, with the major components of the GA-4 package indicated. All components illustrated in Figure 5.2 were modeled using brick elements. The square blocks shown in red are homogeneous regions representing the four fuel assemblies within the package. The fuel assemblies are contained within the cruciform stainless steel fuel support structure (FSS) and FSS liner. The helium gas in the gaps between the homogenized fuel assembly regions and the FSS plates was explicitly modeled with solid elements. The model includes a composite representation of the layers of the cruciform inner frame of the FSS, which consists of thin sheets of stainless steel enclosing boron carbide rods. The thin steel of the FSS liner is represented with a single layer of nodes (illustrated in light blue in the diagram in Figure 5.2).

The GA-4 gamma shield (represented by three layers of elements illustrated in multiple colors in Figure 5.2), consisting of a rectangular tube of DU, encloses the FSS liner. The DU gamma shield is in non-loadbearing contact with the square cross-section of the FSS liner, and has rounded outer corners, in order to fit within the cross-sectional geometry of the steel package body. The rectangular stainless steel package body forms the inner surface of the liquid neutron shield (NS) tank. The liquid neutron shield tank contains a 56% propylene glycol/water mixture that is modeled as a solid material using the elements shown between the steel package body and the outer wall of the tank. The outer wall of the neutron shield tank is a thin cylindrical stainless steel shell, and is represented in the model as a single layer of elements, as shown in Figure 5.2. This layer constitutes the outer surface of the package assembly.

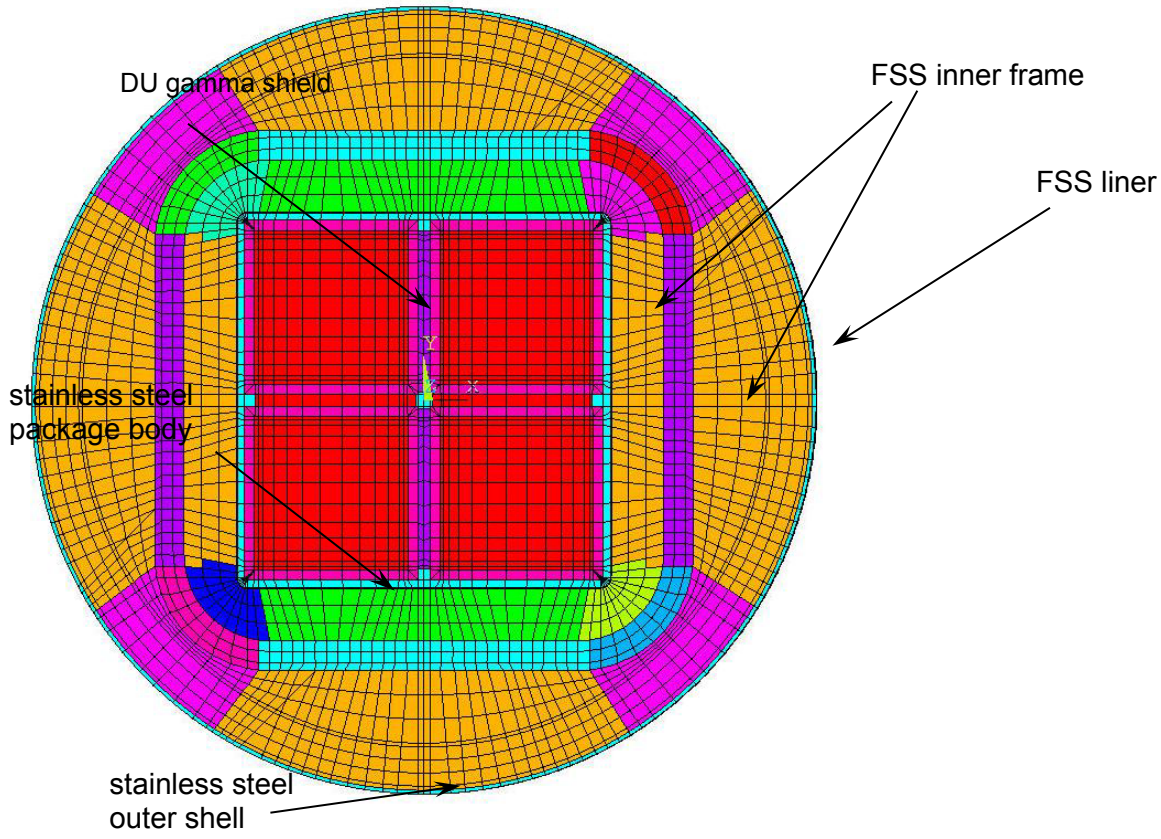

Figure 5.2. Cross-Section of ANSYS Model of GA-4 Package Near Midplane

The diagram in Figure 5.2 shows a cross-section of the package near the center of the axial length of the cask cavity. In this region, there is only liquid in the region between the cask body and the neutron shield tank outer shell. At either end of the package, in the regions covered by the impact limiters, the neutron shield tank is structurally supported by 36 radially distributed stainless steel ribs designated as the impact limiter support structure (ILSS). These ribs extend radially from the thick steel shell of the package body to the thin outer stainless steel shell. In addition to providing structural support, the ribs provide additional pathways for conduction heat transfer from the cask body to the neutron shield tank outer shell. This region is explicitly modeled in detail in the ANSYS model, but for clarity is omitted from the diagram in Figure 5.2.

A slice through the long axis of the model is illustrated in the diagram in Figure 5.3, and shows the modeling of the ends of the package, including the impact limiters, which consist of an internal aluminum honeycomb structure enclosed within a stainless steel skin. The stainless steel shell of each impact limiter was modeled with shell elements. All other components were modeled using brick elements. A detailed representation of the model in the region of the top impact limiter and package closure is illustrated in Figure 5.4. This diagram shows the impact limiter stainless steel skin and a thin air gap between the impact limiter and the external surface of the package. This gap, which conservatively accounts for the tolerance of the fit of the impact limiter onto the package, was represented in the model geometry using SOLID70 brick elements.

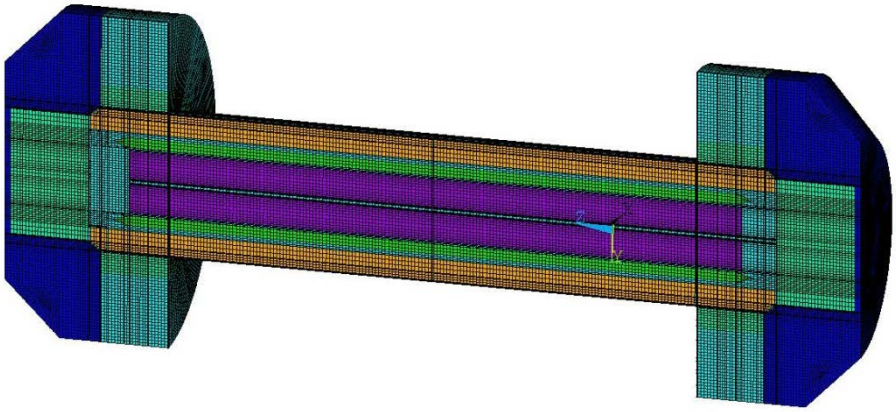

Figure 5.3. GA-4 Package Geometry, Including Impact Limiters

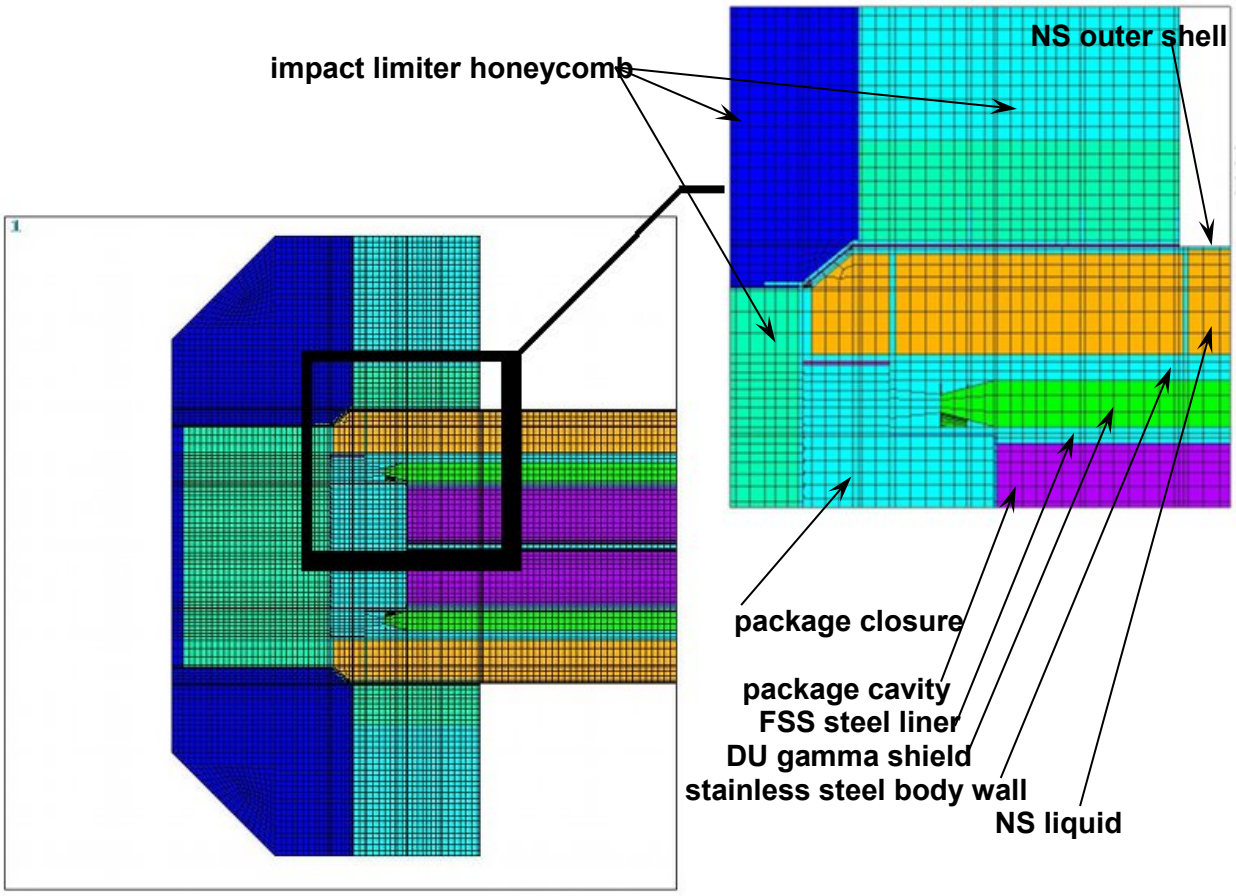

Figure 5.4. GA-4 Package Geometry Model: Impact Limiter Details

For this analysis, the air gap between the closure lid and the impact limiter steel liner was assumed to remain open during the fire and in the post-fire cooldown, even though deformation or warping of the impact limiter in response to the fire conditions could potentially reduce or eliminate this gap. During the fire, this assumption would tend to slow the rate of heat input to the package through the impact limiters, but because very little heat from the fire can enter the package through the highly insulating material of the impact limiters, this assumption would be expected to have a negligible effect on the thermal response of the package. In the post-fire cooldown, however, this assumption would tend to slow the rate of heat removal from the package, by increasing the insulating effect of the impact limiters.

The thermal inertia of an SNF package can result in significantly higher temperatures being reached on some components in the post-fire cooldown, compared to temperatures reached during the fire, particularly for temperatures in nominally cooler regions of the package. It was therefore deemed more important to capture the effect of retaining the air gap throughout the fire scenario, particularly since heat transfer in the package end regions would not be expected to affect the peak component temperatures during the fire, which occur near the package midplane, due to direct heat input from the fire.

The lower end of the package consists of a thick stainless steel bottom plate welded to the steel inner and outer walls of the package. The upper end of the package is sealed with a stainless steel closure assembly that attaches to a stainless steel flange on the steel body wall. Figure

5.5 shows the detailed representation of the closure assembly developed for this model. Helium-filled gaps between the closure assembly and the FSS, and between the stainless steel flange and the closure assembly, were included in the model geometry. These gaps were represented with solid brick elements.

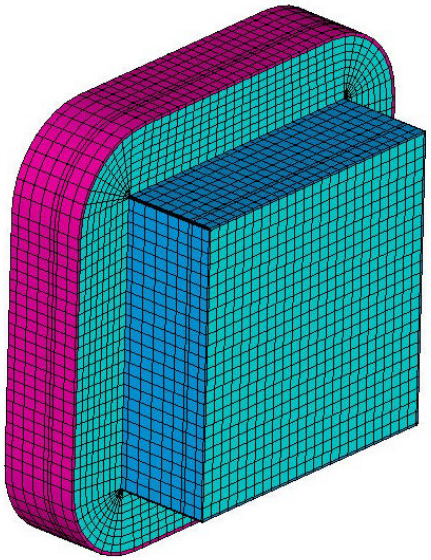

Figure 5.5. GA-4 Package Geometry Model: Closure Lid

Section 6.2 provides a detailed discussion of the modeling assumptions and boundary conditions for the fire analysis. The detailed representation of the package internals was designed to capture all three possible modes of heat transfer (i.e., conduction, convection, and thermal radiation) between all of the components of the model. Conduction is handled inherently in ANSYS by the elements and corresponding material properties representing each component, but convective and radiative mechanisms must be carefully implemented to properly capture the physical behavior of the system. The representation of the fuel assemblies is particularly important in appropriately modeling the thermal response of the fuel rods and predicting the peak cladding temperature. Heat transfer within the fuel assemblies is primarily by conduction and thermal radiation, with convection only a relatively minor contributor.

The fuel assemblies were modeled as homogeneous regions with an effective radial conductivity determined using an effective conductivity model (Bahney and Lotz 1996) that is widely used in the nuclear industry in safety analysis for SNF packages. In this model, the combined effect of thermal radiation and conduction is characterized using an effective conductivity that is a function of assembly geometry and decay heat. The application of the fuel effective conductivity model developed for this analysis introduces a modification to more accurately account for the temperature gradient between the outermost row of rods in the assembly and the enclosing wall. This is accomplished by including a helium gap between the homogenized material region representing the fuel assembly and the wall of the enclosing basket (in this case the FSS cruciform and liner, as shown in the diagram in Figure 5.2), rather than extending the homogenous region to the wall, as is the approach normally used in the effective conductivity model. An additional feature of this modified representation is that it more

directly takes into account the effect of the non-uniform wall temperature distribution around the fuel assembly, which can be of particular significance in modeling fire scenarios.

Axial conduction within the fuel assembly region was modeled only in the fuel cladding and backfill gas, to be consistent with typical applications of the fuel effective conductivity model, conservatively neglecting axial conduction in the uranium oxide fuel. The axial effective conductivity was determined with a cross-sectional area weighting scheme based on the total cross-sectional area of the assembly. However, to appropriately capture the thermal inertia of the fuel assemblies for the transient response in the fire scenario, the effective density and heat capacity for the fuel region was defined based on volumetric averages of the corresponding properties of the helium gas, fuel rod cladding, and uranium oxide fuel pellets.

An average volumetric heat generation of 2,105 Btu/hr (617 W) was applied over the active fuel length for each fuel assembly. The axial distribution of decay heat was represented by dividing the active fuel length into 16 separate zones, and the local heat load was determined by multiplying the average by an appropriate peaking factor for that particular zone. The peaking factor was determined based on the bounding axial power profile presented in the SAR, which has a normalized peaking factor of 1.1.

The helium gas filling the 0.5075-inch gap between the nominal fuel assembly cross-section and FSS was modeled with solid elements and used standard helium thermal properties for conduction, density, and specific heat. Convection across the gap was accounted for by multiplying the local gas conduction values by an empirically derived[2] Nusselt number of 3.66. Thermal radiation exchange across the gap was modeled with MATRIX50 super elements. These were created by using SHELL57 elements to designate the discrete enclosure. The AUX-12 hidden ray-tracing method was used to compute view factors for each element within the super-element. All other gaps in the package assembly, such as between the closure assembly and FSS, or the impact limiters and package skin were modeled in a similar manner, which included thermal radiation and conduction across surfaces but assumed negligible convection.

Other potential gaps not explicitly modeled within the geometry, such as between the gamma shield and package FSS, and between the gamma shield and stainless steel wall were accounted for by modifying the material properties of the adjacent materials to include the calculated effective properties for the material and gap. For very small gaps, the calculations were based on the following assumptions:

- the thermal radiation view factor is specified as 1.0 (gap completely enclosed)
- the temperature difference across the gap is small
- convection heat transfer across the gap can be neglected.

For the pre-fire steady-state and post-fire transient cooldown analyses, nominal gap distances were used to determine the effective thermal conductivity. During the fire transient, the gaps were assumed to close due to thermal expansion of the package materials, such that the calculated effective thermal conductivity across a gap reduced to the thermal conductivity of the adjacent solid material without the gap. This ensured a conservative approach with respect to the effect of heat transfer across the gaps throughout the entire analysis.

[2] This value is based on thermal measurements in full-scale spent fuel storage systems. See Michener et al. (1995) and Creer et al. (1987).

The impact limiter attachment bolts and the closure assembly bolts were represented as line elements within the model. Small variations in the overall length of individual bolts were accounted for by calculating an equivalent cross-sectional area, which was specified in the real constant properties for the line elements.

5.2.2 Material Properties for GA-4 Package in ANSYS Model

The specific thermal material properties used to represent the components of the GA-4 package and roadway structures in the ANSYS model are listed in detail in Appendices A and B. For elements of the model representing the major components of the package, the specified properties are those of the single material comprising that component. However, for efficiency of meshing, the thin plates of the FSS and enclosed neutron absorber rods, the complex honeycomb structures of the impact limiters, and the fuel assemblies are represented using effective thermal properties defined specifically for the overall region. In addition, the effect of the fire on the integrity of the liquid-filled neutron shield tank was also explicitly modeled with changes in material properties in the transient calculation.

The neutron absorber plates of the FSS are composed of boron carbide rods sandwiched between thin stainless steel (XM-19) panels, with helium surrounding the boron carbide rods. Homogeneous material properties were defined for the elements representing the FSS plates, based on volumetric averaging of the material properties for XM-19 stainless steel, boron carbide, and helium. It was assumed that convection in the helium gas would be negligible in the narrow enclosed space within the FSS plates, and the effective thermal conductivity was calculated based on conduction and thermal radiation heat transfer only. Anisotropic properties were defined for this material, assuming conduction only along the axial length of the FSS, with conduction and thermal radiation through the thickness of the composite plate. Thermal radiation was modeled assuming that the helium-filled space between the boron carbide rods and the enclosing steel plates was very small, completely enclosed within the stainless steel panels, with a very small temperature difference between them.

The stainless steel inner support structure and outer shell of the impact limiters was explicitly modeled using elements with properties of XM-19 stainless steel. Composite material properties were used to model the aluminum honeycomb material enclosed within the steel shell. The design of the impact limiters is defined in the package SAR (General Atomics 1998) as a standard non-reinforced hexagonal aluminum structure, and includes specific regions with differing densities, which are bonded together and to the stainless steel shell with adhesive foam. Effective properties for these regions were determined based on material data for aluminum honeycomb from HEXEL Composites (1999), using a volumetric averaging scheme. This approach included the properties of the adhesive foam as well as the air-filled aluminum honeycomb. The effective thermal conductivity values for the honeycomb regions were calculated assuming the material was isotropic within a region, as indicated by the HEXEL Composites data for the honeycomb.

In the course of the transient calculation, the material properties of the impact limiters were modified to account for structural configuration changes and effects of the fire. Portions of the aluminum honeycomb in the impact limiters are assumed to melt during the fire, due to the extremely high temperatures predicted in this transient. For the aluminum honeycomb material in the impact limiters, local melting would be expected to significantly increase in the void (air) volume compared to the intact honeycomb material. This would tend to increase the insulating effect of the impact limiters, reducing the rate of heat transfer through this material. During the fire portion of the transient, the impact limiters were conservatively assumed to remain intact,

allowing the maximum heat transfer to the package through these components during the fire. However, the assumption of intact impact limiters is no longer conservative in the post-fire cooldown portion of the transient. With larger air regions within the impact limiter structure due to local melting of the honeycomb, the damaged impact limiters would tend to further slow the rate of heat removal from the package during the cooldown transient, compared to the effect of intact impact limiters. The material properties of elements in the ANSYS model representing the honeycomb material were therefore modified in the post-fire portion of the calculation to account for the effects of melting.

Fire damage to the impact limiters was determined from the predicted temperature distribution within these regions at the end of the fire. The percentage of honeycomb nodes above the melting point of the aluminum alloy (approximately 1100°F [593°C]) was used to calculate the total volume of melted aluminum, and the volume of lost honeycomb. It was assumed that the molten aluminum would flow due to gravity to the lowest point on the horizontal side of the impact limiters. Therefore, elements in this region encompassing a volume corresponding to the volume of melted aluminum were modified to have the properties of aluminum alloy, rather than the honeycomb mesh. The remaining volume of the impact limiter was assumed to be a mixture of air (corresponding to the volume of the melted mesh) and unmelted intact honeycomb. The thermal conductivity of the elements representing this volume within the impact limiters was modified using an effective thermal conductivity calculated based on volume-averaging of the thermal properties of air and the unmelted honeycomb mesh material.

The effect of the fire on the material properties of the liquid neutron shield was also explicitly represented in the transient calculation. The neutron shield liquid temperature is calculated to exceed its boiling point very early in the fire transient. Prior to rupture, heat transfer through the liquid in the tank is represented with an effective conductivity relationship based on an empirical correlation (Guyer and Brownell 1989) for convection and conduction heat transfer across a gap between two long, horizontal concentric cylinders at different temperatures. The fluid thermal conductivity used in this relationship was determined based on material property data for propylene glycol and water mixtures provided in the GA-4 SAR (General Atomics 1998). (Appendix B contains a detailed description of this correlation, and verification of its applicability to the geometry of the GA-4 neutron shield tank.)

The neutron shield tank is assumed to rupture when the peak temperature in the liquid is predicted to exceed the boiling point of the water-glycol mixture. After rupture, the neutron shield tank contents are assumed to consist only of air, with heat transfer by conduction and convection. Thermal radiation between the inner walls of the empty tank is also accounted for, by direct calculation between the elements on the inner surface of the tank outer shell and the outer surface of the package body.

The effective conductivity of the material within the neutron shield tank was determined as a function of the average tank temperature and the radial temperature difference between the tank inner and outer surfaces. The radial temperature difference was calculated separately along the flats and corners of the neutron shield, to account for the effect of the non-uniform gap due to the square cross-section of the tank inner surface within the circular outer tank shell. Material properties for the tank were updated between each time-step during the transient solution. The affected nodes were assumed to consist of a 56% propylene glycol solution up to the point where the maximum temperature reached the mixture's boiling point of 276°F (136°C).

The boiling point for the tank contents, and hence the time of assumed tank rupture, was calculated based on the maximum normal operating pressure of the neutron shield tank

(General Atomics 1998), and data for vapor pressure versus temperature of aqueous solutions of propylene glycol (Dow Chemical Company 2003). When the maximum temperature in the tank exceeded the boiling point, it was assumed that rupture had occurred and all the liquid in the tank instantly vaporized. The effective conductivity was then computed using dry air as the medium. This calculation extended through the remainder of the fire and was also continued during the cooldown period. This approach conservatively neglects energy absorbed by the phase change (i.e., the heat of vaporization for the liquid), but this is mainly as a matter of convenience, since this would constitute a very small deduction from the total energy imparted to the package.

5.3 COBRA-SFS Model of GA-4 Package

The GA-4 package was also analyzed with COBRA-SFS (Michener et al. 1995), a thermal-hydraulic code developed for analysis of multi-assembly spent fuel storage and transportation systems. The code uses a lumped-parameter finite-difference approach for predicting flow and temperature distributions in spent fuel transfer, storage and transportation systems, and fuel assemblies under forced and natural circulation flow conditions. It is applicable to both steady-state and transient conditions in single-phase gas-cooled spent fuel packages with radiation, convection, and conduction heat transfer.

The COBRA-SFS model was developed to provide independent verification for the ANSYS model of the GA-4 package (see Section 5.2), and to perform sensitivity studies on various parameters and boundary conditions representing the fire scenario. The COBRA-SFS model includes an approximate representation of the impact limiters, since the accident scenario for this fire is not severe enough to produce conditions that could result in the impact limiters detaching from the package. The impact limiters can have a significant effect on the thermal response of the package, since these structures act as thermal shields on the package ends. They protect the package from the heat of the fire, but they also can inhibit the rate of heat removal from the package in the post-fire cooldown portion of the transient.

As in the evaluations with the ANSYS model, the COBRA-SFS model does not consider the effect of the conveyance. The package is assumed to be uniformly surrounded by the bounding fire temperatures from the FDS analyses (see Section 3.0). The GA-4 package was modeled for the COBRA-SFS calculations in sufficient detail to capture the thermal response of the system components in the radial and axial directions. Material properties used in the model are listed in Appendix A. The four fuel assemblies within the basket are each modeled as rod and subchannel arrays, for appropriate representation of radiation heat transfer as well as conduction and convection. The basket separating and containing the fuel assemblies is represented using multiple layers of solid conduction nodes, to capture the effect of the B_4C poison rods stacked within the steel plates forming the arms of the cruciform structure.

The stainless steel inner liner, DU gamma shield, and stainless steel package body are also represented with multiple layers of solid conduction nodes, to appropriately resolve the temperature gradients through these relatively thick components. In addition, these structures are also subdivided to capture the effects of non-uniform external conditions surrounding the package. A cross-section diagram illustrating the nodding for the COBRA-SFS model is shown in Figure 5.6.

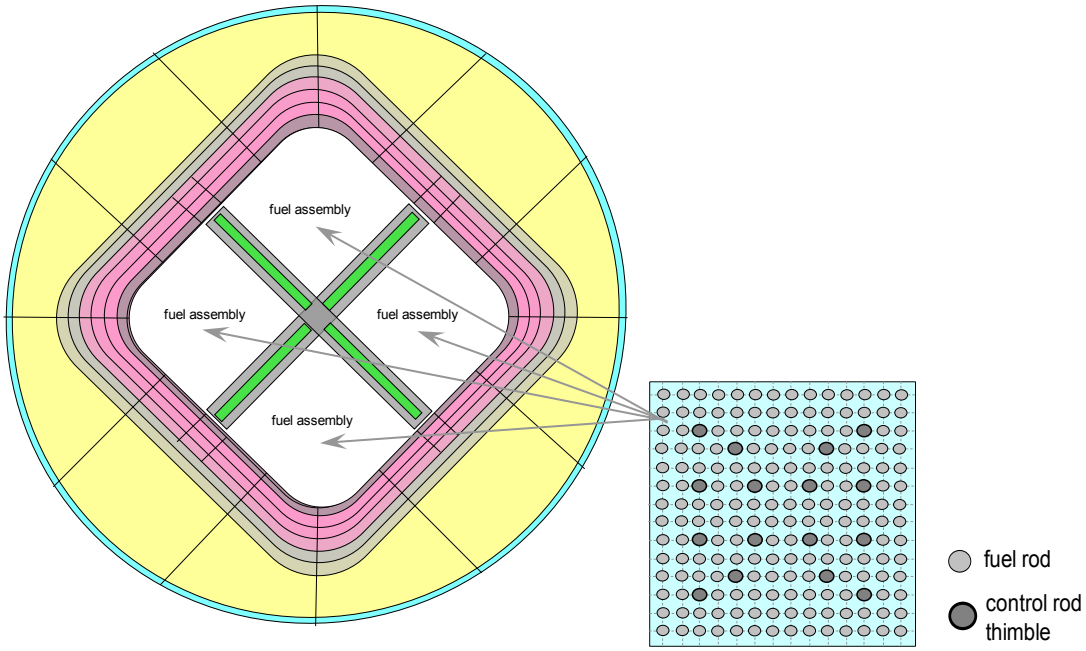

Figure 5.6. Cross-section of COBRA-SFS Model of GA-4 Package, Including Fuel Assemblies, Basket, Package Body, and Neutron Shield

The impact limiters on the package ends are modeled as a one-dimensional axial heat transfer path through a series of layers representing the material structure of the impact limiter. This includes an air gap between the package end and the thin stainless steel casing of the impact limiter, a thick layer of high-impact aluminum honeycomb, a thin layer of low-impact honeycomb material, and the thin stainless steel outer shell. The effect of the overhang of the impact limiter on the sides of the package is modeled using non-uniform material properties, to capture the effect of the concentric annular ring of the impact limiter sides that fit down over the ends of the package. The effective conductivity of this layer includes the effect of the small air gap between the cask outer shell and the impact limiter, the inner stainless steel casing of the impact limiter, the thick ring of high-impact honeycomb, and the thin stainless steel outer shell of the impact limiter.

The neutron shield tank initially contains a liquid 56% propylene glycol/water mixture with maximum design pressure of 150 psig (1.135 MPa), which corresponds to a boiling temperature of 276°F (135.6°C). However, the tank is not an American Society of Mechanical Engineers (ASME) pressure vessel, and in the SAR analyses for the HAC fire at 1472°F (800°C), it is conservatively assumed that in the initial steady-state, the tank has already ruptured and contains only air. This simplification is not used in the analysis of the Newhall Pass tunnel fire, for either the ANSYS model or the COBRA-SFS model. In both evaluations, the neutron shield is initially represented using the SAR model for the effective conductivity of the liquid-filled neutron shield between nodes representing the outer surface of the package body and the thin outer shell of the tank.

This representation is used until the point in the transient where the maximum temperature in the neutron shield region exceeds the boiling point of the glycol/water mixture. For the cases representing the Newhall Pass fire, this time is affected by the temperature transient in the preheating phase of the fire scenario at a particular location, and varies from less than 30 minutes to more than an hour. When this limiting temperature is reached, the medium within the tank is assumed to be dry air, and thermal radiation between the tank inner surfaces is added to the model. The internal surfaces of the shield tank are specified with a uniform emissivity of 0.9 after the assumed loss of liquid contents, to conservatively represent the effect of sooting, on the assumption that highly sooted fire gas could enter the ruptured and fully vented tank.

6.0 ANALYSIS METHOD

This section presents the initial conditions, modeling assumptions, and boundary conditions used with the detailed analysis models described in Section 5.0 to predict the transient response of the GA-4 package to the Newhall Pass fire scenario. The models account for all significant heat transfer paths to and from the package by means of conduction, convection, and thermal radiation during the fire and in the post-fire cooldown. All transients evaluated in the analysis of the Newhall Pass tunnel fire scenario were assumed to begin from the design-basis steady-state for NCT. Section 6.1 describes the significant assumptions and simplifications used in developing the thermal models. Section 6.2 describes the fire scenarios assumed for the transient analyses, and the boundary conditions used for the calculations.

6.1 Thermal Modeling Assumptions

Computational modeling requires simplifying assumptions for even the most detailed representation of a physical system. The assumptions used in developing the detailed geometry models of the GA-4 package are discussed in Section 5.0. This section summarizes the major assumptions relevant to analysis of the response of this package if it were exposed to the conditions of the Newhall Pass tunnel fire scenario. These assumptions apply to both the ANSYS and the COBRA-SFS models, unless specifically noted otherwise.

1. Initial conditions for the package are defined as steady-state NCT at 100°F (38°C) ambient with insolation (10 CFR 71 2003). This assumption conservatively neglects the effect of the actual conditions at the time of the Newhall Pass tunnel fire accident (i.e., at night, with ambient temperature below 50°F [10°C]).
2. The decay heat load in the GA-4 package is assumed to be at its maximum design-basis value of 2105.4 Btu/hr (0.617 kW) per assembly, with a total package decay heat load of 8,423 Btu/hr (2.468 kW). This is a bounding assumption, as the actual decay heat load of an SNF package may be lower than the design-basis configuration.
3. Material properties of package components specified as inputs to the thermal models are listed in Appendix A. These were obtained from the GA-4 SAR (General Atomics 1998), with the following exceptions;
    a. The temperature-dependent thermal conductivity values used in the SAR for XM-19 stainless steel are lower bounding values based on properties of high alloy steels[1]. At NCT, the thermal conductivity values from the SAR are approximately 20% below values published in material data sheets for XM-19 stainless steels. This is conservative for the NCT analysis, but is non-conservative for the fire analysis, in which higher thermal conductivity for the steel results in more rapid heating of the package during the fire. Therefore, thermal conductivity values specific to XM-19 steel[2] were used in the fire analyses.
    b. The thermal conductivity for DU reported in the SAR is for a temperature of approximately 100°F (68°C), and does not take into account the significant increase in thermal conductivity with increasing temperature for this material. As with XM-19, this is a conservative approximation for NCT, but is non-conservative for the fire analysis.

[1] The SAR values used for thermal conductivity of XM-19 steel are from Material Group E “high alloy steels” in Table I-4.0 of the ASME code, 1986.
[2] Values used are for Allegheny Ludlum ATI 50™ Alloy (UNS S20910), Type XM-19. See the Technical Data Sheet in Appendix A.

Therefore, temperature-dependent thermal conductivity values were used for the DU in the thermal analyses, as documented in Appendix A.

4. Clearance gaps within the package (e.g., between the inner liner and the gamma shield, between poison rods and the structural plates of the cruciform basket) are modeled at nominal values, based on design drawings.

   a. Gaps are assumed closed due to thermal expansion during the fire transient, to conservatively maximize heat transfer into the package.

   b. Gaps are assumed open, and at nominal cold values during the cooldown portion of the transient, to conservatively limit the rate of heat removal from the package.

5. The content of the neutron shield tank is conservatively represented to maximize heat transfer through this region during the fire, and minimize it during the post-fire cooldown.

   a. Initial steady-state is represented with the effective conductivity model from the SAR, to account for natural circulation of the neutron shield liquid. This model is used in the fire transient until the peak temperature exceeds 276°F (136ºC), the liquid saturation temperature corresponding to the maximum operating pressure for the tank.

   b. The liquid is assumed lost when the predicted peak temperature in the neutron shield region exceeds 276°F (136°C). Thermal energy absorbed in the vaporization of the liquid is conservatively neglected.

   c. After loss of the liquid, heat transfer between the inner surface of the neutron shield tank outer shell and outer surface of the package body is assumed to consist of thermal radiation plus natural convection and conduction through air for the remainder of the fire and post-fire cooldown transient. The inner surfaces of the tank are assumed to be affected by soot, and the emissivity is conservatively specified at 0.9. Mainly because of the high thermal radiation heat flux at the elevated fire temperatures, this results in a higher heat transfer rate into the package through the neutron shield during the fire than would be achieved with only conduction and natural convection heat transfer through the propylene glycol/water mixture, if it were assumed that the neutron shield tank did not rupture during the fire.

6. The exterior surface of the neutron shield tank is assumed to have an emissivity of 0.15, as specified in the SAR, for the initial pre-fire steady-state calculation. At the start of the fire, the package surface emissivity is set to 0.9, to represent the effect of sooting of the outer surface of the package and impact limiters. This value is also used throughout the post-fire cooldown. (This is slightly more conservative than the value of 0.8 to 0.85 documented in the SAR for the package surfaces in the HAC fire.)

7. Convection heat transfer during the fire is conservatively modeled assuming forced convection to the package from the hot external environment. The total fire duration is defined as the time interval between the initiation of the transient and the end of the fire on the last vehicle to ignite (i.e., vehicle #31, which is nearest the entrance of the tunnel). This approach assumes that as long as there is an intense vehicle fire within the tunnel, forced air convection will continue through the tunnel, due to the chimney effect of the tunnel slope and the natural draft of the fire. Natural convection boundary conditions are re-established only after the end of the fire on the last vehicle to ignite in the tunnel (typically, vehicle #31, as discussed in Section 3.0.)

8. For the post-fire cooldown portion of the transient following the 6-hour FDS simulation of the fire, the air temperature is assumed to gradually drop to 100°F (38°C) with insolation, to conservatively bound long-term ambient conditions. This air temperature is treated as

an AST, and no additional evaluations are needed to account for thermal exchange with the tunnel surfaces. This is a conservative assumption, as information in the MAIT report (CHP 2007) indicates that the tunnel surfaces had cooled to near-ambient conditions within a few hours of the end of the intense portion of the fire, due to the well-ventilated conditions in the tunnel. The tunnel walls would be expected to be far below 100°F (38°C) by approximately 10 hours into the overall transient scenario.

9. During the fire, the aluminum impact limiters are assumed to remain intact within their stainless steel outer shells, and are represented with effective thermal material properties for the honeycomb material, based on bulk density and thermal conductivity of the component materials. This assumption maximizes heat input to the package during the fire by conduction through the impact limiters.

10. After the fire, the elements representing the honeycomb were modified to account for melting of the aluminum due to the heat of the fire. This assumption maximizes the thermal resistance to heat removal from the package by conduction through the impact limiters. Unmelted portions were treated as a combination of aluminum honeycomb and air, and melted portions were assumed to have the thermal properties of aluminum alloy 5052. It was also assumed that the molten aluminum would settle to the bottom of the impact limiters. The effective thermal material properties of the various elements of the impact limiters affected by melting were calculated using a volume-averaging scheme. (Section 5.2 discusses this modeling approach in detail.)

11. The latent heat absorbed by the honeycomb material in the phase change due to melting is conservatively neglected.

12. The effect of the conveyance carrying the GA-4 package is conservatively neglected. The fire is assumed fully engulfing and any shielding effect that the conveyance might have on the package is neglected.

6.2 Thermal Boundary Conditions for GA-4 Package Models

The boundary conditions for the thermal analysis define the external environment that the GA-4 package experiences during the fire and post-fire cooldown. As described in Section 2.0 in the detailed description of the fire, the Newhall Pass tunnel fire began at the tunnel exit and swept through to the tunnel entrance, successively engulfing the vehicles within the tunnel. Due to uncertainty in the fire timeline and in the available fuel load for the fire, five different cases have been developed to represent the fire scenario.

Two locations within the tunnel have been identified as potentially providing the most severe conditions for an SNF package exposed to this fire scenario. One is the hottest fire location, corresponding to the location of the hottest individual vehicle fire within the tunnel. The other is the longest fire location, corresponding to the last vehicle to enter the tunnel, and therefore the last one to be consumed by the fire. Figure 6.1 summarizes the fire boundary conditions derived from the FDS results for the package at the hottest location, (vehicle #22, #23 or #26, near the center of the tunnel). (The boundary temperatures for case NIST-05 have been omitted from these plots, since the FDS results for that case are identical to the results for case NIST-01, as discussed in Section 3.4).

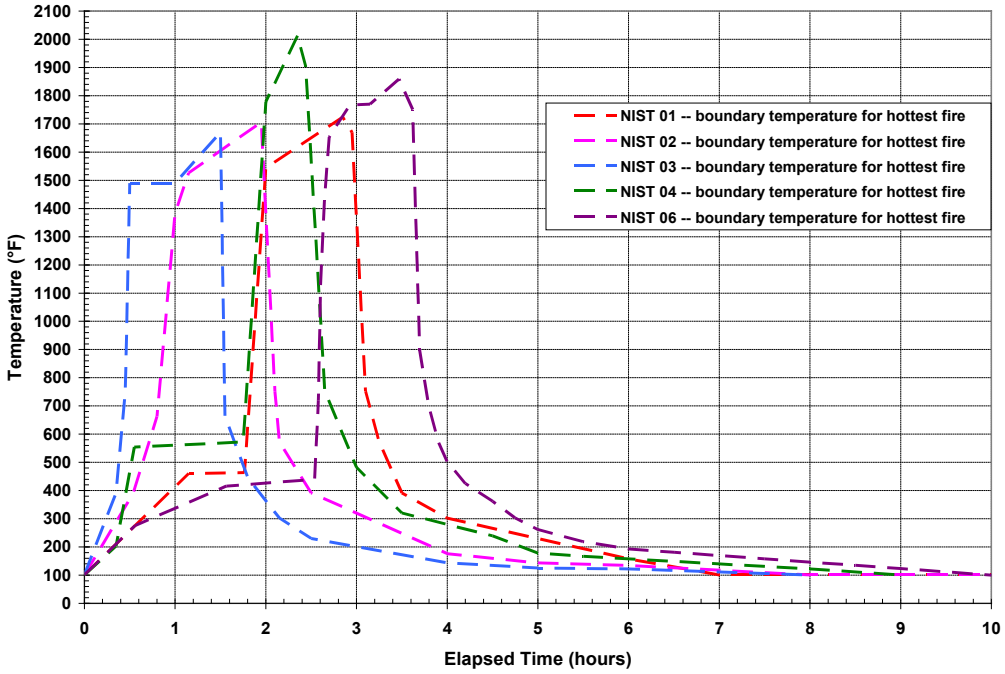

Figure 6.1. Fire Boundary Temperatures for Hottest Fire (all cases)

Figure 6.2 shows the fire boundary conditions for the package at the location with the longest overall fire duration, (vehicle #30 or #31, near the tunnel entrance). In all cases, the emissivity of the fire environment surrounding the package is specified at 1.0, since the boundary temperatures are based on ASTs from the FDS model results. The external surfaces of the package are represented with an emissivity of 0.9 to conservatively represent the effect of sooting. This value is also applied to the inner surfaces of the neutron shield tank after rupture.

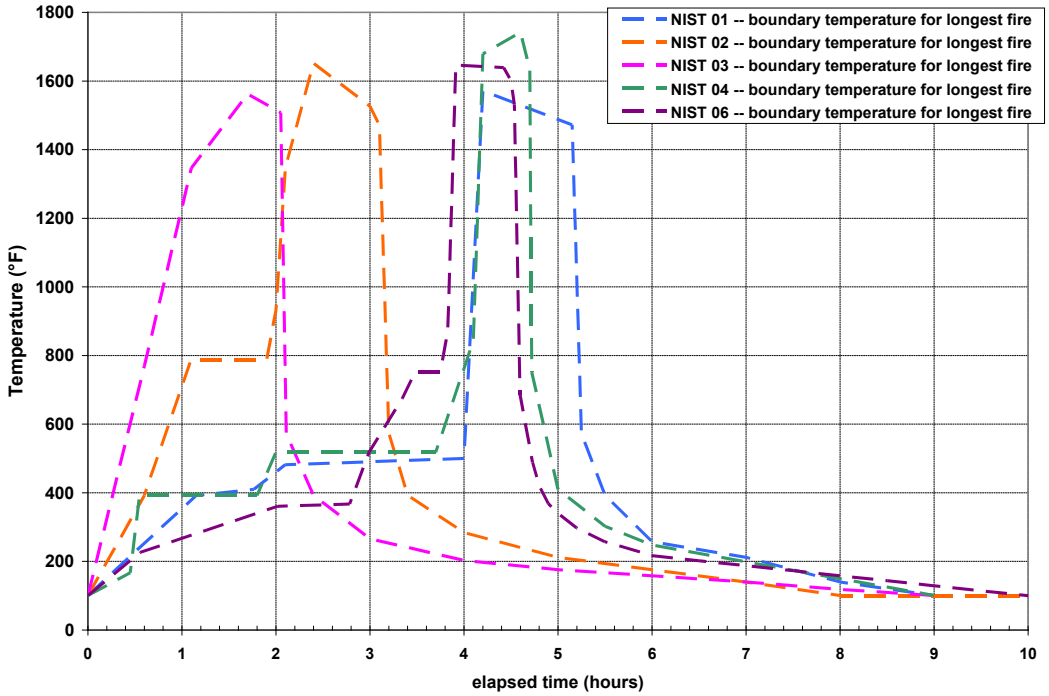

Figure 6.2. Fire Boundary Temperatures for Longest Fire (all cases)

As noted in Section 6.1 in the presentation of modeling assumptions, convection heat transfer at the SNF package surface during the fire was treated in both models as forced convection. Along the package body and the sides of the impact limiters, the Nusselt number is defined using a correlation (Kreith and Bohn 2001)[3] for axial flow over a flat or slightly curved surface at zero angle of attack, and has the form

$$Nu = a(\mathrm{Re}_L^b + c)\,\mathrm{Pr}^d \quad \text{(turbulent regime; } \mathrm{Re}_L > 5.0\text{x}(10^5),\ \mathrm{Pr} > 0.5) \qquad (6.1)$$

where

a = 0.036
b = 0.8
c = -23,200
d = 0.3333
L = characteristic length (in this case, the exposed package body or impact limiter side)
Pr = Prandtl Number
Re_L = $\rho U_\infty L / \mu$

[3] Source reference for this correlation is Kreith and Bohn 2001; primary references cited are Rohsenow, Patankar and Spalding, and Bejan.

where

ρ = fluid density
U_∞ = free-stream external velocity
μ = fluid viscosity

On the flat ends of the impact limiters, the Nusselt number is defined using a correlation for forced convection from an isothermal disk or circular plate with axis perpendicular to the flow direction (Kreith and Bohn 2001). The correlation has the form

$$Nu = a\,\mathrm{Re}_D^{\,b}\,\mathrm{Pr}^{\,c} \quad (900 < \mathrm{Re}_D < 30{,}000) \tag{6.2}$$

where

a = 0.591
b = 0.564
c = 0.3333
ReD = $\rho U_\infty D / \mu$

where

ρ = fluid density
U_∞ = free-stream external velocity
D = diameter of disk or plate
μ = fluid viscosity

In the above correlations, fluid properties are evaluated at the film temperature, defined as the average of the wall surface temperature and the ambient temperature, which in this application is the fire temperature. The free-stream external velocity was specified at a bounding value of 12 ft/s (3.7 m/s), based on the velocities predicted in the FDS simulations.

7.0 ANALYSIS RESULTS

This section presents the results of the thermal analyses of the GA-4 package exposed to the conditions of the Newhall Pass tunnel fire scenario. As noted in Section 6.0, all transient evaluations initiated a steady-state solution for NCT, obtained with the ANSYS and COBRA-SFS models of the GA-4 package. The results obtained with these models predict similar peak component temperatures for NCT, and the results are consistent with the values reported in the package SAR (General Atomics 1998). The peak cladding temperature predicted with the ANSYS model is 306°F (152°C), and the COBRA-SFS model predicts 294°F (145°C). This is a difference of about 4%, and is consistent with the expected differences between the results obtained with a detailed thermal-hydraulic model of the fuel assemblies compared to the results obtained with the k-effective model for the fuel. The k-effective model for the homogenized fuel assembly is designed to yield results that are 5-15% conservative, compared to results obtained with a CFD model of a fuel assembly (Bahney and Lotz 1996).

Figure 7.1 shows the peak component temperatures predicted with the ANSYS and COBRA-SFS models of the GA-4 at NCT, compared to the results reported in the GA-4 SAR (General Atomics 1998). Figure 7.2 shows a color thermograph of the ANSYS model temperature results for the package cross-section for this initial steady state. In the graphic produced with ANSYS, the text data includes the line “TIME = 0.5.” This time-stamp appears on the plot because the NCT steady-state analysis was run as a transient, to ensure a smooth transition within the ANSYS calculation between the initial conditions and the transient fire analysis. The NCT analysis was run as a transient solution with an arbitrary time-step, updating temperature-dependent material properties and external convection coefficients until the solution did not change significantly between time-steps. Time-stamps on graphics produced using ANSYS include the arbitrary 0.5 hours of the NCT analysis, and therefore are off-set by 0.5 hour compared to line plots (for both COBRA-SFS and ANSYS results), which are referenced to the start of the fire as time zero. This feature is carried through all of the color thermographs shown in this section for the ANSYS transient results.

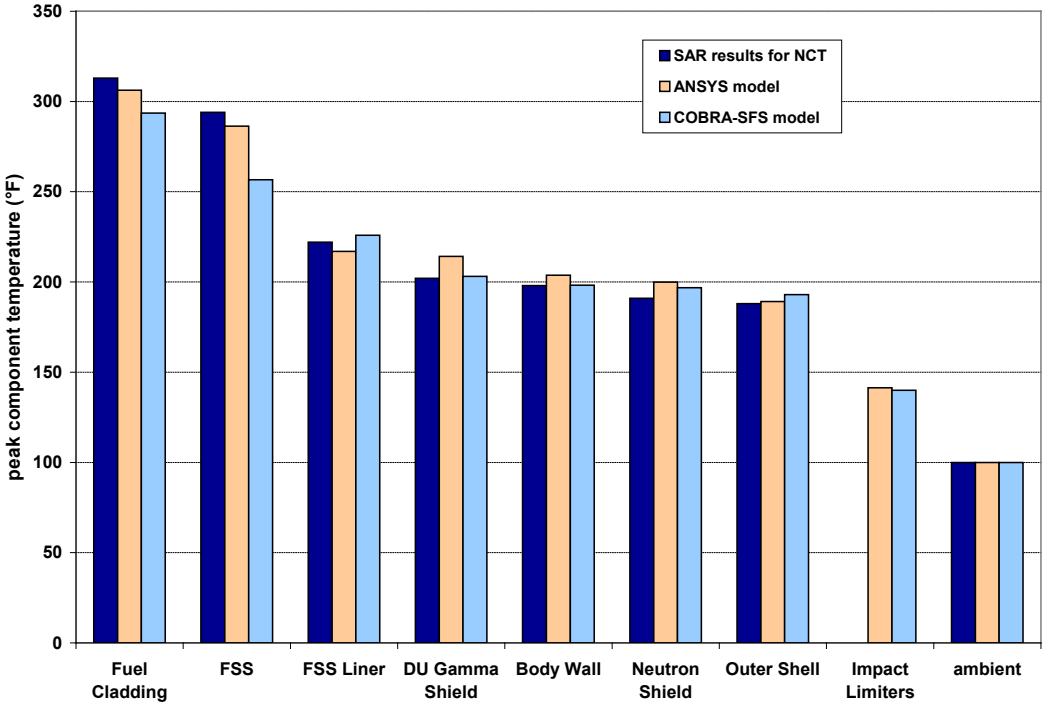

Figure 7.1. Initial Conditions for Fire Transient Analyses: GA-4 at NCT

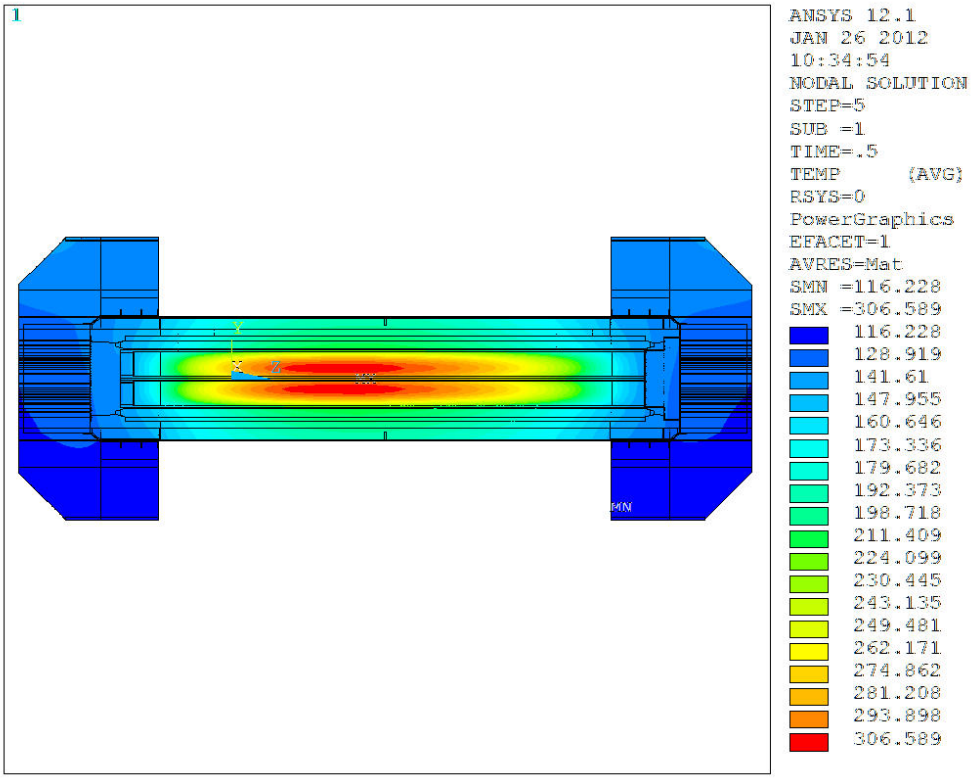

Figure 7.2. Thermal Cross-Section of GA-4 Package at NCT (temperatures in °F)

The thermal analysis of the five cases defined in Section 4.0 are discussed in separate sections, with separate discussion of each of the two potential locations considered for the package in the fire. Detailed thermograph plots of the GA-4 package temperature evolution during these long-duration fire transients (out to 10 hours) are provided in Appendix C. The discussion presented here provides an overview of the package thermal response to the fire conditions, with comparisons of results from the full range of cases evaluated.

Section 7.1 presents results for case NIST-01, which is the base case for this fire scenario, and constitutes a reasonable bounding scenario for the known fire conditions. Section 7.2 presents results for case NIST-02, which evaluates the effect of assuming a faster spread rate for the fire through the tunnel (and consequently results in a shorter overall fire duration). Section 7.3 presents results for case NIST-03, which evaluates the effect of an even faster assumed spread rate, such that the overall fire duration spans the shortest time possible, within the known fire timeline. Section 7.4 presents results for case NIST-04, in which the assumed burn rate for the individual vehicle fires is doubled, resulting in a shorter, more intense fire at each location. Section 7.5 presents results for case NIST-06, which evaluates the effect of realistic estimates of available fuel for the fire, based on actual cargo carried by each vehicle, rather than the bounding average value assumed for all vehicles (including those running empty) for cases NIST-01 through NIST-04. Section 7.6 presents a summary and comparison evaluation of all cases modeled.

7.1 Thermal Results for NIST-01

As discussed above, the boundary conditions at the hottest fire location and longest fire location for case NIST-01 provide a bounding scenario for the Newhall Pass fire. Section 7.1.1 presents the results obtained with the ANSYS and COBRA-SFS models for the hottest fire of this case, and Section 7.1.2 presents the results obtained for the longest fire of this case.

7.1.1 NIST-01: Hottest Fire

In this case, the fire at the hottest location (vehicle #23) does not begin until about 1.8 hours into the transient, and lasts for approximately one hour. The ambient temperature seen by the package conservatively bounds the fully engulfing fire conditions predicted for this case (see Section 4.0). At the location of vehicle #23, the fire effects are modeled by a rise in ambient temperature to about 460°F (238°C) during the first 1.2 hours of the fire, and is held at this value until the local fire begins on vehicle #23. When the fire reaches this location, the ambient temperature seen by the GA-4 package rises rapidly, reaching 1562°F (850°C) in about 15 minutes, then rising more slowly to a peak of 1724°F (940°C) near the end of the approximately hour-long fire. After the fire consumes this vehicle, the local temperature drops rapidly, beginning the post-fire cooldown at this location in the tunnel (as shown by the fire modeling results in Figure 3.2 and the local fire boundary conditions in Figure 4.1 for this case).

Figure 7.3 illustrates the thermal response of the GA-4 package to the fire transient with color thermographs showing radial and axial cross-sections of the package at 3 hours, near the end of the local fire on vehicle #23. These graphics show that the fuel region is at this point the coldest part of the package cross-section, with the peak fuel temperature occurring at the outer corners of the assembly, where the fuel is most exposed to the external fire conditions.

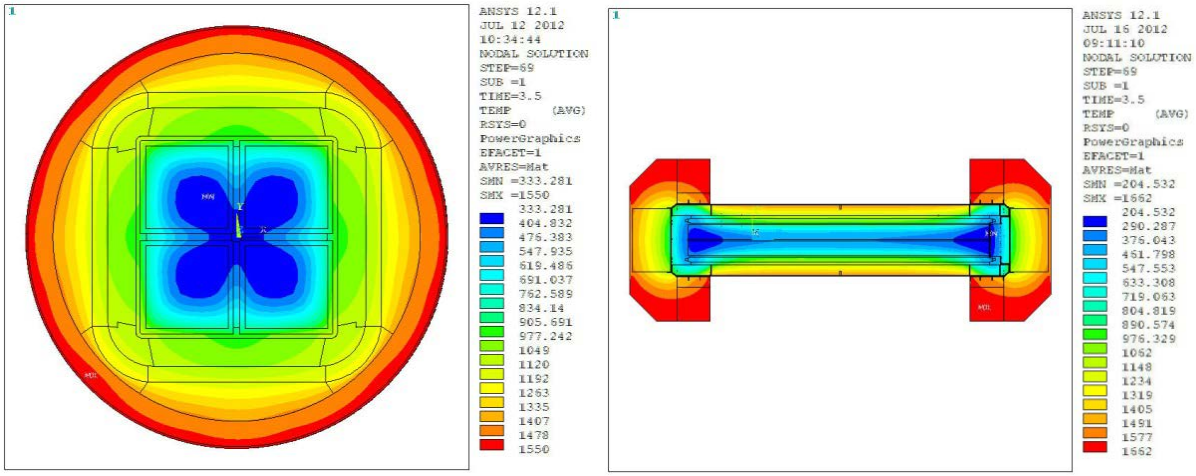

Figure 7.3. ANSYS Model: Radial and Axial Temperature (°F) Distributions in GA-4 Package at End of Fire on Vehicle #23 (hottest fire location) in Case NIST-01

The ANSYS model predicts a maximum temperature of 1081°F (583°C) at the outermost corners of the fuel region, a value slightly above the short-term temperature limit of 1058°F (570°C) for zircaloy cladding. The COBRA-SFS model, with a more realistic representation of the thermal response of the fuel, predicts a maximum peak cladding temperature of 882°F (472°C). This is considerably below the short-term limit for zircaloy cladding in accident conditions. The evolution of the peak component temperatures throughout the fire transient is illustrated in detail by the plots of peak temperatures on individual components of the package, shown in Figure 7.4 for the ANSYS model results and in Figure 7.5 for the COBRA-SFS model results.

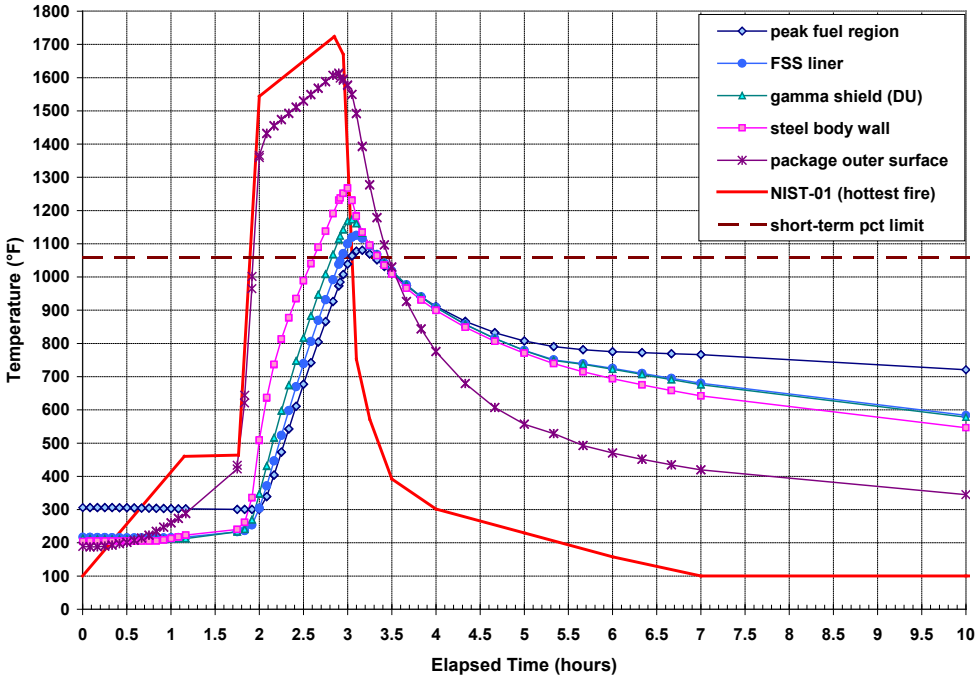

Figure 7.4. ANSYS Results: Peak Component Temperatures in GA-4 Package for Hottest Fire in Case NIST-01

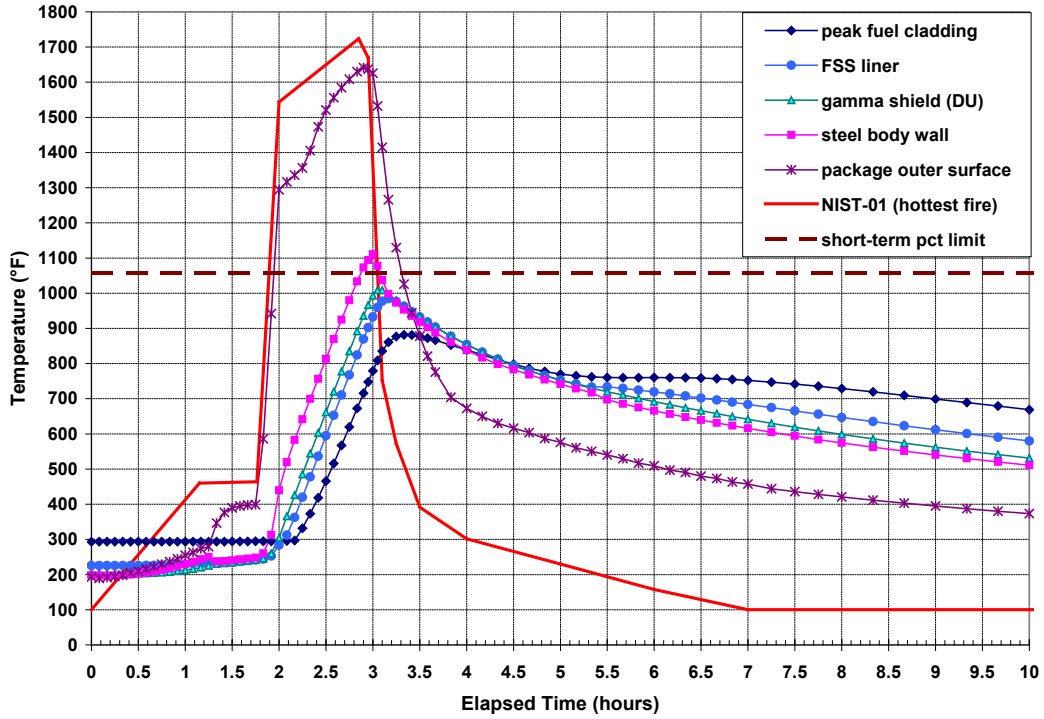

Figure 7.5. COBRA-SFS Results: Peak Component Temperatures in GA-4 Package for Hottest Fire in Case NIST-01

The plots in Figure 7.4 and Figure 7.5 show a relatively steady decrease of all package components in the post-fire cooldown, except for the peak fuel cladding temperature. The overall maximum peak cladding temperature actually occurs after the end of the fire, and this temperature decreases more slowly than the peak temperatures on internal components that do not generate heat. At about 5.5 hours, the maximum peak cladding temperature exhibits a slight increase, to a secondary peak at about 6.5 hours. This behavior is due to the thermal inertia of the fuel, and the decreased rate of heat removal at the higher ambient temperatures during the fire and much of the long cooldown period, compared to the design-basis ambient condition of 100°F (38°C). In more severe fire conditions than those of this case of the Newhall Pass Tunnel fire, this characteristic secondary peak in the maximum cladding temperature can exceed the peak reached during the actual fire (NUREG/CR-6886 2009; NUREG/CR-6894 2007; NUREG/CR-7206 2015).

7.1.2 NIST-01: Longest Fire

The fire on vehicle #31 is the last of the intense vehicle fires in the Newhall Pass tunnel, and in this case, it is initiated at about 4 hours into the transient (see Figure 4.1). At the location of vehicle #31, the fire is modeled with an ambient temperature that rises to about 480°F (249°C) during the first 2 hours of the fire, due to the flow of hot gases from the fire as it engulfs the other vehicles in the tunnel in succession. As a bounding assumption, the temperature at the location of vehicle #31 is specified at this value until the fire reaches it. Once the fire reaches this vehicle, the boundary temperature representing the fire at this location rises rapidly to 1571°F (855°C) then drops gradually to 1479°F (804°C) over a period of approximately one hour.

After the fire has consumed this vehicle, the local temperature drops rapidly, since this is the end of the total fire duration and the beginning of the post-fire cooldown. This is the point at which forced convection within the tunnel is assumed to abruptly end (at this location and at the hottest fire location), and the convection boundary condition for both the ANSYS and the COBRA-SFS model is reset to free convection in still air.

Figure 7.6 illustrates the thermal response of the GA-4 package to the fire transient with color thermographs showing radial and axial cross-sections of the package at 5 hours, approximately 9 minutes before the end of the local fire on vehicle #31. As with the results in Figure 7.3 for the hottest fire location (vehicle #23), these graphics show that the fuel region is the coldest part of the package cross-section at the end of the fire, with the peak fuel temperature occurring at the outer corners of the assembly, where the fuel is most exposed to the external fire conditions.

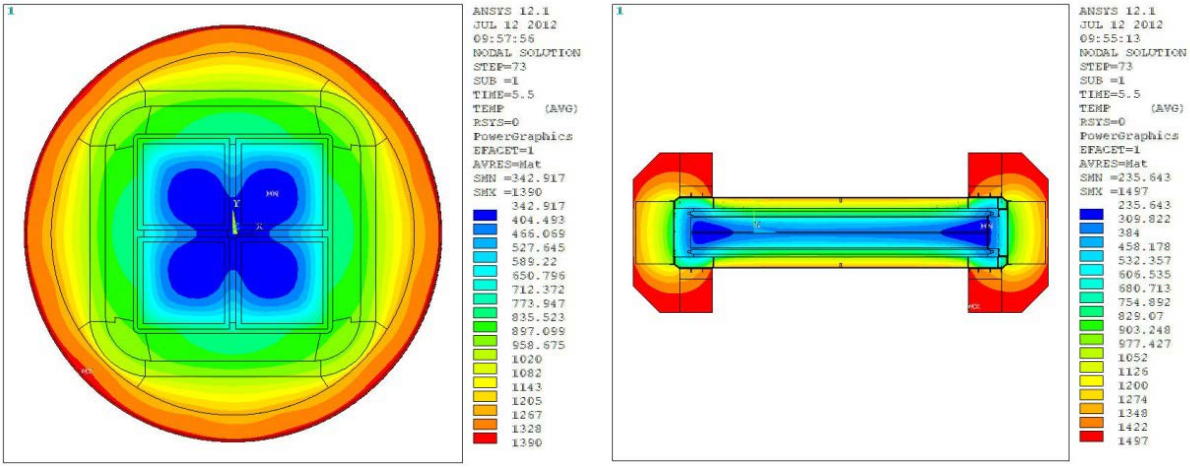

Figure 7.6. ANSYS Model: Radial and Axial Temperature (°F) Distributions in GA-4 Package at End of Fire on Vehicle #31 (longest fire location) in Case NIST-01

For the longest fire location in the tunnel for this case, the ANSYS model predicts a maximum temperature of 954°F (512°C) in the fuel region. This is somewhat lower than the maximum of 1081°F (583°C) predicted for the hottest fire location for this case, and is below the short-term temperature limit of 1058°F (570°C) for zircaloy cladding. The COBRA-SFS model also predicts a lower maximum peak cladding temperature for this longest fire location, compared to the hottest fire location. The peak cladding temperature is only 767°F (408°C) for the longest fire of this case, compared to the 882°F (472°C) value predicted for the hottest fire of this case. This indicates that the longest fire for the NIST-01 case is less severe than the hottest fire, in terms of its potential effect on the GA-4 package, even with the long “preheat” of the package prior to the fire reaching the location of vehicle #31.

The evolution of the peak component temperatures throughout the fire transient is illustrated in detail by the plots of peak temperatures on individual components of the package, shown in Figure 7.5 for the ANSYS model results and in Figure 7.8 for the COBRA-SFS model results. As in the plots in Figure 7.4 and Figure 7.5 for the hottest fire location, the peak temperatures show a relatively steady decrease for all package components in the post-fire cooldown. The peak fuel region temperature (in the ANSYS model) and the peak cladding temperature (in the COBRA-SFS model) also show a steady decrease, but at a slower rate, due to thermal inertia of the heat generating fuel assemblies, and the prolonged period with ambient temperatures above the design-basis value of 100°F (38°C).

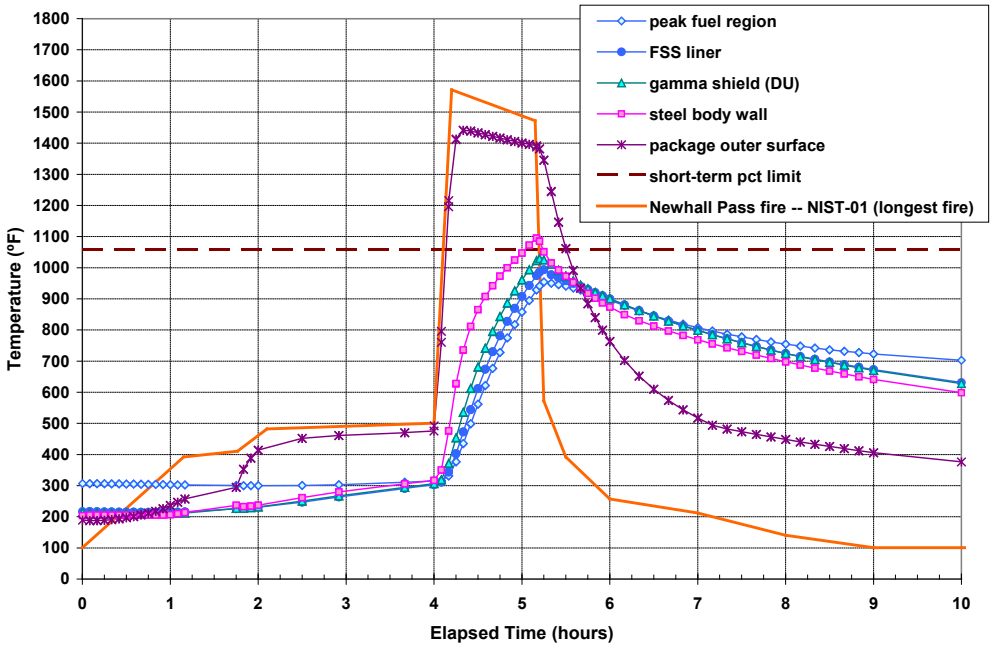

Figure 7.7. ANSYS Results: Peak Component Temperatures in GA-4 Package for Longest Fire in Case NIST-01

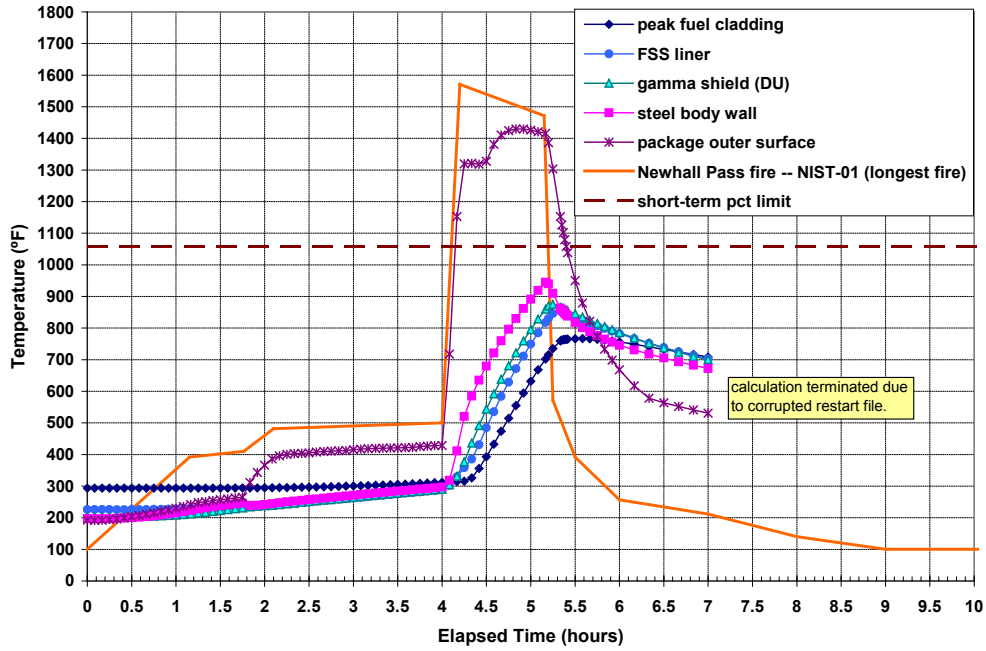

Figure 7.8. COBRA-SFS Results: Peak Component Temperatures in GA-4 Package for Longest Fire in Case NIST-01

The overall maximum peak cladding temperature actually occurs after the end of the fire, and this temperature decreases more slowly than the internal components that do not generate heat. The transient calculation with the COBRA-SFS model was terminated prematurely at 7 hours, due to computer file problems, so this case does not extend long enough to exhibit the secondary maximum observed in the cooldown for the hottest fire location in this case.

However, it is clear from the rate of change of the peak cladding temperature that thermal inertia is taking its toll in the cooldown period for this transient, as well.

As discussed in Section 6.0, the boundary conditions at the hottest fire location and longest fire location for case NIST-01 of the Newhall Pass fire scenario both provide a conservative fire environment for the GA-4 package. Based on the results obtained in the analysis of this fire scenario with the ANSYS model and the COBRA-SFS model, the package experiences higher peak temperatures in the hottest fire case, with the package near the middle of the tunnel. With the package located near the tunnel entrance, even with the long preheat of the package prior to the fire on vehicle #31, peak component temperatures are somewhat lower, reflecting the lower peak fire temperature at this location.

7.2 Thermal Results for NIST-02

The assumed faster spread rate for the fire in case NIST-02, compared to NIST-01, results in a shorter overall duration for the fire scenario. The period of intense fires on the vehicles is a little more than 3 hours, compared to nearly 5.5 hours for NIST-01. Case NIST-02 has somewhat lower peak fire temperatures, even though the local fire duration on a given vehicle is approximately the same as in NIST-01. The shorter overall time for case NIST-02 is a more realistic estimate of the fire duration, based on available information. The 5.5 hours predicted for case NIST-01 is bounding, as it slightly exceeds the maximum possible duration of visible fire in the tunnel.

The boundary conditions at the hottest fire location (vehicle #23, near the middle of the tunnel) for case NIST-02 provide a less severe fire scenario for the GA-4 package than does case NIST-01 at this location. However, for the longest fire location (vehicle #31, at the tunnel entrance), NIST-02 provides a more severe fire scenario than does the corresponding case for NIST-01. Section 7.2.1 illustrates this with results obtained with the ANSYS and COBRA-SFS models for the hottest fire of this case, and Section 7.2.2 shows the results obtained for the longest fire of this case.

7.2.1 NIST-02: Hottest Fire

In this case, the fire at the hottest location (vehicle #23) begins at approximately 45-50 minutes into the fire, and is essentially identical to the fire on this vehicle in case NIST-01. In case NIST-02, the preheat at this location, due to the fire upstream on other vehicles in the tunnel, results in a gradual increase of the local ambient temperature to about 660°F (349°C) during the first 50 minutes of the fire transient. Once the fire reaches vehicle #23, the local temperature increases very rapidly, rising to 1562°F (850°C) in the first 10-15 minutes of the local fire, then rising at a much more gradual rate to a peak of 1706°F (930°C) over the next 40-45 minutes. The fire on vehicle #23 ends at approximately 2 hours, and the local temperature drops rapidly in the post-fire cooldown at this location, as the fire continues to spread through the tunnel to vehicles beyond #23 (as shown by the fire modeling results in Figure 3.3 and the local fire boundary conditions in Figure 4.2 for this case).

Figure 7.9 illustrates the thermal response of the GA-4 package to the fire transient with color thermographs showing radial and axial cross-sections of the package at 2 hours, when the fire is just ending on vehicle #23. As with the results from case NIST-01, these graphics show that the fuel region is the coldest part of the package cross-section at the end of the fire, with the peak fuel temperature occurring at the outer corners of the assembly, where the fuel is most exposed to the external fire conditions.

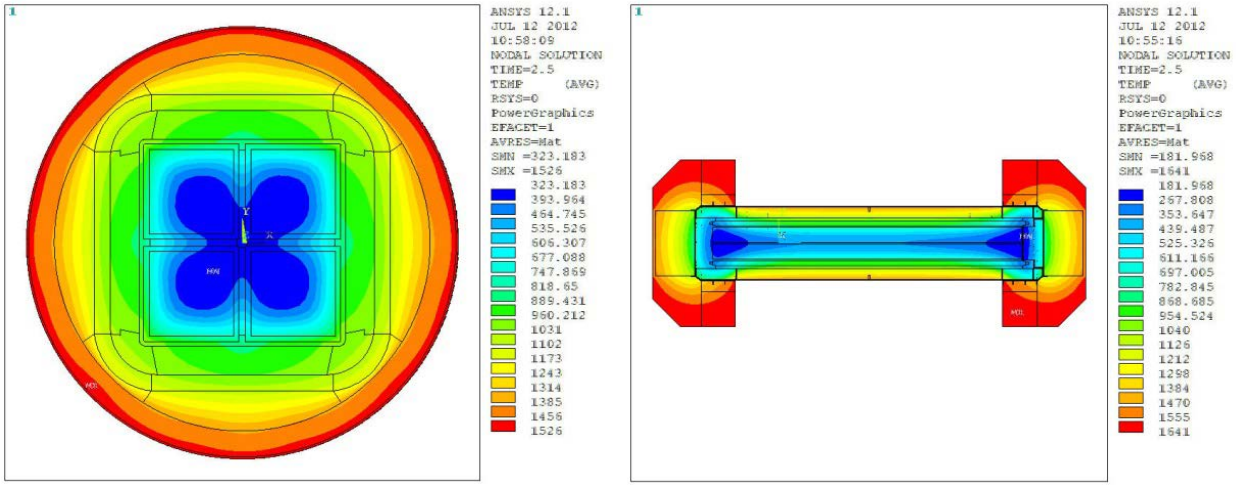

Figure 7.9. ANSYS Model: Radial and Axial Temperature (°F) Distributions in GA-4 Package at End of Fire on Vehicle #23 (hottest fire location) in Case NIST-02

The ANSYS model predicts a maximum temperature of 1010°F (543°C) in the fuel region for this case, a value below the short-term temperature limit of 1058°F (570°C) for zircaloy cladding. The COBRA-SFS model, with a more realistic representation of the thermal response of the fuel, predicts a maximum peak cladding temperature of 818°F (436°C). This is considerably below the short-term limit for zircaloy cladding. The evolution of the peak component temperatures is illustrated in more detail by the plots of peak temperatures on individual components of the package, shown in Figure 7.10 for the ANSYS model results and in Figure 7.11 for the COBRA-SFS model results.

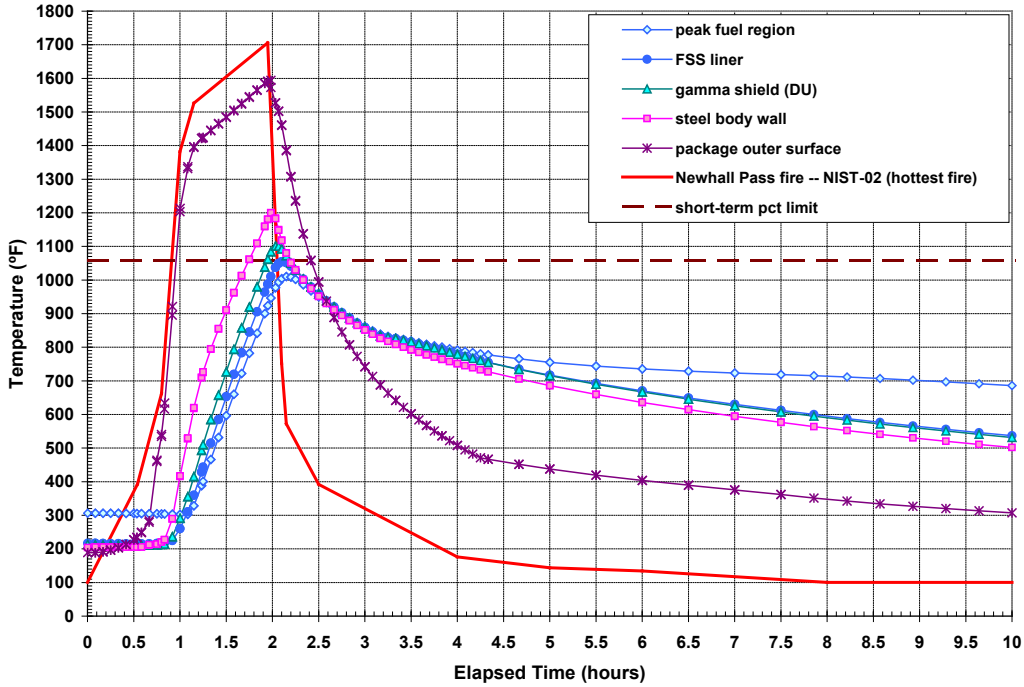

Figure 7.10. ANSYS Results: Peak Component Temperatures in GA-4 Package for Hottest Fire in Case NIST-02

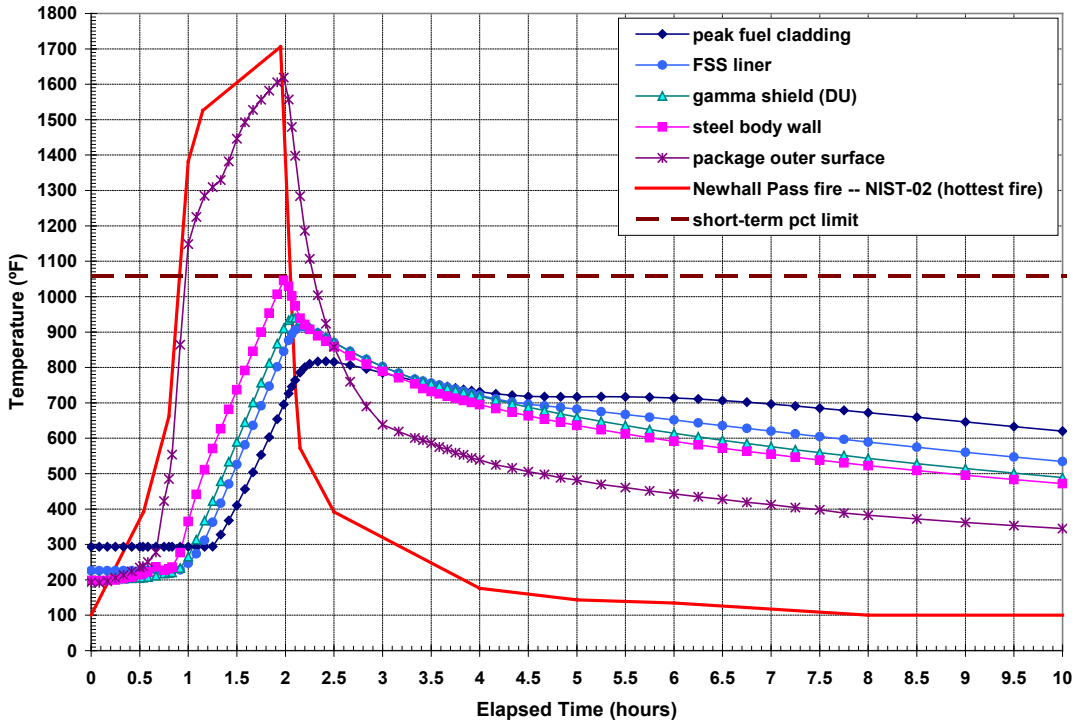

Figure 7.11. COBRA-SFS Results: Peak Component Temperatures in GA-4 Package for Hottest Fire in Case NIST-02

The plots in Figure 7.10 and Figure 7.11 show that, as in case NIST-01, the overall maximum peak cladding temperature occurs after the end of the local vehicle fire, and decreases more slowly than the other internal components that do not generate heat. At about 5 hours, the peak clad temperature predicted with the COBRA-SFS model (Figure 7.11) begins a slight increase, to a secondary peak at about 6 hours. As noted above in the discussion of case NIST-01 (see Section 7.1), this behavior is due mainly to the thermal inertia of the fuel, and therefore occurs over approximately the same time span.

7.2.2 NIST-02: Longest Fire

The fire on vehicle #31 is the last of the intense vehicle fires in the Newhall Pass tunnel, and in case NIST-02, it is initiated at about 2 hours into the transient. This coincides with the time of the end of the fire at the hottest fire location, on vehicle #23. Due to the faster spread rate assumed for this case, a larger number of vehicles are burning at any one time during the transient. In case NIST-02, when the fire reaches vehicle #31, six other vehicles are still actively burning (#24 through #30). For case NIST-01, only three vehicles (#28, #29, and #31) are actively burning at that point in the transient.

The compressed timeframe of the fire in case NIST-02, with more vehicles burning at a given time, results in a more rapid increase in the local ambient temperature at the location of vehicle #31. In case NIST-02, the temperature at the location of vehicle #31 rises to about 800°F (427°C) during the first hour of the transient, compared to only about 480°F (249°C) in the 4 hours it takes the fire to reach vehicle #31 in case NIST-01. The fire on vehicle #31 is somewhat hotter than the fire on this vehicle in case NIST-01 and more sharply peaked over the duration of the fire. In case NIST-02, the fire temperature on vehicle #31 initially rises rapidly to 1346°F (730°C) in the first few minutes, then increases to about 1652°F (900°C) over the next 20 minutes. The fire temperature then drops gradually to about 1472°F (800°C) over a period of approximately 45 minutes.

Figure 7.12 illustrates the thermal response of the GA-4 package to the fire transient with color thermographs showing radial and axial cross-sections of the package at 3 hours, approximately 6 minutes before the end of the local fire on vehicle #31. As with the results for the hottest fire location for this case (vehicle #23), and for case NIST-01 (see Section 7.1), these graphics show that the fuel region is the coldest part of the package cross-section at the end of the fire, with the peak fuel temperature occurring at the outer corners of the assembly, where the fuel is most exposed to the external fire conditions.

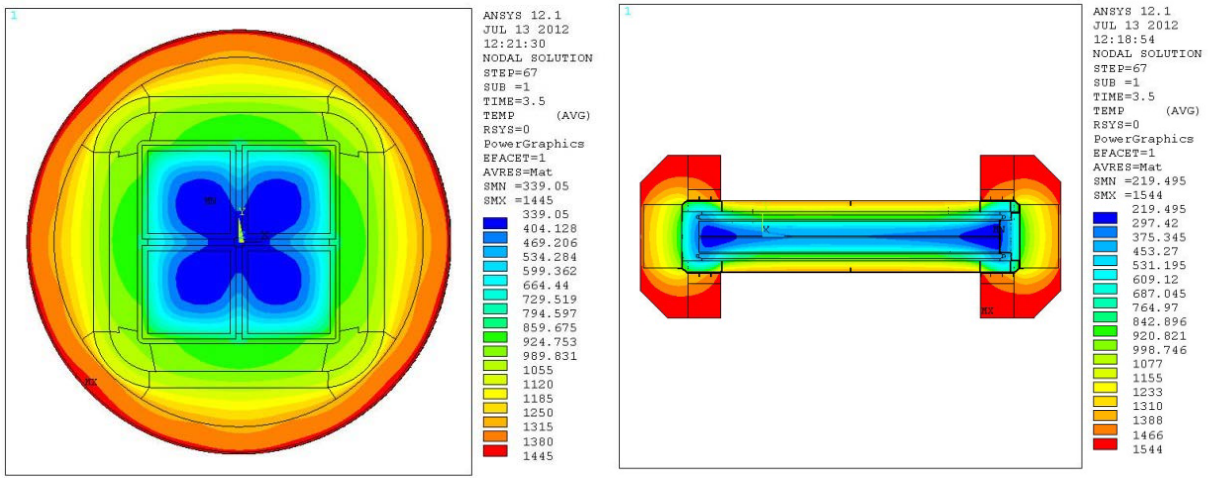

Figure 7.12. ANSYS Model: Radial and Axial Temperature (°F) Distributions in GA-4 Package at End of Fire on Vehicle #31 (longest fire location) in Case NIST-02

For this location in the tunnel, the ANSYS model predicts a maximum temperature of 1020°F (549°C) in the fuel region, which is below the short-term temperature limit of 1058°F (570°C) for zircaloy cladding. It is also lower than the peak fuel region temperature of 1081°F (583°C) that the ANSYS model predicts for the fuel region with the package in the hottest fire location of case NIST-02. For this case, the peak fuel region temperature predicted for the longest fire (on vehicle #31), is slightly above the peak temperature of 1010°F (543°C) predicted for the hottest fire (on vehicle #23). The COBRA-SFS model also predicts a higher maximum peak cladding temperature of 834°F (445°C) for the longest fire of NIST-02, compared to the 818°F (436°C) value predicted for the hottest fire of this case. This trend is consistent with the ANSYS model results, indicating that the longest fire for case NIST-02 is slightly more severe than the hottest fire, in terms of its potential effect on the GA-4 package.

The evolution of the peak component temperatures throughout the fire transient is illustrated in detail by the plots of peak temperatures on individual components of the package, shown in Figure 7.13 for the ANSYS model results and in Figure 7.14 for the COBRA-SFS model results. The more intense preheat of the package before the local fire on vehicle #31 results in rising temperatures on all package components, including the FSS liner, and the peak fuel cladding temperature begins to rise earlier in the transient than in the longest fire for case NIST-01. As in the plots in Figure 7.10 and Figure 7.11 for the hottest fire location, the peak temperatures show a relatively steady decrease for all package components in the post-fire cooldown.

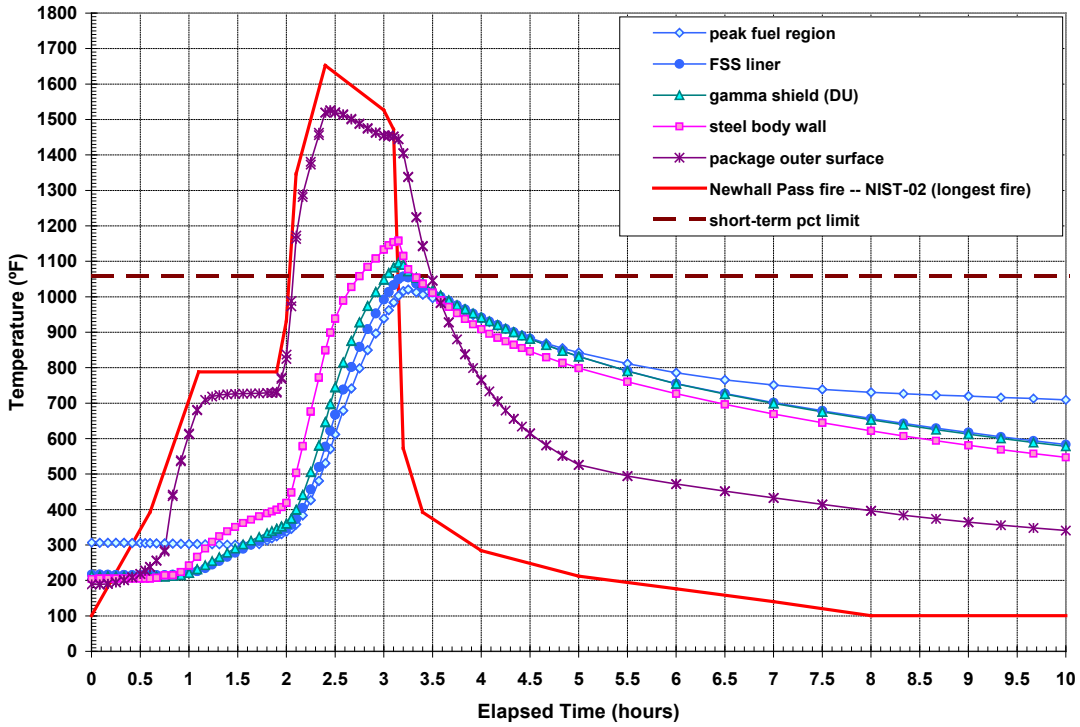

Figure 7.13. ANSYS Results: Peak Component Temperatures in GA-4 Package for Longest Fire in Case NIST-02

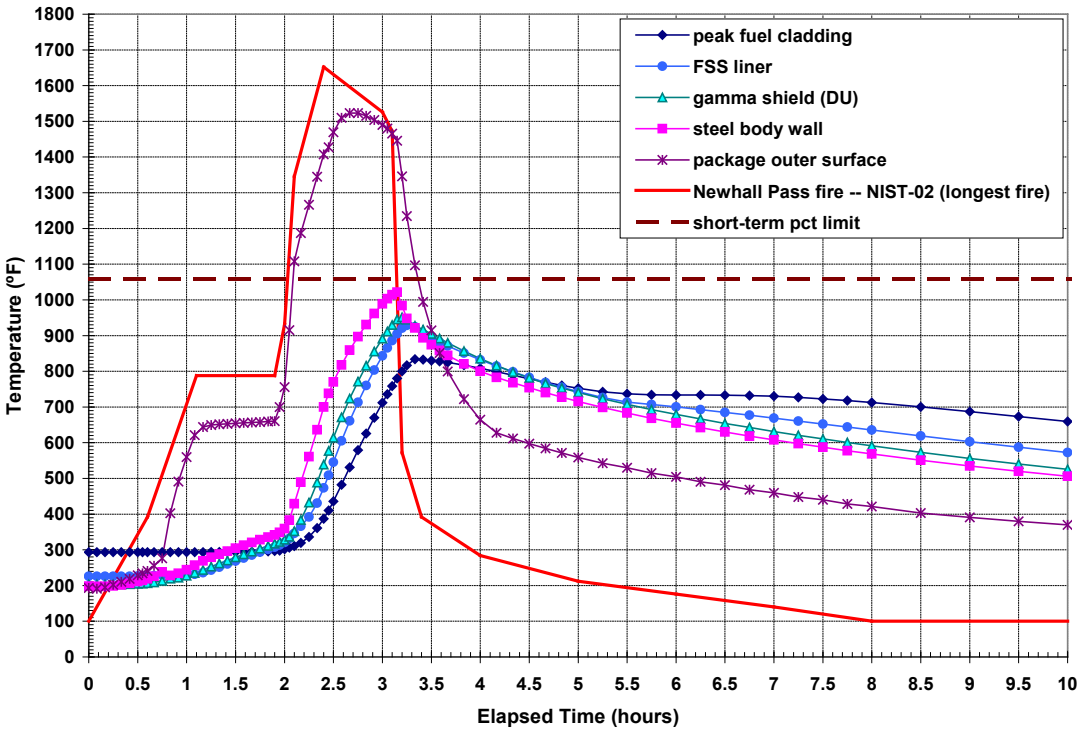

Figure 7.14. COBRA-SFS Results: Peak Component Temperatures in GA-4 Package for Longest Fire in Case NIST-02

As noted for all cases discussed above, the overall maximum peak cladding temperature occurs after the end of the fire, and this temperature decreases more slowly than the internal components that do not generate heat. At about 6 hours, the maximum peak cladding temperature predicted with the COBRA-SFS model (Figure 7.14) exhibits a slight increase, to a secondary peak at about 7 hours. This behavior is due to the thermal inertia of the fuel, and the decreased rate of heat removal at the higher ambient temperatures during the fire and much of the long cooldown period.

7.3 Thermal Results for NIST-03

In case NIST-03, the spread rate for the fire is assumed to be faster than in NIST-01 or NIST-02, and results in the shortest possible total fire duration that fits within the known timeline of the Newhall Pass fire. The fast spread rate results in an overall duration of only about 2 hours for the intense portion of the fire scenario, compared to just over 3 hours for case NIST-02, and approximately 5 hours for case NIST-01. The shorter overall fire duration in case NIST-03 results in slightly lower peak fire temperatures, even though the local fire duration on a given vehicle is approximately the same as in NIST-01 and NIST-02.

The boundary conditions at the hottest fire location (vehicle #22, near the middle of the tunnel) for case NIST-03 provide a slightly less severe fire scenario for the GA-4 package than does case NIST-01 or NIST-02 at this location. For the longest fire location (vehicle #31, at the tunnel entrance), NIST-03 predicts a slightly higher peak fire temperature than does the corresponding case for NIST-01. However, it is significantly below the peak fire temperature predicted for the longest fire in case NIST-02.

The preheating at the longest fire location results in higher ambient temperatures for case NIST-03 prior to the fire in this location than in the other cases. Due to the rapid spread rate assumed in this case, all of the vehicles in the tunnel are still burning at the time of the start of the fire on vehicle #31. As a result, the fires at the two locations overlap in time by about half an hour; that is, the first half of the ~1-hour fire duration at the longest fire location (vehicle #31) occurs during the last half of the ~1-hour fire duration at the hottest fire location (vehicle #22).

Based on the fire timeline from the MAIT report, this case may provide the most realistic estimate of the fire spread rate, as it is the only one that fills the tunnel from end to end with fire for a significant period of time. However, it does not produce the most severe fire environment for the GA-4 package, compared to the bounding fire scenarios evaluated. Section 7.3.1 illustrates this with results obtained with the ANSYS and COBRA-SFS models for the hottest fire of this case, and Section 7.3.2 shows the results obtained for the longest fire of this case.

7.3.1 NIST-03: Hottest Fire

In this case, the fire at the hottest location (vehicle #22, near the center of the tunnel) begins at approximately 30 minutes into the fire. The preheat at this location due to the fire upstream on other vehicles in the tunnel is therefore quite short, and reaches only to about 600°F (316°C) before the fire reaches this location. Once the fire reaches vehicle #22, the local temperature increases very rapidly, rising to about 1490°F (810°C), where it holds relatively steady for 25-30 minutes, then rising gradually to a peak of 1670°F (910°C) over the remaining 30-35 minutes of the fire on vehicle #22. This local fire ends at approximately 90-95 minutes, and the local temperature drops rapidly in the post-fire cooldown at this location, as the fire continues to

spread through the tunnel to vehicles beyond #22 (as shown by the fire modeling results in Figure 3.4 and the local fire boundary conditions in Figure 4.3 for this case).

Figure 7.15 illustrates the thermal response of the GA-4 package to the fire transient with color thermographs showing radial and axial cross-sections of the package at 1.5 hours, within ~3 minutes of the end of the local fire on vehicle #22. These graphics show that the fuel region is at this point the coldest part of the package cross-section, with the peak fuel temperature occurring at the outer corners of the assembly, where the fuel is most exposed to the external fire conditions.

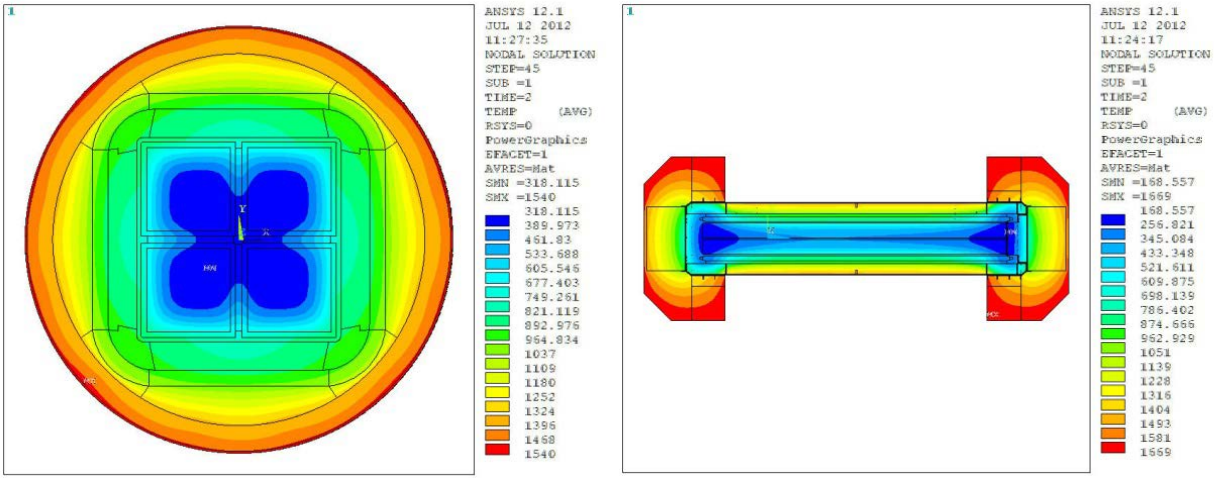

Figure 7.15. ANSYS Model: Radial and Axial Temperature (°F) Distributions in GA-4 Package at End of Fire on Vehicle #22 (hottest fire location) in Case NIST-03

The ANSYS model predicts a maximum temperature of 921°F (494°C) in the fuel region for this case, a value significantly below the short-term temperature limit of 1058°F (570°C) for zircaloy cladding. The COBRA-SFS model, with a more realistic representation of the thermal response of the fuel, predicts an even lower value, with a maximum peak cladding temperature of only 742°F (394°C). This is far below the short-term limit, and slightly below the long-term limit of 752°F (400°C) for zircaloy cladding, which is applicable to NCT.

The evolution of the peak component temperatures is illustrated in more detail by the plots of peak temperatures on individual components of the package, shown in Figure 7.16 for the ANSYS model results and in Figure 7.17 for the COBRA-SFS model results. These plots show that in general, this case does not impose as severe a fire transient on the GA-4 package as the conditions for case NIST-01 and case NIST-02. The results obtained for case NIST-03 suggest that a realistic representation of the Newhall Pass Tunnel fire scenario may not be significantly worse for the GA-4 package than the design-basis HAC fire. It is clearly not as severe as the fire scenario produced by the bounding assumptions of case NIST-01.

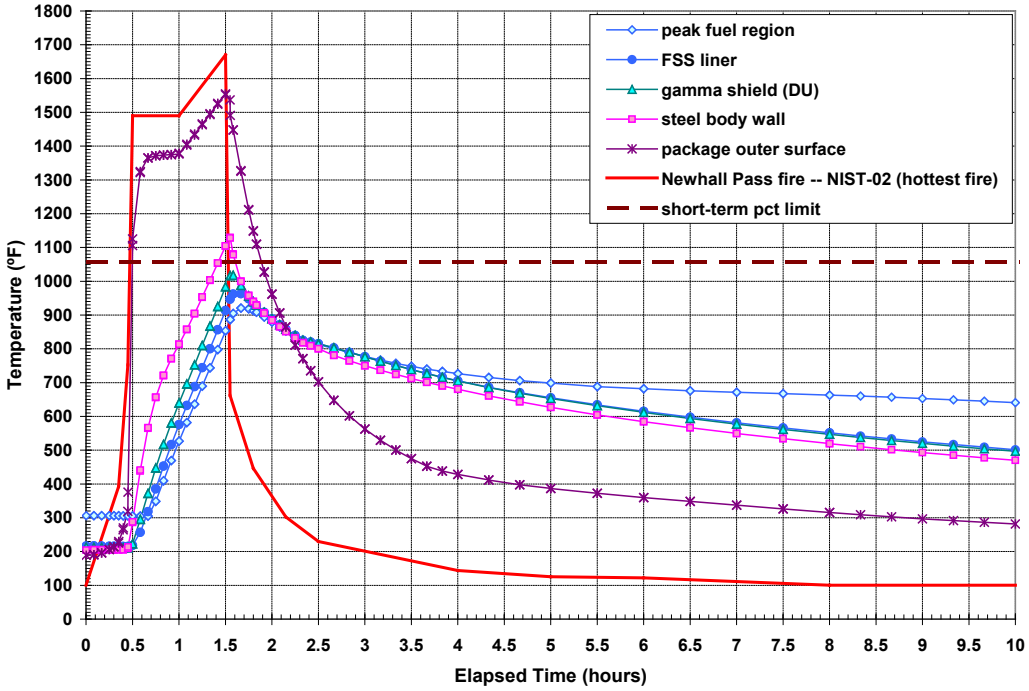

Figure 7.16. ANSYS Results: Peak Component Temperatures in GA-4 Package for Hottest Fire in Case NIST-03

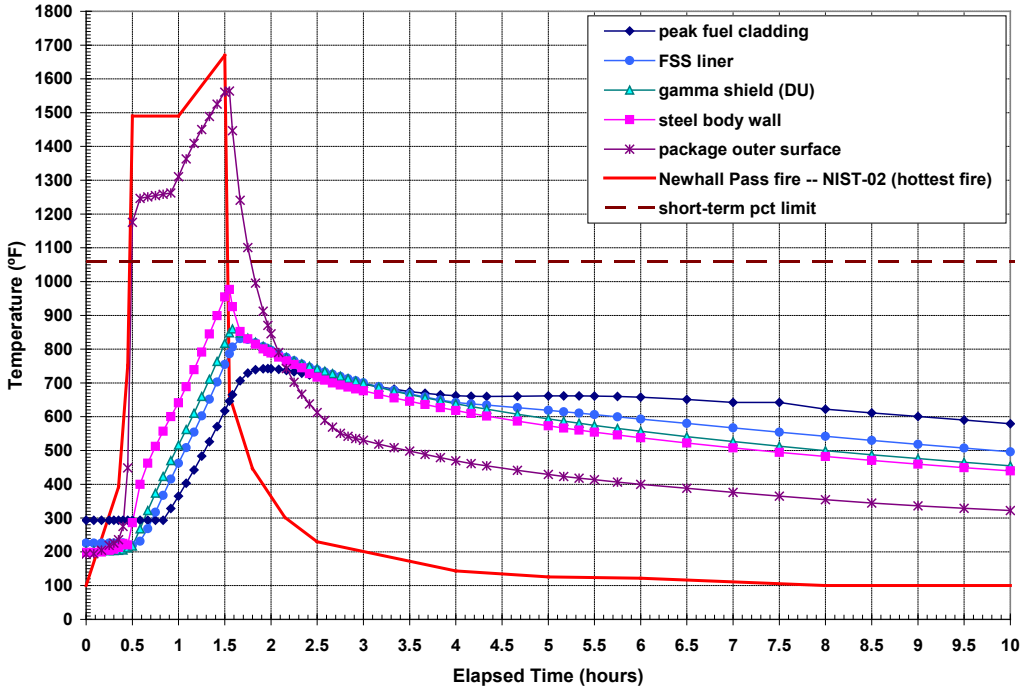

Figure 7.17. COBRA-SFS Results: Peak Component Temperatures in GA-4 Package for Hottest Fire in Case NIST-03

As noted in the discussion of cases NIST-01 and NIST-02, the plots for case NIST-03, in Figure 7.16 and Figure 7.17, show a relatively steady decrease of all package components in the post-fire cooldown. The overall maximum peak cladding temperature occurs after the end of the fire, and this temperature decreases more slowly than the internal components that do not generate heat. At about 5 hours the maximum peak cladding temperature predicted with the COBRA-SFS model (Figure 7.17) exhibits a very slight increase, to a secondary peak at about 6 hours. As noted previously, this behavior is due to the thermal inertia of the fuel.

7.3.2 NIST-03: Longest Fire

Due to the rapid spread rate assumed in case NIST-03, the fire on vehicle #31 begins within 1 hour of the start of the fire, and at least 30 minutes before the end of the fire on vehicle #22 (near the center of the tunnel). As the fire spreads through the tunnel, there is a rapid increase in the local ambient temperature near vehicle #31, exceeding 1231°F (666°C) by the end of the first hour of the transient. This intense preheating obscures the precise time of the beginning of the fire on vehicle #31, but it is reasonable to suppose that it has begun by the end of the first hour. In the second hour of the transient, the temperature at the location of vehicle #31 continues to rise for ~40 minutes, reaching a peak value of 1562°F (850°C), then decreases slightly over the remaining ~20 minutes of the fire to about 1486°F (808°C) near the end of the fire. The fire temperature then drops abruptly, indicating the end of the intense local fire on vehicle #31, effectively reaching the end of the fire transient, after a total duration of just over 2 hours.

Figure 7.18 illustrates the thermal response of the GA-4 package to the fire transient with color thermographs showing radial and axial cross-sections of the package at 2 hours, approximately 5 minutes before the end of the local fire on vehicle #31. As with the results in Figure 7.15 for the hottest fire location (vehicle #22) in this case, these graphics show that the fuel region is the coldest part of the package cross-section at the end of the fire, with the peak fuel temperature occurring at the outer corners of the assembly, where the fuel is most exposed to the external fire conditions.

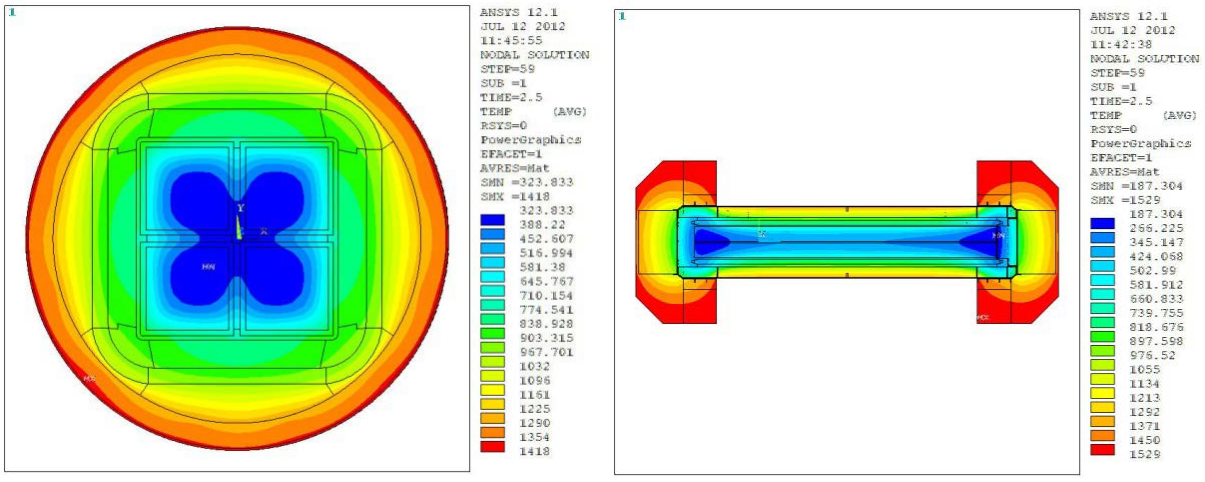

Figure 7.18. ANSYS Model: Radial and Axial Temperature (°F) Distributions in GA-4 Package at End of Fire on Vehicle #31 (longest fire location) in Case NIST-03

For this location in the tunnel, the ANSYS model predicts a maximum temperature of 913°F (489°C) in the fuel region, which is well below the short-term temperature limit of 1058°F (570°C). It is also lower than the peak fuel region temperatures that the ANSYS model predicts with the package at this location in cases NIST-01 and NIST-02. As in case NIST-02, the significant preheating at the location of the vehicle #31 results in case NIST-03 predicting that the peak fuel region temperature for the longest fire location would be very close to the peak temperature predicted for the hottest fire location.

The COBRA-SFS model predicts a maximum peak cladding temperature of 742°F (394°C) for the hottest fire of NIST-03. This model predicts essentially the same peak for the longest fire for this case, with a peak of 745°F (396°C). The results from both the ANSYS model and the COBRA-SFS model show that the main effect of the faster spread rates assumed for the fire in cases NIST-02 and NIST-03 is to raise the overall ambient temperature more uniformly throughout the tunnel, as the burn-times of the individual vehicle fires overlap more closely than in the slower spread rate assumed for NIST-01. The faster spread rate also tends to compress the overall fire duration, however, so that the tunnel air temperatures remain high for a shorter period of time overall. The net effect produces lower peak fire temperatures, and consequently lower temperatures are predicted for the components of the GA-4 package when exposed to these cases for the Newhall Pass fire scenario. These results are illustrated by the evolution of the peak component temperatures, shown in Figure 7.19 for the ANSYS model results and in Figure 7.20 for the COBRA-SFS model results.

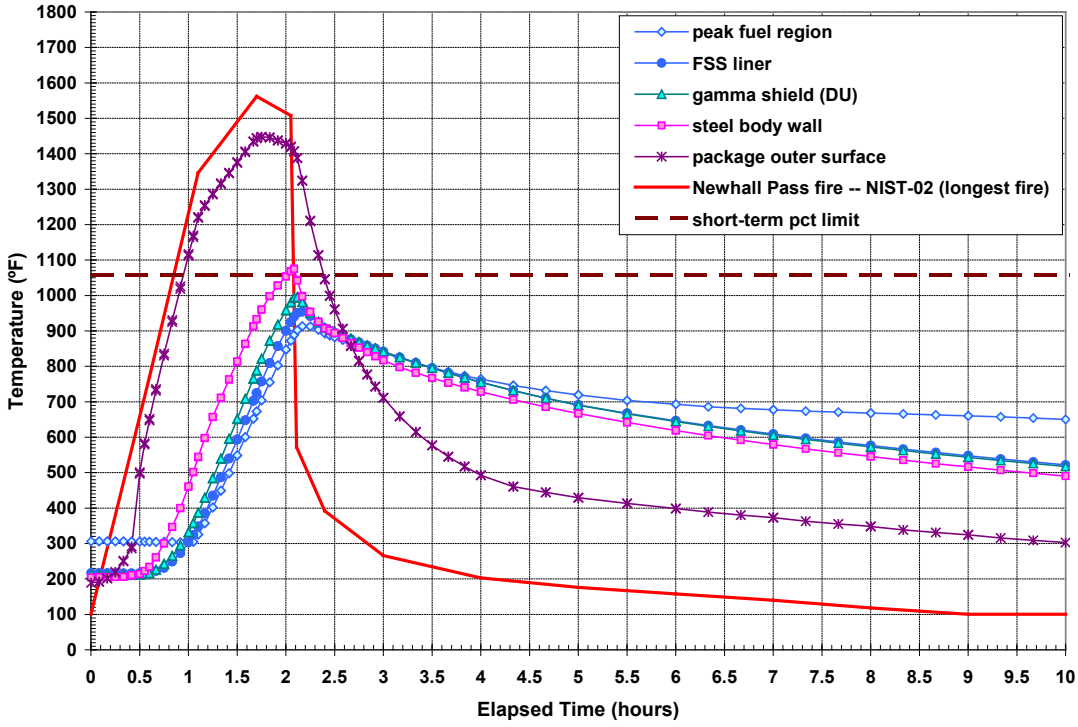

Figure 7.19. ANSYS Results: Peak Component Temperatures in GA-4 Package for Longest Fire in Case NIST-03

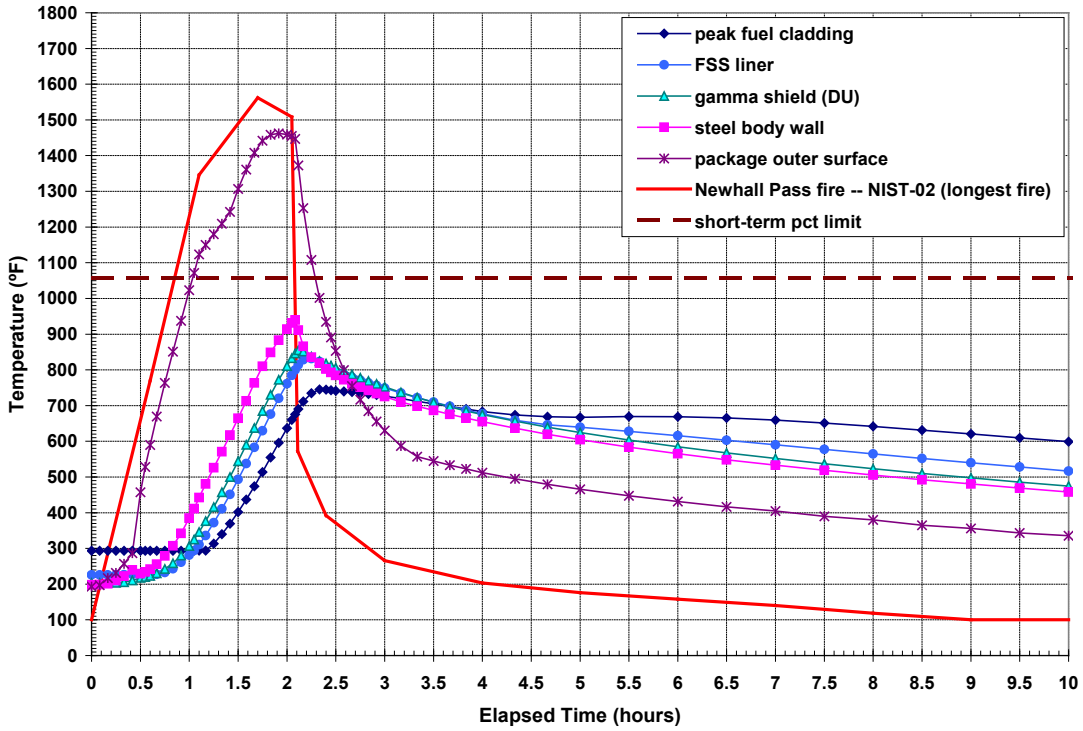

Figure 7.20. COBRA-SFS Results: Peak Component Temperatures in GA-4 Package for Longest Fire in Case NIST-03

The plots in Figure 7.19 and Figure 7.20 show a relatively steady decrease of all package components in the post-fire cooldown, except for the peak fuel cladding temperature. The overall maximum peak cladding temperature occurs after the end of the fire, and this temperature decreases more slowly than the internal components that do not generate heat. At about 5.5 hours, the maximum peak cladding temperature predicted with the COBRA-SFS model (Figure 7.20) exhibits a slight increase, to a secondary peak at about 6.5 hours. As discussed above for the similar results seen in case NIST-01 and case NIST-02, this behavior is due primarily to the thermal inertia of the fuel.

7.4 Thermal Results for NIST-04

The results for cases NIST-01, NIST-02, and NIST-03 show that within the bounds of the known fire timeline, a slower spread rate for the fire through the tunnel, which results in a longer overall fire duration, produces more severe conditions for the GA-4 package in the Newhall Pass Tunnel fire scenario. Case NIST-04 assumes the same relatively slow spread rate as case NIST-01, resulting in a total fire duration of approximately 5 hours. However, for case NIST-04, the burn rate for the individual vehicle fires is doubled, producing shorter, more intense local fires.

The peak fire temperature for every vehicle in the tunnel is higher in case NIST-04 than in the cases discussed above, even though the total fire duration is approximately the same as in NIST-01. However, the local fire duration on each vehicle is shorter (30-40 minutes, rather than approximately 1 hour), since the available fuel for a given fire is consumed in approximately half the time. The results obtained with the thermal models of this package are evaluated to determine if this case is more severe or less severe than the base case (NIST-01).

Section 7.4.1 shows the results obtained with the ANSYS and COBRA-SFS models for the hottest fire of this case, and Section 7.4.2 shows the results obtained for the longest fire of this case.

7.4.1 NIST-04: Hottest Fire

The temperatures representing the fire on vehicle #22 range from 1778°F (970°C) at the beginning of the local fire to a peak of 2012°F (1100°C), rising steadily for a period of approximately 20 minutes. This fire is initiated at about 1.8 hours into the transient, as is the hottest fire in case NIST-01, but with the higher burn rate postulated for the vehicle fires in NIST-04, the local fire on vehicle #22 lasts for less than 45 minutes, rather than a full hour. After the fire consumes this vehicle, the local temperature drops rapidly, beginning the post-fire cooldown at this location in the tunnel (as shown by the fire modeling results in Figure 3.5 and the local fire boundary conditions in Figure 4.4 for this case).

Figure 7.21 illustrates the thermal response of the GA-4 package to the fire transient with color thermographs showing radial and axial cross-sections of the package at 2.5 hours, approximately 5 minutes before the end of the local fire on vehicle #22. These graphics show that the fuel region is at this point the coldest part of the package cross-section, with the peak fuel temperature occurring at the outer corners of the assembly, where the fuel is most exposed to the external fire conditions.

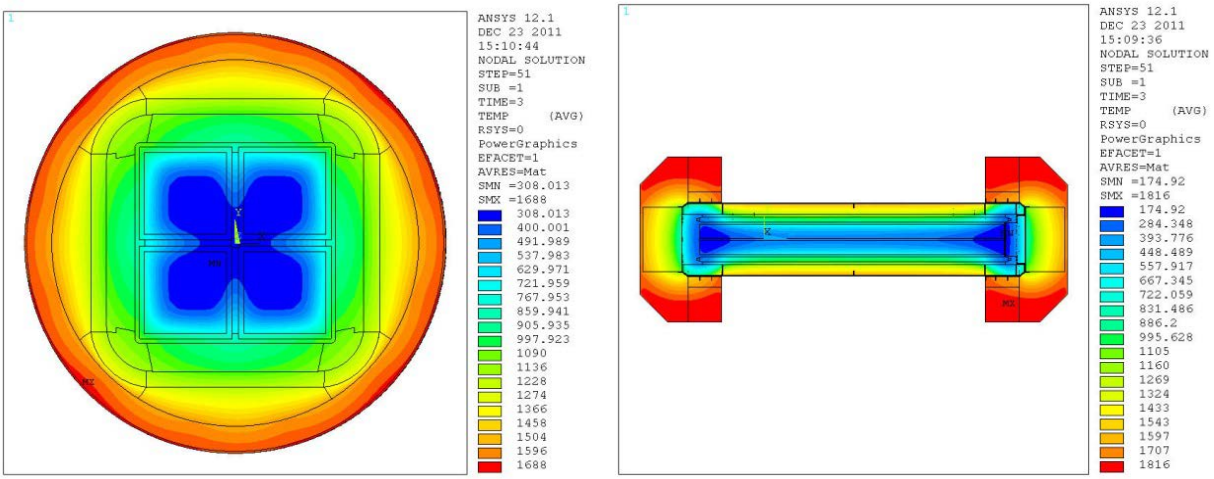

Figure 7.21. ANSYS Model: Radial and Axial Temperature (°F) Distributions in GA-4 Package at End of Fire on Vehicle #22 (hottest fire location) in Case NIST-04

The ANSYS model predicts a maximum temperature of 1074°F (579°C) in the fuel region for the hottest fire location of case NIST-04, which is slightly below the peak temperature of 1081°F (583°C) in the fuel region predicted for the hottest fire of case NIST-01 (see Section 7.1). For this fire scenario, the longer duration of the local vehicle fire is a more important factor than the maximum fire temperature in determining the response of the fuel to this fire transient.

As in case NIST-01, the ANSYS model predicts that the peak temperature in the fuel region for case NIST-04 slightly exceeds the short-term temperature limit of 1058°F (570°C) for zircaloy cladding, but by a smaller margin. The COBRA-SFS model, with a more realistic representation of the thermal response of the fuel, predicts a maximum peak cladding temperature of 853°F

(456°C), which is considerably below the short-term temperature limit for zircaloy cladding. The evolution of the peak component temperatures, shown in Figure 7.22 for the ANSYS model results and in Figure 7.23 for the COBRA-SFS model results, illustrates the overall response of the GA-4 package to this fire scenario at the hottest fire location.

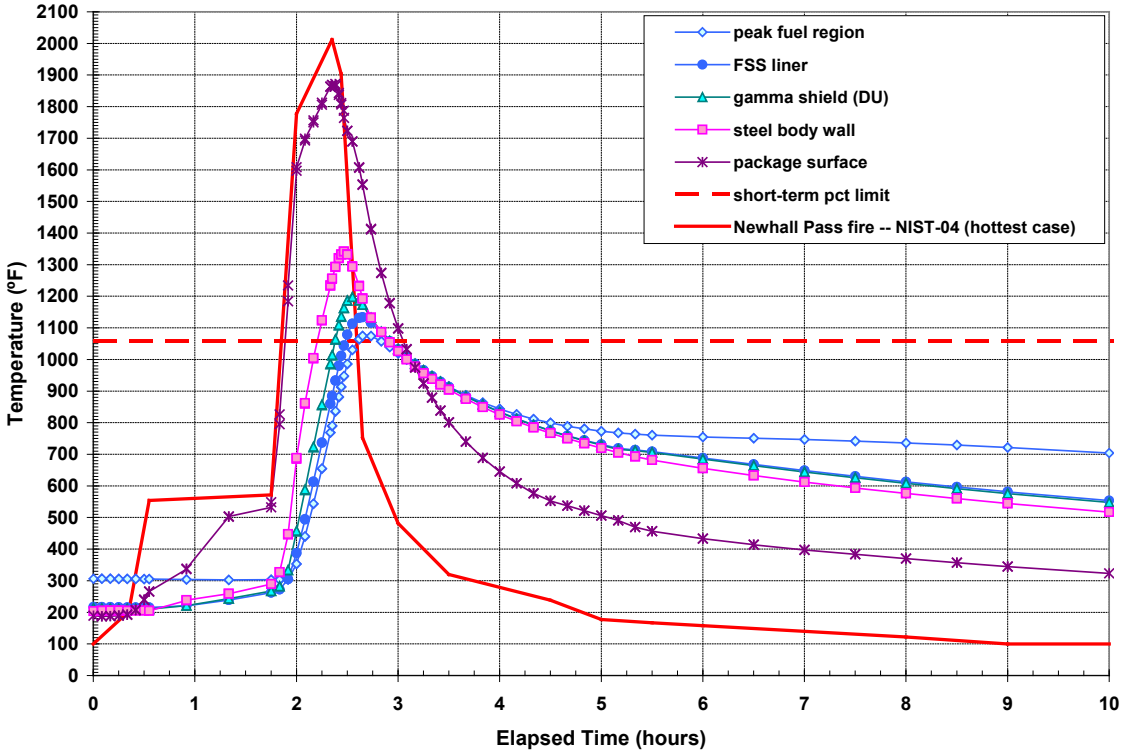

Figure 7.22. ANSYS Results: Peak Component Temperatures in GA-4 Package for Hottest Fire in Case NIST-04

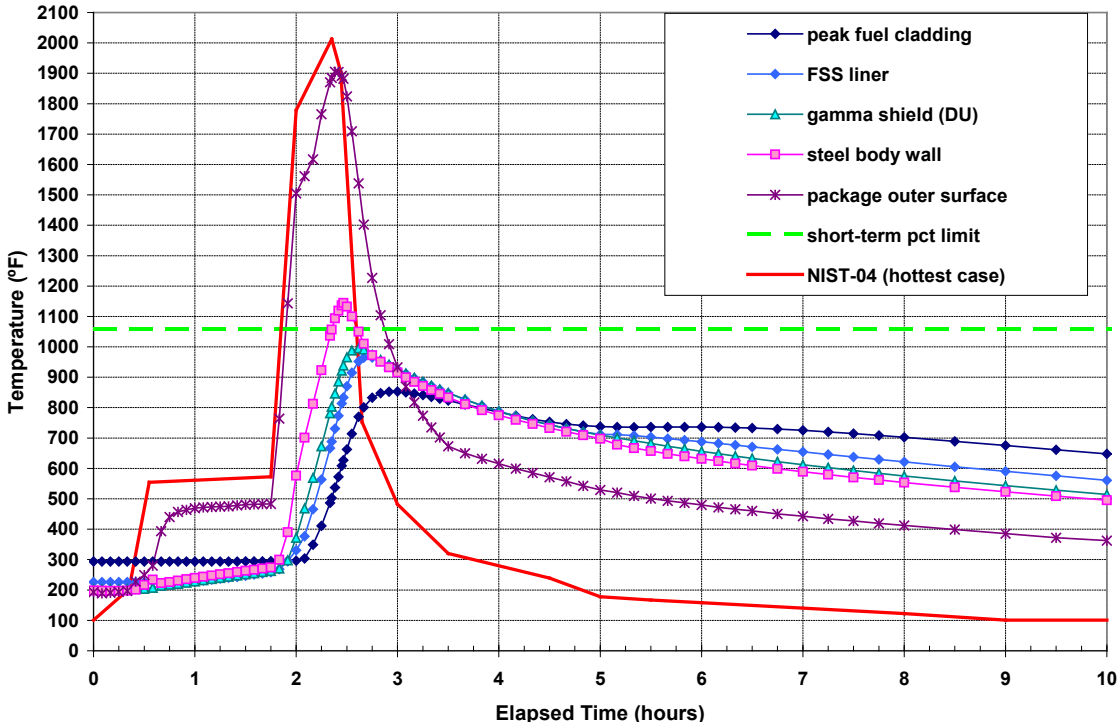

Figure 7.23. COBRA-SFS Results: Peak Component Temperatures in GA-4 Package for Hottest Fire in Case NIST-04

As in the previous cases discussed above, a relatively steady decrease of all package peak component temperatures is seen in Figure 7.22 and Figure 7.23 in the post-fire cooldown, except for the peak fuel cladding temperature. The overall maximum peak cladding temperature occurs after the end of the fire, and this temperature decreases more slowly than the internal components that do not generate heat. At about 5 hours, the maximum peak cladding temperature predicted with the COBRA-SFS model (Figure 7.23) exhibits a slight increase, to a secondary peak at about 6 hours. This behavior is due to the thermal inertia of the fuel, and the decreased rate of heat removal at the higher ambient temperatures during the fire and much of the long cooldown period.

7.4.2 NIST-04: Longest Fire

The fire on vehicle #31 is the last of the intense vehicle fires in the Newhall Pass tunnel, and in case NIST-04, it is initiated at about 4 hours into the transient. This is essentially the same time as in case NIST-01, which assumes the same spread rate. The boundary temperature at this location rises to about 400°F (204°C) during the first 30 minutes of the fire, then to about 518°F (270°C) after approximately 2 hours, due to the flow of hot gases from the fire as it engulfs the other vehicles in the tunnel in succession. These preheating temperatures are comparable to the values in case NIST-01, which has essentially the same overall fire duration, but are significantly lower than in the cases with faster assumed spread rates (NIST-02 and NIST-03).

Once the fire reaches vehicle #31, at just over 4 hours, the boundary temperature representing the fire at this location rises rapidly to 1679°F (915°C) then continues to rise gradually to 1742°F (950°C) over a period of approximately 25 minutes. In the remaining 4 minutes of the fire on this vehicle, the temperature drops to about 1632°F (889°C), then plummets to about 752°F

(400°C). Since this is the last vehicle involved in the tunnel fire, the end of this fire is the beginning the post-fire cooldown. At this time in the fire duration, the forced convection boundary condition on the package (in both the hottest fire location and the longest fire location) is replaced with natural convection to still air.

Figure 7.24 illustrates the thermal response of the GA-4 package to the fire transient with color thermographs showing radial and axial cross-sections of the package at 4.5 hours, approximately 9 minutes before the end of the local fire on vehicle #31. As with the results in Figure 7.21 for the hottest fire location (vehicle #22), these graphics show that the fuel region is the coldest part of the package cross-section at the end of the fire, with the peak fuel temperature occurring at the outer corners of the assembly, where the fuel is most exposed to the external fire conditions.

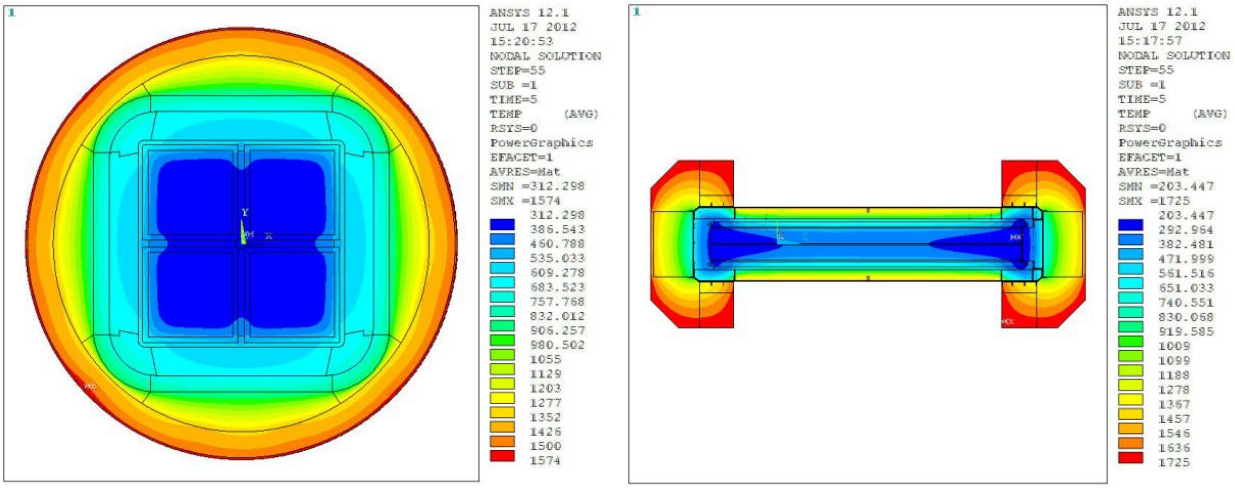

Figure 7.24. ANSYS Model: Radial and Axial Temperature (°F) Distributions in GA-4 Package at End of Fire on Vehicle #31 (longest fire location) in Case NIST-04

For the longest fire location in the tunnel for this case, the ANSYS model predicts a maximum temperature of only 867°F (464°C) in the fuel region. This is below the short-term temperature limit of 1058°F (570°C) for zircaloy cladding, and is also significantly lower than the peak fuel region temperature of 1074°F (579°C) that the ANSYS model predicts for the hottest fire location of case NIST-04. The COBRA-SFS model also predicts a lower maximum peak cladding temperature for this longest fire location, compared to the hottest fire location. The peak cladding temperature is only 693°F (367°C) for the longest fire of this case, compared to the 853°F (456°C) value predicted with the COBRA-SFS model for the hottest fire of this case.

This trend is consistent with the ANSYS model results for the previous cases, indicating that the longest fire for case NIST-04 is significantly less severe than the hottest fire, in terms of its potential effect on the GA-4 package, even with the long preheat of the package prior to the fire reaching the location of vehicle #31. The evolution of the peak component temperatures in response to this local fire are shown in Figure 7.25 for the ANSYS model results and in Figure 7.26 for the COBRA-SFS model results.

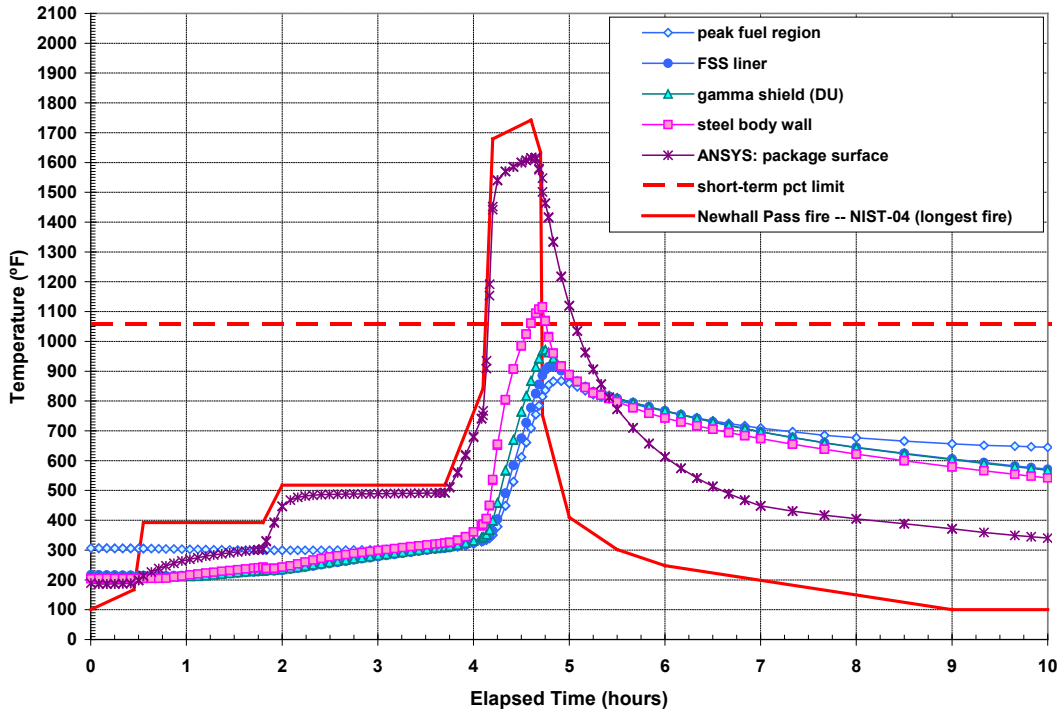

Figure 7.25. ANSYS Results: Peak Component Temperatures in GA-4 Package for Longest Fire in Case NIST-04

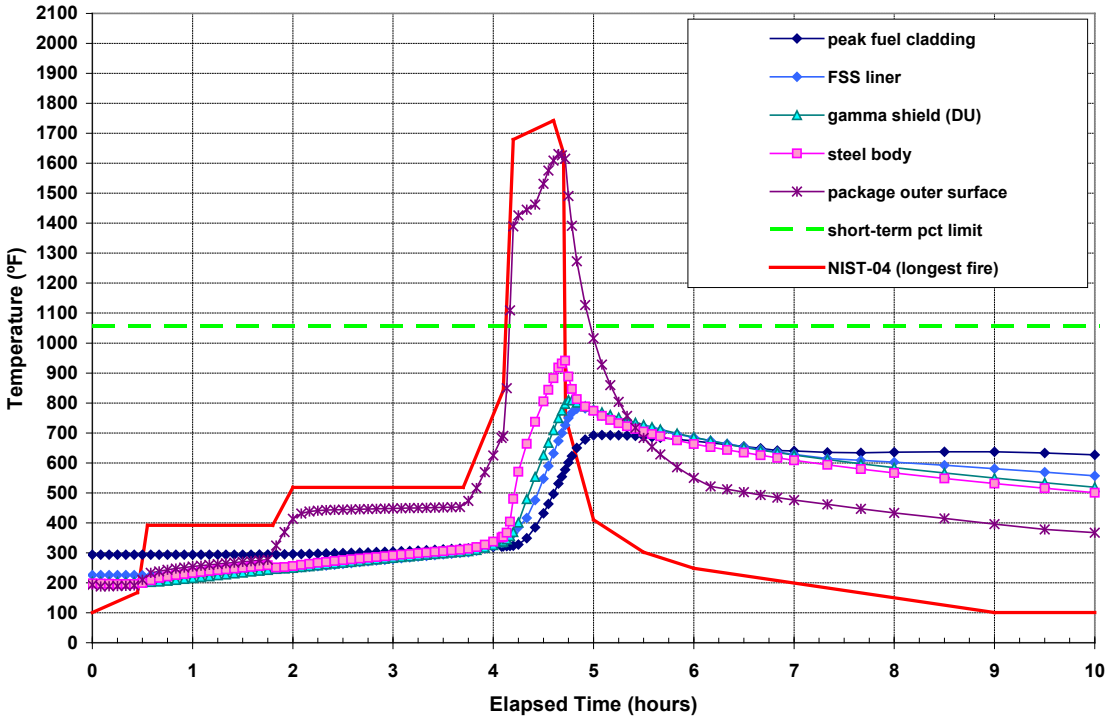

Figure 7.26. COBRA-SFS Results: Peak Component Temperatures in GA-4 Package for Longest Fire in Case NIST-04

As with the results presented above for cases NIST-01, -02, and -03, the plots in Figure 7.25 and Figure 7.26 show a relatively steady decrease of all package components in the post-fire cooldown, except for the peak fuel cladding temperature. The overall maximum peak cladding temperature occurs after the end of the fire, and this temperature decreases more slowly than the internal components that do not generate heat. At about 8 hours, the maximum peak cladding temperature predicted with the COBRA-SFS model (Figure 7.26) exhibits a slight increase, to a secondary peak at about 8.5 hours. This behavior is due to the thermal inertia of the fuel, and the decreased rate of heat removal at the higher ambient temperatures during the fire and much of the post-fire cooldown.

As discussed in Section 6.0, the boundary conditions at the hottest fire location and longest fire location for case NIST-04 of the Newhall Pass fire scenario both provide a conservative fire environment for the GA-4 package. Based on the results obtained in the analysis of this fire scenario with the ANSYS model and the COBRA-SFS model, the package experiences less severe conditions than in case NIST-01, even though the peak fire temperatures are hotter. The shorter duration of the individual vehicle fires, due to the higher specified burn rate, is more important than the higher peak fire temperatures (compared to NIST-01) in evaluating the GA-4 package response to this fire scenario.

7.5 Thermal Results for NIST-06

The results for cases NIST-01, NIST-02, NIST-03, and NIST-04 show that, all other things being equal, a longer overall fire duration and longer individual vehicle fires within the total fire duration, produces more severe conditions for the GA-4 package in the Newhall Pass Tunnel fire scenario. The long-duration fire cases (NIST-01 and NIST-04) are bounding on the two cases with possibly more realistic fire duration estimates (NIST-02 and NIST-03). However, in all of these cases, the combustible mass of fuel was represented for a “typical” cargo on all vehicles, even the ones running empty, to bound the large uncertainty in available fuel for the fire. Case NIST-06 was developed to investigate the effect of the actual cargo loads of the various vehicles, insofar as they could be determined from the available information. Case NIST-06 assumes the same relatively slow spread rate as case NIST-01 as a bounding conservatism, resulting in a total fire duration of approximately 4.5 hours.

Case NIST-06 also assumes the same burn rate for the vehicle fires, but because the fuel load varies with vehicle contents (or lack of contents, for the vehicles running empty), the fire duration on each vehicle varies significantly, from less than 30 minutes to slightly more than an hour. Due to the variable cargo loads, the hottest fire location is on vehicle #26. The longest fire location is vehicle #31, which actually is the last vehicle to burn in all cases and therefore experiences the longest period at elevated temperatures within the tunnel during fire. However, in case NIST-06, the fire on this vehicle is of very short duration (~26 minutes) and reaches a relatively low peak fire temperature, since it was running empty at the time of the accident. As a conservatism, the longest fire location in case NIST-06 is defined as vehicle #30. The fire on this vehicle is predicted to last nearly twice as long as the fire on vehicle #31, and reaches a significantly higher peak fire temperature (as shown in Figure 3.7). The fire on vehicle #30 ends at essentially the same time as the fire on vehicle #31, such that the total fire duration is the same with either vehicle location selected as the longest fire location.

The results obtained for case NIST-06 with the thermal models of the GA-4 package are evaluated to determine if this more realistic case is more severe or less severe than the base case (NIST-01). Section 7.5.1 shows the results obtained with the ANSYS and COBRA-SFS models for the hottest fire of this case, and Section 7.5.2 shows the results obtained for the longest fire of this case.

7.5.1 NIST-06: Hottest Fire

The temperatures representing the fire on vehicle #26 range from 1176°F (636°C) at the beginning of the local fire and reach a peak of 1878°F (1025°C), rising over a period of approximately 50 minutes. This fire is initiated at about 2.55 hours into the transient, and lasts for about 80 minutes, which is about 20 minutes longer than the local fire duration at the hottest fire location (vehicle #23) in case NIST-01. After the fire consumes this vehicle, the local temperature drops rapidly, beginning the post-fire cooldown at this location in the tunnel (as shown by the fire modeling results in Figure 3.7 and the local fire boundary conditions in Figure 4.5 for this case).

Figure 7.27 illustrates the thermal response of the GA-4 package to the fire transient with color thermographs showing radial and axial cross-sections of the package at 3.5 hours, approximately 10 minutes before the end of the local fire on vehicle #26. These graphics show that in this case, as in all the other cases evaluated, the fuel region is at this point the coldest part of the package cross-section, with the peak fuel temperature occurring at the outer corners of the assembly, where the fuel is most exposed to the external fire conditions.

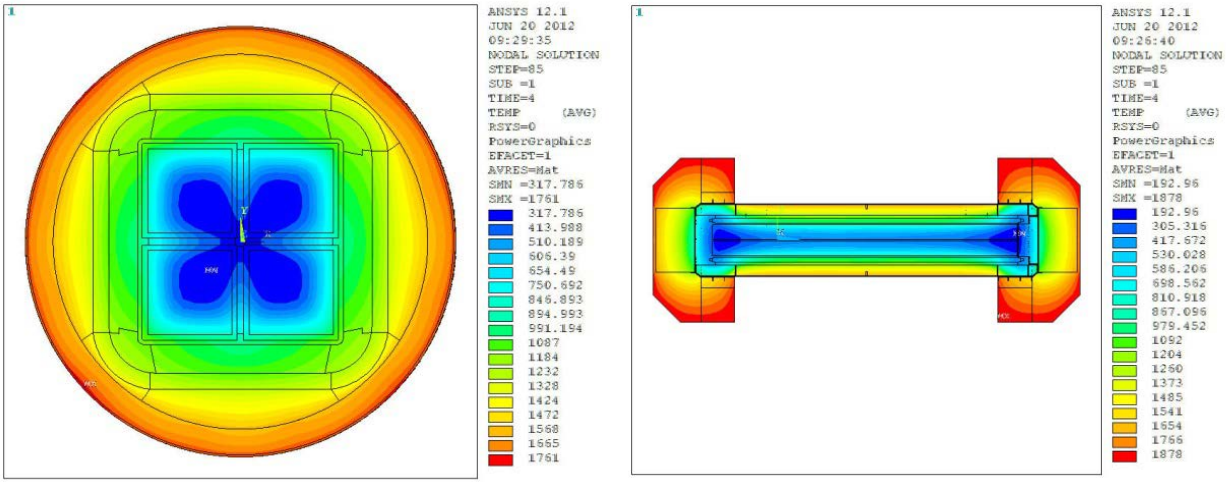

Figure 7.27. ANSYS Model: Radial and Axial Temperature (°F) Distributions in GA-4 Package at End of Fire on Vehicle #26 (hottest fire location) in Case NIST-06

The ANSYS model predicts a maximum temperature of 1217°F (658°C) in the fuel region for the hottest fire location of case NIST-06. The COBRA-SFS model, with a more realistic representation of the thermal response of the fuel, predicts a maximum peak cladding temperature of 994°F (534°C). For both models, this maximum temperature is significantly higher than the maximum values predicted for the other four cases. This is an interesting result, because the hottest fire for case NIST-06 actually has a lower peak temperature than the hottest fire in case NIST-04, and is only slightly higher than the peak temperature in case NIST-01.

The significant difference appears to be the duration of the local fire exposure for each case. In case NIST-01, the hottest fire lasts approximately 65 minutes; in case NIST-04, it lasts only about 43 minutes. In case NIST-06, the fire at the hottest fire location lasts approximately 80 minutes. This is also the cause of the larger divergence between the peak cladding temperature results obtained with the ANSYS model and the COBRA-SFS model, compared to the cases with shorter fire durations. The k-effective model for the fuel region is a steady-state model, and does not adequately approximate transient heat transfer behavior within the fuel bundle in response to the fire. The k-effective model is by design conservative, and this conservatism tends to increase with increasing temperature. As a result, in this case, the ANSYS model predicts a peak fuel cladding temperature that is significantly above the short-term temperature limit of 1058°F (570°C) for zircaloy cladding. The COBRA-SFS model, with a more physically accurate representation of the thermal response of the fuel, predicts a maximum peak cladding temperature that is somewhat lower than this limit. Figure 7.28 illustrates the increasing conservatism of the k-effective model in the plot comparing the peak cladding temperature over time for the conditions of the hottest fire location.

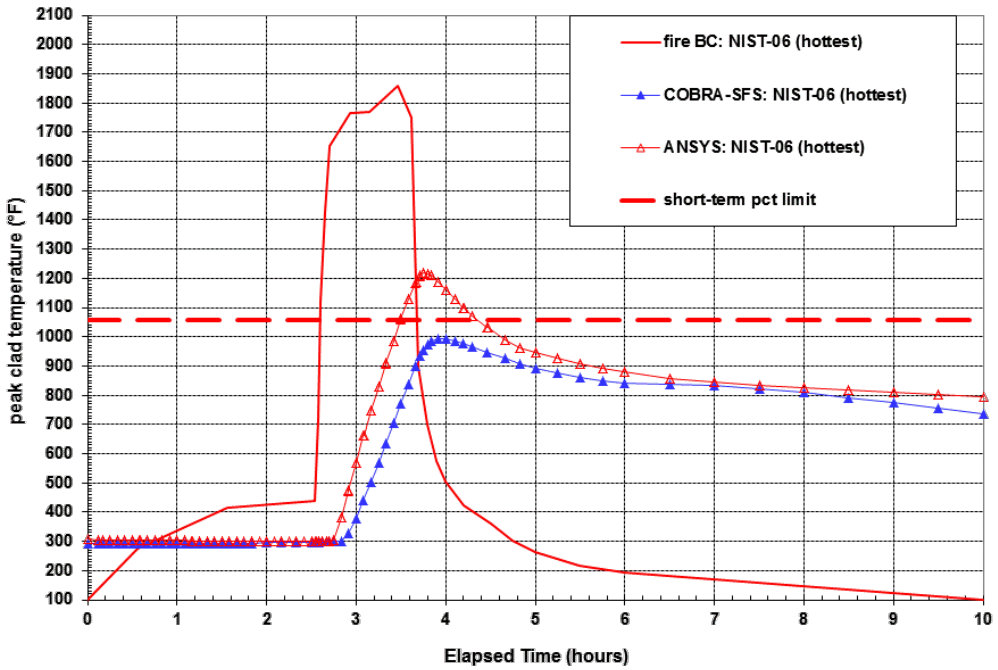

Figure 7.28. ANSYS Results: Peak Fuel Temperatures in GA-4 Package for Hottest Fire in Case NIST-06

As shown in Figure 7.28, the ANSYS model results are initially only slightly more conservative than the COBRA-SFS model results, such that the difference hardly shows on the scale of the plot that includes the fire transient. However, as the boundary temperature representing the fire rises and the transient becomes more severe, the difference between the predicted values from the two models increases, with the ANSYS model showing a more conservative response. After the fire, in the post-fire cooldown, as conditions begin to approach a new steady-state, the difference between the predicted values for the two models once again becomes small, with the ANSYS model only slightly more conservative than the COBRA-SFS model. This difference is reflected in the evolution of the peak temperatures of the inner components of the package, as shown in Figure 7.29 for the ANSYS model results and in Figure 7.30 for the COBRA-SFS model results.

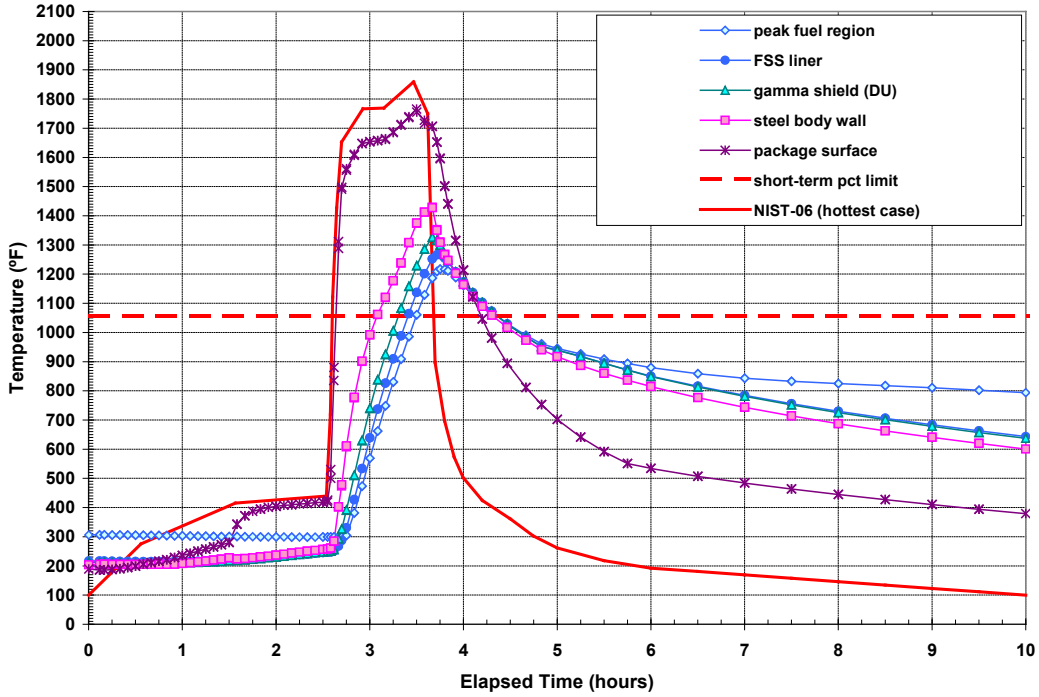

Figure 7.29. ANSYS Results: Peak Component Temperatures in GA-4 Package for Hottest Fire in Case NIST-06

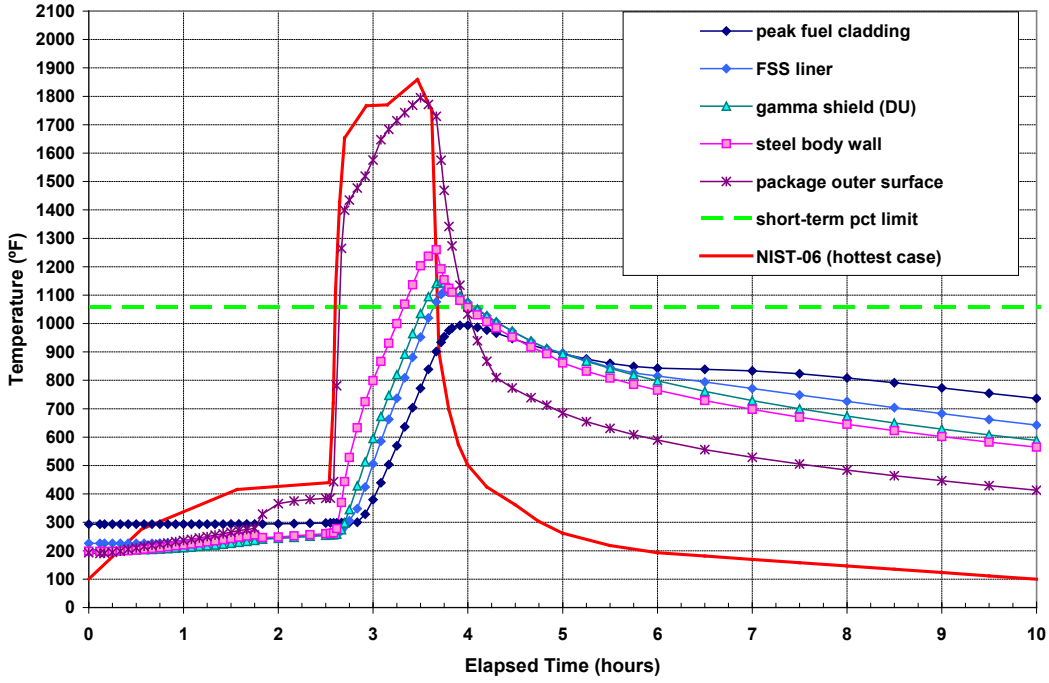

Figure 7.30. COBRA-SFS Results: Peak Component Temperatures in GA-4 Package for Hottest Fire in Case NIST-06

As in the previous cases discussed above, a relatively steady decrease of all package peak component temperatures is seen in Figure 7.29 and Figure 7.30 in the post-fire cooldown, except for the peak fuel cladding temperature. The overall maximum peak cladding temperature occurs after the end of the fire, and this temperature decreases more slowly than the internal components that do not generate heat. At about 6 hours, the maximum peak cladding temperature predicted with the COBRA-SFS model (Figure 7.30) exhibits a slight increase, to a secondary peak at about 6.5 hours. This behavior is due to the thermal inertia of the fuel, and the decreased rate of heat removal at the higher ambient temperatures during the fire and much of the long cooldown period.

7.5.2 NIST-06: Longest Fire

The fire on vehicle #30 is initiated at about 3.8 hours into the transient, and is the last of the vehicles in the tunnel that has a substantial cargo to be consumed by the fire. The boundary temperature at this location rises to about 361°F (183°C) during the first 2 hours of the fire, then to about 553°F (289°C) by the time of the start of the local vehicle fire, due to the flow of hot gases from the fire as it engulfs the other vehicles in the tunnel in succession. This preheating is more gradual than in case NIST-01, but reaches higher temperatures prior to the local vehicle fire. However, the preheating temperatures reached in case NIST-06 for the longest fire location are significantly lower than in the cases with faster assumed spread rates for the fire (NIST-02 and NIST-03).

Once the fire reaches vehicle #30, the boundary temperature representing the fire at this location rises rapidly to 1646°F (897°C), which bounds the maximum temperature reached in the fire on this vehicle for this case. The fire temperature holds steadily near this value for nearly the entire 43 minutes of the fire duration, then drops rapidly to about 752°F (400°C) in less than 5 minutes. This coincides with the end of the shorter fire on the empty vehicle (vehicle #31) that is the vehicle nearest the tunnel entrance, signaling the end of this fire and the beginning of the post-fire cooldown. At this point in the fire calculation, the forced convection boundary condition on the package (in both the hottest fire location and the longest fire location) is replaced with natural convection to still air.

Figure 7.31 illustrates the thermal response of the GA-4 package to the fire transient with color thermographs showing radial and axial cross-sections of the package at 4.5 hours, approximately 6 minutes before the end of the local fire on vehicle #30. As with the results in Figure 7.27 for the hottest fire location (vehicle #26), these graphics show that the fuel region is the coldest part of the package cross-section at the end of the fire, with the peak fuel temperature occurring at the outer corners of the assembly, where the fuel is most exposed to the external fire conditions.

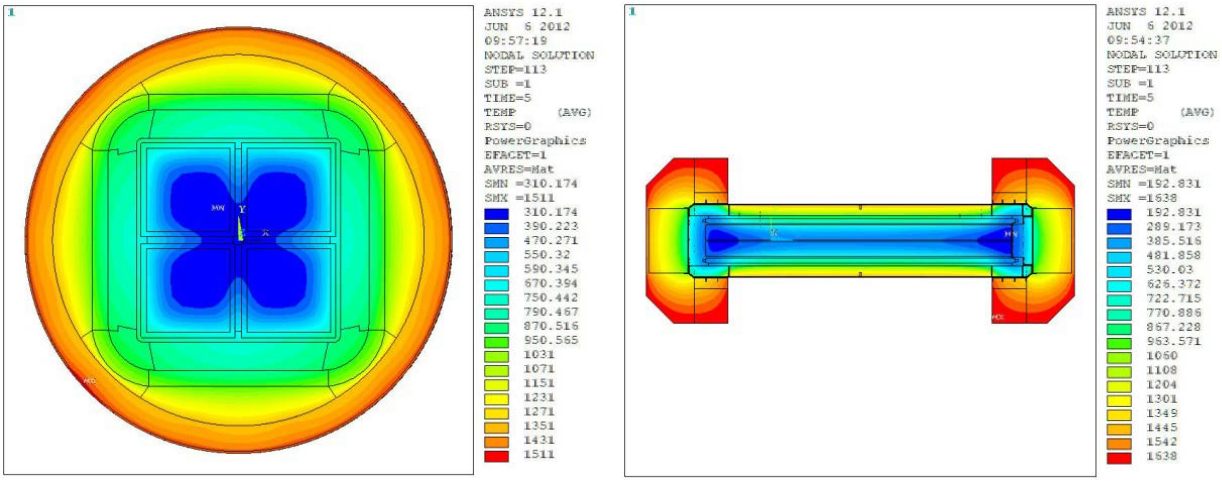

Figure 7.31. ANSYS Model: Axial and Radial Temperature (°F) Distributions in GA-4 Package at ~6 minutes Before End of Fire on Vehicle #30 (longest fire location) in Case NIST-06

For the longest fire location in the tunnel for this case, the ANSYS model predicts a maximum temperature of only 882°F (472°C) in the fuel region. This is below the short-term temperature limit of 1058°F (570°C) for zircaloy cladding, and substantially lower than the maximum fuel region temperature predicted for the hottest fire of this case. It is also significantly lower than the highest value that the ANSYS model predicts for the longest fire in all other cases evaluated. This is due primarily to the short duration of this local fire (less than 40 minutes).

The COBRA-SFS model also predicts a lower maximum peak cladding temperature for this longest fire location, compared to the hottest fire location. The peak cladding temperature is only 702°F (372°C) for the longest fire of this case, compared to the 994°F (534°C) value predicted with the COBRA-SFS model for the hottest fire of this case. This trend is consistent with the ANSYS model results, indicating that the longest fire for case NIST-06 is significantly less severe than the hottest fire, in terms of its potential effect on the GA-4 package, even with the long preheat of the package prior to the fire reaching the location of vehicle #30. The evolution of the peak component temperatures in response to this local fire are shown in Figure 7.32 for the ANSYS model results and in Figure 7.33 for the COBRA-SFS model results.

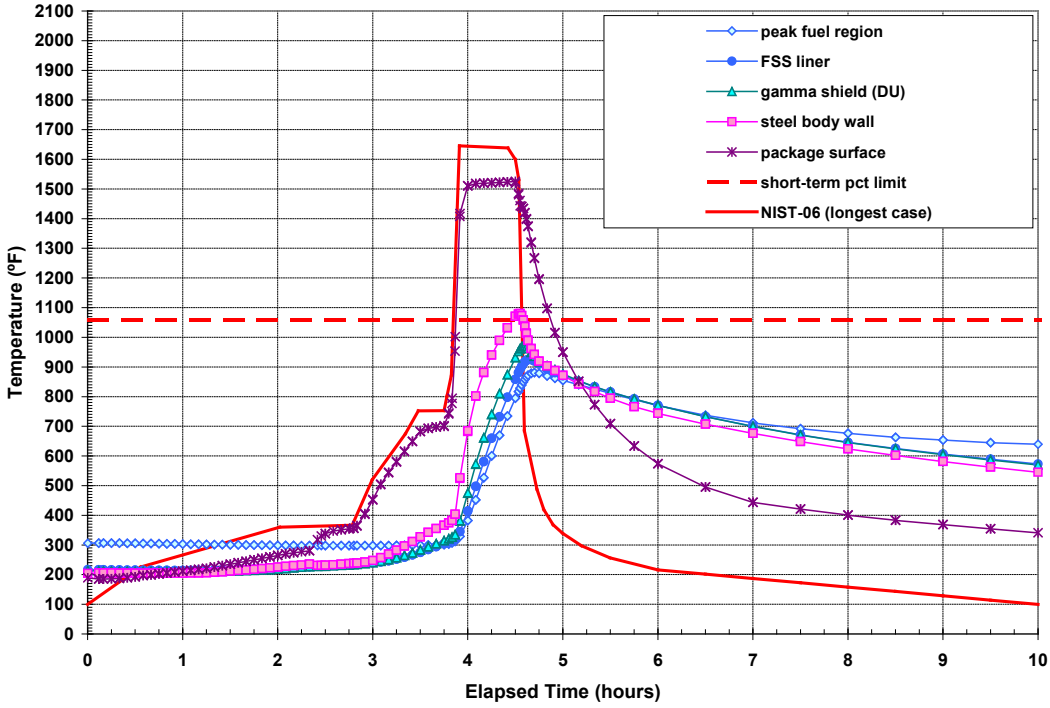

Figure 7.32. ANSYS Results: Peak Component Temperatures in GA-4 Package for Longest Fire in Case NIST-06

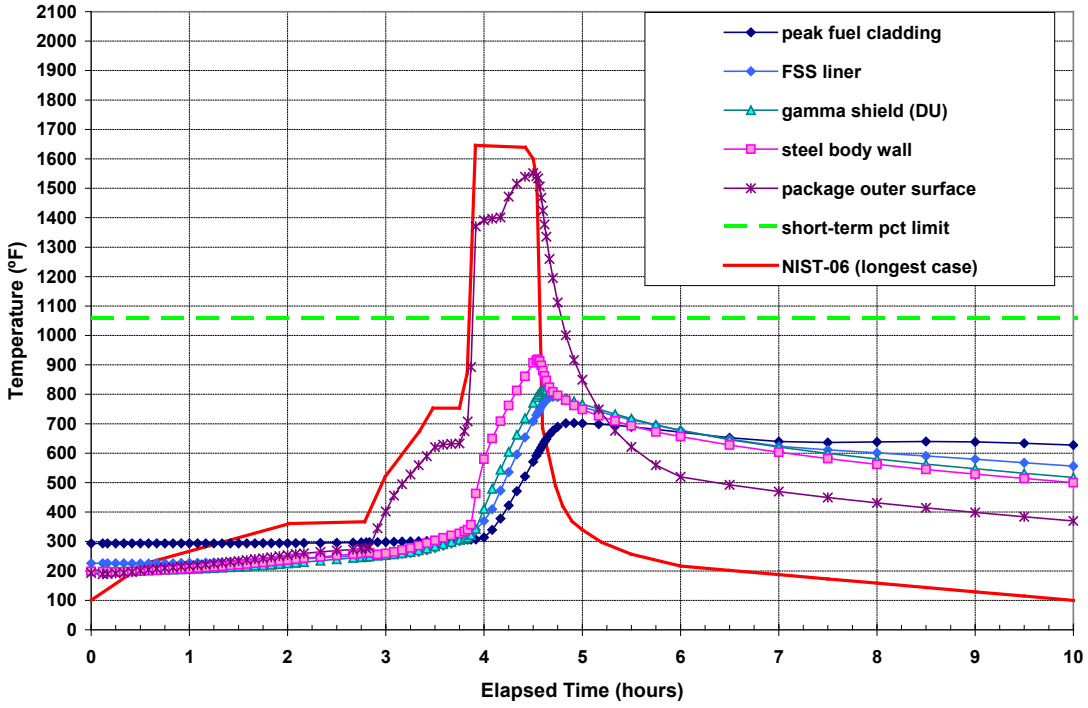

Figure 7.33. COBRA-SFS Results: Peak Component Temperatures in GA-4 Package for Longest Fire in Case NIST-06

As with the results presented above for cases NIST-01, -02, -03, and -04, the plots in Figure 7.32 and Figure 7.33 show a relatively steady decrease of all package components in the post-fire cooldown. The overall maximum peak cladding temperature occurs after the end of the fire, and this temperature decreases more slowly than the internal components that do not generate heat. At about 8 hours, the maximum peak cladding temperature predicted with the COBRA-SFS model (Figure 7.33) exhibits a slight increase, to a secondary peak at about 9 hours. This behavior is due to the thermal inertia of the fuel and the decreased rate of heat removal at the higher ambient temperatures during the fire and most of the post-fire cooldown.

7.6 Summary of Thermal Results for All Cases

In assessing the potential effects of the Newhall Pass Tunnel fire scenario on an SNF package, the results presented in Sections 7.1 through 7.5 show that there are two significant issues to consider; how hot did the fire get, and how long did it last. The fire duration involves both the overall duration of the fire within the tunnel, and the duration of the local vehicle fire at the postulated location of the SNF package. Table 7.1 summarizes the peak temperatures obtained for the cases evaluated, tabulated with the peak fire temperature, and fire duration. (Note that for convenience, the hottest fire is denoted by "A" and the longest fire is denoted by "B" in the case numbers in Table 7.1).

The results in Table 7.1 suggest that the total fire duration may be the most important factor in determining the response of the peak fuel temperature to the fire scenario. This is more clearly illustrated by the bar charts in Figure 7.34 (for the hottest fire locations) and Figure 7.35 (for the longest fire locations) for each case.

Table 7.1. Maximum Peak Fuel Cladding Temperatures for All Cases

Case	Peak Fire °F (°C)	Total Fire Duration (hours)	Local Fire Duration (minutes)	ANSYS: Peak Fuel Region °F (°C)	COBRA-SFS: Peak Cladding °F (°C)
NIST-01-A	1721 (938)	5.1	65	1081 (583)	882 (472)
NIST-01-B	1579 (859)		56	954 (512)	767 (408)
NIST-02-A	1706 (930)	3.0	67	1010 (544)	818 (436)
NIST-02-B	1648 (898)		64	1020 (549)	834 (445)
NIST-03-A	1668 (909)	2.0	62	921 (494)	742 (395)
NIST-03-B	1570 (854)		64	913 (490)	745 (396)
NIST-04-A	1991 (1088)	4.7	43	1074 (579)	853 (456)
NIST-04-B	1736 (947)		36	867 (464)	693 (367)
NIST-06-A	1861 (1016)	4.5	78	1217 (659)	994 (534)
NIST-06-B	1646 (897)		43	881 (472)	702 (372)

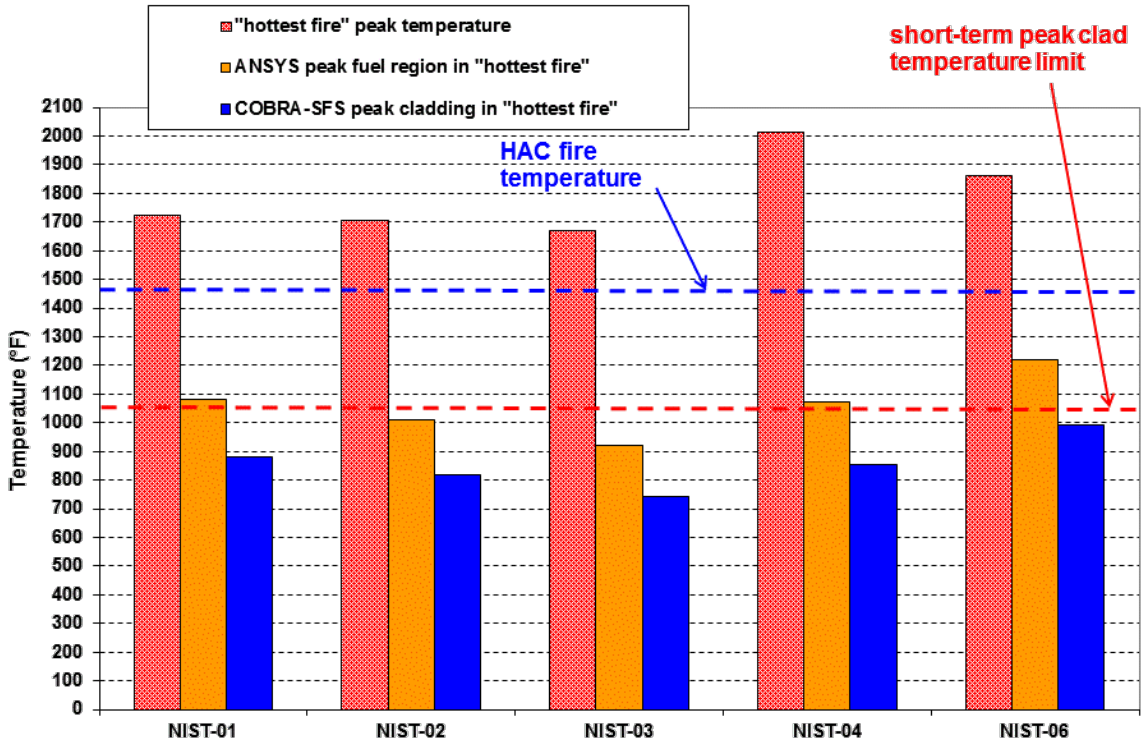

Figure 7.34. Comparing Maximum Temperatures in All Cases for “Hottest Fire”

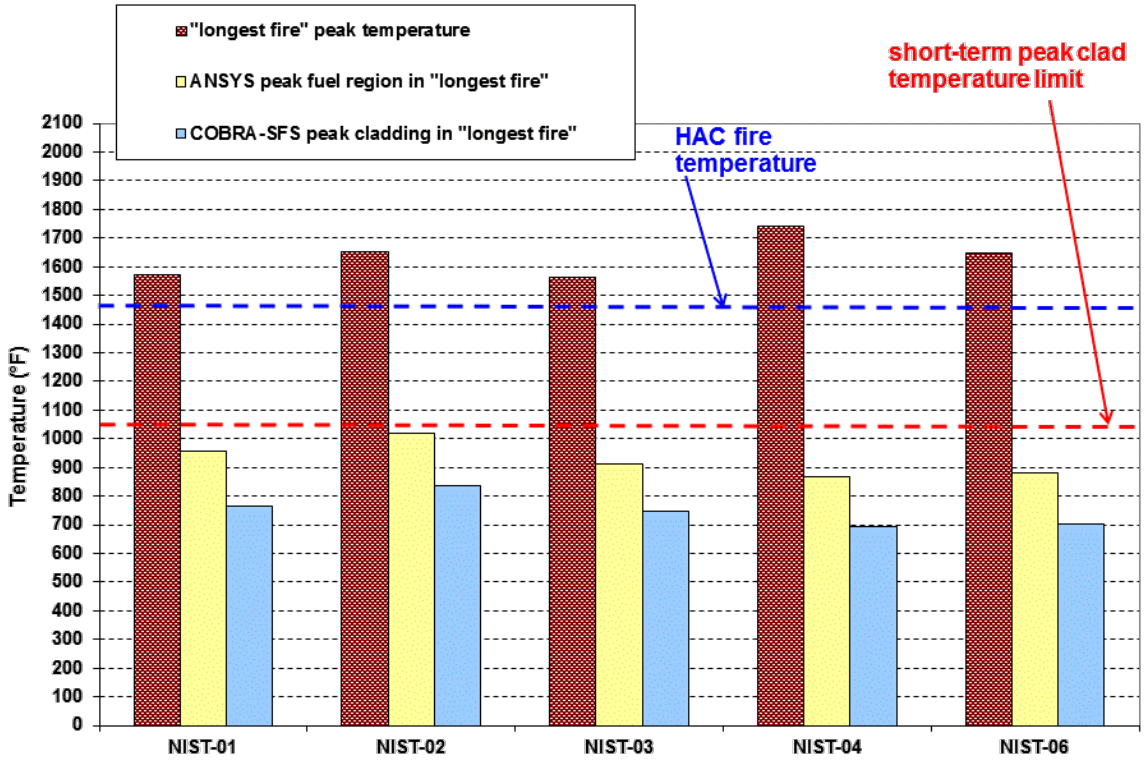

Figure 7.35. Comparing Maximum Temperatures in All Cases for “Longest Fire”

Figure 7.34 for the hottest fire comparison shows two interesting trends for the three cases with bounding fuel load assumed for the fire (NIST-01, -02, and -03). As discussed in Sections 7.1, 7.2, and 7.3, cases NIST-01, -02, and -03 show that the predicted maximum peak clad temperature for the hottest fire decreases with decreasing total overall fire duration (for essentially constant local fire duration), even though the peak fire temperature decreases only slightly with decreasing total fire duration for these three cases.

Similarly, the importance of the local fire duration at the hottest fire location is shown by the comparison between case NIST-01 and NIST-04 in Figure 7.31. These cases are essentially identical, except for the specified burn rate, which results in individual vehicle fires that are only about half as long as the corresponding vehicle fires in NIST-01. The higher burn rate in case NIST-04 yields a peak fire temperature that is significantly hotter than that in case NIST-01, but the maximum peak clad temperature (from the COBRA-SFS model) and the maximum peak fuel region temperature (from the ANSYS model) are slightly *lower* than the values predicted for case NIST-01. This suggests that a shorter fire can have less severe effects on a SNF package, even if it reaches a higher temperature than a longer fire. It is not so much the heat coming into the package from the fire that adversely affects the fuel; it is the lack of heat removal from the fuel during and after the fire (in the cooldown portion of the fire transient) that is more likely to be the problem.

The comparison between case NIST-06 and NIST-01 in Figure 7.34 further supports this trend. The hottest fire in case NIST-06 has a peak temperature approximately midway between those of case NIST-01 and case NIST-04, but the predicted maximum fuel region and peak cladding temperatures for case NIST-06 are higher than those in either NIST-01 or NIST-04. The predicted temperatures for case NIST-06 are in fact the highest of all cases evaluated. This appears to be due primarily to the longer duration of the fire in the hottest fire location for case NIST-06, which is about 15 minutes longer than the corresponding hottest fire in case NIST-01, and about 35 minutes longer than the corresponding fire in case NIST-04.

The trends shown in the chart in Figure 7.35 for the longest fire location (near the tunnel entrance), are similar to those noted above for the comparisons in Figure 7.34, but are somewhat less distinct. The peak fire temperatures are significantly lower than those of the hottest fire for a given case, resulting in significantly less severe fire conditions. The more realistic estimate of combustible load for each vehicle evaluated in case NIST-06 results in a less severe fire at the longest fire location, compared to the “typical” load assumed for all vehicles in cases NIST-01 through -04.

The most severe fire conditions at the location of vehicle #31 (the vehicle nearest the tunnel entrance) are for case NIST-02, rather than case NIST-01, comparing the four cases with uniform combustible fuel loads on all vehicles. This may be due in part to the relatively high “pre-fire” temperatures at this location for the two hours prior to the fire reaching vehicle #31. In case NIST-01, the ambient temperature at this location prior to the beginning of the local vehicle fire is much lower, compared to the conditions at this location in case NIST-01. In case NIST-03, the ambient temperature rises more rapidly than in case NIST-02, but the entire fire duration in case NIST-03 is only about two hours.

Although the pre-fire conditions at the longest fire location are significantly hotter than the design-basis steady-state conditions for the GA-4 package, these results suggest that the preheating time in this fire scenario is not long enough to significantly affect the overall fuel cladding temperatures prior to the fire. In all cases evaluated, the peak cladding temperature does not show a noticeable increase until after the start of the local vehicle fire, and the highest

temperature on the outer corner rod of an assembly, which is the location most exposed to the fire, increases by less than 100°F (55°C), even with up to 4 hours of preheating in this fire scenario.

This result may seem inconsistent with the significant effect that the thermal inertia of the package has on the slow cooldown rate of the package and the secondary maximum in the peak cladding temperature observed in all cases. It is, in fact, the same phenomenon, but in reverse. It takes time to heat up the relatively massive stainless steel package body and DU gamma shield enough to significantly affect the radial gradient within the fuel assemblies. For some time during the preheating period, the fuel region (which is initially the hottest part of the package), continues to dump heat to the package body and gamma shield, even as these components are being heated from the outside by the increasing ambient boundary temperature.

8.0 POTENTIAL CONSEQUENCES

Potential adverse consequences of a severe accident involving an SNF transportation package fall into two categories; loss of shielding, and a failure of containment boundary of the package. Loss of neutron or gamma shielding could potentially result in a direct radiation dose to an individual in close proximity to the package. Failure of any of the components that make up the containment boundary (e.g., package seals) could result in a release of radioactive material from inside the package, potentially resulting in a direct radioactive dose to first-responders at the scene of the accident, or possibly to members of the public in the surrounding area. Loss of shielding as a potential consequence of the Newhall Pass tunnel fire scenario is discussed in Section 8.1. Package seal performance is discussed in Section 8.2 and Section 8.3 evaluates the potential for a release from the GA-4 package as a result of the conditions predicted for this conservative representation of the Newhall Pass Tunnel fire scenario.

8.1 Potential for Loss of Shielding

The potential for increased neutron and gamma radiation dose rates from the GA-4 package as a result of exposure to the Newhall Pass tunnel fire scenario was evaluated. Direct radioactive dose rate limits are specified in 10 CFR 71 for normal conditions and accident conditions. As a licensed transportation package, the design basis of the GA-4 complies with the regulatory limits for all conditions of transport.

Section 8.1.1 describes the consequences of loss of neutron shielding for the GA-4 in the Newhall Pass tunnel fire scenario. Section 8.1.2 discusses the potential for loss of gamma shielding.

8.1.1 Neutron Shielding

Neutron shielding for the GA-4 package is provided by neutron-absorbing liquid in an annular tank surrounding the steel body of the package (see Sections 5.1 and 5.2 for details of package geometry). The shielding material is a mixture of 56% propylene glycol and water, with 1% dissolved boron. The neutron shield tank is not generally expected to survive the hypothetical accident conditions prescribed in 10 CFR 71 for SNF transportation packages, which include a 30-minute fully engulfing fire at “1475°F (800°C).”

The GA-4 package is designed to be in compliance with the regulatory limits for all conditions of transport. Loss of the neutron shield tank contents is a design-basis assumption for HAC, and analyses presented in the package SAR (General Atomics 1998) assume loss of the neutron shield in all accident scenarios, including the HAC fire. The conditions of the Newhall Pass Tunnel fire, although more severe than the HAC fire, can do no more damage to the neutron shield of the GA-4 than is assumed *a priori* in the HAC fire evaluations. Therefore, the GA-4 package would be expected to remain below the dose limits after loss of neutron shielding in the Newhall Pass tunnel fire scenario, as well.

8.1.2 Gamma Shielding

Gamma shielding for the GA-4 is provided by a 2.64-inch (6.7-cm) thick layer of DU encased in the stainless steel body of the package. The DU layer extends a few inches beyond the full axial length of the package inner cavity, to assure complete coverage of the active fuel length, and is positioned between the stainless steel inner liner and the 1.5-inch (3.81-cm) thick stainless steel body of the package.

The Newhall Pass Tunnel fire scenario does not expose the package to impacts that would exceed its design-basis loading, and therefore would not be expected to cause structural damage to the package. The DU material experiences a significant increase in temperature as a result of thermal exposure, but the performance of the DU gamma shield is unaffected by this transient. The peak temperatures predicted for the DU gamma shield for the bounding cases developed to model this fire are listed in Table 8.1. This table shows that the peak temperature in the DU material is conservatively estimated to be in the range 800°F (427°C) to 1200°F (650°C) for the ten cases evaluated. This is significantly below this material's melting temperature of 2070°F (1132°C).

Table 8.1. Summary of Peak Temperatures in DU Gamma Shielding Material

Case	Peak Fire Temperature (°F)	ANSYS Model (°F)	COBRA-SFS Model (°F)
NIST-01-A	1724	1173	1009
NIST-01-B	1571	1025	875
NIST-02-A	1706	1101	940
NIST-02-B	1652	1096	951
NIST-03-A	1670	1018	860
NIST-03-B	1562	995	855
NIST-04-A	2012	1198	995
NIST-04-B	1742	963	810
NIST-06-A	1859	1326	1149
NIST-06-B	1646	971	816

These results show that the gamma shielding of the GA-4 can be expected to remain intact and functional even if subjected to the severe conditions of the Newhall Pass Tunnel fire scenario. Therefore, the GA-4 package would be expected to remain below the HAC dose limits (10 CFR 71 2003).

8.2 Performance of Package Containment Seals

Based on the results of the thermal analysis (as discussed in Sections 7.1 through 7.6), there is a possibility of a release from the package because of failure of components that make up the containment boundary of the package. Calculated temperatures in the region of the lid closure seal, drain valve/port, and gas sample valve/port seals during the transient exceed the continuous-use temperature limits for the seal material. Therefore, the potential exists for the release of contents from the package in this fire scenario.

Section 8.2.1 presents the operating temperature limits for the seal material used in the GA-4 package. Section 8.2.2 provides a detailed discussion of seal temperatures predicted for the GA-4 package in the Newhall Pass Tunnel fire scenario.

8.2.1 Operating Temperature Limits for GA-4 Package Seal Material

The containment boundary for the GA-4 package is maintained by the seals on the package lid, drain valve and port, and gas sample valve and port. The package lid seal consists of primary and secondary O-rings at the interface of the lid and the package stainless steel body. The gas sample valve is located within the package lid, and the drain valve is located in the steel base of the package. The gas sample valve is sealed with primary and secondary O-rings, and for transport conditions, the outer face of the port is fitted with a steel plug that is threaded to a specified torque of 20 ft-lb. The drain valve is sealed within its access port with primary, secondary, and tertiary O-rings. The drain valve cover and drain port plug are also sealed with O-rings, in addition to being threaded, and are torqued to 20 ft-lb.

The O-ring seals at all locations are ethylene propylene, which has a continuous-use temperature limit of 302°F (150°C). Figure 8.1 shows a graph of the temperature limit on this material as a function of exposure time. As exposure temperature increases, the time limit for allowed exposure decreases. (Note that the horizontal axis, Exposure Time, in this plot is on a logarithmic scale.) The maximum temperature this material is rated to withstand without effectively immediate failure is 790°F (421°C), but it will tolerate this exposure for only six minutes.

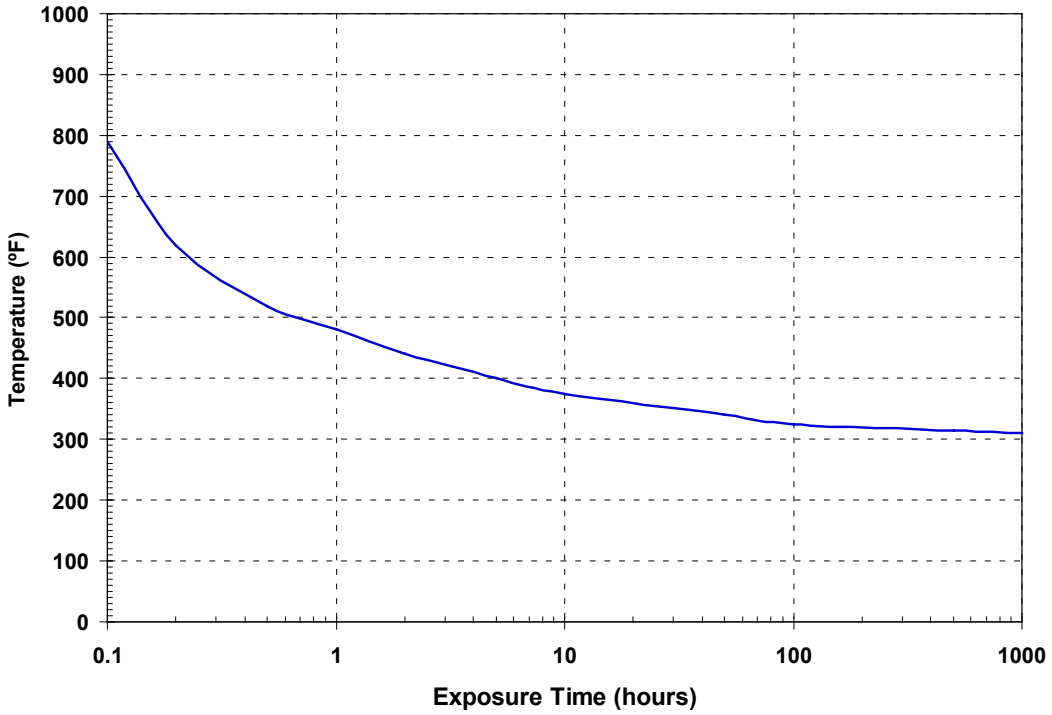

Figure 8.1. Operating Temperature Limit as a Function of Exposure Time for Ethylene Propylene Seal Material (based on data presented in the GA-4 SAR [General Atomics 1998])

8.2.2 Seal Temperatures in the Newhall Pass Tunnel Fire Scenario

All of the containment boundary seals in the GA-4 package are in locations that are covered by either the top or bottom impact limiter assembly. In the HAC fire (30 minutes at 800°C) analysis presented in the package SAR (General Atomics 1998), the predicted peak temperatures on these components do not exceed the bounds of the operating temperature limit curve shown in Figure 8.1. However, in the bounding conditions postulated for the Newhall Pass tunnel fire scenario, the higher fire temperatures and longer duration of the fire result in temperatures that exceed the documented performance capabilities of this hydrocarbon seal material.

Table 8.2 shows the temperatures predicted with the ANSYS model for the three seal locations during the fire scenario. The COBRA-SFS model predicts somewhat more conservative temperatures, due to the more simplified modeling approach used to represent the package end regions, compared to the ANSYS model.

Table 8.3 shows the temperature predictions in these locations from the COBRA-SFS model calculations.

Table 8.2. Summary of Peak Seal Temperatures from ANSYS Model Results

Case	Peak Fire Temperature (°F)	Lid Seal (°F)	Gas Sample Port Seal (°F)	Drain Valve Seal (°F)
NIST-01-A	1721	630	529	633
NIST-01-B	1579	626	533	618
NIST-02-A	1706	586	495	591
NIST-02-B	1648	649	548	644
NIST-03-A	1668	533	443	532
NIST-03-B	1570	578	484	571
NIST-04-A	1991	583	495	590
NIST-04-B	1736	552	474	545
NIST-06-A	1861	545	459	532
NIST-06-B	1646	668	562	678

Table 8.3. Summary of Peak Seal Temperatures from COBRA-SFS Model Results

Case	Peak Fire Temperature (°F)	Lid Seal (°F)	Gas Sample Port Seal (°F)	Drain Valve Seal (°F)
NIST-01-A	1721	974	894	908
NIST-01-B	1579	897	831	848
NIST-02-A	1706	948	861	873
NIST-02-B	1648	926	864	879
NIST-03-A	1668	905	821	833
NIST-03-B	1570	883	813	827
NIST-04-A	1991	981	870	882
NIST-04-B	1736	906	810	825
NIST-06-A	1861	1039	956	969
NIST-06-B	1646	883	797	811

These results show that the highest temperatures reached in the seal regions are in the range that the seal material would be expected to be able to withstand for up to 10 to 20 minutes without exceeding operating temperature limits. However, in the Newhall Pass Tunnel fire scenario, the seal regions on the GA-4 package would be expected to experience elevated temperatures for several hours, not just a few minutes. Table 8.4 summarizes the peak temperatures predicted for the lid seal region for the various cases evaluated. This table reports the peak temperatures during the fire portion of the transient and also in the cooldown portion of the transient, which is when the highest seal region temperature occurs in all cases. Table 8.4 also includes the length of time the seal region is above the 30-minute exposure, 5-hour exposure, and long-term exposure temperature limits.

Table 8.4. Summary of Peak Lid Seal Temperatures during Phases of Transient

ANSYS lid seal temperatures summary:				**Total Time Above 30-minute exposure limit of 520°F (hours)**	**Total Time Above 5-hr exposure limit of 400°F (hours)**	**Total Time Above long-term limit of 302°F (hours)**
	peak seal temperature during:					
Case	**"Hottest" Fire (°F)**	**"Longest" Fire (°F)**	**Post-fire Cooldown (°F)**			
NIST-01-A	499		630	2.62	7.25	>7.5
NIST-01-B		486	626	2.17	5.25	>5.7
NIST-02-A	505		586	1.80	5.2	>8.4
NIST-02-B		583	649	2.50	6.1	>7.7
NIST-03-A	411		533	0.67	3.5	7.4
NIST-03-B		494	578	1.5	4.9	>8.5
NIST-04-A	455		583	1.83	5.0	>7.7
NIST-04-B		429	552	1.17	4.4	>5.8
NIST-06-A	527		668	2.8	6.2	>6.8
NIST-06-B		447	545	1.2	4.1	>5.9

The time-at-temperature results for the drain valve seal and gas sample port seal are similar to the results for the lid seal. The heat-up and cooldown curves for these seals slightly lag the corresponding time values for the lid seal, due to their more protected locations within the closure lid and package base, respectively. The peak temperatures on the valve seals are essentially the same or slightly lower than the values predicted for the lid seal, and therefore the temperature response of the lid seal can be considered as bounding on the behavior of all seals in the package.

The results in Table 8.4 show that the highest seal temperatures occur during the cooldown phase of the transient, rather than during the period of fire exposure for the GA-4 package. The impact limiters shield the seal regions from direct exposure to the fire, and therefore limit the temperature rise on these components during the fire. In the post-fire cooldown of the package, however, the insulating effect of the impact limiters slows the rate of heat removal from the ends of the package, and the high temperatures developed in the central region of the package during the fire result in heat flowing toward the cooler ends. The temperature in these regions continues to increase long after the end of the fire portion of the transient.

In all cases evaluated, the seal region temperatures are predicted to exceed all exposure temperature limits at some point in the cooldown portion of the transient. Seal failure, which is

defined as the inability of the seal material to maintain a stable differential between the internal pressure within the package cavity and the external ambient pressure, must be assumed under these conditions. Experimental measurements of the performance of elastomer seals at elevated temperatures (NUREG/CR-7115 2012) show that seal failure is a complex process, not a simple pass/fail test. It is possible that in some circumstances some sealing capability would remain even after exposure to excursion temperatures well above the rated operating temperatures for the seal material. However, for the purposes of determining the potential release from the GA-4 package in this fire scenario, a simple pass/fail criterion is used to evaluate potential seal performance.

Since the temperatures predicted in these transients exceed the maximum recommended service temperature for the seal material, the seals are assumed to fail. The assumption of complete seal failure is bounding for the performance of the GA-4 package seals, and may be quite conservative. Nevertheless, this assumption is the basis for determining that a release is possible from the GA-4 package in this fire scenario due to package containment boundary leakage. The analyses presented in the following sections determine the character and amount of material that could be released.

8.3 Potential Release Issues

NRC staff evaluated the potential for release of radioactive material from the GA-4 package as a consequence of the Newhall Pass Tunnel fire scenario. Based on the results of the thermal analysis (as discussed in Sections 7.1 through 7.6), there is the possibility of a release from the package due to failure of components of the containment boundary of the package. Calculated temperatures in the region of the lid, drain valve, and gas sample port seals during the transient are expected to exceed the continuous-use temperature limits for the seal material. In addition, the peak fuel cladding temperatures (presented in Section 7.0) predicted in some cases reach the range where burst rupture of zircaloy cladding can occur. There is therefore the potential for release of fission products and spent fuel particles, in addition to CRUD[1] particulate, which is assumed to undergo 100% spallation from the rod surfaces in accident conditions (NUREG/CR-6487 1996).

Results of fuel performance analyses for the conditions encountered in this fire scenario are presented in Section 8.3.1. Results of evaluations of the potential for release from fuel rods to the GA-4 package cavity are presented in Section 8.3.2. Evaluations of the potential for release from the GA-4 package to the surrounding environment are presented in Section 8.3.3.

8.3.1 Fuel Rod Cladding Performance

Spent fuel has two potential sources of radioactive material that could serve as source terms for a release from an SNF transportation package; the CRUD on the rod outer surface, and the radioactive material (fission products and fuel fragments) confined within the metal cladding. The Standard Review Plan (NUREG-1617 2000) specifies the assumption of 100% spallation of CRUD from fuel rod surfaces for HAC analyses. For consistency, this assumption is also applied to the Newhall Pass Tunnel fire scenario. Determining the amount of material that could

[1] **C**halk **R**iver **U**nknown **D**eposit; generic term for material deposited on the rod surface from the coolant during reactor operations. The significant activated element is Cobalt-60. Regulatory guidance specifies a bounding value of 140 μCi/cm^2 for spent fuel rods in PWR assemblies. A bounding estimate for total activity due to CRUD can be calculated from the total fuel rod surface area and the age of the fuel (i.e., time out of the reactor).

potentially be released from within the rods, however, requires additional analysis of fuel rod behavior for the conditions of the fire scenario. If it can be shown that the fuel rods remain intact throughout the fire scenario, there would be no release of material from within the rods. If conditions are such that the fuel rods could fail, the nature and severity of the potential failure must be evaluated.

The predicted fuel cladding temperatures obtained with the ANSYS and COBRA-SFS models of the GA-4 in the Newhall Pass Tunnel fire scenario are presented in Section 7.0 for the bounding cases evaluated. As discussed in Section 7.0, the fuel cladding temperature results obtained with the ANSYS model are more conservative, compared to the COBRA-SFS model results, due to the more conservative representation of the fuel using the homogeneous k-effective model. However, this model is generally used in design-basis evaluations of fuel temperatures in SNF packages, and for completeness, the evaluation of fuel cladding performance for the conditions predicted in the Newhall Pass Tunnel fire scenario is performed for the thermal results obtained with both models.

Based on the fuel cladding temperatures predicted in the thermal modeling, predicted fuel cladding rupture temperatures were obtained using the burst rupture model in the FRAPTRAN1.4 code (NUREG/CR-7023 2011), a fuel performance code for calculating light water reactor fuel rod behavior in severe transient conditions. This approach was also used in the evaluation of fuel cladding performance presented in the study of the MacArthur Maze fire scenario (NUREG/CR-7206 2015).

In the FRAPTRAN1.4 analyses, initial conditions for the hottest fuel rod were determined from a steady-state calculation using FRAPCON-3.4 (NUREG/CR-7022 2011) for the design-basis fuel in the GA-4 package, WE 14x14 (standard) fuel with average burnup of 33 GWd/MTU, initial room temperature pressurization of 460 psig. The FRAPCON calculation essentially “ages” the assembly to the internal pressure corresponding to its final burnup. The rod in this condition was then subjected to the time history of the maximum cladding surface temperatures predicted with the thermal models for the various bounding cases defining the Newhall Pass fire scenario, using FRAPTRAN1.4.

In the FRAPTRAN code, burst rupture is evaluated with a burst stress/strain model developed from test data obtained for loss-of-coolant accident analysis. Burst rupture is the expected mechanism of failure for fuel rods in the reactor core when subjected to severe accident conditions, and is a potential failure mode for spent fuel at high temperatures. In the fire scenario, the fuel rods are predicted to experience a similar thermal transient, consisting of an essentially adiabatic heat-up during the fire, and therefore burst rupture is a reasonable mechanism of potential failure for spent fuel rods. Evaluations of creep rupture failure performed for fuel in the GA-4 package exposed to the MacArthur Maze fire scenario (NUREG/CR-7206 2015) showed that rods could also fail by creep rupture in a long-term fire scenario, at a slightly higher cladding temperature than was obtained for the same conditions with the burst rupture model in FRAPTRAN. Therefore, creep rupture modeling evaluations were also performed for the fuel rods in the Newhall Pass fire scenario, using the FRAPCON-3.4 code (NUREG/CR-7022 2011) in conjunction with the DATING code (Simonen and Gilbert 1988). The version of the code used in this analysis has been updated with creep coefficients from creep tests on irradiated cladding (Gilbert et al. 2002). The creep rupture modeling evaluations showed that fuel would not fail at the temperatures predicted for the Newhall Pass Tunnel fire scenario. This is consistent with the results obtained for the MacArthur Maze fire scenario, in which the creep rupture model predicted a rupture temperature of 1229°F (665°C). This temperature is not exceeded in any case of the Newhall Pass Tunnel fire scenario.

The burst rupture model predicts rupture at a single location along the axial length of a fuel rod. The temperature predictions obtained with both the COBRA-SFS model and with the ANSYS model show that the highest temperatures occur near the axial center of the active fuel region, and therefore rod rupture would be expected near the middle of the rod. Since the design-basis fuel for the GA-4 is low burnup (i.e., no more than 45 GWd/MTU), the degree of pellet-clad interaction would be relatively limited, and a single rod breach would be expected to effectively depressurize the fuel rod. Therefore, no additional ruptures are predicted on a given rod, and potential release calculations are based on one rupture per rod.

Table 8.5 summarizes the results of the burst rupture analyses as applied to the five cases evaluated for the Newhall Pass fire scenario. These results are also illustrated graphically in Figure 8.2. For the peak fuel region temperature histories predicted in these cases with the ANSYS model, the FRAPTRAN analysis predicts burst rupture at 1038°F (559°C). This relatively low predicted rupture temperature reflects the conservatism in the cladding temperature history predicted in the thermal analysis, and the uncertainty in the FRAPTRAN predictions at the relatively low heating rate for the cladding in this fire scenario. For the more realistic temperature histories predicted with the COBRA-SFS model, the FRAPTRAN analyses predict that burst rupture would not occur for the conditions postulated for these bounding cases representing the Newhall Pass Tunnel fire scenario, although clad ballooning is predicted to occur for the most severe case (NIST-06-A). In the less severe conditions of the HAC fire, the stress in the cladding is not generally expected to exceed the elastic limit, and therefore burst rupture would not be predicted with the models in the FRAPTRAN code.

Table 8.5. Results of Fuel Performance Analyses in the Newhall Pass Fire Scenario

	ANSYS Model Results		**COBRA-SFS Model Results**	
Case	**Peak Fuel Region Temperature (°F (°C))**	**Fuel Failure Predicted?**	**Maximum Peak Cladding Temperature (°F (°C))**	**Fuel Failure Predicted?**
NIST-01-A	1081 (583)	yes	882 (472)	no
NIST-01-B	954 (512)	no	767 (408)	no
NIST-02-A	1010 (544)	no	818 (436)	no
NIST-02-B	1020 (549)	no	834 (445)	no
NIST-03-A	921 (494)	no	742 (395)	no
NIST-03-B	913 (490)	no	745 (396)	no
NIST-04-A	1074 (579)	yes	853 (456)	no
NIST-04-B	867 (464)	no	693 (367)	no
NIST-06-A	1217 (659)	yes	994 (534)	no
NIST-06-B	881 (472)	no	702 (372)	no

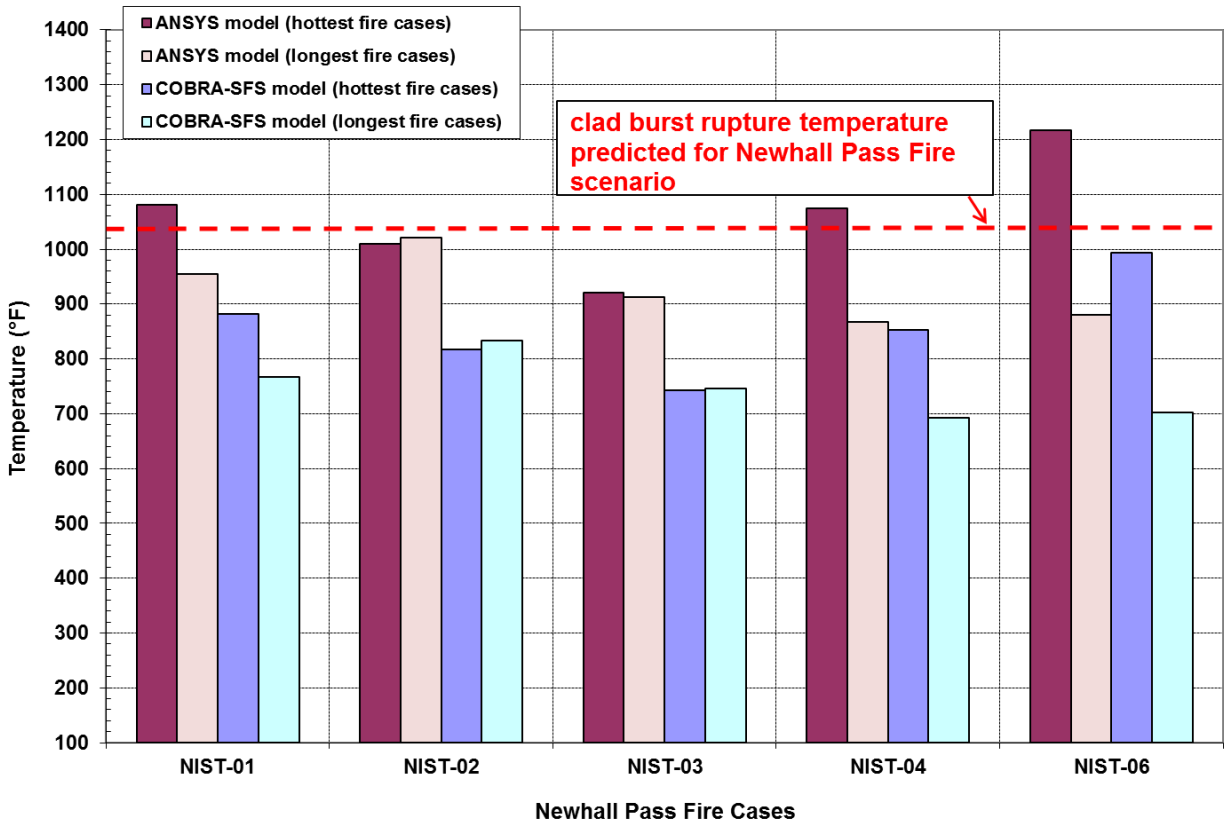

Figure 8.2. Predicted Burst Rupture Temperature Compared to Maximum Fuel Rod Temperatures from Thermal Analysis Models

The FRAPTRAN code was designed to predict nuclear fuel behavior during reactor accidents. In particular, failure models have been developed to provide reasonably accurate predictions for Reactivity Initiated Accident (RIA) and Loss-Of-Coolant Accident (LOCA) failures. For the case of a fire accident scenario in transportation of spent nuclear fuel, potential cladding failure can occur as a result of temperature increase and the associated rod internal pressure increase. These concurrent temperature and pressure increases can result in sufficient stress to cause ballooning and rupture of the cladding due to rapid high temperature creep. In a FRAPTRAN calculation of such an event, if the temperature and stress in the cladding are such that the cladding deforms to its uniform elongation in the hoop/circumferential direction, fuel rod ballooning is predicted. If the stress exceeds a correlated temperature-dependent level, cladding rupture will be predicted.

Ballooning and rupture models such as those in the FRAPTRAN code have been developed with the specific intent to accurately predict cladding failures during a LOCA, where the temperature increase rate is typically much higher (on the order of 10°C/s or higher) than in the case of fire scenarios (typically on the order of 0.2°C/s for the HAC fire, and for the MacArthur Maze fire scenario, conservatively estimated to be 0.27°C/s). For a given stress level, a slower heatup rate will generally tend to result in a lower rupture temperature, but there is very little data in the FRAPTRAN validation database that has heatup rates below 1°C/s. There is much more data at higher heating rates, ranging from 5°C/s to >30°C/s, as fully documented in the FRAPTRAN code manual (NUREG/CR-7023 2011). Due to the sparseness of the data showing burst rupture at temperatures below 1292°F (700°C), burst rupture temperatures in this range

predicted with FRAPTRAN, particularly for conditions with a heatup rate below 1°C/s have a greater uncertainty than predictions obtained for higher heating rates, where the database is more fully populated. In particular, predictions of burst rupture temperatures lower than 667°C (1232°F), which is the lowest burst rupture temperature in this subset of the code's validation database, should be evaluated as indicative of the possibility of rupture, rather than absolute indicators that rupture would occur for such conditions

Based on the ANSYS model results, predicted maximum fuel region temperatures exceed the calculated burst temperature obtained in the FRAPTRAN analysis for three of the five cases evaluated with the package at the hottest location in the tunnel (near the center of the tunnel). Predicted maximum fuel region temperatures do not exceed the calculated burst temperature in any of the five cases with the package at the longest fire location (near the tunnel entrance). For the COBRA-SFS results, the predicted maximum fuel cladding temperature does not exceed the calculated burst temperature in any of the cases, with the package at either location.

The temperature predictions obtained with the ANSYS model for the fuel region throughout the fire transient in all cases evaluated are documented in detail in Appendix C. These results show that in the three cases where the peak cladding temperatures exceed the predicted burst rupture temperature, less than 25% of the fuel region in each assembly of the GA-4 package is expected to reach or exceed this temperature for the conditions of the Newhall Pass Tunnel fire scenario. In most cases, a significant fraction of the rods in the inner region of the assembly do not exceed 752°F (400°C) at any point in the transient. The COBRA-SFS model results predict that none of the rods in the package would reach maximum peak temperatures above the calculated burst temperature for this fire scenario. In all cases, the maximum fuel cladding temperatures predicted with the more realistic representation of the fuel assemblies in the COBRA-SFS model remain below the cladding burst rupture temperature predicted for the conditions of the Newhall Pass Tunnel fire scenario.

Because the more conservative results obtained with the ANSYS model show that fuel failure could potentially occur for this fire scenario, and the predicted seal temperatures from both models indicate that seal failure would occur, the possibility of a release from the package cannot be entirely ruled out. For the purpose of evaluating the potential release from the GA-4 package in the Newhall Pass Tunnel fire scenario, the analysis for the MacArthur Maze fire is assumed to be bounding on any possible release from the package in the Newhall Pass Tunnel fire scenario. Even though this conservative evaluation shows that only a small number of rods could potentially fail in the Newhall Pass Tunnel fire scenario, imposing the potential release calculated based on conditions of the MacArthur Maze fire scenario in effect assumes that all rods in the package fail. This is extremely conservative for the potential release to the package, and for the potential release from the package to the environment, such that the potential release results for the MacArthur Maze fire scenario effectively bound the maximum possible release from the package in the Newhall Pass Tunnel fire scenario.

8.3.2 Potential Release to GA-4 Package Cavity

As noted above, the same potential release to the package cavity as determined in the comparable analysis for the MacArthur Maze fire scenario (NUREG/CR-7206 2015) is assumed for the Newhall Pass Tunnel fire scenario. For completeness of the documentation of the analysis of the Newhall Pass Tunnel fire scenario in the current document, the rod release analysis developed for the MacArthur Maze fire scenario (and presented in NUREG/CR-7206 2015) is repeated here.

Determining potential release quantities from an SNF package involves first determining the amount of material that is available for release from the fuel rods, and then determining the amount of this material that can be released from the package. This section presents analyses performed by NRC staff to determine the total amount of activity that could be released from the four assemblies defining the design-basis payload for the package, as described in the GA-4 SAR. Analyses to determine the potential for release from the package to the environment are presented in Section 8.3.3.

Typically, release quantities are expressed in terms of *release fractions*, a ratio calculated as the amount of material actually released divided by the total amount available for release. Regulatory guidance for determining the releasable source term for SNF transportation packages is provided in the *Standard Review Plan for Transportation Packages for Spent Nuclear Fuel: Final Report*, NUREG-1617 and in *Containment Analysis for Type B Packages Used to Transport Various Contents*, NUREG/CR-6487. The release fractions specified in these documents are listed in Table 8.6. These release fractions define bounding values for the fraction of material that is assumed to be released from the fuel rods to the package under NCT and HAC.

Table 8.6. Bounding Values of Release Fractions from Ruptured Fuel Rods

Radionuclide Group	Release Fraction	
	(NCT)	(HAC)
non-reactive gases (e.g., Kr-85)	0.3	0.3
volatile gases (e.g., cesium and iodine compounds)	0.0002	0.0002
particulate (fuel fragments or fines)	0.00003	0.00003
CRUD spallation fraction	0.15	1.0

The potential release from the GA-4 package corresponding to the release fractions in Table 8.6 is a function of the contents of the package. The radionuclide inventories for the two design-basis fuel configurations for the GA-4 package were obtained using ORIGEN-ARP (Gauld et al. 2009). The source term inventories obtained in these calculations are listed in Table 8.7. Consistent with the criticality and shielding calculations in the GA-4 package SAR (General Atomics 1998), WE 14x14 fuel at 35 GWd/MTU burnup and 10-years cooling is bounded by WE 15x15 at 35 GWd/MTU and 10-years cooling. Therefore, all source term and potential release calculations are performed assuming 10-year-old WE 15x15 fuel at 35 GWd/MTU, even though the thermal analysis is based on WE 14x14 fuel geometry. This is a conservative assumption, since the temperatures obtained with WE 14x14 fuel would be slightly higher than those predicted for WE 15x15 fuel for the same design-basis decay heat loading. Table 8.7 lists the calculated source terms for a single assembly. The total inventory within the GA-4 is four times the quantities listed in this table, since this package can carry up to four fuel assemblies.

Table 8.7. Radionuclide Inventory for a Single Assembly in the GA-4 Package

Nuclide	Activity (Ci)	
	WE 15x15 (45 GWD/MTU; 15 yrs cooled)	**WE 15x15 (35 GWD/MTU; 10 yrs cooled)**
Ag-110m	2.44E-03	2.42E-01
Am-241	5.56E+03	3.54E+03
Am-242		1.59E+01
Am-242m	2.15E+01	1.60E+01
Am-243	9.68E+01	4.74E+01
Ba-137m	1.78E+05	1.57E+05
Ce-144	3.21E+00	2.84E+02
Cm-242	1.77E+01	1.32E+01
Cm-243	5.71E+01	3.22E+01
Cm-244	9.37E+03	3.99E+03
Cm-245	1.64E+00	
Cs-134	2.78E+03	1.01E+04
Cs-137	1.88E+05	1.66E+05
Eu-152	6.17E+00	7.38E+00
Eu-154	5.41E+03	5.54E+03
Eu-155	8.50E+02	1.23E+03
H-3	6.42E+02	6.37E+02
Kr-85	8.28E+03	9.80E+03
Np-239	9.68E+01	4.74E+01
Pm-147	6.01E+03	2.27E+04
Pr-144		2.84E+02
Pr-144m		3.97E+00
Pu-238	8.78E+03	5.31E+03
Pu-239	6.51E+02	6.41E+02
Pu-240	1.26E+03	1.04E+03
Pu-241	1.50E+05	1.60E+05
Pu-242	6.98E+00	4.22E+00
Rh-106		1.17E+03
Ru-106	4.74E+01	1.17E+03
Sb-125	4.41E+02	1.28E+03
Sm-151	7.47E+02	7.02E+02
Sn-119m		2.47E-02
Sn-121		1.80E+01
Sn-121m	2.94E+01	2.32E+01
Sr-90	1.19E+05	1.14E+05
Tc-99	3.38E+01	2.74E+01
Te-125m	1.08E+02	3.13E+02
U-234	1.91E+00	1.98E+00
U-237		3.84E+00
Y-90	1.19E+05	1.14E+05
Zr-93	4.26E+00	3.46E+00

The bounding values for release fractions defined in Table 8.6 were applied to the source terms listed in Table 8.7 to determine a bounding estimate of the activity that could be released from the four fuel assemblies to the GA-4 package interior in the MacArthur Maze fire scenario (NUREG/CR-7206 2015). Figure 8.3 shows the activity released to the package for the source term inventory from Table 8.7 for the bounding configuration of 10-year-cooled WE 15x15 fuel at 35 GWd/MTU. Figure 8.4 shows the activity released to the package for the source term inventory from Table 8.4 for 15-year-cooled WE 15x15 fuel at 45 GWd/MTU.

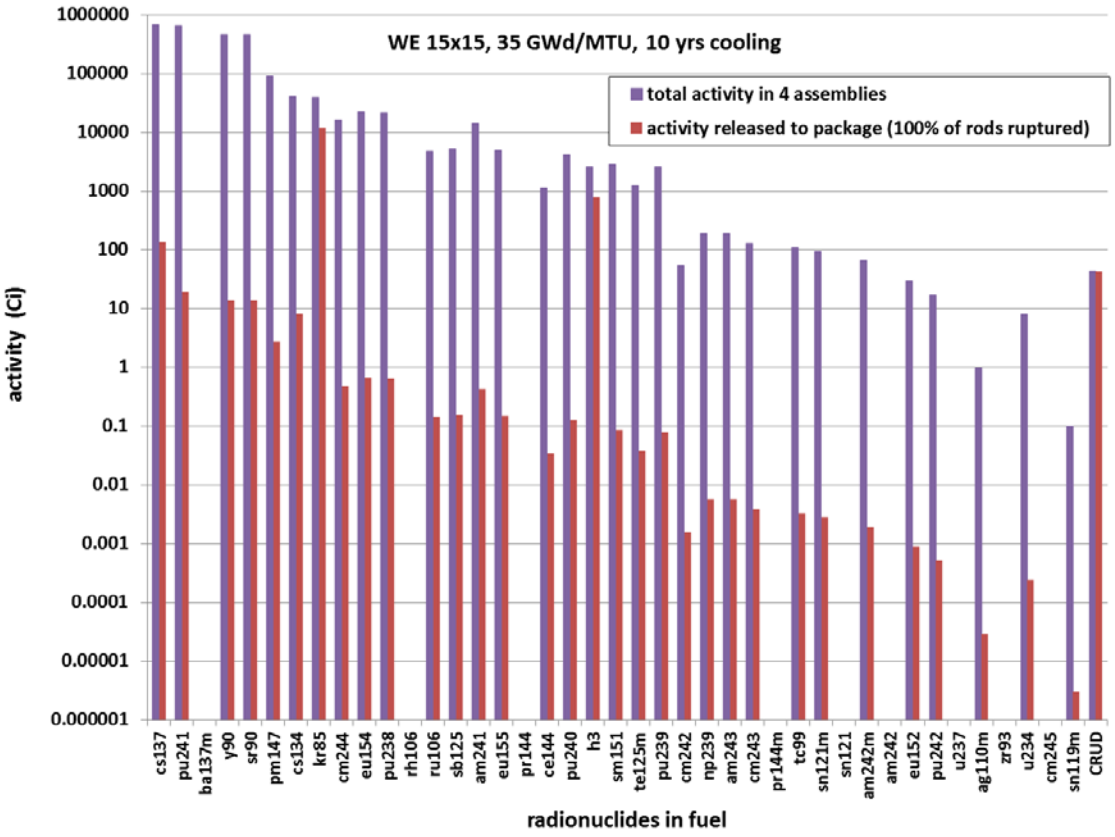

Figure 8.3. Summary of Activity in Radionuclides Released to GA-4 Package Cavity from WE 15x15 (35GWd/MTU, 10-yrs-cooled fuel) for Bounding Release Fractions Specified in NUREG-1617

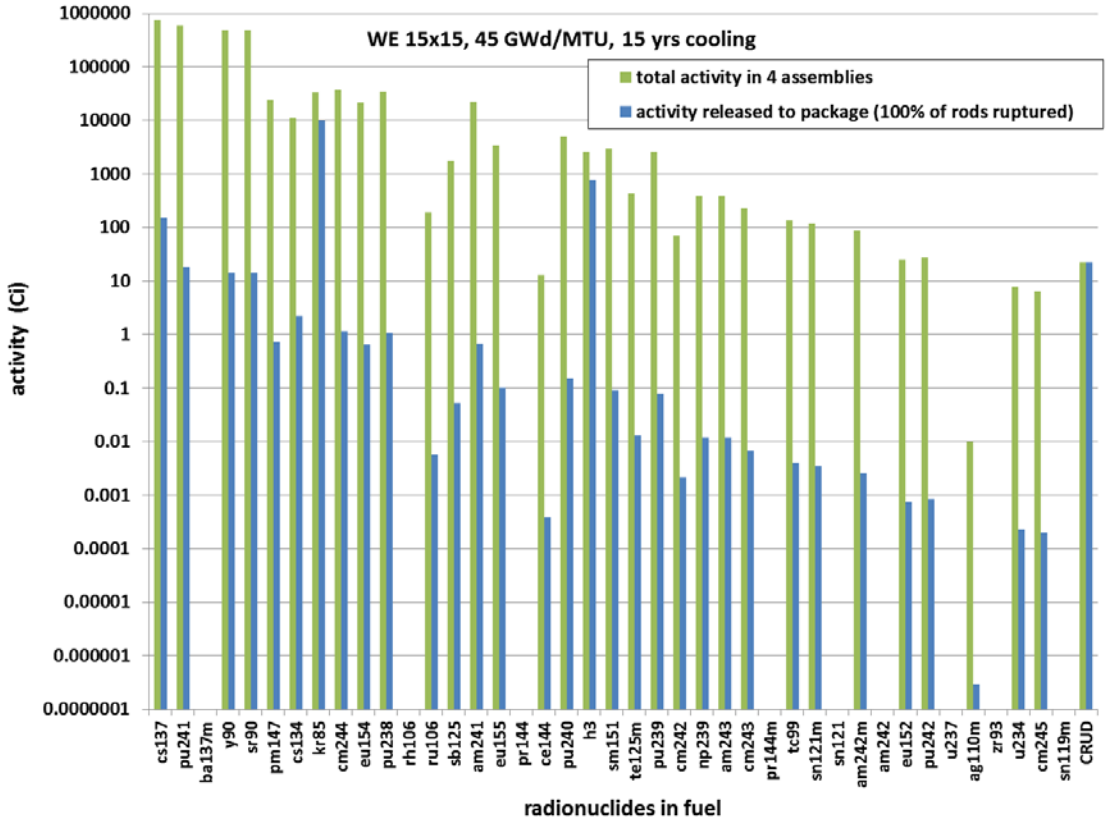

Figure 8.4. Summary of Activity in Radionuclides Released to GA-4 Package Cavity from WE 15x15 (45 GWd/MTU, 15-yrs-cooled fuel) for Bounding Release Fractions Specified in NUREG-1617

8.3.3 Potential Release from GA-4 Package in Newhall Pass Tunnel Fire Scenario

As noted above, the potential release from the GA-4 package in the Newhall Pass Tunnel fire scenario is bounded by the potential release determined for this package in the MacArthur Maze fire scenario. For completeness in the current document, the potential release analysis for the MacArthur Maze fire scenario is reproduced here, echoing the documentation of the analysis in NUREG/CR-7206.

Release rates from SNF packages are typically calculated for NCT and HAC using models based on guidance in NUREG/CR-6487, which contains models that reference ANSI standards for leakage tests on packages for shipment of radioactive materials (ANSI N14.5 1997). The analyses presented in the GA-4 SAR show that as long as the package seals remain intact, the package can be expected to meet all containment requirements, and potential releases from the package would be well below regulatory limits. However, the GA-4 package seals are predicted to exceed operational temperature limits in these bounding fire scenarios. In addition, it is conservatively assumed that all rods would rupture in the MacArthur Maze fire scenario. Therefore, there is the potential for leakage of radioactive material from the GA-4 package at some point in the cooldown transient of this bounding fire scenario.

Determining an appropriate leak rate for the package in the conditions predicted for a fire scenario in which the seals are expected to fail presents an interesting challenge. The models for leak rates derived from the ANSI standard ANSI N14.5 are not based on the assumed seal conditions in this fire scenario, and there is very little information in the literature on leak rates associated with *failed* seals. In typical engineering applications, the leak rates of failed seals are unacceptable by definition, and their potential magnitude is of no practical interest. What little information to be found tends to focus rather narrowly on special applications where time-to-failure could be a critical design parameter (e.g., equipment that will be sent into orbit). In these types of studies, the focus is on the time interval, not the leak rate itself, and the work is mainly interested in modes of seal failure or seal behavior prior to failure.

A modeling approach to determine a reasonable bounding leak rate for the GA-4 package for the portion of the transient following the time after assumed seal failure due to exceeding thermal operating limits was developed for the evaluation of the MacArthur Maze fire scenario (NUREG/CR-7206 2015). Section 8.3.3.1 repeats the presentation of this model, for completeness in the documentation of the Newhall Pass Tunnel fire scenario evaluations. Section 8.3.3.2 presents the potential release calculations for the GA-4 package, based on the leak rates determined with this model, for the bounding case of the MacArthur Maze fire scenario.

8.3.3.1 Leak Rate Model for GA-4 Package without Seals

For leak rate modeling, the interface between the closure lid and end flange of the package body end flange is of greatest significance. (There is also the potential for leakage paths through the gas sample valve/port and the drain valve/port; this is discussed in Section 8.3.3.2.) Failure of the seals in the fire scenario is conservatively treated in this evaluation as if the seals simply cease to exist after exceeding the operating temperature limits on the lid seal. This timeframe conservatively bounds the interval of the estimated time when all seals are predicted to have exceeded operating temperature limits. The possibility of damaged seal material affecting the geometry of the leakage path is ignored. If it is assumed that there is no O-ring seal material remaining in the seal grooves of the lid and flange, the only barrier to flow through the interface is the actual physical contact between these two components.

The closure lid and body flange both have smooth metal surfaces where the two components are in contact, and the closure bolts are torqued to a specified pre-load, such that there is a positive and essentially uniform clamping force at the interface. The evaluations investigating the response of the lid closure bolts to the extreme thermal environment of the MacArthur Maze fire scenario (NUREG/CR-7206 2015), show definitively that the bolts maintain a positive clamping force throughout the fire transient, including the long cooldown back to ambient conditions. The thermal and structural stresses on the lid closure bolts in the MacArthur Maze fire scenario bound the much less severe conditions of the Newhall Pass tunnel fire scenario. Therefore, the maximum potential leak rate for the Newhall Pass tunnel fire scenario is bounded by the leak rate calculated for the MacArthur Maze fire scenario.

Flow of gas through the very narrow space between the closure lid and body flange can be treated as analogous to fluid flow through fractured material in which the local scale of motion can be approximated by the cubic law for flow between parallel plates. This is a simplified form of the momentum conservation equation, and is a function of the geometry of the flow path and the driving pressure difference between the package interior and the external environment

(Brown 1987). A formulation of this relationship, expressed in cylindrical coordinates, is given by

$$Q_{LR} = 2\pi \left(\frac{d_e^3}{12\mu}\right)\left(\frac{\Delta P}{\ln(r_o/r_i)}\right) \tag{8.2}$$

where

Q_{LR} = volumetric flowrate through the leakage path
d_e = equivalent gap between surfaces in contact
μ = viscosity of flowing gas
ΔP = driving pressure difference
r_o = outer radius
r_i = inner radius

The equivalent gap between the surfaces in contact is the critical unknown in the above equation, since all other parameters can be readily determined from the geometry of the GA-4 package closure lid and flange, and the conditions calculated for the MacArthur Maze fire scenario with the thermal models. The actual gap is a function of the surface roughness of the components in contact and the clamping force holding them together. This gap cannot readily be estimated with any degree of certainty without knowing the exact microscale geometry of the surfaces involved.

Therefore, an alternative approach was developed by considering another much simpler physical process in which the gap between two surfaces in direct contact has an important effect on physical behavior; the flow of heat between two surfaces in direct or very close contact. The thermal resistance between two such components is a strong function of the contact pressure and surface texture of the two surfaces, and is typically expressed in terms of the overall thermal contact resistance, as

$$R_{tc} = \frac{d_e}{k} \tag{8.3}$$

where

R_{tc} = thermal contact resistance (m^2-K/W) as a function of contact pressure and surface texture for two surfaces in direct contact
d_e = equivalent gap between surfaces in contact
k = thermal conductivity of gas in spaces between contacting surfaces

Using thermal contact resistance data for stainless steel surfaces (Shajaefard and Goudarzi 1987) as a function of contact pressure and surface roughness at the interface, and assuming helium gas in the very constrained spaces between the contacting surfaces, the above relationship can be used to determine an equivalent gap for the closure lid and package flange in the Newhall Pass Tunnel fire scenario.

The results for evaluations of the lid closure bolt response to the MacArthur Maze fire scenario using detailed finite element analysis modeling provide a history of the clamping force between the closure lid and package body flange. Figure 8.5 shows the estimated equivalent gap after seal failure, based on the contact resistance as a function of the lid/flange contact pressure due to the clamping force, and the thermal conductivity of helium gas.

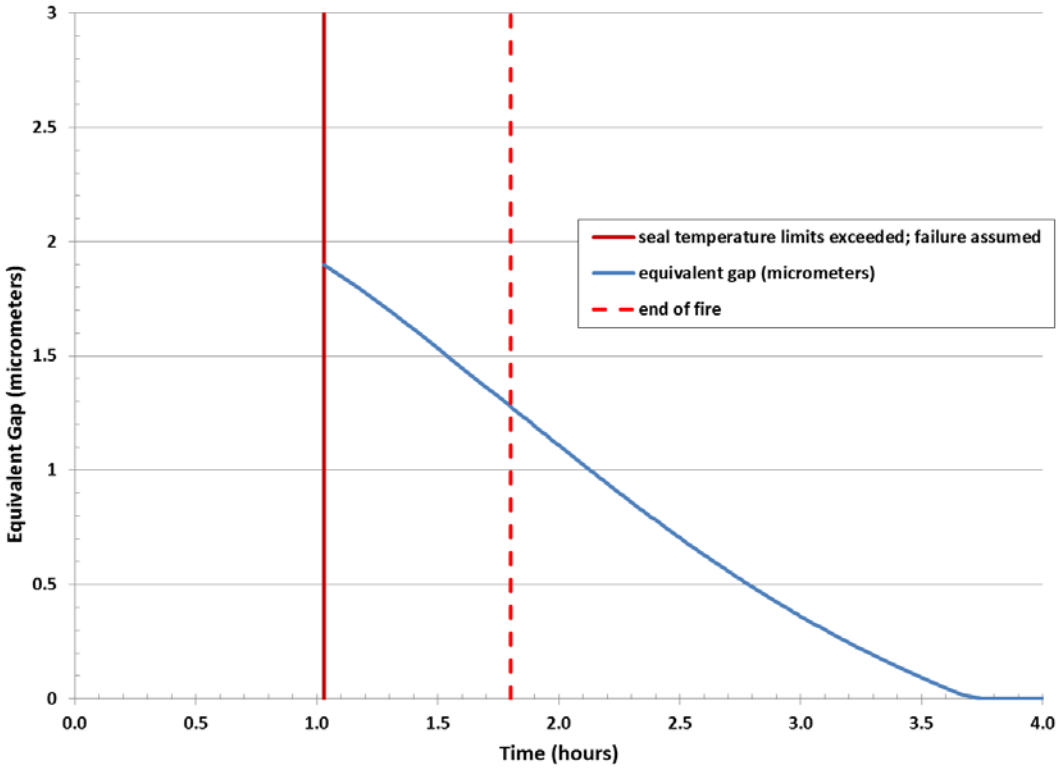

Figure 8.5. Equivalent Gap between Closure Lid and Package Body Flange after Seal Failure for Bounding Conditions of the MacArthur Maze Fire Scenario

The clamping force on the lid increases during the post-fire cooldown, due to differential thermal contraction between the nickel alloy closure bolts and the stainless steel lid and package body. The effect is to essentially close the gap entirely, for all practical purposes, by about 3.75 hours into the fire transient. This effectively limits the window of time in which material could leak out of the package to less than 3 hours. This has the effect of greatly reducing the potential for a substantial release of radioactive material from the package, as shown by the release evaluations in Section 8.3.3.2.

8.3.3.2 Bounding Release Estimate for Newhall Pass Tunnel Fire Scenario

Using the leak rate model and equivalent gap width relationship presented in Section 8.3.3.1, a conservative bounding estimate was obtained for potential release of radioactive material from the GA-4 package in the MacArthur Maze fire scenario. The leak rate obtained with this model is a function primarily of the cavity gas pressure developed during the transient and the bolt temperature history. The conditions of pressure and temperature in the MacArthur Maze fire scenario effectively bound the conditions of the Newhall Pass Tunnel fire scenario. This is illustrated in Figure 8.6, with a comparison of the bounding cavity gas pressure calculated for the MacArthur Maze fire scenario, compared to the cavity gas pressure predicted for the bounding cases defining the Newhall Pass Tunnel fire scenario. The calculated cavity gas pressures conservatively neglect the effect of mass loss due to leakage, and the pressure is calculated based on the average cavity gas temperature, using the ideal gas law.

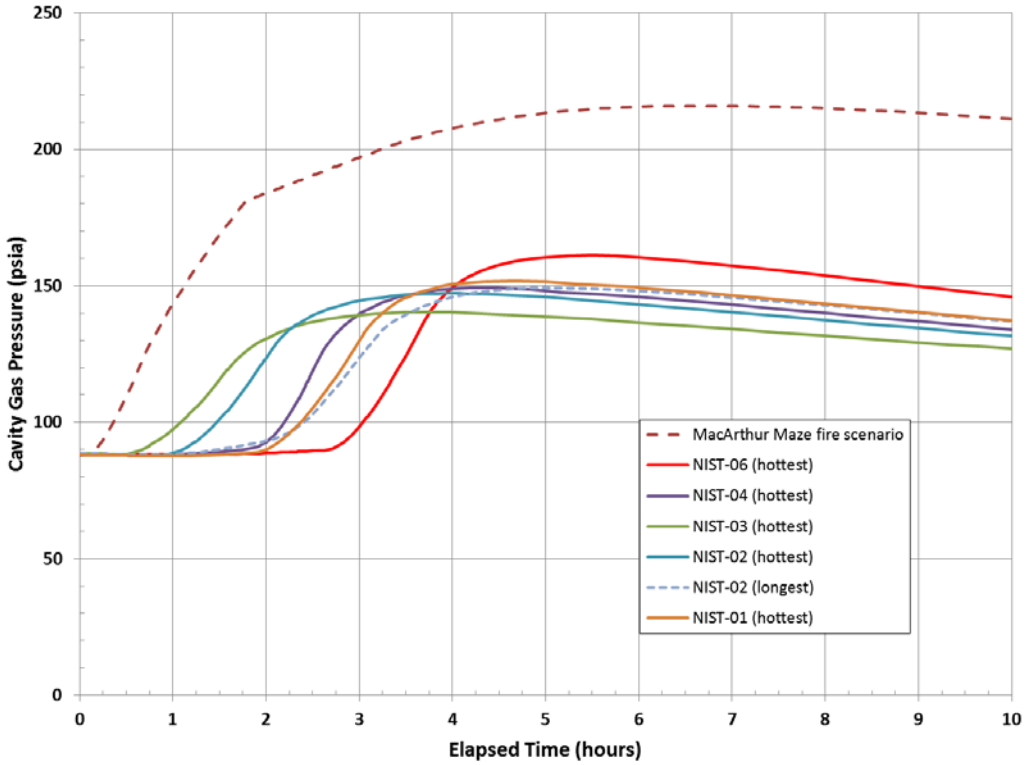

Figure 8.6. Cavity Gas Pressure for Bounding Cases for Newhall Pass Tunnel Fire Scenario Compared to Bounding Value from the MacArthur Maze Fire Scenario

The plot in Figure 8.6 clearly shows that for the bounding conditions defined to model the Newhall Pass Tunnel fire scenario, the cavity gas pressure is significantly lower than that predicted for the MacArthur Maze fire scenario. Similarly, the gas temperature and the package component temperatures (including the lid and lid closure bolts) are lower in the results obtained for the Newhall Pass Tunnel fire scenario. The results obtained with this leak rate model for the MacArthur Maze fire are bounding for the Newhall Pass Tunnel fire scenario. The results obtained in the analysis of the MacArthur Maze fire scenario (reported in NUREG/CR-7206 2015) are repeated here, for completeness.

The fluid viscosity of pure helium was used for this calculation, rather than attempting to quantify the viscosity of the mixture of helium and fission gases that would actually be in the package following the rod ruptures. This is a conservative assumption, since the viscosity of the mixture would be higher than the viscosity of pure helium. The difference between the mixture property and that of pure helium would in any case be expected to be small, since the gas released from the fuel rods would consist mainly of helium.

The pressure difference driving the volumetric flow through the interface between the package cavity and ambient was calculated assuming a constant external ambient pressure of 1 atm. The internal cavity pressure was calculated using the ideal gas law, based on the average gas temperature predicted with the ANSYS thermal model. The initial pressure in the cavity was assumed to be at the Maximum Normal Operating Pressure (MNOP) for the GA-4 package. This is a conservative initial pressure, as it corresponds to the pressure effect of 100% of the fuel rods in the package having ruptured, and the density change is determined for B&W 15x15

fuel[2], which is the most limiting fuel configuration for the maximum operating pressure. This approach provides a bounding estimate of the cavity internal pressure throughout the fire transient, and avoids the complication of changing the gas density in the package at the predicted time of rod rupture in this analysis.

Figure 8.7 shows the predicted leak rate as a volumetric flow of helium gas through the equivalent gap. Two leak rate calculations were performed; a bounding case in which the package gas density was assumed to remain constant throughout the transient, and a more realistic case in which the change in gas density (and hence pressure) due to outflow of gas from the package was accounted for. The difference between the two cases is relatively small, due to the small leak rates predicted for this configuration with the closure lid clamped tightly to the package body flange throughout the transient.

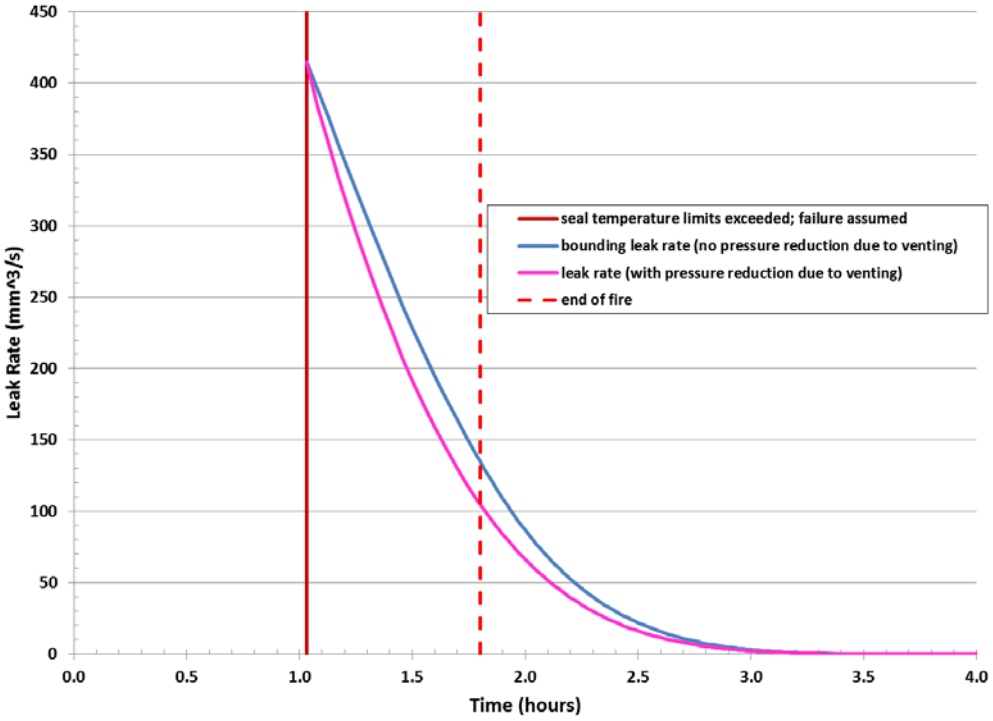

Figure 8.7. Volumetric Leak Rate for GA-4 Package after Seal Failure in the MacArthur Maze Fire Scenario

The release calculations were performed assuming the bounding leak rate over time (as shown in Figure 8.7), providing a bounding estimate of potential release from the package. The activity within the package cavity was assumed to be uniformly distributed within the gas, with all particulate (i.e., fuel fines and spalled CRUD) suspended in the gas as an aerosol. The total release of each component was calculated simply as the activity of that component times the volumetric fraction of gas escaping from the package.

[2] For the thermal analysis, the most limiting fuel is WE 14x14, and this is the fuel configuration represented in the thermal models, as described in Sections 5 and 6. However, for maximum cavity pressure evaluations, as presented in the SAR, B&W 15x15 is the limiting configuration, due to the fuel rod design of this fuel assembly. Therefore, the cavity pressure obtained assuming 100% rod rupture (for four assemblies) with this fuel design was used, as a conservatism in the leak rate evaluations.

A number of additional conservatisms were incorporated into the release calculation, including the following assumptions:

- the entire quantity of fuel particulate was assumed to remain suspended in the gas within the cavity; the possibility of particulate settling or plating out on internal package structures was ignored

- the filtering effect of the equivalent gap size was neglected; the maximum size of the equivalent gap is only about two micrometers, and is much smaller than the upper bound of 10 micrometers on respirable particle size; the release calculations do not consider that a large percentage of the fuel particulate and CRUD particles simply could not escape from the package, due to the small size of the gap.

These assumptions result in a very conservative estimate of the amount of activity that could escape from the package in the approximately 2.7 hours that the package could sustain a significant leakage.

The activity of the large number of radionuclides comprising the estimated release can be more conveniently expressed in combined form, as a function of their combined isotopic A_2 limit[3] values from 10 CRF 71, Appendix A.

The A_2 value for a mixture of normal form material can be determined using the following relationship from 10 CFR 71, (Appendix A, Section IV.d), as

$$A_2 \; for \; mixture = \frac{1}{\left[\sum_{i=1}^{n} \frac{f(i)}{A_2(i)}\right]}$$

where

n = number of radionuclides in mixture
$f(i)$ = fraction of total mixture activity due to the i^{th} component
$A_2(i)$ = A_2 value for the i^{th} component

Using this approach, the A_2 for the mixture of radionuclides in the estimated potential release from the GA-4 package is calculated as 88 Ci (3.25 TBq) for WE 15x15 fuel at 45 GWd/MTU, 15 yrs cooling. The corresponding result for WE 15x15 fuel at 35 GWd/MTU, 10-yrs cooling is a mixture A_2 of 143 Ci (5.3 TBq). The calculation of the mixture A_2 for each fuel configuration includes all fission gas and particulate released from the fuel, plus the CRUD assumed to spall from the exterior surfaces of the rods.

[3] An A_2 quantity is defined in 49 CFR 173.403 as the maximum activity of a Class 7 (radioactive) material permitted in a Type A package, which does not require an accident resistant design. The amount of material that constitutes an A_2 quantity depends on its specific activity and other radiological properties. Appendix A of 10 CFR 71 specifies the specific A_2 quantities for a large number of radioactive materials, and defines methods for calculating values for materials not listed in the table. Spent nuclear fuel requires a Type B package, which can carry more than an A_2 quantity of radioactive material, but must retain the integrity of containment and shielding under normal conditions of transport (as per 49 CFR 173) and meet the release limits of less than an A_2 per week for hypothetical accident conditions.

Based on the leak rate model, the total release from the package is estimated as 21 Ci (0.78 TBq) for the higher burnup fuel, and as 24.5 Ci (0.91 TBq) for the lower burnup fuel. Expressed as an A_2 fraction, relative to the mixture A_2 for each configuration, these release rates are 0.24 and 0.17, respectively. Therefore, the bounding estimate of the total release from the package is 0.24 of the mixture A_2 calculated assuming WE 15x15 fuel at 45 GWd/MTU, 15 yrs cooling. As mentioned above, if the effect of particulate settling and the restriction of large particulate from passing through a small gap were taken into account, the release estimate would be significantly reduced.

The evaluations of potential release from the GA-4 package assume that the estimated release by way of the closure lid is sufficiently conservative to be bounding on the possible contribution of leakage through the drain valve/port and gas sampling valve/port, which form part of the containment boundary of the GA-4 package. These components also contain seals that would be expected to exceed their operating temperature limits in this fire scenario, as discussed in Section 8.2 above. However, these penetrations of the package are less than an inch in diameter, compared to the approximately 2-ft diameter of the closure lid rim, and therefore do not provide a significant increase in the area available for potential leakage. In addition, the ports consist of long and convoluted flow paths that would tend to filter any particulate that might be carried through them to the ambient environment. The gas sample port is effectively blocked by the sample valve itself, which in addition to having primary and secondary O-ring seals, is threaded into place over a length of several inches. Also, for transport conditions, the outer face of the gas sample port is plugged with a threaded cover that extends to a depth of more than an inch. Similarly, the drain port is plugged by the drain valve, and capped with a threaded drain valve cover and port plug.

Based on the geometry of the valve/ports in this package, it is reasonable to assume that leakage from the package at these locations due to failed seals would be much less likely to be significant compared to leakage through for the much larger area and more direct flow path of the closure lid seal region. The conservative assumptions regarding the amount of material that could be transported out of the package through the lid closure/flange equivalent gap are sufficient to bound any possible contribution of the valve/port leakage paths. It is therefore justifiable to neglect the effect of the valve/ports, without compromising the conservatism of the estimated leak rate and total package release calculations.

9.0 OVERALL SUMMARY AND CONCLUSIONS

The U.S. Nuclear Regulatory Commission has established requirements for packaging and transportation of spent nuclear fuel (SNF) assemblies under NCT and for hypothetical accident conditions (HAC). These requirements (10 CFR 71) conservatively bound the conditions that an SNF package might be subjected to in the course of its service life. However, real-world accidents of greater severity are certainly possible, and rare as they may be, the NRC has proactively undertaken the examination of such accidents, to determine what the potential consequences might be, were such an accident ever to involve an SNF package.

Three previous studies of transportation accidents, one resulting in a fire in a railroad tunnel (NUREG/CR-6886 2009), one in a highway tunnel (NUREG/CR-6894 2007), and one on a highway interchange (NUREG/CR-7206 2015) were undertaken with four different SNF package designs. Based on conservative scenarios constructed from these real-world fire conditions, the results of these studies have shown that the design basis for SNF packages is sufficiently robust for them to survive such beyond-design-basis conditions without adverse consequences to public safety. In all cases evaluated, the modeling results showed that the various SNF packages would be expected to maintain required shielding for ionizing radiation, and also would maintain the integrity of the containment boundary sufficiently to limit potential release of radioactive material from the packages to within regulatory bounds for accident conditions.

The Newhall Pass Tunnel accident of October 12, 2007 was selected as a fourth study in this series of evaluations of real-world accidents because of the long duration of the fire and the wide range of potential fire exposure scenarios, due to the large number of vehicles involved in the accident and fire. Since this was a highway accident, the only type of SNF package that could potentially be involved would be a LWT package. The General Atomics GA-4 LWT transportation package was selected for this investigation, mainly because it can carry a relatively large payload for an over-the-road transportation package, and therefore the potential consequences of package failure could be more severe than for packages with smaller payload capacities. The GA-4 package is designed to transport up to four intact PWR spent fuel assemblies, with a maximum total package decay heat load of 2.5 kW. (This is the same package that was evaluated in the MacArthur Maze highway interchange fire and roadway collapse (NUREG/CR-7206 2015).)

Bounding Scenario for the Newhall Pass Tunnel Accident

The Newhall Pass Tunnel accident consisted of a chain reaction traffic collision and fire involving 33 commercial tractor-trailer rigs and one passenger vehicle, on a section of the southbound Interstate 5 truck route where it passes under the main north-south lanes of Interstate 5. A fire started within the close pile-up of vehicles near the tunnel exit and spread rapidly into the tunnel, eventually filling the entire tunnel and destroying the twenty-four tractor-trailer rigs that were trapped within it. The cargoes of the trucks consisted mainly of foodstuffs, and none were carrying hazardous flammable material (i.e., no gasoline tankers, such as in the Caldecott Tunnel fire (NUREG/CR-6894 2007) and the MacArthur Maze fire (NUREG/CR-7206 2015.) The severe tunnel-filling fire is estimated to have lasted more than 2 hours, and possibly as long as 5 hours. (Refer to Figure 1.2, which shows a sonar image of the configuration of the destroyed vehicles within the tunnel, prior to the beginning of salvage operations. See Section 2.0 for a detailed discussion of the fire scenario, with images obtained by first-responders at the scene.)

Based on fire modeling with the FDS code, and physical examination of material samples obtained from the remnants of the vehicles removed from the tunnel, a bounding fire scenario was defined for thermal evaluations of the potential effects of this fire on an SNF package. Due to uncertainties in the overall fire timeline and incomplete information on the actual cargo of some of the trucks, five specific fire modeling cases were defined to bound the possible range of fire conditions. The fire modeling approach utilized a feature in FDS that allows the fire behavior to be defined with a total mass of fuel and a specified burn time. Based on the available information, a bounding "fuel budget" was developed for a typical vehicle within the tunnel, consisting of the combustible components of the vehicle, plus an estimated combustible mass for a typical cargo.

Cases were developed for assumed fire spread rates that spanned the range of uncertainty in the actual duration of the intense fire within the tunnel, estimated as ranging from 2 hours to 5 hours. To verify the conservatism of the "typical" fuel budget, with respect to the actual fuel load available on each vehicle, combustible mass of the actual cargo for each of the vehicles in the tunnel was estimated, based on information extracted from the MAIT report (CHP 2007). The temperatures obtained with these modeling assumptions represent conservative bounding values for the fire that destroyed the vehicles and their cargoes in this accident.

Thermal Modeling Approach and Summary of Results

Detailed thermal models of the GA-4 package were constructed for the ANSYS and COBRA-SFS codes, for transient evaluations to determine the temperature response of the package to bounding cases defining the fire scenario. These evaluations also included the post-fire cooldown transient, and all evaluations were run out to approximately 10 hours. This is not long enough for the package to have returned to steady-state, but in this fire scenario, the relatively short cooldown time is sufficient for all component temperatures in the package to be trending downward. (For fires of greater severity than the Newhall Pass Tunnel fire, the time to this turn-around is generally many hours longer, resulting in peak component temperatures [including peak fuel cladding temperatures] occurring long after the end of the fire, as noted in documentation of the previous studies mentioned above.)

The initial condition of the package at the start of the fire scenario in each case was defined as steady-state NCT. The tunnel fire consisted of a series of fires on the individual vehicles, as the fire spread through the tunnel, with the overlap of vehicle fires in a given case determined by the specified spread rate. The results of the FDS modeling were used to identify the vehicle with the hottest fire in a given case, to define the most adverse location for the SNF package within the tunnel, with respect to peak fire temperature exposure. Because of the length of the fire, these results were also used to identify the location with the longest exposure to elevated temperatures during the fire in a given case. In all cases, the hottest location corresponded to a vehicle near the center of the tunnel, and the longest fire location corresponded to the last vehicle to be consumed by the fire (i.e., the vehicle closest to the tunnel entrance). The complex and dynamic fire conditions predicted with FDS for the vehicle at the hottest fire location and the vehicle at the longest fire location were represented for the GA-4 package as a fully engulfing pool fire in the thermal analyses for each case.

Thermal evaluations of the package response to the various bounding cases developed to represent the Newhall Pass Tunnel fire scenario show that the peak temperatures would be expected to be higher for the fire at the hottest fire location, compared to the longest fire location in all cases. The results obtained with the ANSYS model are conservative with respect to the COBRA-SFS model, due mainly to the simplifications in the representation of the fuel region in

the ANSYS model. In three of the five cases, the ANSYS model predicts that the peak cladding temperature in response to the fire at the hottest fire location would be expected to exceed the short-term limit of 1058°F (570°C) for zircaloy cladding, shortly after the end of the vehicle fire at that location. The corresponding results from the COBRA-SFS model show that this limit would not be exceeded in any of these cases. Both models predict that the peak cladding temperature would remain below this limit in all cases for the local vehicle fire at the longest fire location.

The maximum peak cladding temperature in the transient is predicted with the ANSYS model to be 1217°F (659°C), compared to 994°F (534°C) predicted with the COBRA-SFS model for the same bounding case. Both models predict temperatures in the regions of the package seals that are within the seal material operating temperature limits during the fire portion of the transient for each case evaluated. However, in all cases, both models predict that the seal temperature limits will be exceeded for several hours of the post-fire cooldown transient, due to the thermal inertia of the package and the insulating effect of the impact limiters attached to the ends of the package.

Fuel Rod Performance Evaluation

Based on the predicted fuel cladding temperatures from the ANSYS and COBRA-SFS modeling, fuel performance was evaluated using the burst rupture model in the FRAPTRAN-1.4 code (NUREG/CR-7023 2011). For the fuel region temperature histories predicted for the five cases evaluated in this fire scenario with the ANSYS model, the FRAPTRAN analysis predicts cladding burst rupture at 1038°F (559°C). For the fuel cladding temperature histories predicted with the COBRA-SFS model for these five cases, the FRAPTRAN analysis predicts that although some rods may experience ballooning in the most severe case (NIST-06, for the hottest fire location), rod burst rupture would not be expected to occur in any of these cases. Based on the predicted burst rupture temperature, fuel failure is predicted with the ANSYS model for three of the five cases considered with the GA-4 package at the hottest fire location in the tunnel.

These results suggest that although fuel failure is possible as a result of the conditions of the Newhall Pass Tunnel fire, a realistic assessment of the fire conditions and realistic thermal modeling would show that fuel would not be expected to fail. However, as a bounding evaluation the potential release from the GA-4 package in the Newhall Pass Tunnel fire scenario is assumed to be potentially the same as that predicted for the MacArthur Maze fire scenario (NUREG/CR-7206 2015). In the MacArthur Maze fire scenario, the potential consequences are evaluated assuming that all rods in the package fail. This is extremely conservative, and effectively bounds the maximum possible release from the package in the Newhall Pass Tunnel fire scenario.

Potential Radiological Consequences

Neutron and gamma radiation dose rates from the GA-4 package as a result of the postulated conditions of the Newhall Pass Tunnel fire scenario will not exceed the design basis of the package, which is well within the regulatory limits for hypothetical accident conditions. The neutron shielding is lost early in the transient in all cases, but loss of the neutron shield tank contents is a design-basis assumption for this package in all HAC analyses. The conditions of the Newhall Pass Tunnel fire can do no more damage to the GA-4 package neutron shield than is assumed *a priori* in the HAC analyses. The gamma shielding for the GA-4 is provided by a layer of DU within the stainless steel package body. The shielding function of this material is not affected by the temperatures it is predicted to reach in the Newhall Pass Tunnel fire

scenario. There is no credible scenario in this fire accident that could result in neutron and gamma dose rates from the design-basis GA-4 package exceeding the regulatory limits for accident conditions.

Loss of the package seals due to exceeding seal material thermal limits means that there is the potential for radioactive material to escape from the package. Rupture of all rods in the package is assumed as a bounding limit, even though conservative estimates of maximum fuel temperature histories from the ANSYS modeling for the various cases indicate that only a relatively small percentage of rods would be expected to exceed the burst rupture temperature in this scenario. (Evaluations for the temperatures predicted with the COBRA-SFS model indicate that no rods would be likely to fail in this fire scenario.) In addition, 100% spalling of CRUD from the external surfaces of the fuel rods is assumed, per NRC guidance.

With these extremely conservative assumptions, the package release evaluation for the GA-4 in the MacArthur Maze fire scenario (NUREG/CR-7206 2015) is by definition bounding on the potential release from the package in the Newhall Pass Tunnel fire. Conservative and bounding modeling assumptions for the MacArthur Maze fire scenario show that the maximum possible release total release is 0.24 of the A_2 quantity calculated for total activity of the mixture of radionuclides (comprised of fission gases, fuel particulate and CRUD) released from the package. The regulatory limit specifies a maximum allowable release rate of an A_2/week. The predicted total release estimate of approximately one-fourth of a mixture A_2 is below the prescribed limit for safety, and indicates that the potential release from this package in either the MacArthur Maze fire scenario or Newhall Pass Tunnel fire scenario would not pose a risk to public health and safety.

10.0 REFERENCES

10 CFR 71. 2003. "Packaging and Transportation of Radioactive Material." *Code of Federal Regulations*, U.S. Nuclear Regulatory Commission, Washington, D.C.

ANSI N14.5. 1997. *American National Standard for Radioactive Materials—Leakage Tests on Packages for Shipment.* American National Standards Institute.

ANSYS, Inc. 2003. *ANSYS Users Guide for Revision 8.0.* ANSYS, Inc., Canonsburg, Pennsylvania.

Bahney RH III and TL Lotz. 1996. *Spent Nuclear Fuel Effective Thermal Conductivity Report*, BBA000000-01717-5705-00010 Rev. 00, TRW Environmental Safety Systems, Inc., Fairfax, Virginia.

Brown R. 1987. "Fluid Flow through Rock Joints: The Effect of Surface Roughness." *Journal of Geophysical Research*, 92(B2):1337-1347.

CHP – California Highway Patrol. 2007. *Multi-Disciplinary Accident Investigation Team Report, Interstate 5 Truck Route Tunnel Collision and Fire, October 12, 2007* (MAIT Report). California Highway Patrol, Southern Division (SF-34-07), Newhall Area, CHP 558 (REV 6-99) OPI 061.

Creer JM, TE Michener, MA McKinnon, JE Tanner, ER Gilbert, and RL Goodman. 1987. *The TN-24P PWR Spent-Fuel Storage Cask: Testing and Analysis*. EPRI-NP-5128/PNL-6054, Electric Power Research Institute, Palo Alto, California.

General Atomics. 1998. GA-4 Legal Weight Truck Spent Fuel Shipping Cask Safety Analysis Report for Packaging (SARP), Document No. 910469, Revision G, General Atomics, August 1998. (Public version available online in ADAMS: ML070020004, ML070020006, and ML070020007.)

HEXCEL. 2003. HexWeb Honeycomb Attributes and Properties. Available at http://www.hexcel.com/Resources/DataSheets/Brochure-Data-Sheets/Honeycomb_Attributes_and_Properties.pdf.

Kreith F and MS Bohn. 2001. *Principles of Heat Transfer*, 6th edition, Brooks/Cole, Forest Grove, California.

McGrattan KB, B Klein, S Hostikka, and J Floyd. 2008. *Fire Dynamics Simulator (Version 5), User's Guide*. Special Publication 1019-5, National Institute of Standards and Technology, U.S. Department of Commerce, Washington, D.C.

Michener TE, DR Rector, JM Cuta, RE Dodge, and CW Enderlin. 1995. *COBRA-SFS: A Thermal-Hydraulic Code for Spent Fuel Storage and Transportation Casks*. PNL-10782, Pacific Northwest National Laboratory, Richland, Washington.

NUREG/CR-6487. 1996. *Containment Analysis for Type B Packages Used to Transport Various Contents*, BL Anderson, RW Carlson, and LE Fischer. U.S. Nuclear Regulatory Commission, Washington, D.C.

NUREG/CR-6886. 2009. *Spent Fuel Transportation Package Response to the Baltimore Tunnel Fire Scenario.* U.S. Nuclear Regulatory Commission, Washington, D.C.

NUREG/CR-6894. 2007. *Spent Fuel Transportation Package Response to the Caldecott Tunnel Fire Scenario*. U.S. Nuclear Regulatory Commission, Washington, D.C.

NUREG/CR-7022, Vol. 1. 2011. *FRAPCON-3.4: A Computer Code for the Calculation of Steady-State Thermal-Mechanical Behavior of Oxide Fuel Rods for High Burnup*. U.S. Nuclear Regulatory Commission, Washington, D.C.

NUREG/CR-7023, Vol. 1. 2011. *FRAPTRAN 1.4: A Computer Code for the Transient Analysis of Oxide Fuel Rods.* U.S. Nuclear Regulatory Commission, Washington, D.C.

NUREG/CR-7101. 2011. *Structural Material Analyses of the Newhall Pass Tunnel Fire, 2007*, U.S. Nuclear Regulatory Commission, Washington, D.C.

NUREG/CR-7115. 2012. *Performance of Metal and Polymeric O-Ring Seals in Beyond-Design-Basis Temperature Excursions*. U.S. Nuclear Regulatory Commission, Washington, D.C.

NUREG/CR-7206[1]. 2015. *Spent Fuel Transportation Package Response to the MacArthur Maze Fire Scenario*. U.S. Nuclear Regulatory Commission, Washington, D.C.

NUREG-1617. 2000. *Standard Review Plan for Transportation Packages for Spent Nuclear Fuel: Final Report*. U.S. Nuclear Regulatory Commission, Washington, D.C.

The Dow Chemical Company. 2003. *A Guide to Glycols.* Available at *http://www.dow.com/webapps/lit/litorder.asp?filepath=propyleneglycol/pdfs/noreg/117-01682.pdf*. The Dow Chemical Company, Midland, Michigan.

[1] U.S. Nuclear Regulatory Commission plans to post this document on the Federal Register for Public Comment. Following such posting, and resolution of any comments received, the NRC plans to issue this report as NUREG/CR-7206. The current report, on the Newhall Pass Tunnel fire, will undergo a similar posting, and is expected to be released as NUREG/CR-7207, following resolution of any public comments received.

APPENDIX A

MATERIAL PROPERTIES FOR COBRA-SFS MODEL OF GA-4 PACKAGE

APPENDIX A

MATERIAL PROPERTIES FOR COBRA-SFS MODEL OF GA-4 PACKAGE

Table A.1. Internal Fill Gas—Helium at Atmospheric Pressure

Temperature (°F)	Enthalpy (Btu/lbm)	Thermal Conductivity (Btu/hr-ft-°F)	Specific Heat (Btu/lbm-°F)	Specific Volume (ft^3/lbm)	Viscosity (lbm/hr-ft)
0	100	0.078	1.24	83.33	0.0410
200	348	0.097	1.24	119.76	0.0533
400	596	0.115	1.24	156.25	0.0641
600	844	0.129	1.24	192.31	0.0727
800	1092	0.138	1.24	229.36	0.0823
1000	1340	0.138	1.24	265.25	0.0907
2552	3264	0.138	1.24	549.00	0.1138

Table A.2. External Ambient Air at Atmospheric Pressure

Temperature (°F)	Enthalpy (Btu/lbm)	Thermal Conductivity (Btu/hr-ft-°F)	Specific Heat (Btu/lbm-°F)	Specific Volume (ft^3/lbm)	Viscosity (lbm/hr-ft)
60	124.5	0.0146	0.24	13.5669	0.0434
300	182.1	0.0193	0.243	19.8325	0.058
400	206.5	0.0212	0.245	22.4432	0.063
500	231.1	0.0231	0.247	25.0539	0.068
600	256	0.025	0.25	27.6645	0.072
700	281.1	0.0268	0.253	30.2752	0.077
800	306.7	0.0286	0.256	32.8859	0.081
900	332.5	0.0303	0.259	35.4966	0.085
1000	358.6	0.0319	0.262	38.1072	0.0889
2000	617.2	0.0471	0.2586	64.214	0.1242
4000	1522	0.0671	0.4524	116.428	0.1242

Table A.3. Material Properties

Specific Heat (Btu/lbm-°F)	Density (lbm/ft^3)	Thermal Conductivity (Btu/hr-ft-°F)	Emissivity	Description	Source
0.11	492.5	see Eq. (A-1)	see Table A.4	SA-240, Type XM-19 stainless steel, for basket plates, inner liner, package body, and neutron shield tank outer shell	Density and specific heat from GA-4 SAR (General Atomics 1998); thermal conductivity from ATI 50™ Technical Data Sheet (see below)
0.065	1185.4	14.8	0.5	Depleted uranium for gamma shielding	Specific heat from Table 3.2-1 of GA-4 SAR; density from SAR Section 2.3, p. 2.3-1; thermal conductivity from W21 SAR (see Appendix B)
0.29	151	15.0	0.8	Boron carbide rods within basket plates	Table 3.2-1 of GA-4 SAR, p. 3.2-2
0.787	61.72	$k_{Nsliq.}$ = 0.186 k_{eff} = 5.92	N/A	60% propylene glycol and water mixture (neutron shield)	Table 3.2-2 of GA-4 SAR (selected value at 194ºF), and correlation for k_{eff} of liquid (see Eq. (A-3))

Emissivity values for thermal radiation exchange were obtained from Table 3.2-3 of the GA-4 SAR. However, the emissivity of package surfaces exposed to the fire was conservatively represented with a value of 0.9, rather than the "0.8 or 0.85" listed in the SAR. Table A.4 summarizes the emissivity values used for the XM-19 stainless steel components during the various phases of the fire scenario.

Table A.4. Emissivity Values for XM-19 Stainless Steel Components

Emissivity	Component	Transient Conditions
0.20	steel inner liner basket plates package body inner surface	pre-fire steady state, fire, and post-fire cooldown
0.20	package body outer surface NS tank shell inner surface	pre-fire steady state
0.15	NS tank shell outer surface	pre-fire steady state
0.9	package body outer surface NS tank shell inner surface NS tank shell outer surface	fire and post-fire cooldown

Temperature-dependent thermal conductivity (in units Btu/hr-ft^2-°R) for XM-19 stainless steel was evaluated in the COBRA-SFS model using a linear regression fit to ATI 50 thermal conductivity data (see Appendix B for the material data sheet). The relationship from this fit is

$$k_{XM-19} = a_0 + a_1 T \tag{A.1}$$

where

a_0 = 5.4446
a_1 = 0.0047
T = material temperature (°R)

The relationship in Eq. (A.1) is a polynomial curve fit to the same data used to derive the linear equation presented in the GA-4 SAR, which has the form

$$k_s = a_0 + a_1 T \tag{A.2}$$

where

a_0 = 3.6 (empirical coefficient)
a_1 = 0.00532 (empirical coefficient)
T = material temperature (°R)

These two equations give essentially identical results for temperatures below about 1000°F (538°C), but Equation (A.1) is more conservative by 15-20% at the highest range of temperatures encountered in the fire scenario.

The formula for the effective conductivity used to model natural convection in the liquid neutron shield is documented in the GA-4 SAR as

$$k_{eff} = \frac{a_0 k_{NSliq.} \,\mathrm{Pr}\, Gr_D}{\left(a_1 + \mathrm{Pr}\right)^{a_2}} \tag{A.3}$$

where

a_0 = 0.135 (empirical coefficient)
a_1 = 1.36 (empirical coefficient)
a_2 = 0.278 (empirical coefficient)
$k_{NSliq.}$ = thermal conductivity of neutron shield liquid (60% propylene glycol/water mixture)
Pr = Prantdl Number
Gr_D = Grashoff number, using thickness of liquid layer in the neutron shield tank as the characteristic length

Source for Thermal Conductivity of XM-19 stainless steel:

ATI Allegheny Ludlum

ATI 50™ Technical Data Sheet

Thermal Expansion (mean coefficient over range)

Temperature Range			
°F	°C	in/in/°F x 10^{-6}	mm/mm/°C x 10^{-6}
75-200	24-93	9.0	16.2
75-400	24-204	9.3	16.7
75-600	24-316	9.6	17.3
75-800	24-427	9.9	17.9
75-1000	24-538	10.2	18.4
75-1200	24-649	10.5	19.0
75-1400	24-760	10.8	19.6
75-1600	24.871	11.1	20.0

Thermal Conductivity

Temperature			
°F	°C	Btu-in/ft^2 * hr-°F	W/m * K
200	93	103	14.3
400	204	113	16.3
600	316	125	17.9
800	427	136	19.5
1000	538	144	21.1
1200	649	158	22.7
1400	760	170	24.3
1600	871	181	25.9

Source for Thermal Conductivity of Depleted Uranium:

Table 3.2-1 - W21 Canister Homogenous Material Properties (3 pages)

Material	Temperature (°F)	Thermal Conductivity (BTU/hr-ft-°F)		Density[1] (lb/ft^3)	Specific Heat (BTU/lb-°F)
Lead[3]	-58	21. 7		708	0.030
	32	20.4			0.030
	81	20.0			
	158	19.9			0.031
	248				0.032
	261	19.4			
	338				0.032
	428	18.4			0.033
	608				0.033
	621	16.4			
	698				0.051
	833	10.1			
BORAL®[4]		Through	Axial		
	-40	59.7[6]	63.2[6]	160	0.191[6]
	77	59.0	64.2		0.217
	212	58.1	65.3		0.246
	392	58.5	66.8		0.271
	482	58.3	67.1		0.280
	572	58.1	67.4		0.288
	662	57.7	67.4		0.293
	752	57.3	67.3		0.298
	842	56.2	66.4		0.304
	932	55.2	65.5		0.308
	1472	48.9[6]	60.1[6]		0.329[6]
Depleted Uranium[5]	68	14.6		1183	0.028
	140	15.0			0.028
	437	17.5			0.031
	824	19.3			0.038

Table 3.2-1 Notes:

(1) Single values are shown for homogeneous material density since this material property does not vary significantly with temperature.

(2) Material properties are obtained from ASME Boiler and Pressure Vessel Code, Section II, Part D, 1998 Edition.

(3) Touloukian, Y.S., *Thermal Conductivity - Metallic Elements and Alloys*, Thermophysical Properties of Matter, the TPRC Data Series, Vol. 1, 1970.

(4) AAR, Standard Specification for BORAL® Composite Sheet, AAR Advanced Structures.

(5) General Electric, *Properties of Solids, Thermal Conductivity, Metallic Materials*, Heat Transfer Division, July 1974.

(6) Extrapolated value.

APPENDIX B

MATERIAL PROPERTIES FOR ANSYS MODEL OF GA-4 PACKAGE

APPENDIX B

MATERIAL PROPERTIES FOR ANSYS MODEL OF GA-4 PACKAGE

Table B.1. ASME SA-240 Grade XM-19

Temperature (°F)	Thermal Conductivity (Btu/hr-in-°F)	Density (lbm/in^3)	Specific Heat (Btu/lbm-°F)	Description
50	0.65333	0.2850	0.1150	Used for FSS liner, package body, ILSS, bottom plate, outer shell, trunnions, closure
100	0.67333			
300	0.75167			
500	0.83000			
700	0.90833			
900	0.98667			
1100	1.0650			
1300	1.1433			
1500	1.2217			
1700	1.3000			
1900	1.3783			
2100	1.4567			

Table B.2. FSS Inner Frame (XM-19, helium, and boron carbide composite)

Temperature (°F)	Thermal Conductivity (Btu/hr-in-°F)			Density (lbm/in^3)	Specific Heat (Btu/lbm-°F)	Description
	Kxx	Kyy	Kzz			
0	0.32494	0.40625	0.33828	0.19272	0.19893	Calculated composite properties of XM-19 steel, helium, and boron carbide pellets
100	0.33972	0.42913	0.35146	0.19272	0.19893	
200	0.36773	0.46354	0.38037	0.19272	0.19893	
300	0.39439	0.49628	0.40806	0.19272	0.19893	
400	0.42001	0.52716	0.43482	0.19272	0.19893	
500	0.44263	0.55498	0.45892	0.19272	0.19893	
600	0.46443	0.58131	0.48228	0.19272	0.19893	
700	0.48302	0.60502	0.50280	0.19272	0.20954	
800	0.50101	0.62760	0.52280	0.19272	0.22016	
900	0.51884	0.65034	0.54269	0.19272	0.22494	
1000	0.53611	0.67167	0.56210	0.19272	0.22971	
1100	0.55338	0.69302	0.58153	0.19272	0.23821	

Table B.3. Homogeneous Fuel Region for Westinghouse 14x14 OFA

Temperature (°F)	Thermal Conductivity (Btu/hr-in-°F)			Density (lbm/in^3)	Specific Heat (Btu/lbm-°F)	Description
	Kxx	Kyy	Kzz			
0	-	-	0.05923			
75	0.01688	0.01688	-			
100	0.01815	0.01815	0.05923			
150	0.02069	0.02069	-			
200	0.02323	0.02323	0.05923			
250	0.02576	0.02576	-			
300	0.02865	0.02865	0.06163			
350	0.03173	0.03173	-			
400	0.03498	0.03498	0.06436			
450	0.03848	0.03848	-			Used for active fuel assembly region (WE 14x14)
500	0.04220	0.04220	0.06706	0.1446	0.0747	
550	0.04628	0.04628	-			
600	0.05061	0.05061	0.06998			
650	0.05525	0.05525	-			
675	0.05768	0.05768	-			
700	0.06011	0.06011	0.07344			
725	0.06266	0.06266	-			
750	0.06545	0.06545	-			
800	-	-	0.07689			
900	-	-	0.08033			
1000	-	-	0.08143			

Table B.4. Helium

Temperature (°F)	Thermal Conductivity (Btu/hr-in-°F)	Density (lbm/in^3)	Specific Heat (Btu/lbm-°F)	Description
0	0.00650	0.6900 E-5	1.240	
200	0.00808	0.4810 E-5		
400	0.00958	0.3690 E-5		Used for gaps within package assembly
600	0.01075	0.2990 E-5		
800	0.01150	0.2520 E-5		
1400	0.01370	0.1710 E-5		

Table B.5. Air

Temperature (°F)	Thermal Conductivity (Btu/hr-in-°F)	Density (lbm/in^3)	Specific Heat (Btu/lbm-°F)	Description
0	0.001092	0.4994 E-4	0.2396	Used for trunnion air pockets, outer closure assembly gap, and the impact limiter to outer shell gap
32	0.001159	0.5039 E-4	0.2398	
100	0.001297	0.4103 E-4	0.2400	
200	0.001483	0.3484 E-4	0.2411	
300	0.001661	0.3021 E-4	0.2427	
400	0.001833	0.2674 E-4	0.2448	
500	0.002001	0.2390 E-4	0.2473	
600	0.002163	0.2164 E-4	0.2504	
800	0.002469	0.1823 E-4	0.2567	
1000	0.002769	0.1574 E-4	0.2631	
1200	0.003060	0.1383 E-4	0.2688	
1400	0.003331	0.1233 E-4	0.2740	

Table B.6. ASME SA-479 S21800, Nitonic 60

Temperature (°F)	Thermal Conductivity (Btu/hr-in-°F)	Density (lbm/in^3)	Specific Heat (Btu/lbm-°F)	Description
-	1.00	0.2750	0.1150	Used for trunnion sleeves

Table B.7. ASTM A-276 GR 304

Temperature (°F)	Thermal Conductivity (Btu/hr-in-°F)	Density (lbm/in^3)	Specific Heat (Btu/lbm-°F)	Description
-	0.8333	0.2836	0.1100	Used for stiffener ring

Table B.8. Aluminum Honeycomb 220 psi

Temperature (°F)	Thermal Conductivity (Btu/hr-in-°F)	Density (lbm/in^3)	Specific Heat (Btu/lbm-°F)	Description
0	0.22856	0.0024	0.210	Used for honeycomb section 2 of impact limiters
100	0.28238			
200	0.34957			
300	0.40339			

Table B.9. Aluminum Honeycomb 725 psi

Temperature (°F)	Thermal Conductivity (Btu/hr-in-°F)	Density (lbm/in^3)	Specific Heat (Btu/lbm-°F)	Description
0	0.59172	0.0046	0.210	Used for honeycomb section 3 of impact limiters
100	0.73086			
200	0.90488			
300	1.04410			

Table B.10. Aluminum Honeycomb 1400 psi

Temperature (°F)	Thermal Conductivity (Btu/hr-in-°F)	Density (lbm/in^3)	Specific Heat (Btu/lbm-°F)	Description
0	1.0322	0.0061	0.210	Used for honeycomb section 1 of impact limiters
100	1.2751			
200	1.5787			
300	1.8216			

Table B.11. Stainless Steel 304L

Temperature (°F)	Thermal Conductivity (Btu/hr-in-°F)	Density (lbm/in^3)	Specific Heat (Btu/lbm-°F)	Description
-	0.8333	0.2836	0.110	Used for fuel spacer tube

Table B.12. ASTM A-412 Grade XM-11

Temperature (°F)	Thermal Conductivity (Btu/hr-in-°F)	Density (lbm/in^3)	Specific Heat (Btu/lbm-°F)	Description
-99.4	0.52500	0.2830	0.1150	Used for impact limiter shell
203.0	0.65777			
401.0	0.77777			
599.0	0.87500			
797.0	0.97223			
1200.0	1.18750			
1600.0	1.39580			

Table B.13. SB-637 Alloy N07718

Temperature (°F)	Thermal Conductivity (Btu/hr-in-°F)	Density (lbm/in^3)	Specific Heat (Btu/lbm-°F)	Description
-	0.5493	0.2960	0.1040	Used for assembly bolts

Table B.14. Emissivity Values for Radiation Heat Transfer

Component	Material	Emissivity Before Fire	Emissivity During/After	Solar Absorptivity
Inner Steel Surfaces	stainless steel	0.35	0.35	-
Outer Cask Skin	stainless steel	0.15	0.9	0.4
Outer Impact Limiter Shell	steel	0.85	0.9	0.6
Depleted Uranium	depleted uranium	0.5	0.5	-
Fuel Assembly	-	0.7	0.7	-
Boron Carbide Pellets	boron carbide	0.8	0.8	-
Surface Exposed to Fire	-	0.9	0.9	-
Ambient Environment	-	0.9	0.9	-
Inside of Cask Skin	stainless steel	0.9	0.9	-
Outer Surface of Package Body	stainless steel	0.9	0.9	-

Depleted Uranium – See table in Appendix A

Neutron Shield – Effective Conductivity Calculations:
An empirical relationship for effective conductivity incorporating the effects of both conduction and convection was used to determine heat exchange through the liquid neutron shield. The effective conductivity of the fluid within the tank is based on heat transfer between two concentric cylinders. This correlation produces reasonable values of k_{eff}, and the transient conditions are generally within its applicable range. The correlation relates the Nusselt number to the ratio of the effective conductivity over the actual conductivity, and is expressed as

$$\frac{k_{eff}}{k_c} = Nu = 0.386\left(\frac{\mathrm{Pr}}{0.861+\mathrm{Pr}}\right)^{0.25} Ra_c^{0.25} \tag{B.1}$$

where

k_{eff} = effective thermal conductivity of material in node
k_c = thermal conductivity of motionless fluid in node
Nu = Nusselt number
Pr = Prandtl number
Ra_c = modified Rayleigh number

The modified Rayleigh number is defined as:

$$Ra_c = \frac{\left[\ln(D_o/D_i)\right]^4}{L^3\left[D_i^{-0.6} + D_o^{-0.6}\right]^5} Ra \tag{B.2}$$

where

D_o = annulus outer diameter
D_i = annulus inner diameter
Ra = Rayleigh number
L = $(D_o - D_i)/2$

The Rayleigh number is based on the temperature difference across the annular gap and is expressed as:

$$Ra = \frac{g\beta(T_i - T_o)L^3}{\nu\alpha} \tag{B.3}$$

where

g = acceleration of gravity
T_i = inner surface temperature
T_o = outer surface temperature
β = thermal expansion coefficient
α = thermal diffusivity of fluid
ν = kinematic viscosity of fluid

Using the correlations listed above, a macro was written to calculate the effective conductivity after each solution step within the transient model. For conditions below 276°F, the properties of 56% propylene glycol and water were used to calculate the effective conductivity. Once the maximum temperature within the tank exceeded 276°F, the properties of air were used to determine the thermal conductivity.

Verification of Effective Conductivity Model for GA-4 Neutron Shield Configuration

The effective conductivity model described above is based on experimental data for natural convection mixing of fluid between horizontal concentric cylinders. The neutron shield tank of the GA-4 package consists of an inner surface formed by the package body, which is a square with rounded corners, and an outer cylindrical shell. To verify that this empirical model could be applied to the GA-4 package neutron shield geometry, the correlation predictions were compared to results from a computational fluid dynamics (CFD) model.

Calculations were performed with Star-CD[1], for a 2-D "slice" model at the midplane of the package, using two basic configurations to model the GA-4 neutron shield tank. In one model, the neutron shield fluid region is represented as a solid material with thermal conductivity determined using the relationship for the effective thermal conductivity, as defined in Eq. (B.1). In the other model, the neutron shield fluid region is represented as a liquid, with the fluid properties of the propylene-glycol/water mixture reported in the GA-4 SAR [11].

The results of this evaluation are summarized in Table B.15, with comparisons of the maximum and minimum predicted temperatures obtained with the Star-CD model for all cases considered. All calculations in this evaluation were performed at normal conditions of transport. The maximum temperature is the peak temperature in the fuel region[2], and the minimum temperature is the minimum temperature on the package outer shell surface. As shown by the results in Table B.15, a computation mesh that was appropriate for the neutron shield represented as a solid was not sufficient resolution for the CFD model. The number of computational elements required was approximately two orders of magnitude larger.

Star-CD results for the case with the neutron shield represented as a solid material and for the case with the neutron shield represented as a fluid (with an appropriately refined mesh) are shown graphically with color thermographs in Figure B.1. Overall, this evaluation has shown that the effective conductivity model predicts temperatures that are results are consistent with the CFD model results. There is also some indication that the effective conductivity model may yield results that are slightly conservative.

[1] **STAR-CD,** ***Version 4.14 Methodology***, Computational Dynamics Ltd. 2010.

[2] Note that the 2-D "slice" model used in this study oversimplifies features captured in the fully 3-D ANSYS model used for the MacArthur Maze fire calculations. As a result, temperatures predicted for NCT with the fully 3-D ANSYS model differ slightly from the temperatures reported in this study with Star-CD. With the ANSYS model, the peak fuel region temperature is 306°F (152°C) and the minimum outer shell temperature is 188°F (87°C).

Table B.15. Summary of STAR-CD Model Results

Case Description	Peak Fuel Region Temperature, °F (°C)	Minimum Outer Shell Temperature, °F (°C)	Number of Computational Elements	Number of Fluid Elements
Effective conductivity model	302 (150)	194 (90)	3,664	0
Baseline CFD model	312 (156)	194 (90)	3,664	1232
CFD model (2x2 refine, all)	307 (153)	194 (90)	14,596	4928
CFD model (4x4 refine, all)	303 (151)	192 (89)	58,384	19,712
CFD model (5x5 refine) 2x solids	301 (149)	189 (87)	46,936	30,800
CFD model (8x8 refine, all)	300 (149)	189 (87)	233,536	78,848

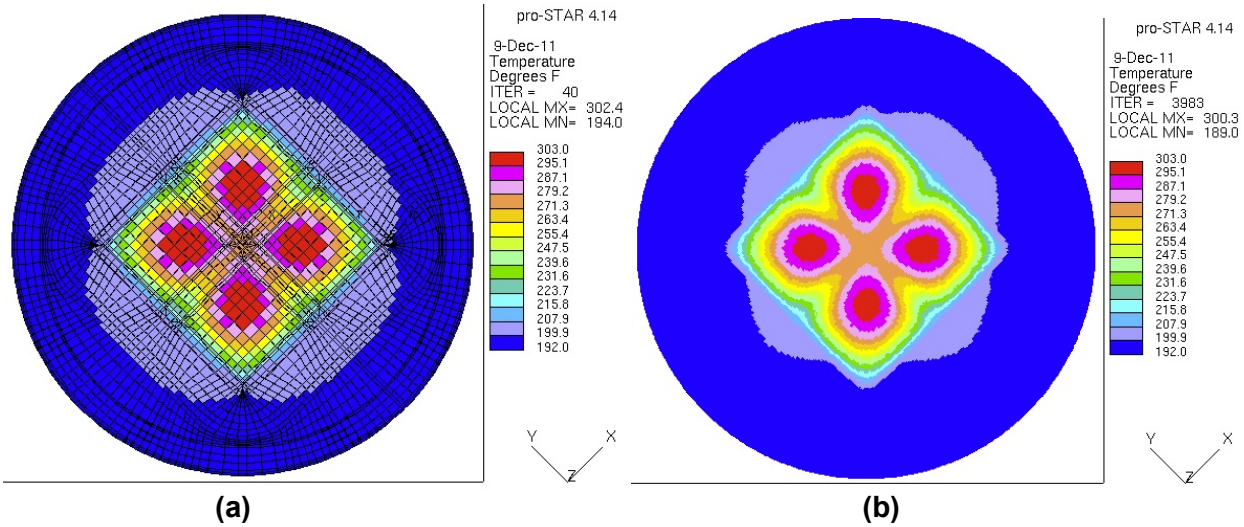

Figure B.1. Midplane Temperature Distributions Predicted with Star-CD Model of GA-4 Package at Normal Conditions of Transport: (a) solid material neutron shield with effective conductivity model, and (b) liquid neutron shield with (8x8) refined mesh.

APPENDIX C

DETAILED TEMPERATURE EVOLUTION FOR GA-4 COMPONENTS IN NEWHALL PASS TUNNEL FIRE SCENARIOS

APPENDIX C

DETAILED TEMPERATURE EVOLUTION FOR GA-4 COMPONENTS IN NEWHALL PASS TUNNEL FIRE SCENARIOS

This appendix is included to supplement the discussion of results presented in Section 7.0 of this report, by providing a detailed picture of the evolution of the package internal temperatures for all cases evaluated in the Newhall Pass fire scenario. Thermographs of cross-sections radially and axially through the center of the package are shown at selected hourly intervals[1] throughout the fire and into the post-fire cooldown. These images clearly illustrate the rapid heat-up of the package outer components in response to the fire environment, and the slow response of the package internal components (including the fuel assemblies), which generally reach their peak temperatures after the end of the fire. The axial cross-section images illustrate the tendency of package components covered by the impact limiters to continue to increase in temperature after the end of the fire. The impact limiters insulate the package ends (including the seals) from the effects of the fire, but they also insulate them from the rapidly cooling ambient post-fire conditions, trapping heat dissipating axially from the hot center of the package.

All cases evaluated were initiated from the same steady-state conditions corresponding to normal conditions of transport (NCT). Therefore, the thermographs for the initial conditions are shown only for the first case presented here, case NIST-01 ("hottest fire").

C.1 NIST-01

The fire conditions predicted with FDS for NIST-01 provide the base case boundary conditions for the thermal evaluations of the GA-4 package response to the Newhall Pass Tunnel fire scenario. In this case, the fuel available for the fire is based on an assumed "typical" cargo load for each vehicle (including those known to have been empty). The fire spread rate is defined such that the total fire duration is approximately 5 hours, slightly longer than the maximum credible duration for the intense vehicle fires in this accident scenario. The burn rate is specified such that the fire on each vehicle lasts approximately 1 hour.

C.1.1 NIST-01: Package at Hottest Fire Location

The "hottest location" for this case is on vehicle #23, near the center of the tunnel. Due to the relatively slow spread rate, the fire on this vehicle does not begin until approximately 1.8 hours into the fire scenario. Figure C.1 shows the engulfing fire boundary temperatures assumed for the two selected fire locations. The local fire duration on vehicle #23 is approximately 1 hour, after which the local ambient temperature drops rapidly, as the fire continues to move toward the tunnel entrance. Approximately an hour after the end of the fire on vehicle #23 (near the center of the tunnel), the local fire is just beginning on vehicle #31 (as discussed in Section C.1.2 below).

[1] The initial steady-state (NCT) prior to the fire is developed in the ANSYS model with a pseudo-transient of 0.5 hours to assure that the package is at thermal equilibrium at the beginning of the transient. The transient time-stamp on the ANSYS graphics include this initial time interval, and are therefore offset by 0.5 hour from the fire transient time. To avoid confusion, the graphics have been labeled with the elapsed time since time zero, at the start of the fire.

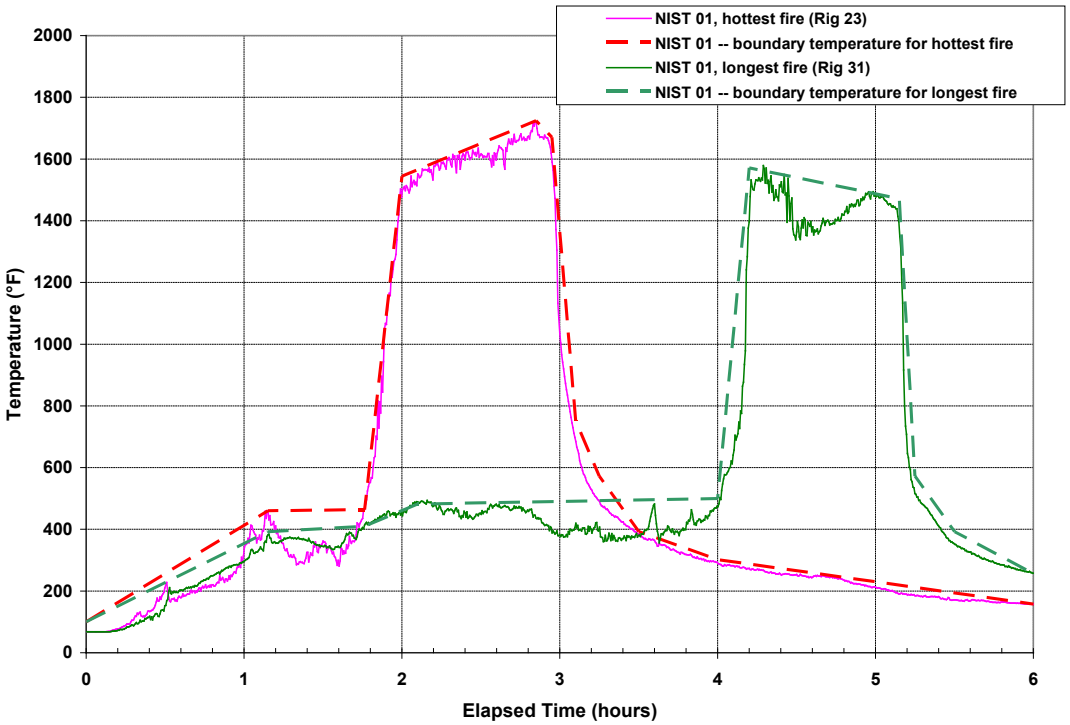

Figure C.1. Boundary Temperatures for Hottest Fire and Longest Fire Locations for Case NIST-01

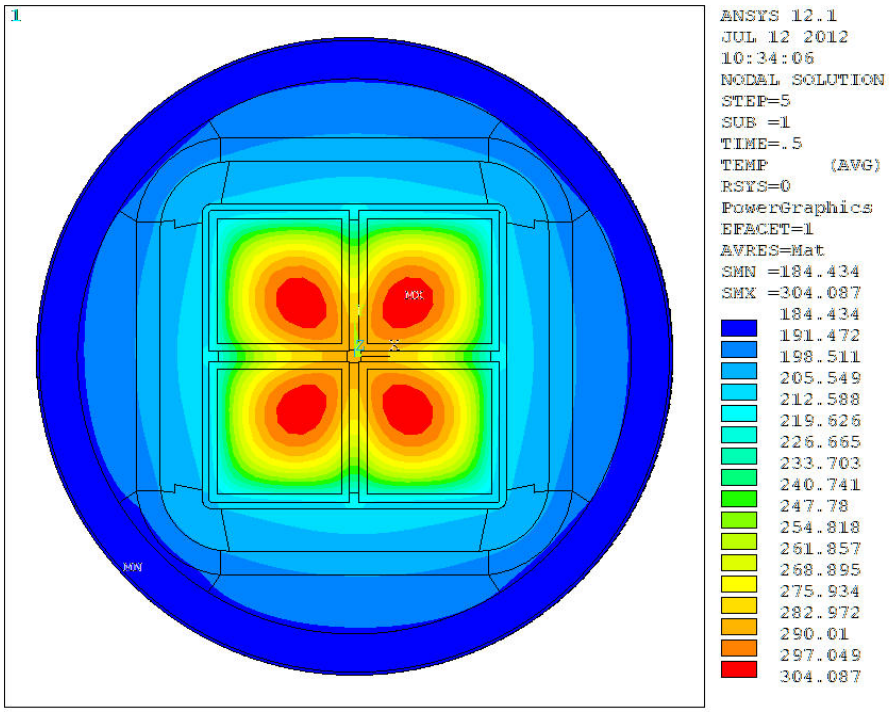

Figure C.2. All Cases: (initial steady-state – ambient temperature 100°F [38°C])

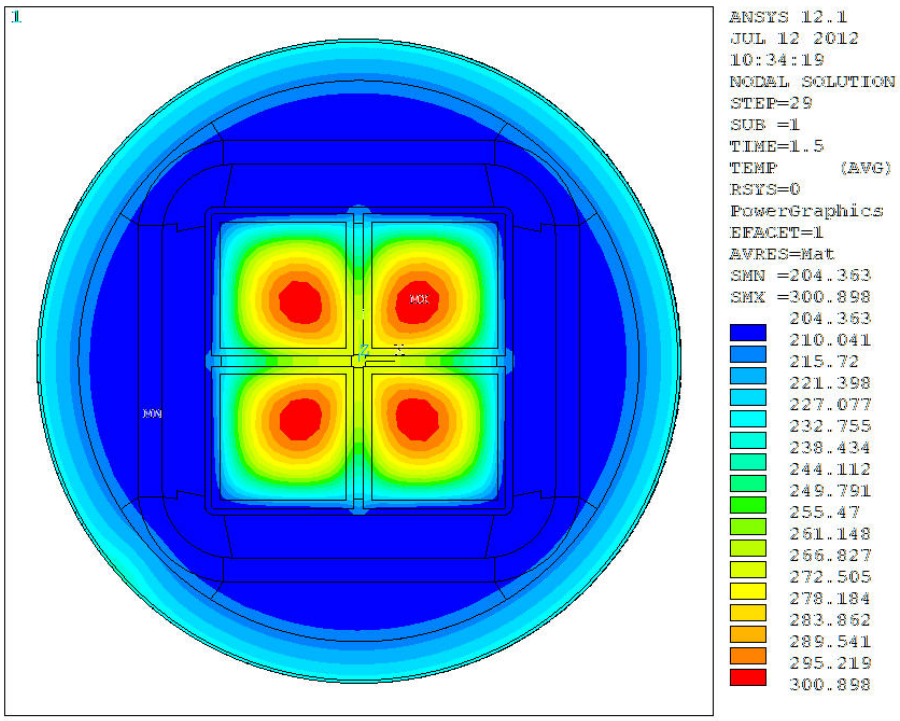

Figure C.3. NIST-01: (at 1 hour – ~45 minutes before fire on vehicle #23 – ambient temperature ~392°F [200°C])

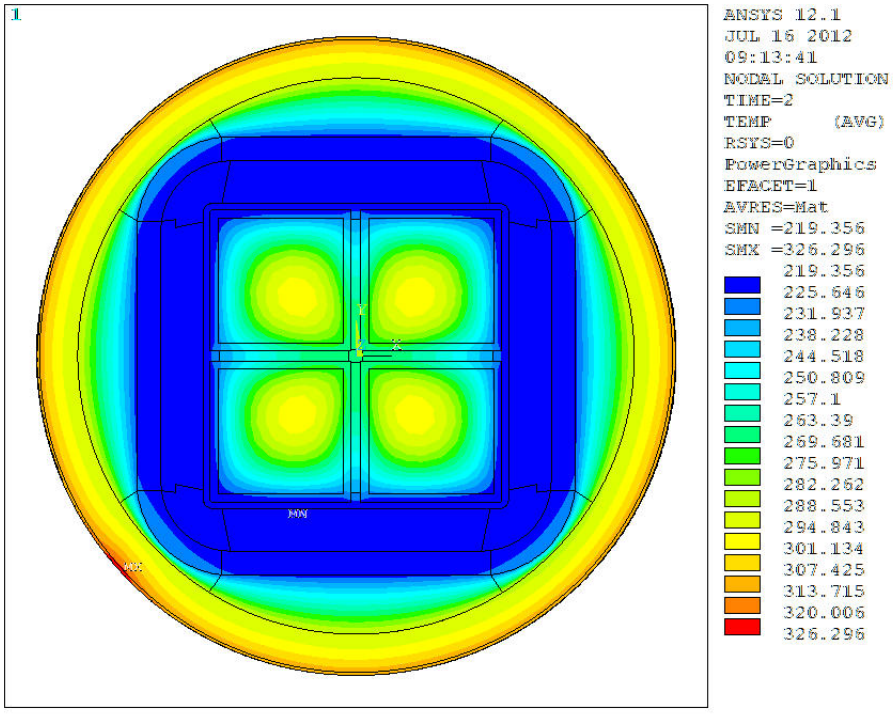

Figure C.4. NIST-01: (at 1.5 hours – ~15 minutes before fire on vehicle #23 – ambient temperature ~465°F [241°C])

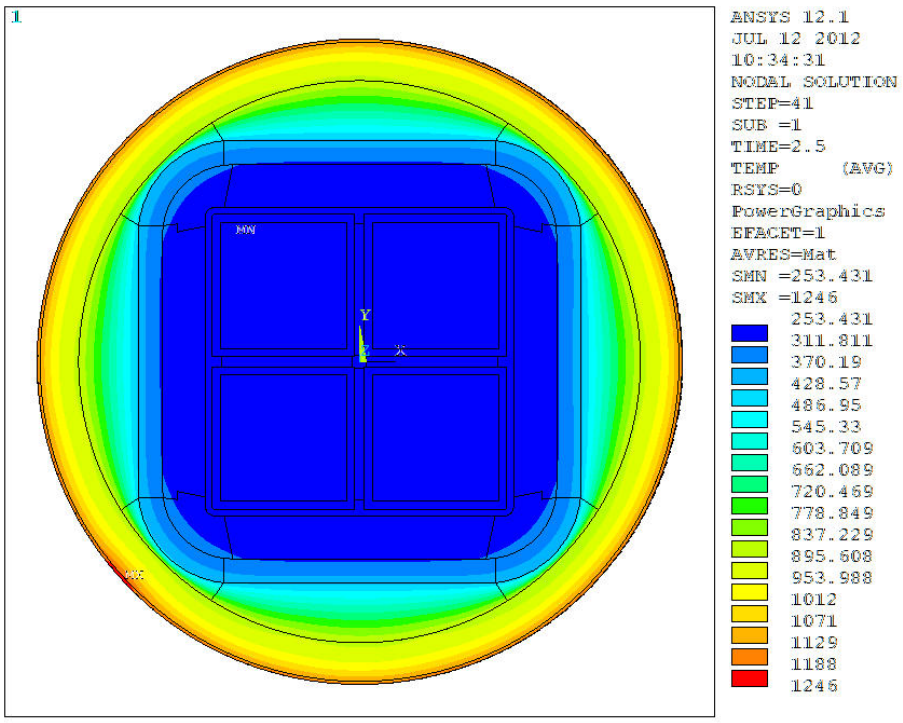

Figure C.5. NIST-01: (at 2 hours – beginning of fire on vehicle #23 – ambient temperature ~1544°F [840°C])

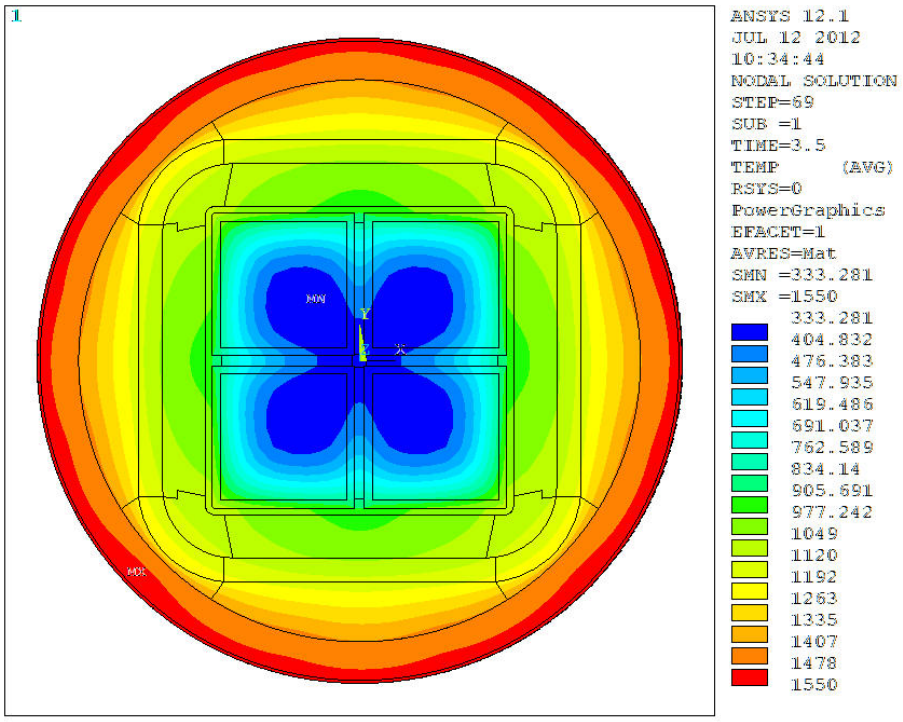

Figure C.6. NIST-01: (at 3 hours – end of fire on vehicle #23 – ambient temperature ~1364°F [740°C])

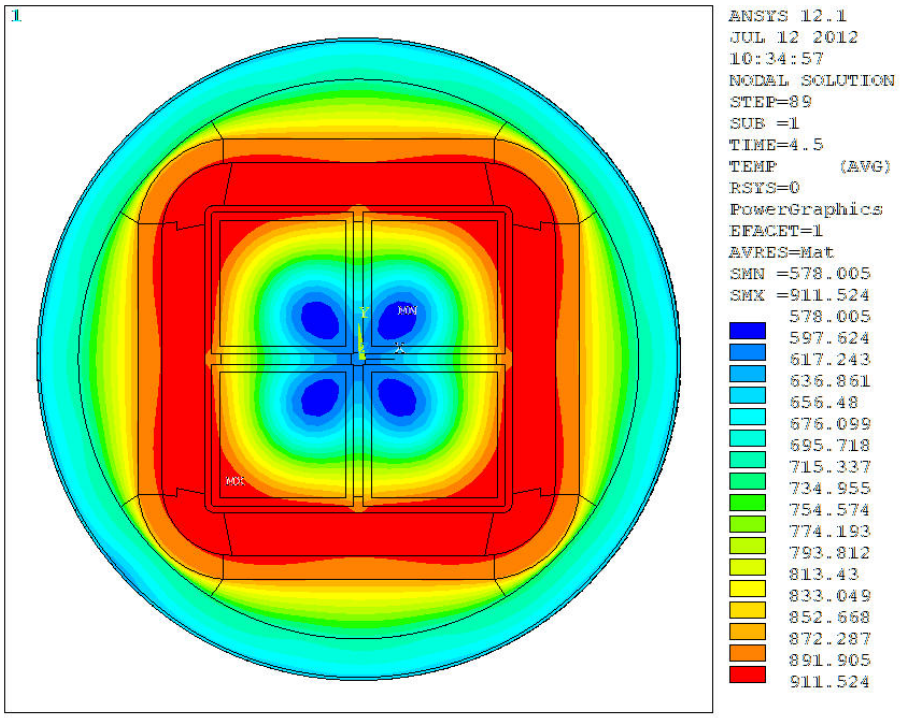

Figure C.7. NIST-01: (at 4 hours – 1 hour after end of fire on vehicle #23 – ambient temperature ~302°F [150°C])

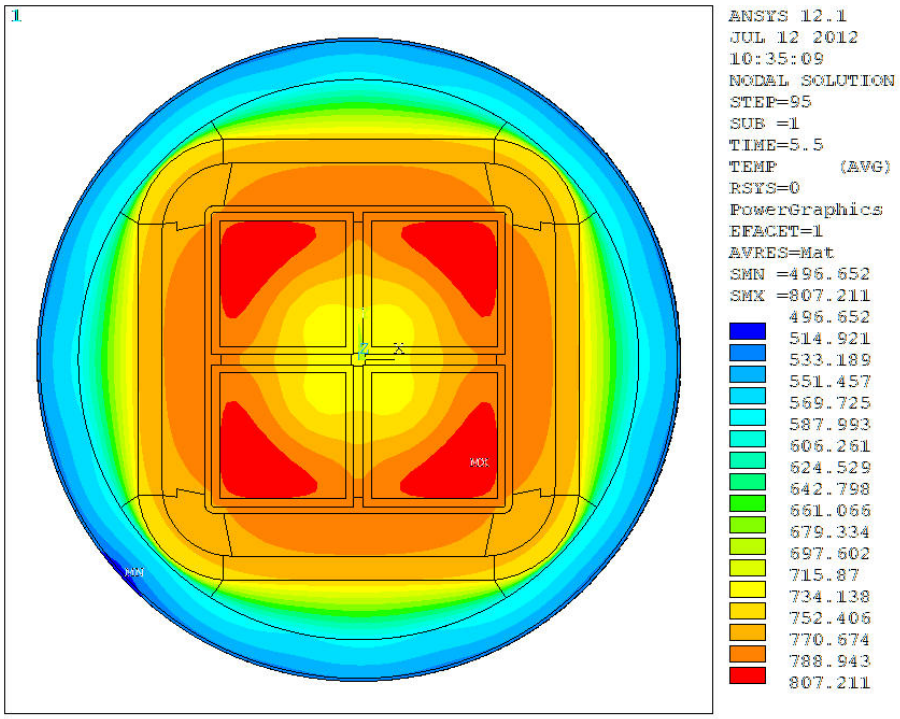

Figure C.8. NIST-01: (at 5 hours – end of all vehicle fires, and 2 hours after end of fire on vehicle #23 – ambient temperature ~230°F [110°C])

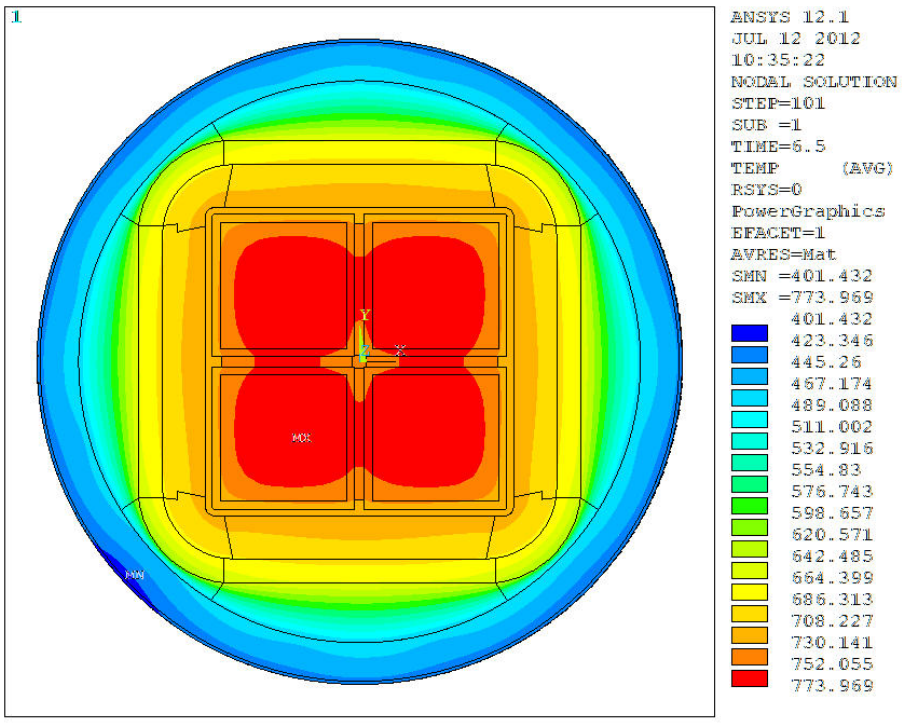

Figure C.9. NIST-01: (at 6 hours – 3 hours after end of fire on vehicle #23 – ambient temperature ~158°F [70°C])

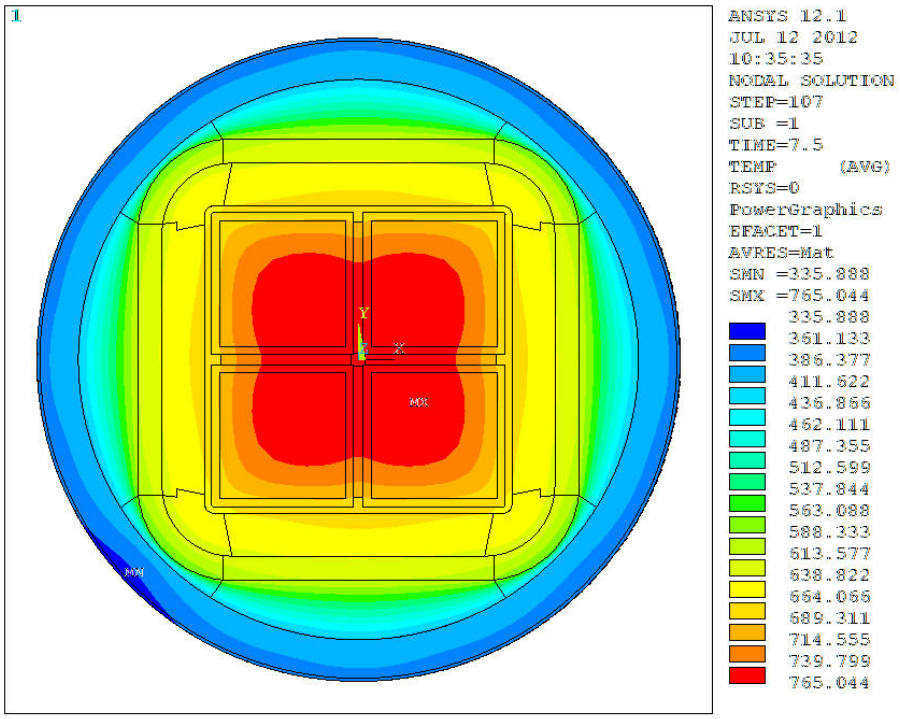

Figure C.10. NIST-01: (at 7 hours – 4 hours after end of fire on vehicle #23 – ambient temperature returned to pre-fire conditions; 100°F [38°C])

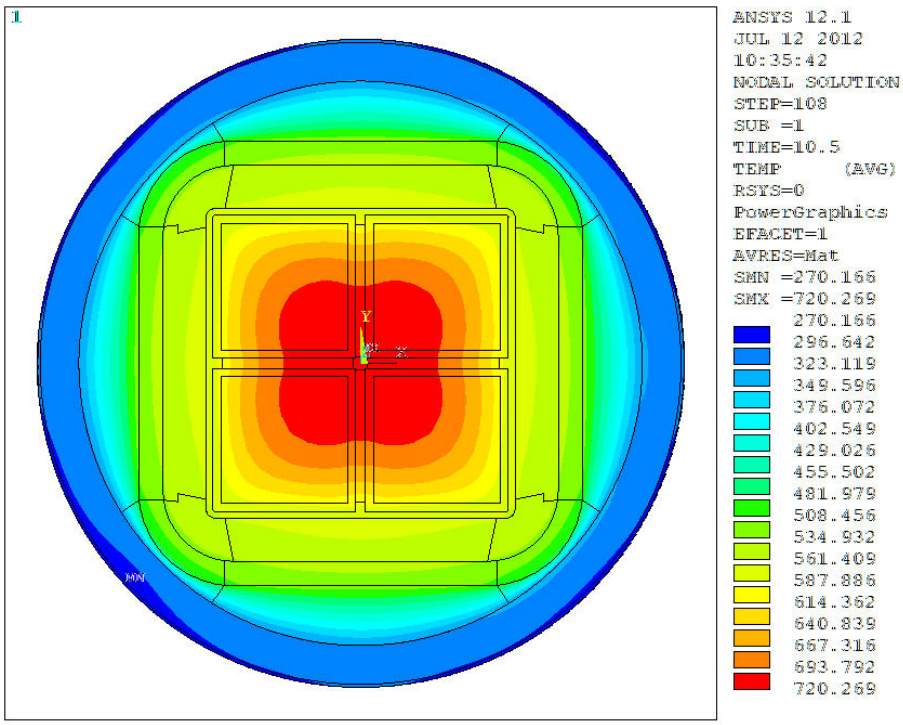

Figure C.11. NIST-01: (at 10 hours – 7 hours after end of fire on vehicle #23 – ambient temperature 100°F [38°C])

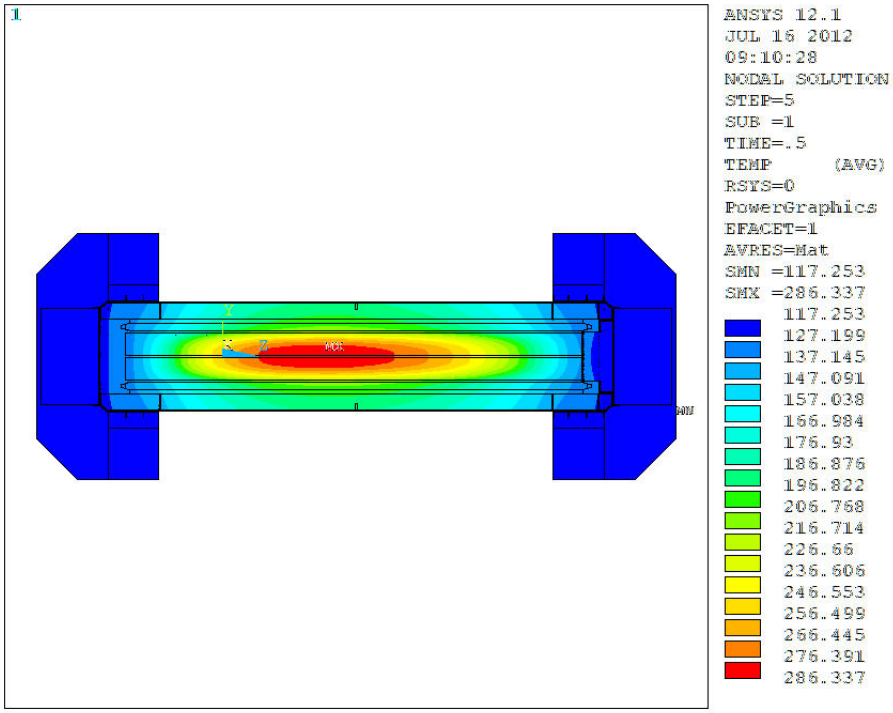

Figure C.12. NIST-01: (initial steady-state)

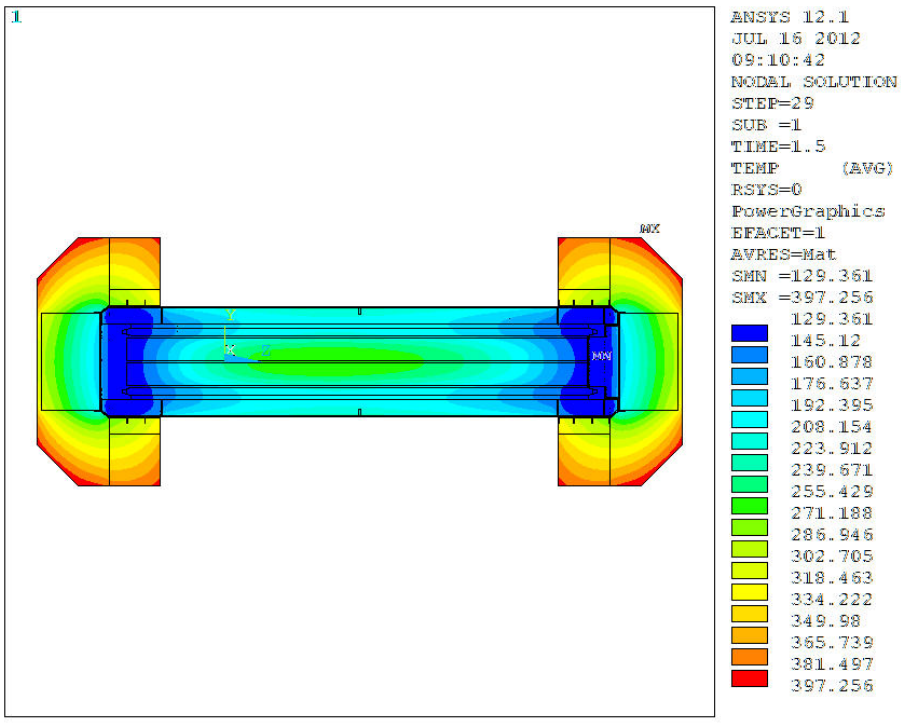

Figure C.13. NIST-01: (at 1 hour – before fire on vehicle #23 – ambient temperature ~392°F [200°C])

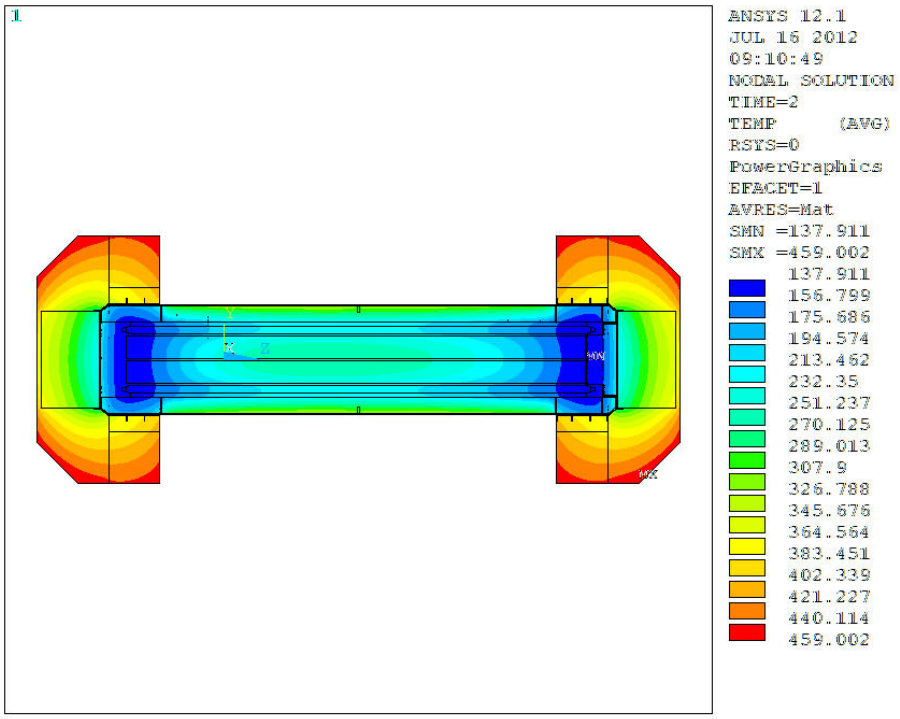

Figure C.14. NIST-01: (at 1.5 hours – ~15 minutes before fire on vehicle #23 – ambient temperature ~465°F [241°C])

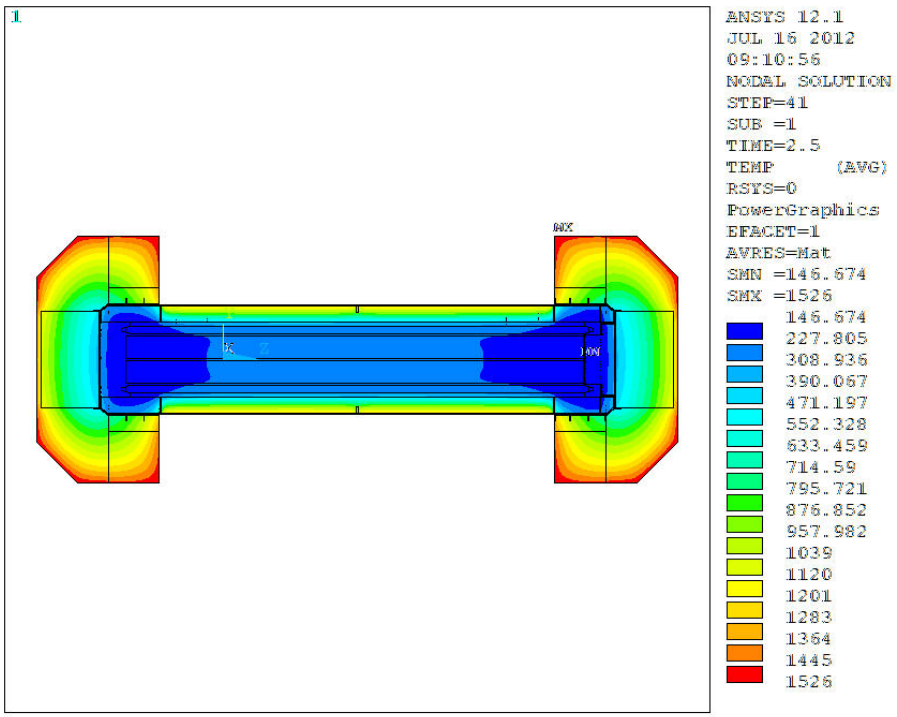

Figure C.15. NIST-01: (at 2 hours – beginning of fire on vehicle #23 – ambient temperature ~1544°F [840°C])

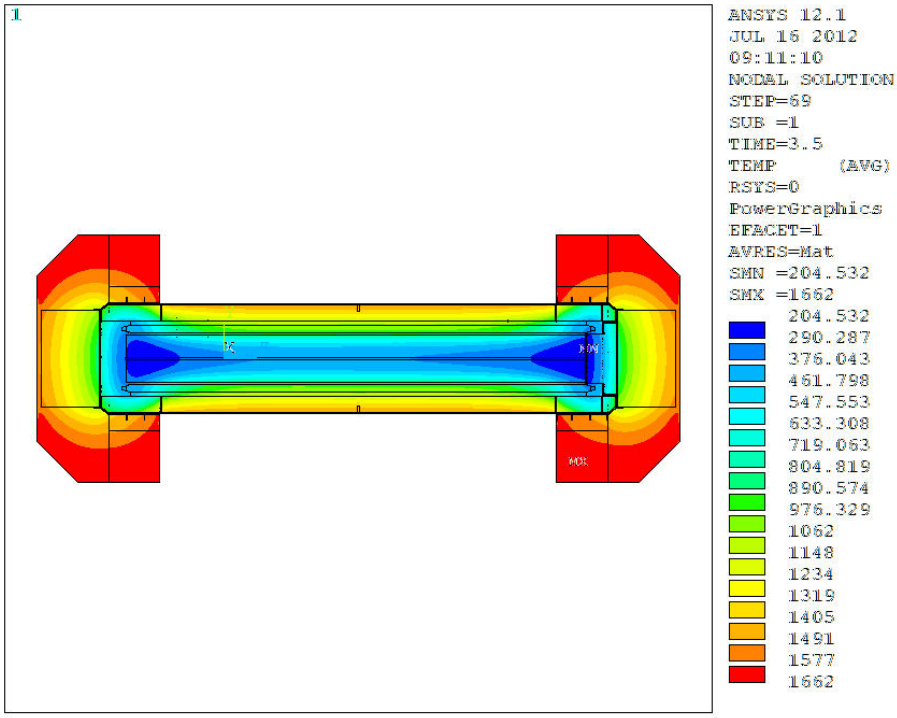

Figure C.16. NIST-01: (at 3 hours – end of fire on vehicle #23 – ambient temperature ~1364°F [740°C])

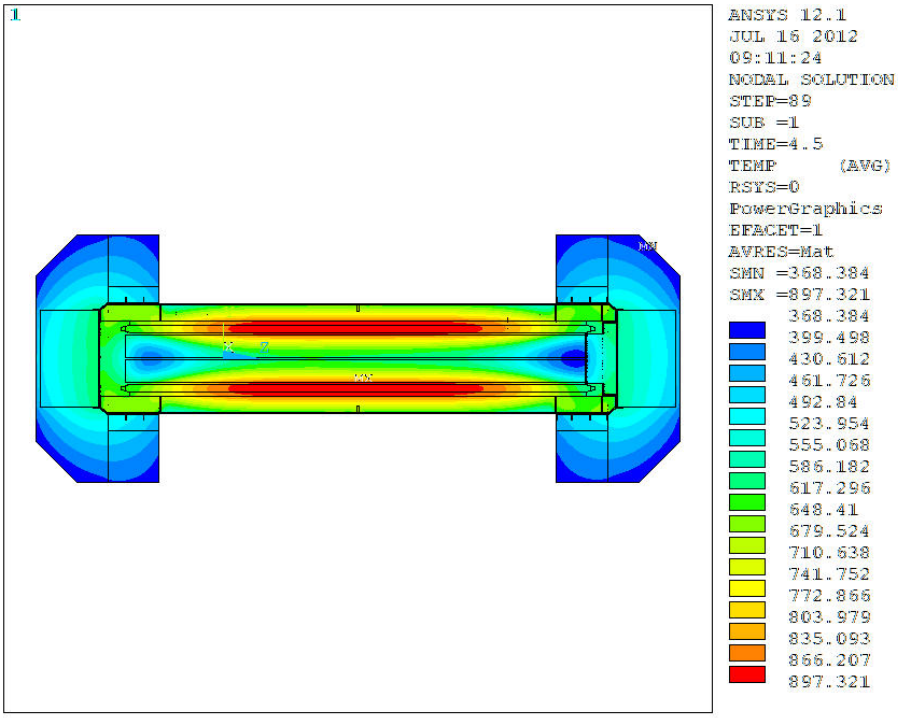

Figure C.17. NIST-01: (at 4 hours – 1 hour after end of fire on vehicle #23 – ambient temperature ~302°F [150°C])

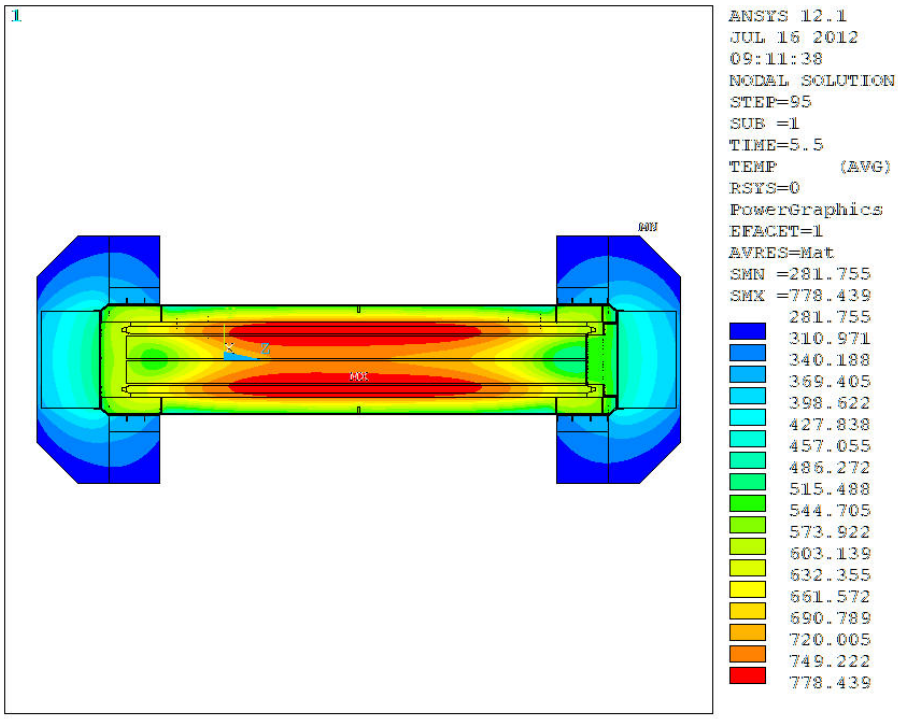

Figure C.18. NIST-01: (at 5 hours – end of all vehicle fires, and 2 hours after end of fire on vehicle #23 – ambient temperature ~230°F [110°C])

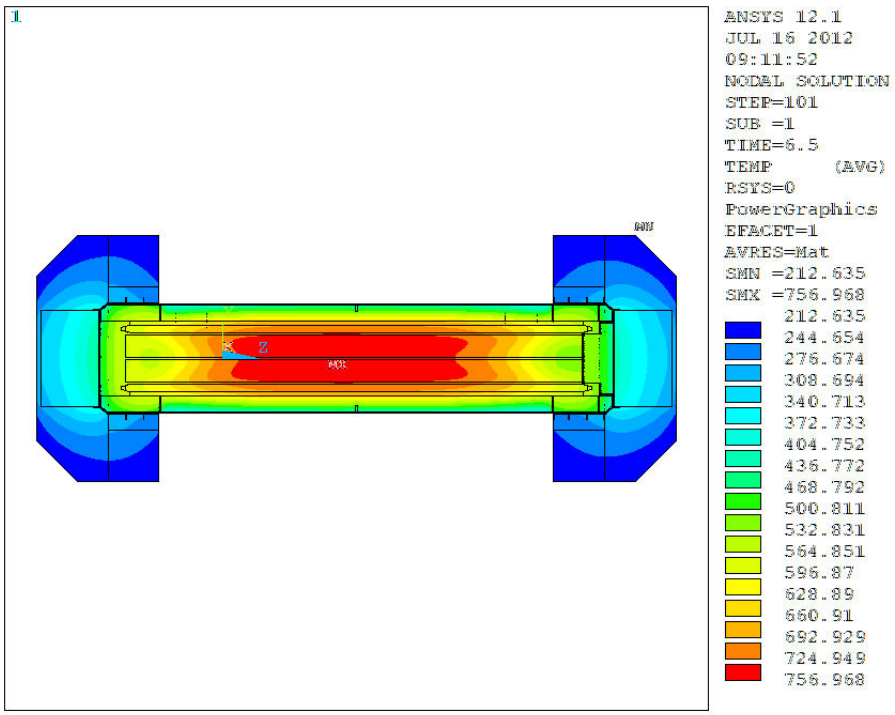

Figure C.19. NIST-01: (at 6 hours – 3 hours after end of fire on vehicle #23 – ambient temperature ~158°F [70°C])

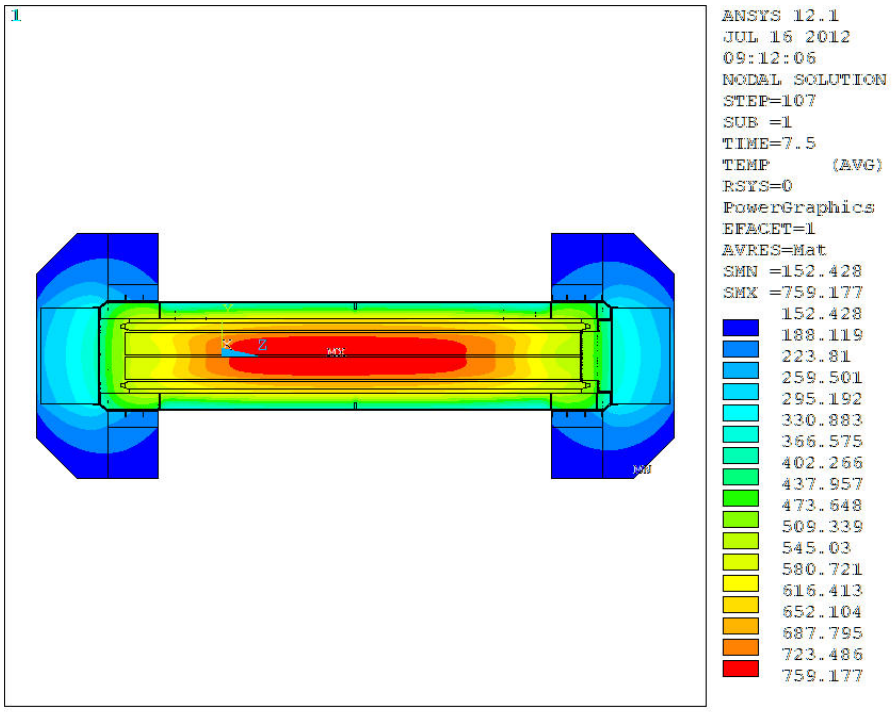

Figure C.20. NIST-01: (at 7 hours – 4 hours after end of fire on vehicle #23 – ambient temperature returned to pre-fire conditions; 100°F [38°C])

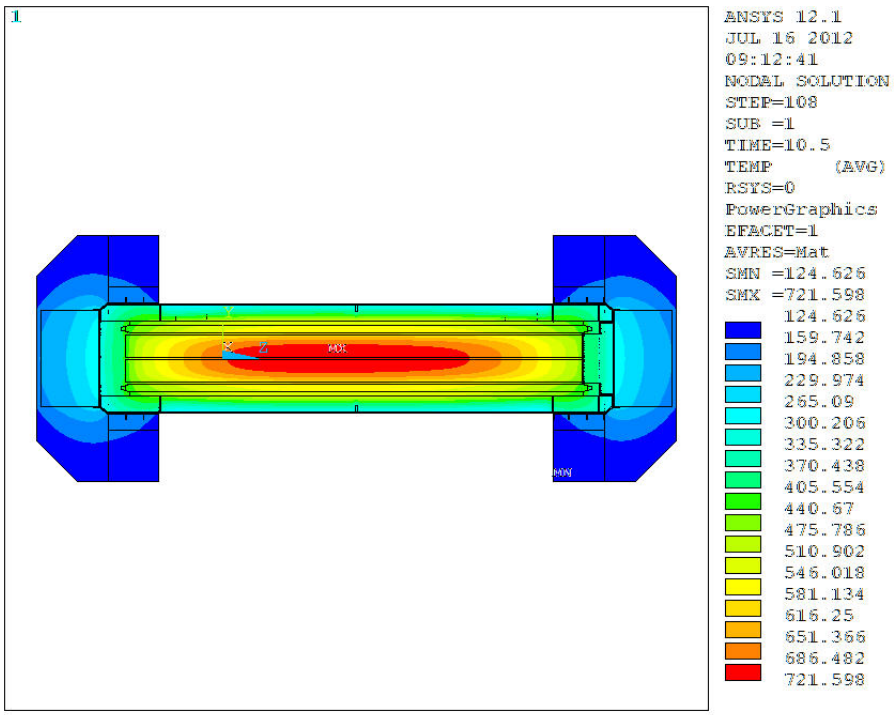

Figure C.21. NIST-01: (at 10 hours – 7 hours after end of fire on vehicle #23 – ambient temperature 100°F [38°C])

C.1.2 NIST-01: Package at Longest Fire Location

The longest fire location for this case is on vehicle #31, near the entrance to the tunnel. Due to the relatively slow spread rate, the fire on this vehicle does not begin until approximately 4 hours into the fire scenario. The package experiences an essentially linear increase in ambient temperature to ~400°F (204°C) during the first hour of the transient, then a more gradual increase to ~500°F (260°C) during the second hour. The ambient temperature is nearly constant at this value for the remaining 2 hours of the 'preheat' before the local fire begins on vehicle #31.

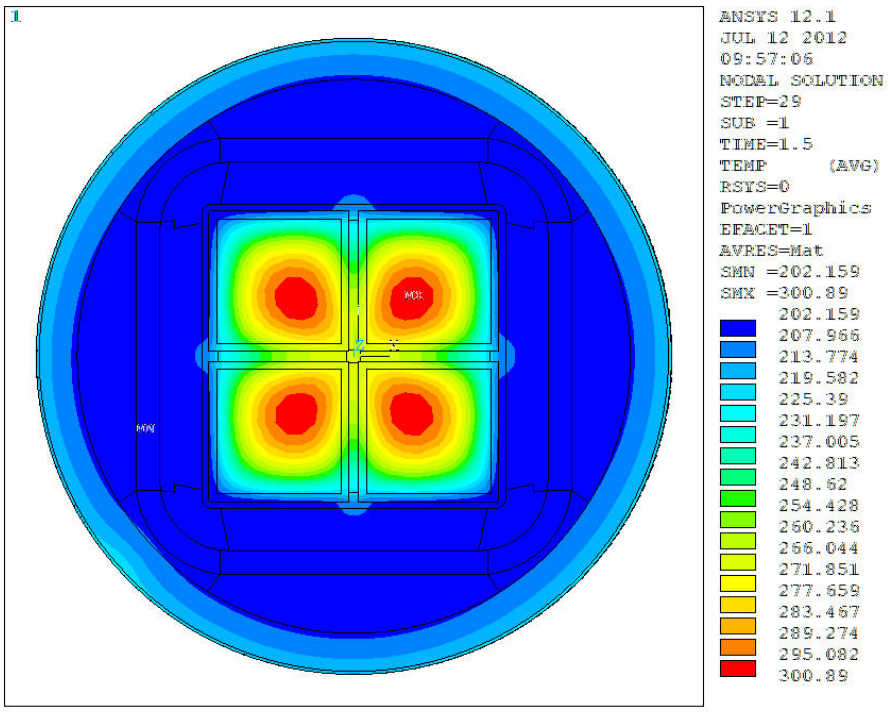

Figure C.22. NIST-01: (at 1 hour – 3 hours before fire on vehicle #31 – ambient temperature ~353°F [179°C])

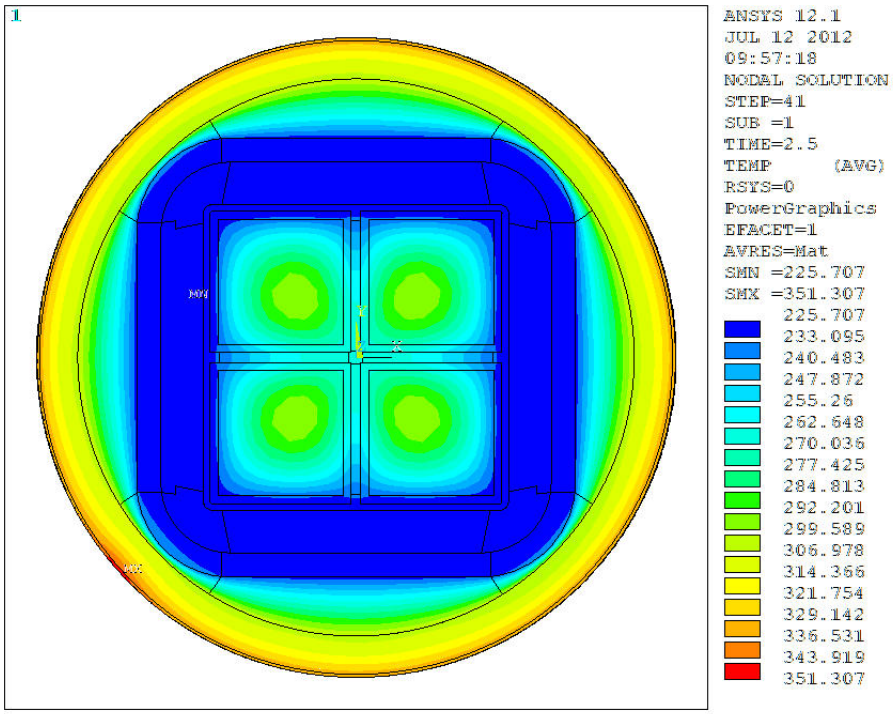

Figure C.23. NIST-01: (at 2 hours – 2 hours before fire on vehicle #31 – ambient temperature ~461°F [238°C])

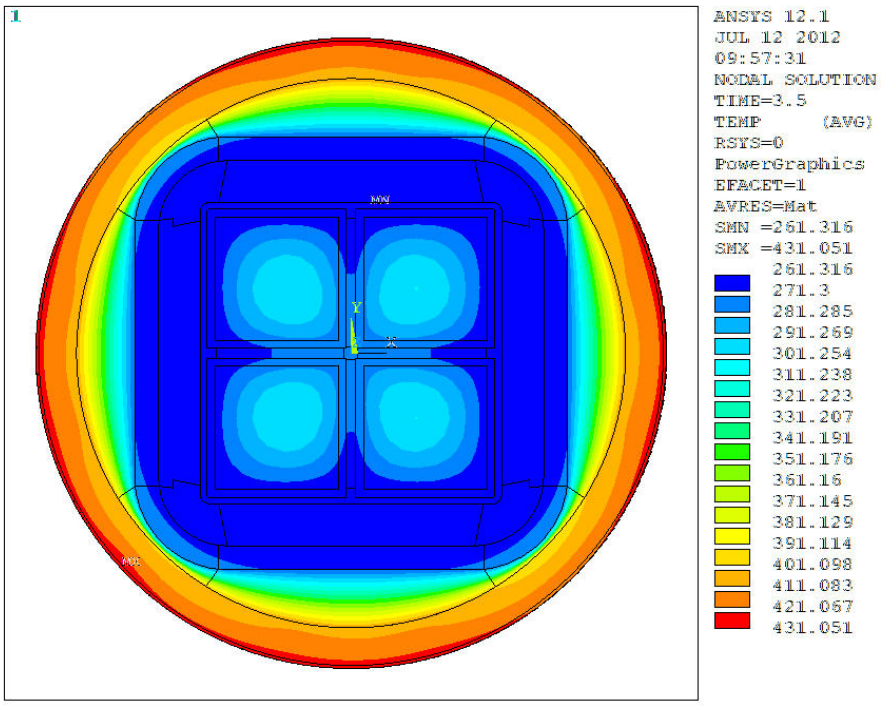

Figure C.24. NIST-01: (at 3 hours – 1 hour before fire on vehicle #31 (and end of fire on vehicle #23) – ambient temperature ~494°F [257°C])

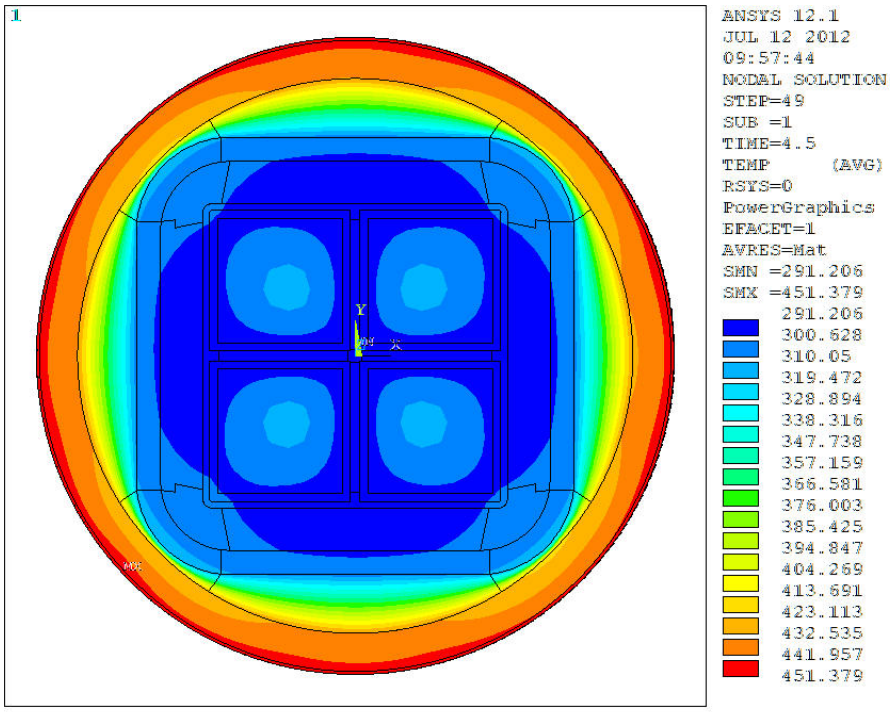

Figure C.25. NIST-01: (at 4 hours – just before beginning of fire on vehicle #31 – ambient temperature 500°F [260°C])

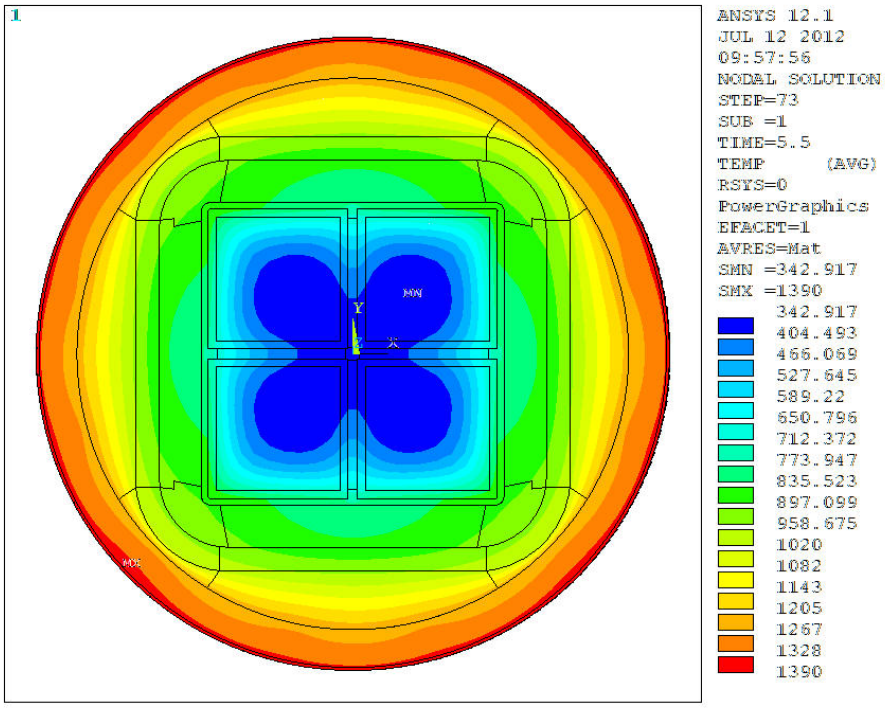

Figure C.26. NIST-01: (at 5 hours – 9 minutes before end of fire on vehicle #31 (and end of all vehicle fires) – ambient temperature 1496°F [813°C])

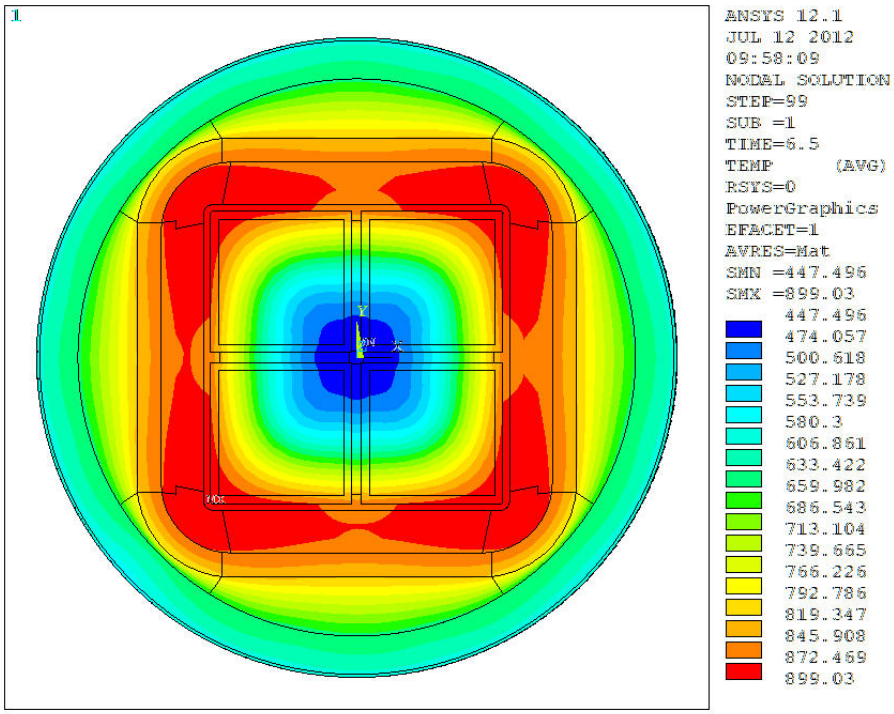

Figure C.27. NIST-01: (at 6 hours – ~1 hour after end of fire on vehicle #31 – ambient temperature 279°F [137°C])

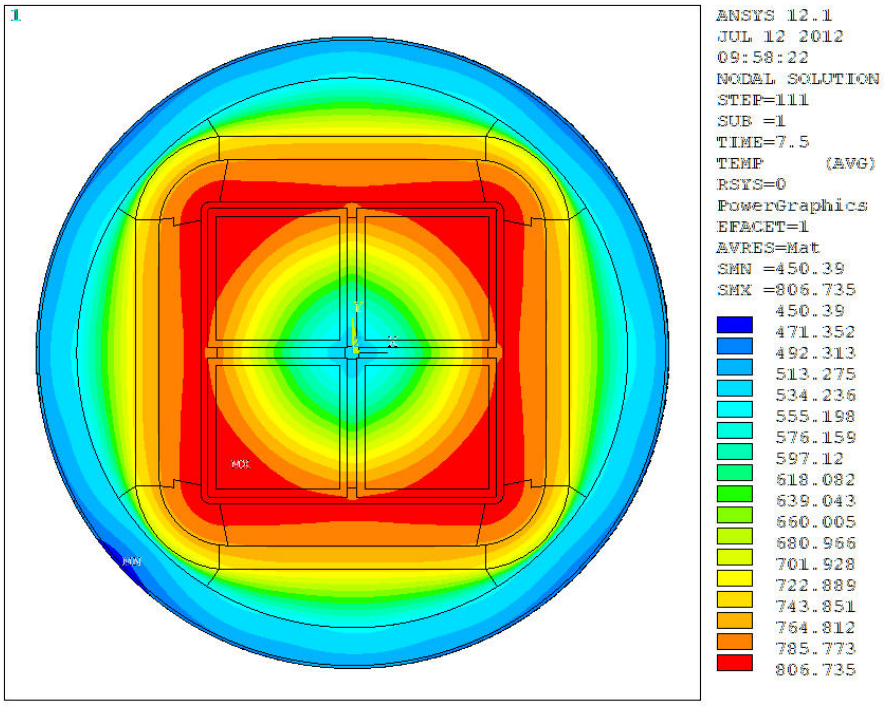

Figure C.28. NIST-01: (at 7 hours – ~2 hours after end of fire on vehicle #31 – ambient temperature 219°F [104°C])

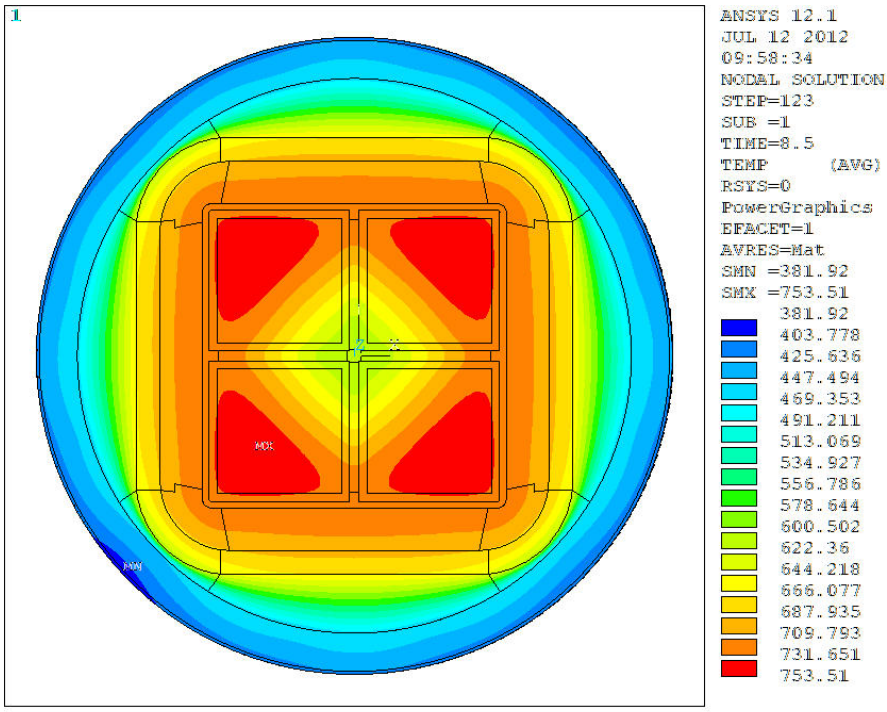

Figure C.29. NIST-01: (at 8 hours – ~3 hours after end of fire on vehicle #31 – ambient temperature 152°F [67°C])

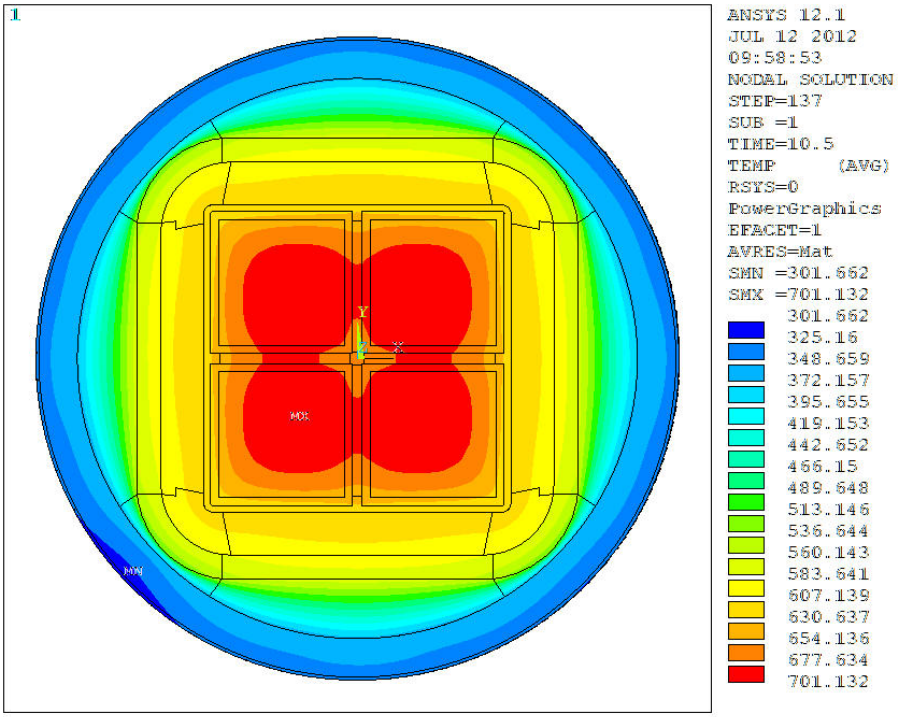

Figure C.30. NIST-01: (at 10 hours – ~5 hours after end of vehicle fires – ambient temperature 100°F [38°C])

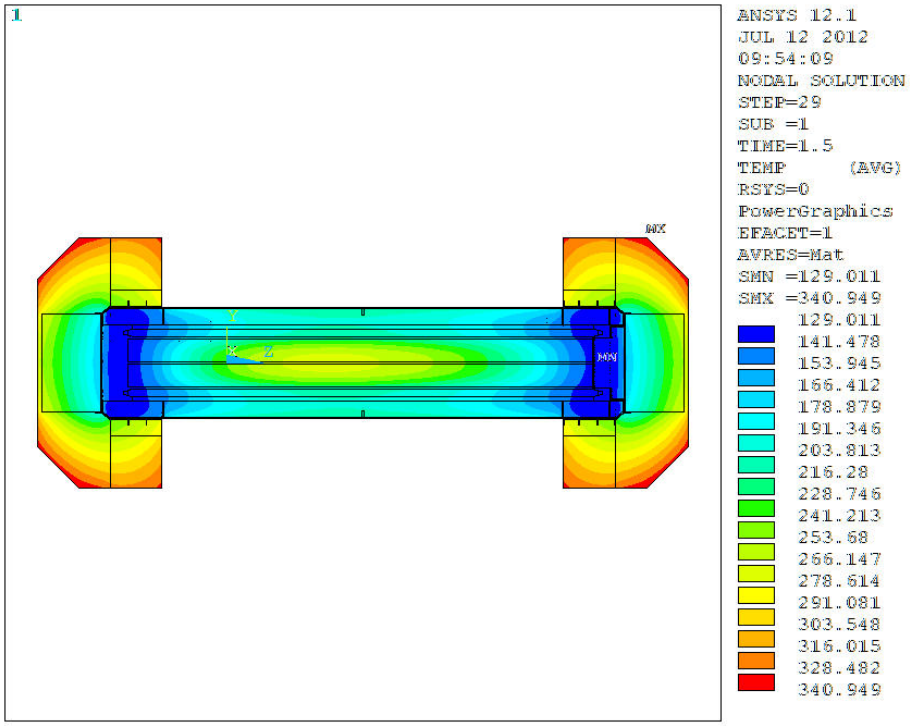

Figure C.31. NIST-01: (at 1 hour – 3 hours before fire on vehicle #31 – ambient temperature ~353°F [179°C])

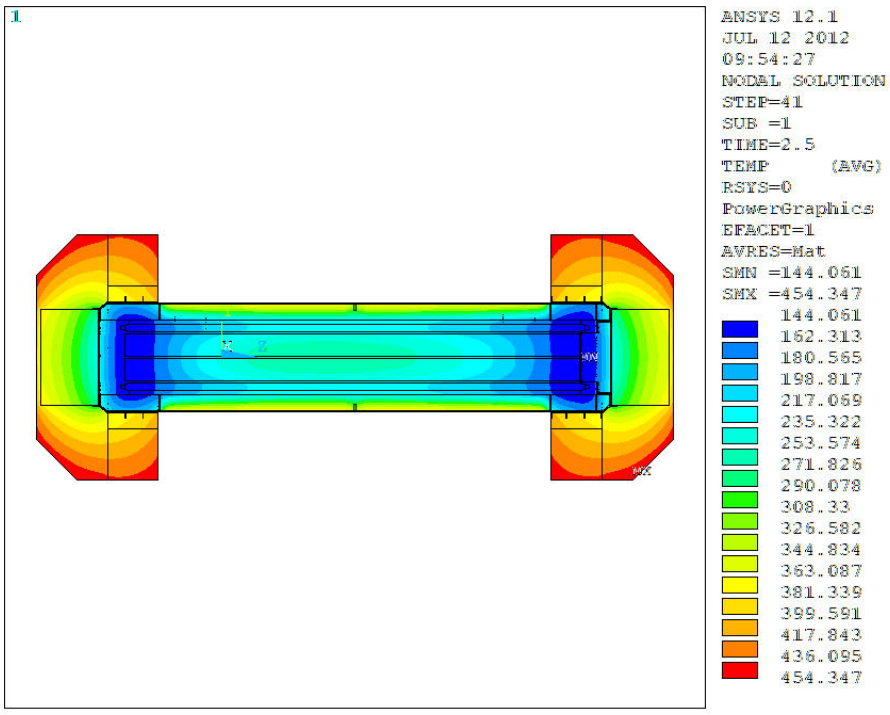

Figure C.32. NIST-01: (at 2 hours – 2 hours before fire on vehicle #31 – ambient temperature ~461°F [238°C])

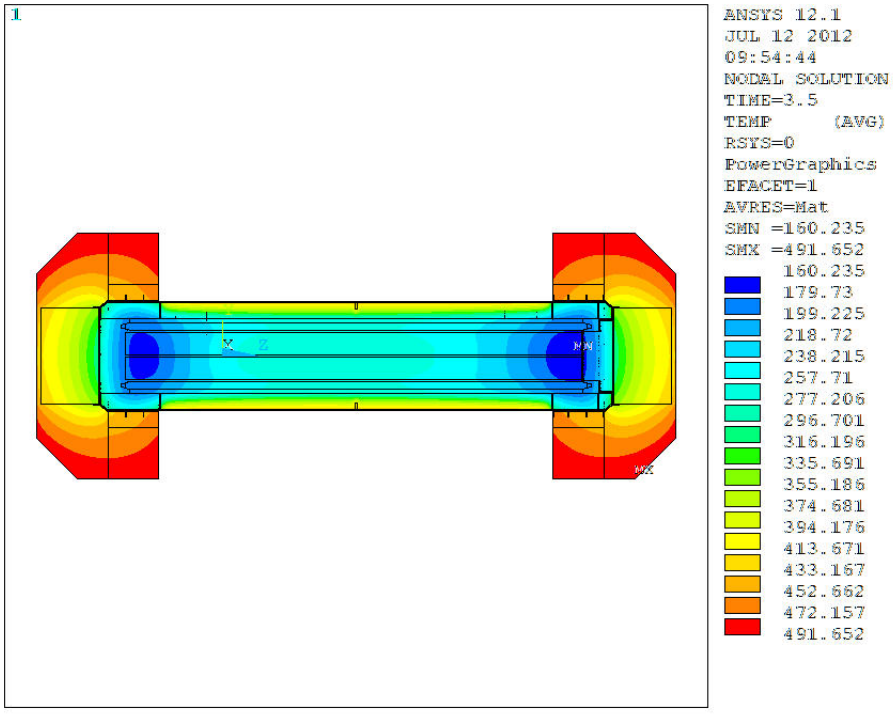

Figure C.33. NIST-01: (at 3 hours – 1 hour before fire on vehicle #31 (and end of fire on vehicle #23) – ambient temperature ~494°F [257°C])

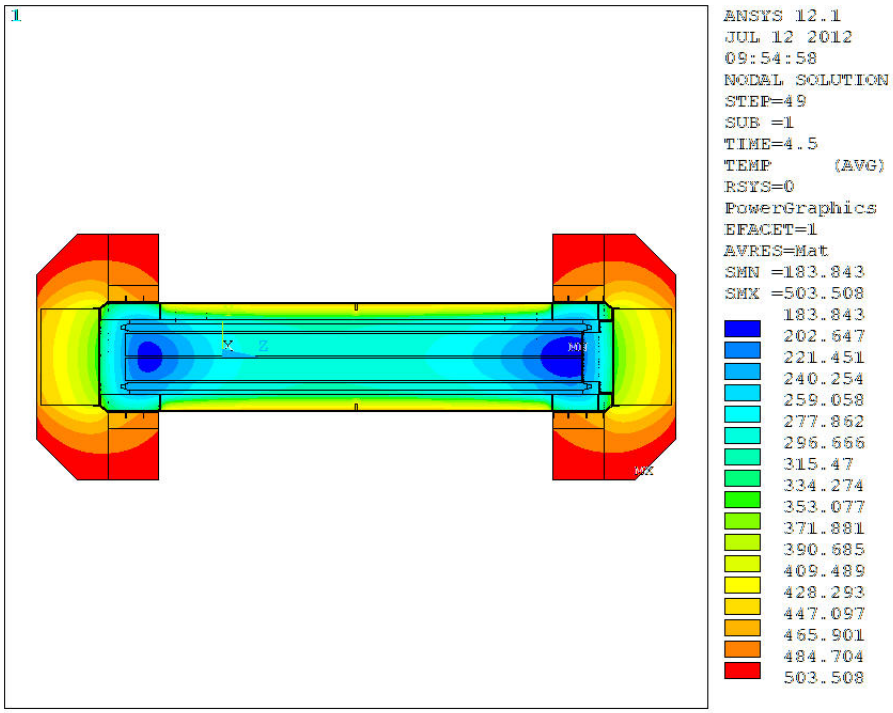

Figure C.34. NIST-01: (at 4 hours – just before beginning of fire on vehicle #31 – ambient temperature 500°F [260°C])

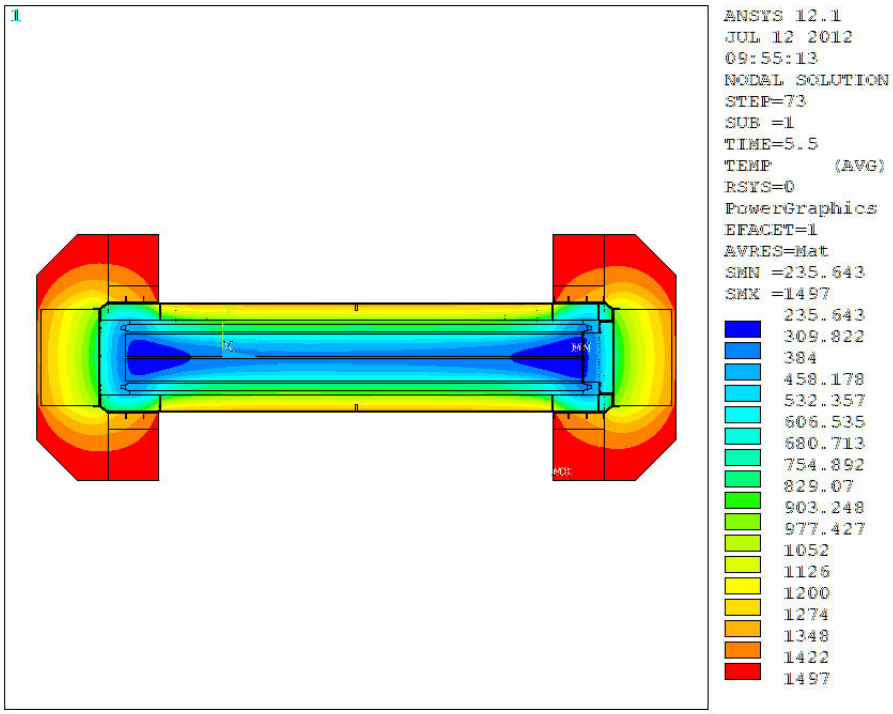

Figure C.35. NIST-01: (at 5 hours – 9 minutes before end of fire on vehicle #31 (and end of all vehicle fires) – ambient temperature 1496°F [813°C])

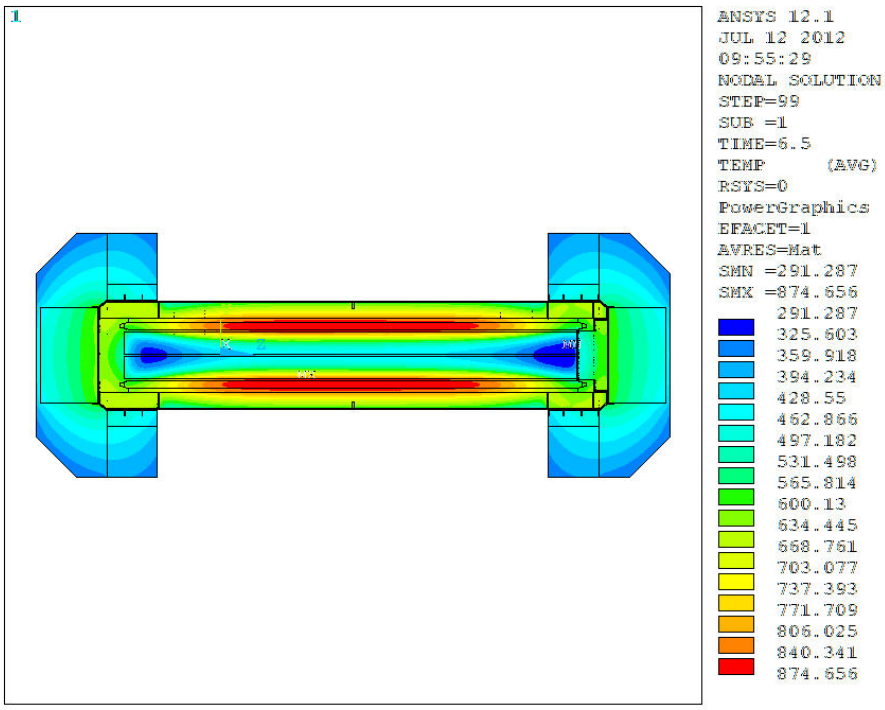

Figure C.36. NIST-01: (at 6 hours – ~1 hour after end of fire on vehicle #31 – ambient temperature 279°F [137°C])

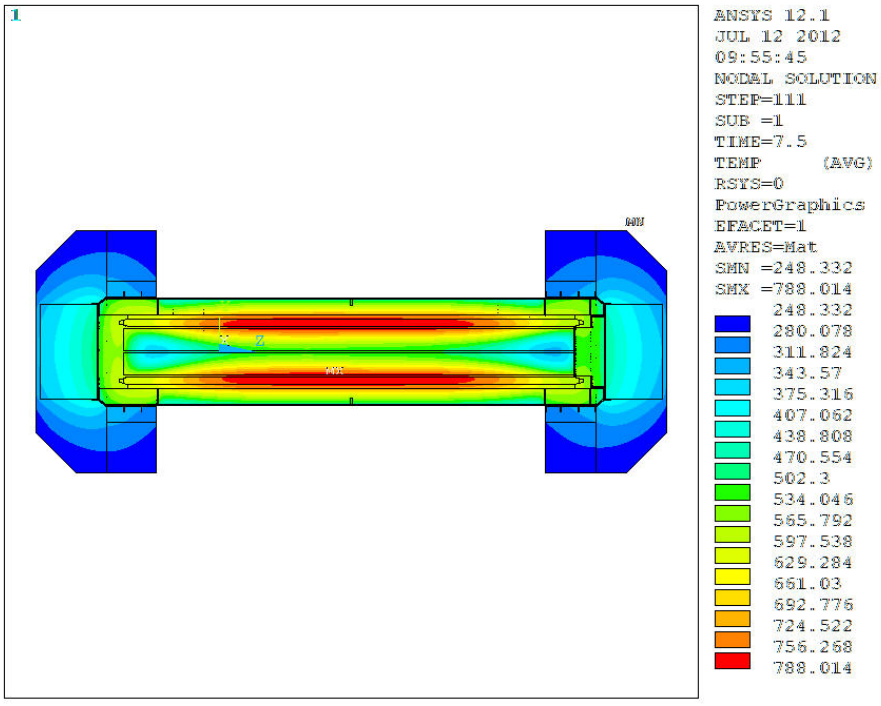

Figure C.37. NIST-01: (at 7 hours – ~2 hours after end of fire on vehicle #31 – ambient temperature 219°F [104°C])

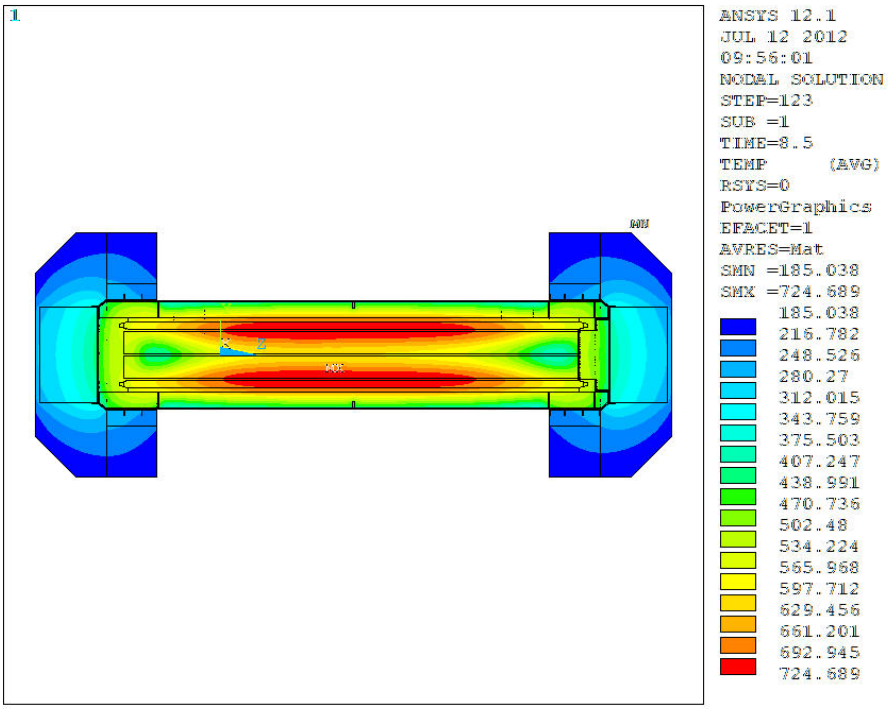

Figure C.38. NIST-01: (at 8 hours – ~3 hours after end of fire on vehicle #31 – ambient temperature 152°F [67°C])

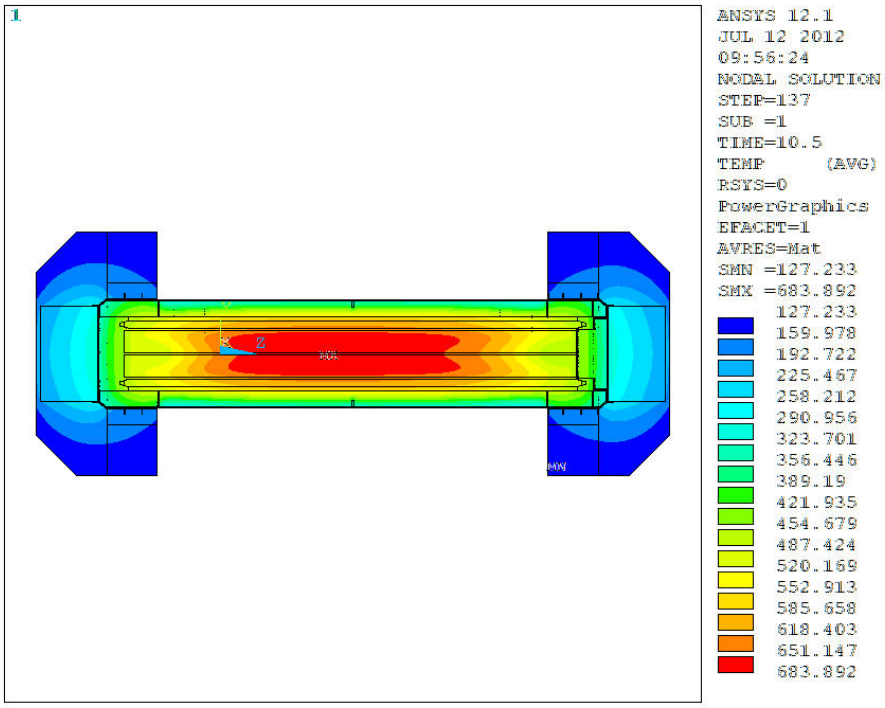

Figure C.39. NIST-01: (at 10 hours – ~5 hours after end of vehicle fires – ambient temperature 100°F [38°C])

C.2 NIST-02

The fire conditions predicted with FDS for NIST-02 are determined for a faster spread rate than the base case (NIST-01), such that the total fire duration is approximately 3 hours, which is 2 hours less than in the base case. As in NIST-01, the fuel available for the fire is based on an assumed typical cargo load for each vehicle (including those known to have been empty). The burn rate is also the same, with the fire on each vehicle lasting approximately 1 hour.

C.2.1 NIST-02: Package at Hottest Fire Location

The hottest fire location for this case is on vehicle #23, near the center of the tunnel. Due to the faster spread rate, the fire on this vehicle begins at approximately 1 hour into the fire scenario, compared to the 2-hour lag time at this location in NIST-01. Similarly, the fire at the longest fire location (vehicle #31), begins at approximately 2 hours into the fire scenario, at approximately the same time that the fire at the hottest fire location is ending. Figure C.40 shows the engulfing fire boundary temperatures assumed for the two selected fire locations.

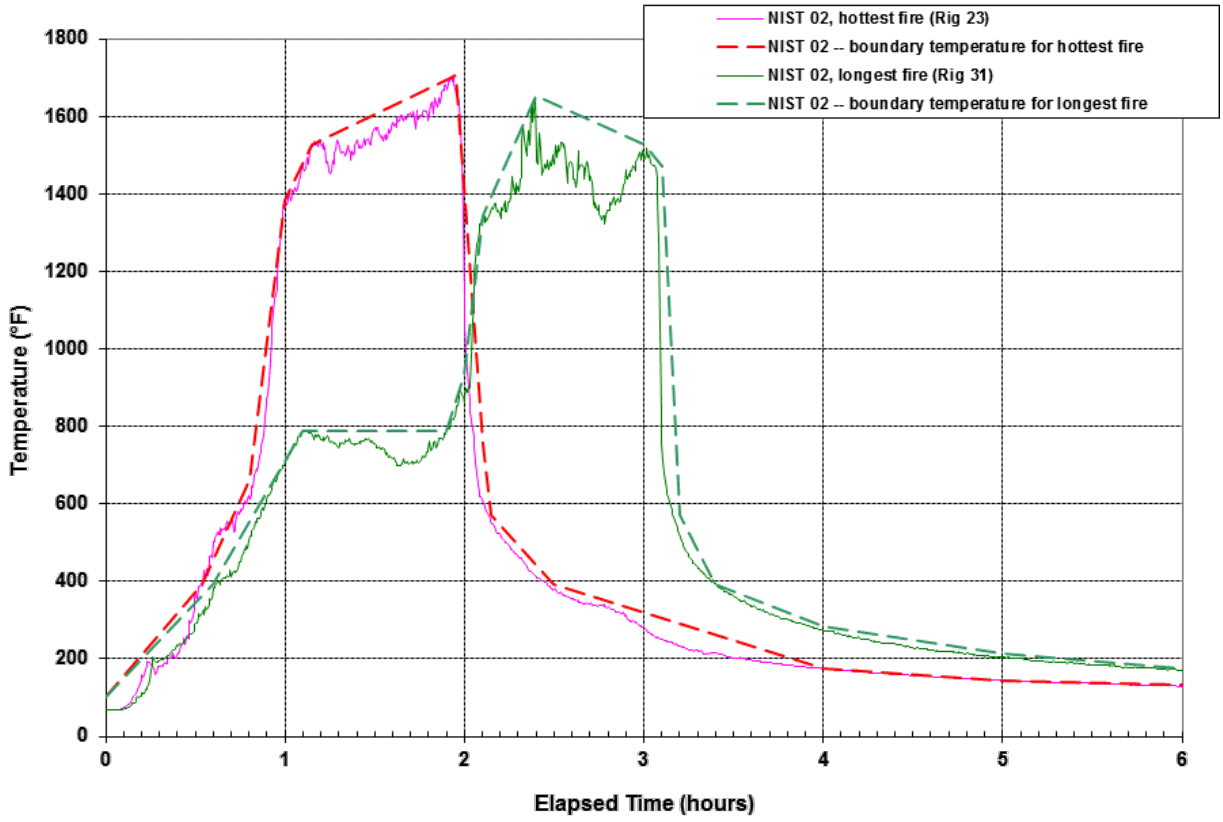

Figure C.40. Boundary Temperatures for Hottest Fire and Longest Fire Locations for Case NIST-02

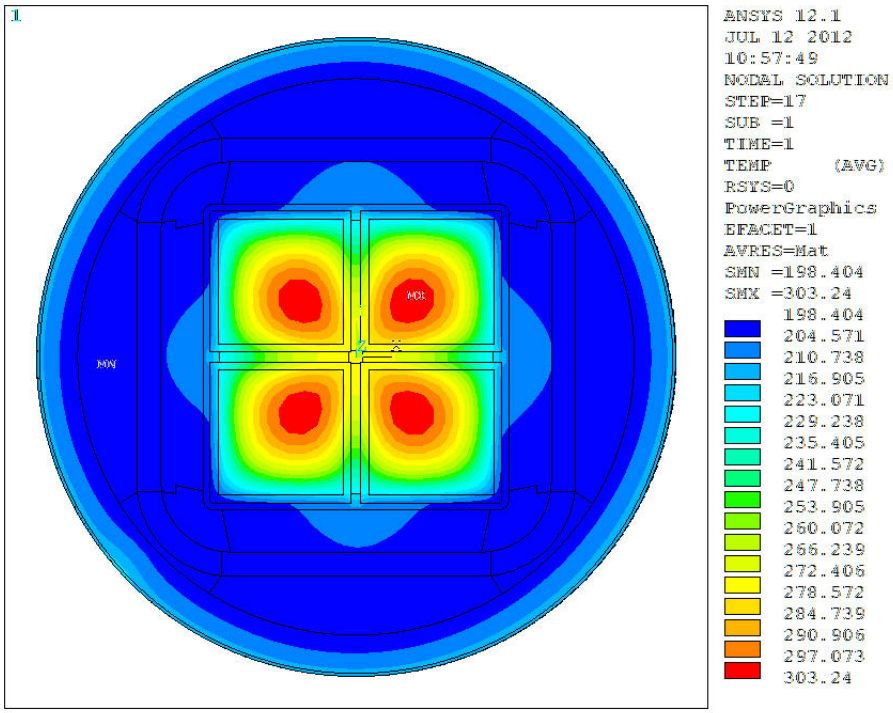

Figure C.41. NIST-02: (at 30 minutes – 18 minutes before beginning of fire on vehicle #23 – ambient temperature 370°F [188°C])

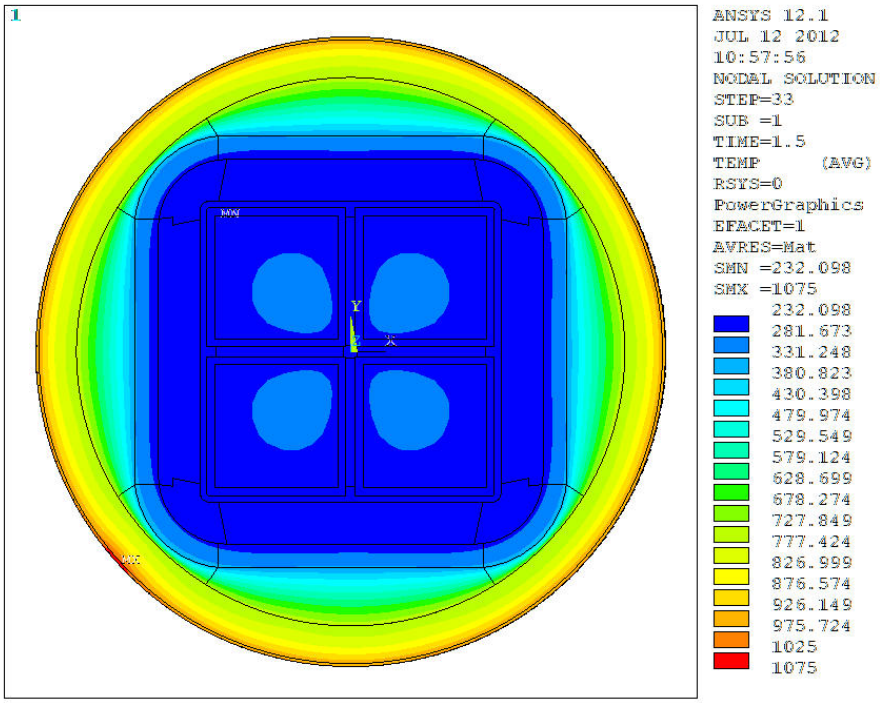

Figure C 42. NIST-02: (at 1 hour – 12 minutes after beginning of fire on vehicle #23 – ambient temperature 1382°F [750°C])

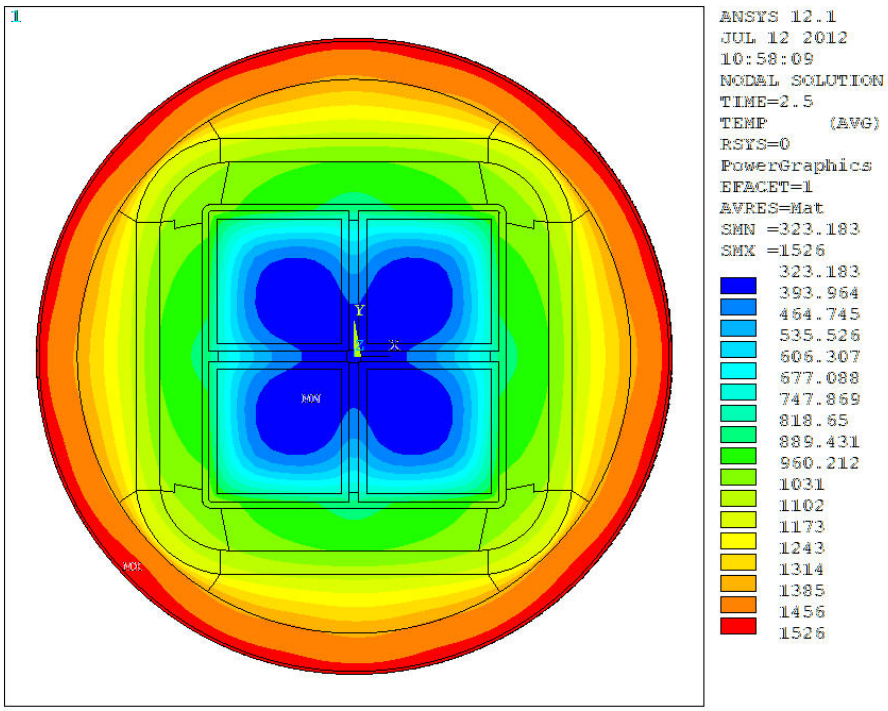

Figure C.43. NIST-02: (at 2 hours – end of fire on vehicle #23 – ambient temperature 1485°F [807°C])

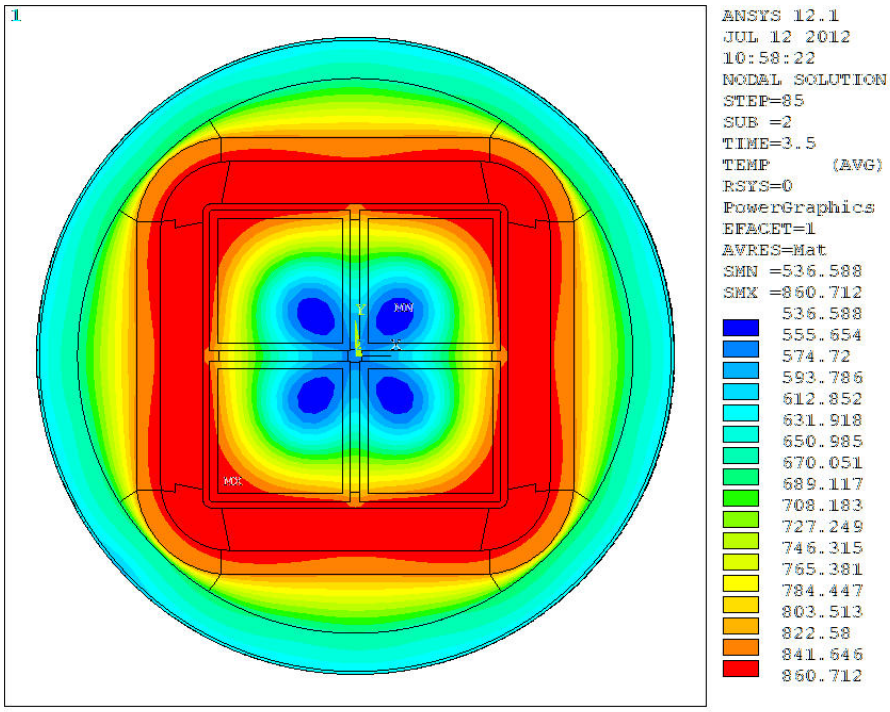

Figure C.44. NIST-02: (at 3 hours – 1 hour after end of fire on vehicle #23 – ambient temperature 344°F [173°C])

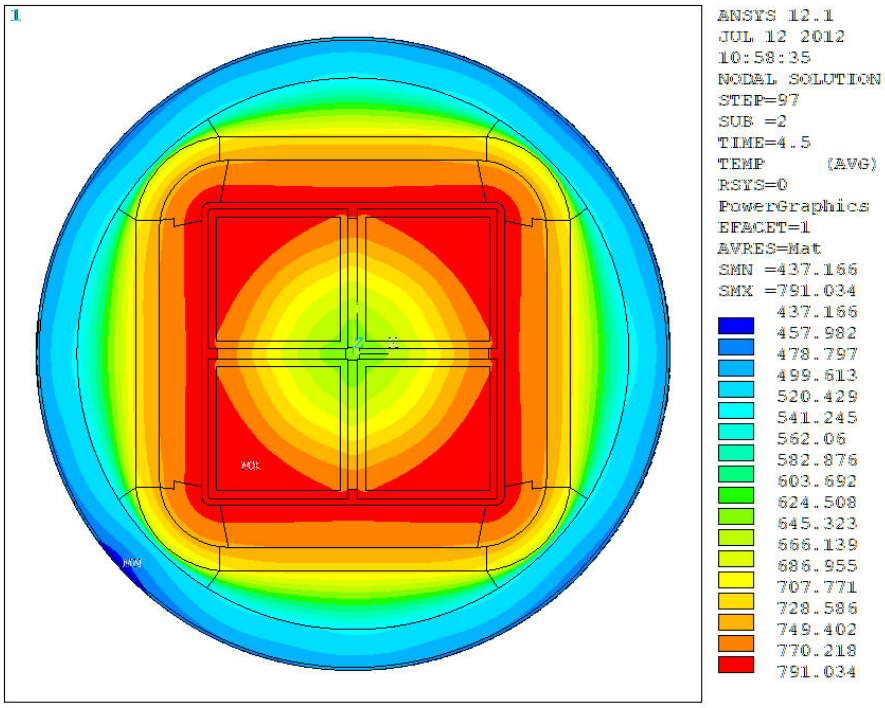

Figure C.45. NIST-02: (at 4 hours – 2 hours after end of fire on vehicle #23 – ambient temperature 200°F [93°C])

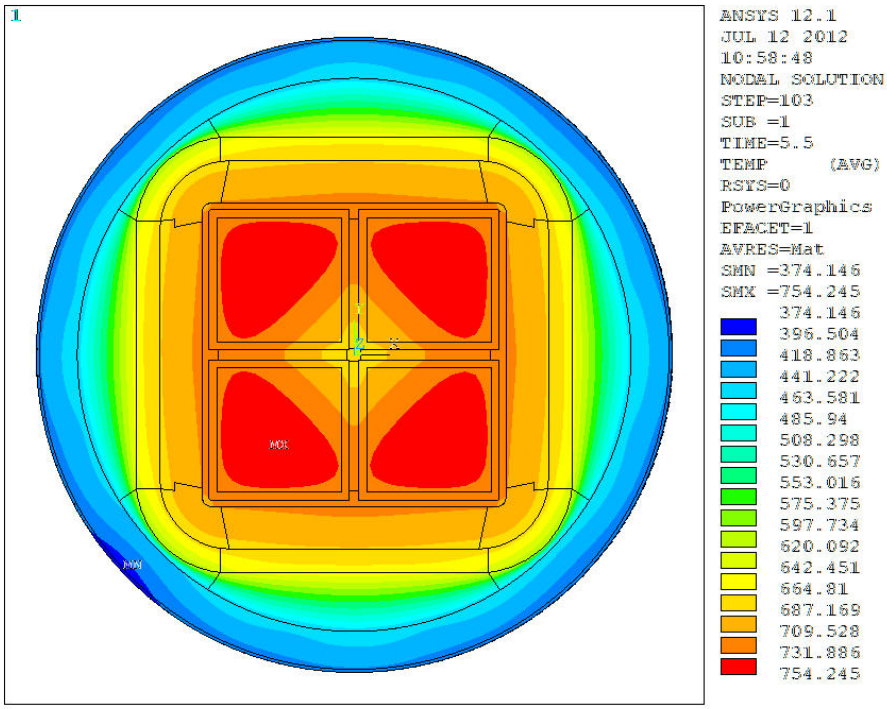

Figure C.46. NIST-02: (at 5 hours – 3 hours after end of fire on vehicle #23 – ambient temperature 154°F [68°C])

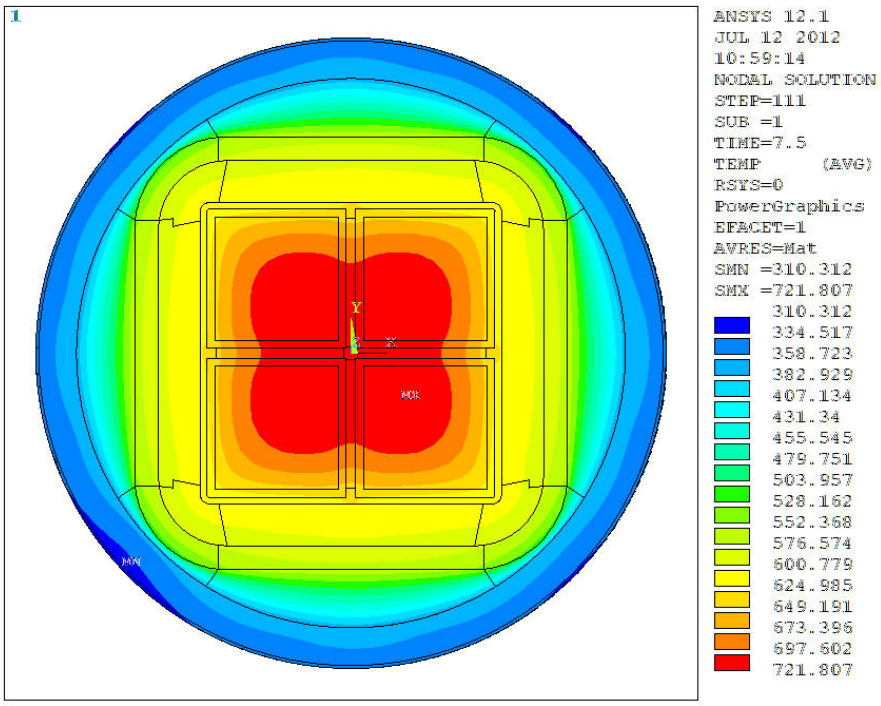

Figure C.47. NIST-02: (at 7 hours – 5 hours after end of fire on vehicle #23 – ambient temperature 126°F [52°C])

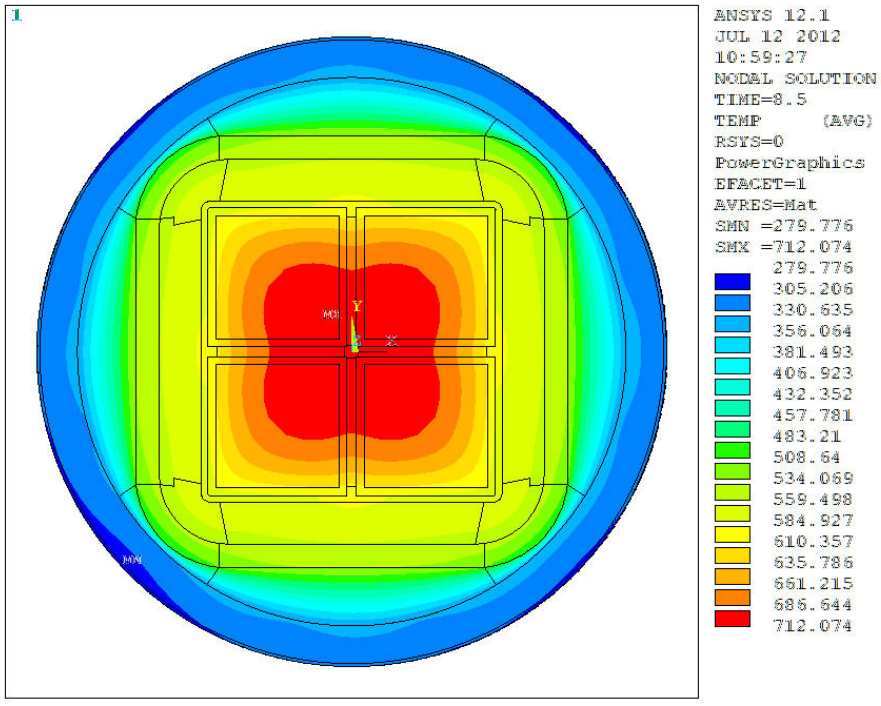

Figure C.48. NIST-02: (at 8 hours – 6 hours after end of fire on vehicle #23 – ambient temperature 100°F [38°C])

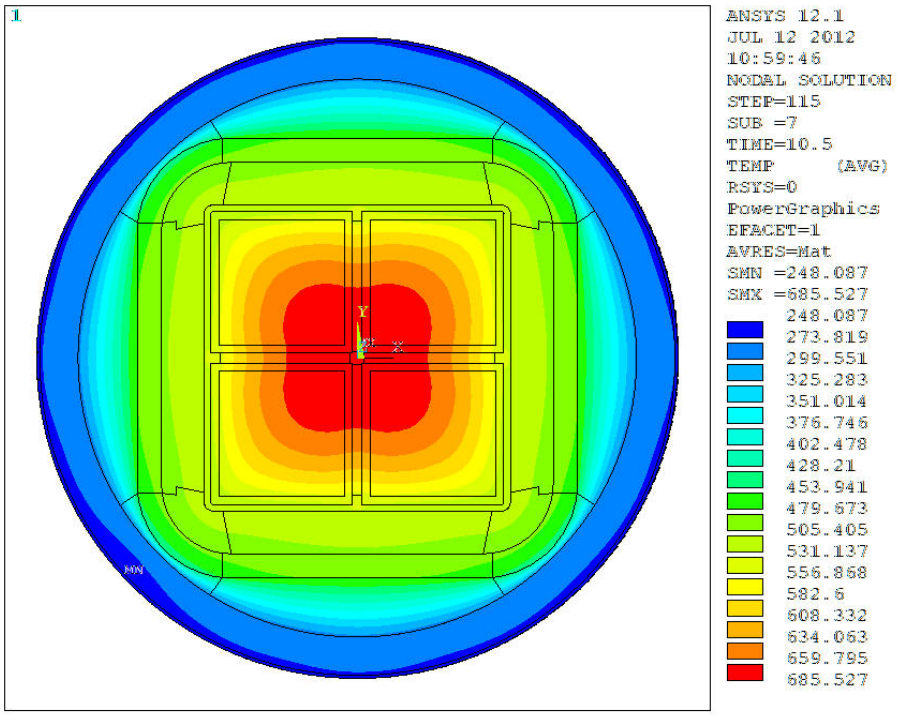

Figure C.49. NIST-02: (at 10 hours – 8 hours after end of fire on vehicle #23 – ambient temperature 100°F [38°C])

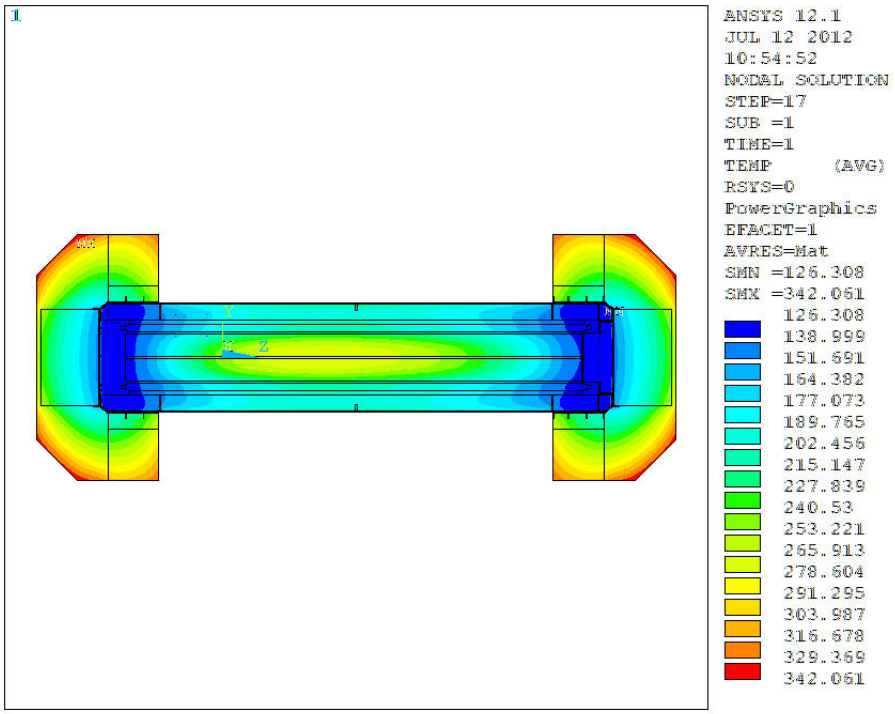

Figure C.50. NIST-02: (at 30 minutes – 18 minutes before beginning of fire on vehicle #23 – ambient temperature 370°F [188°C])

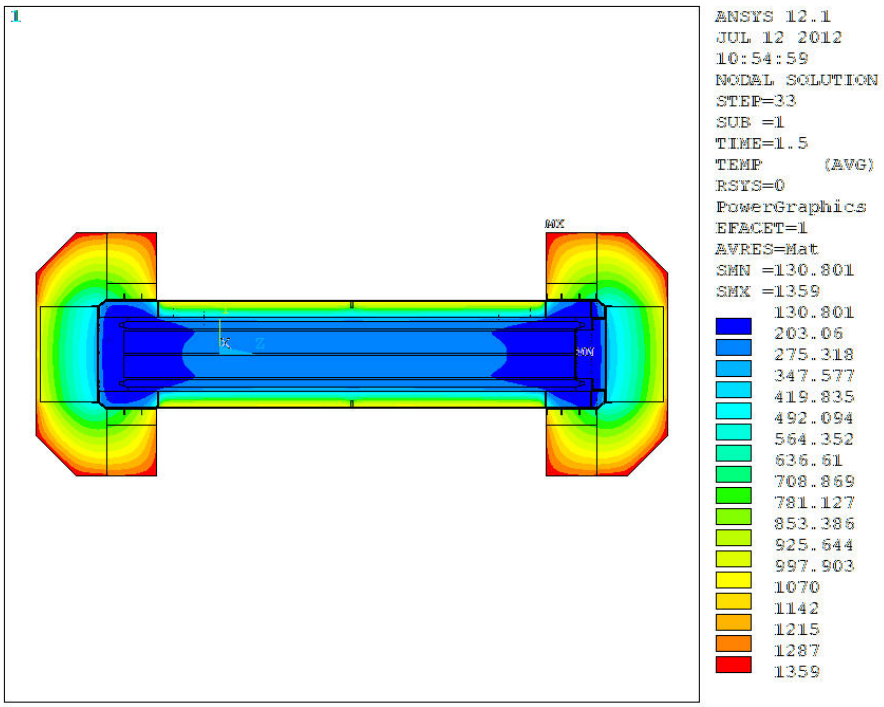

Figure C.51. NIST-02: (at 1 hour – 12 minutes after beginning of fire on vehicle #23 – ambient temperature 1382°F [750°C])

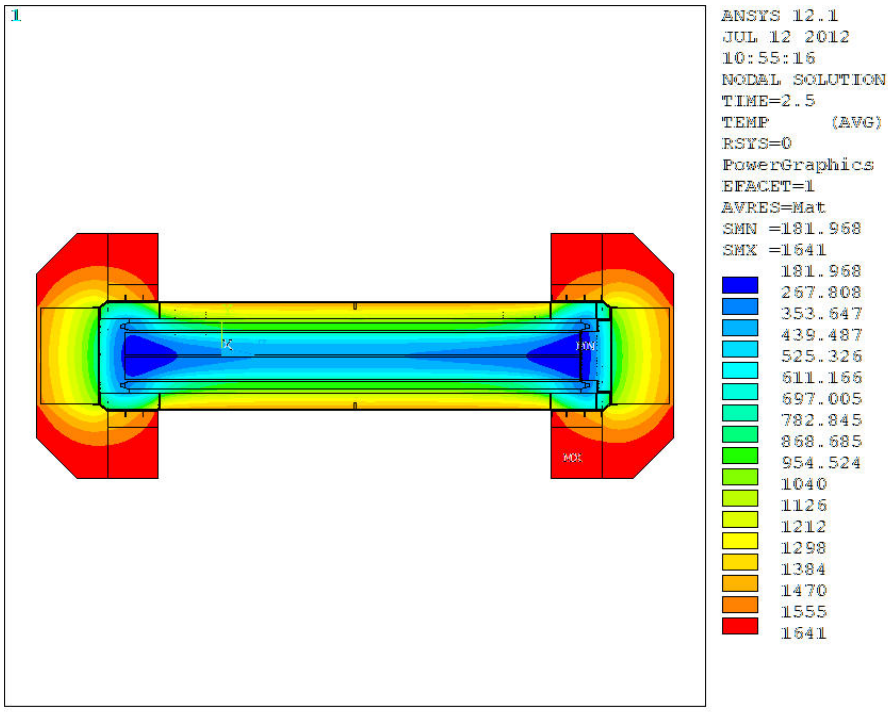

Figure C.52. NIST-02: (at 2 hours – end of fire on vehicle #23 – ambient temperature 1485°F [807°C])

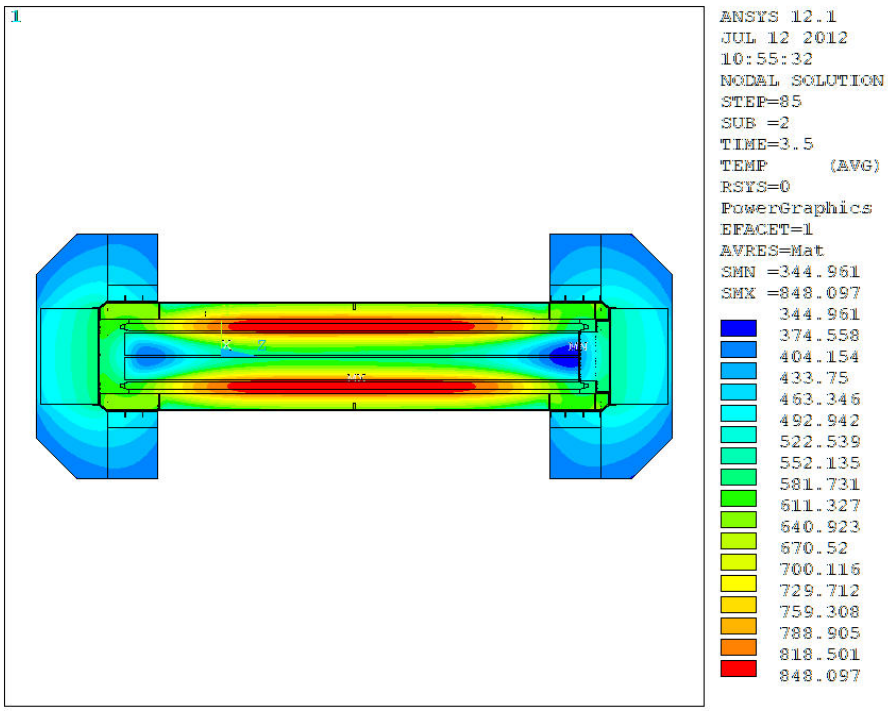

Figure C.53. NIST-02: (at 3 hours – 1 hour after end of fire on vehicle #23 – ambient temperature 344°F [173°C])

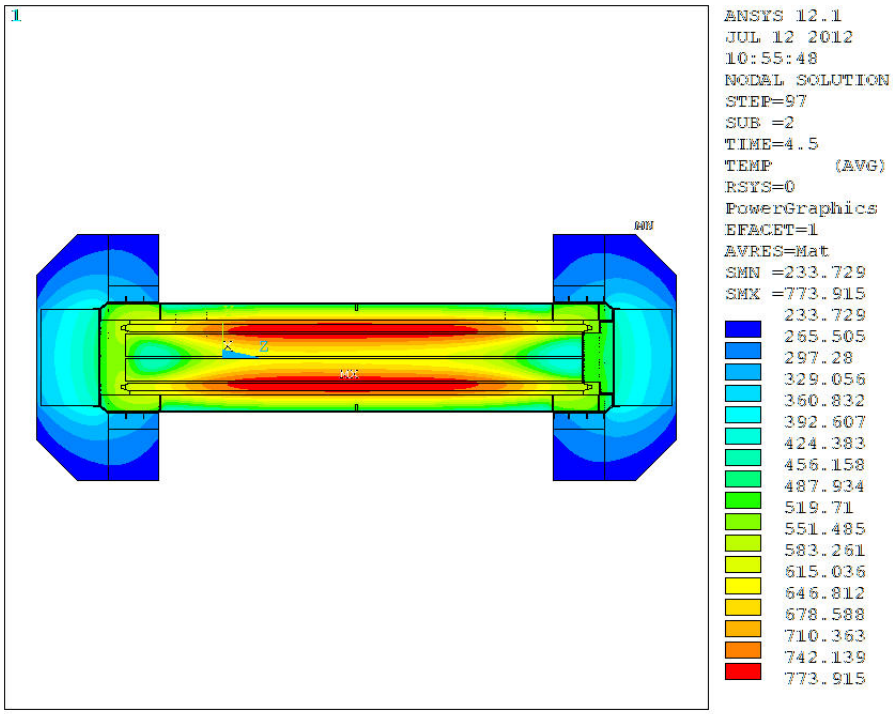

Figure C.54. NIST-02: (at 4 hours – 2 hours after end of fire on vehicle #23 – ambient temperature 200°F [93°C])

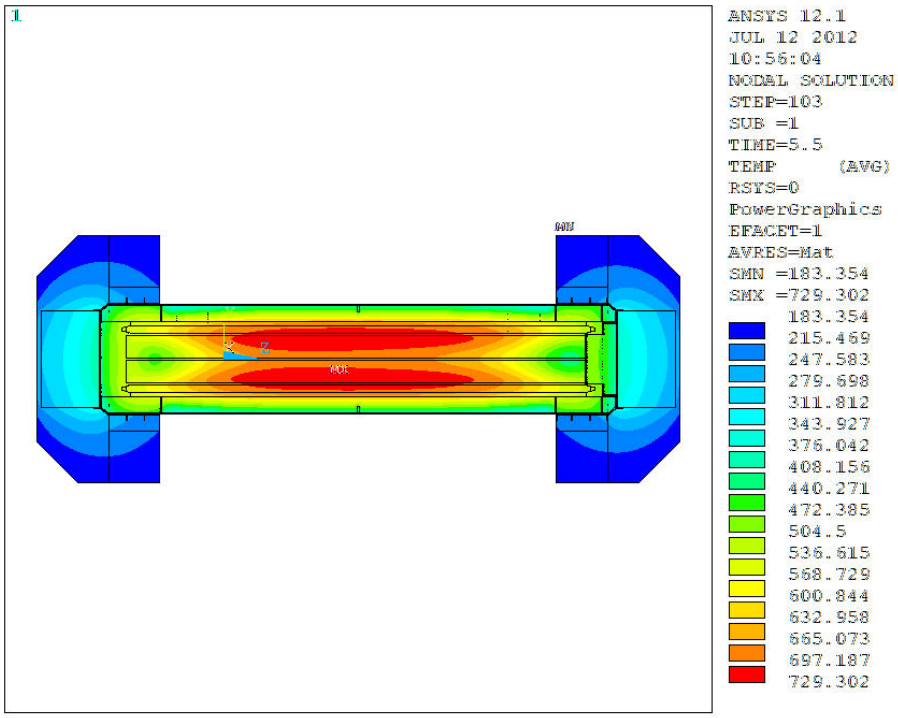

Figure C.55. NIST-02: (at 5 hours – 3 hours after end of fire on vehicle #23 – ambient temperature 154°F [68°C])

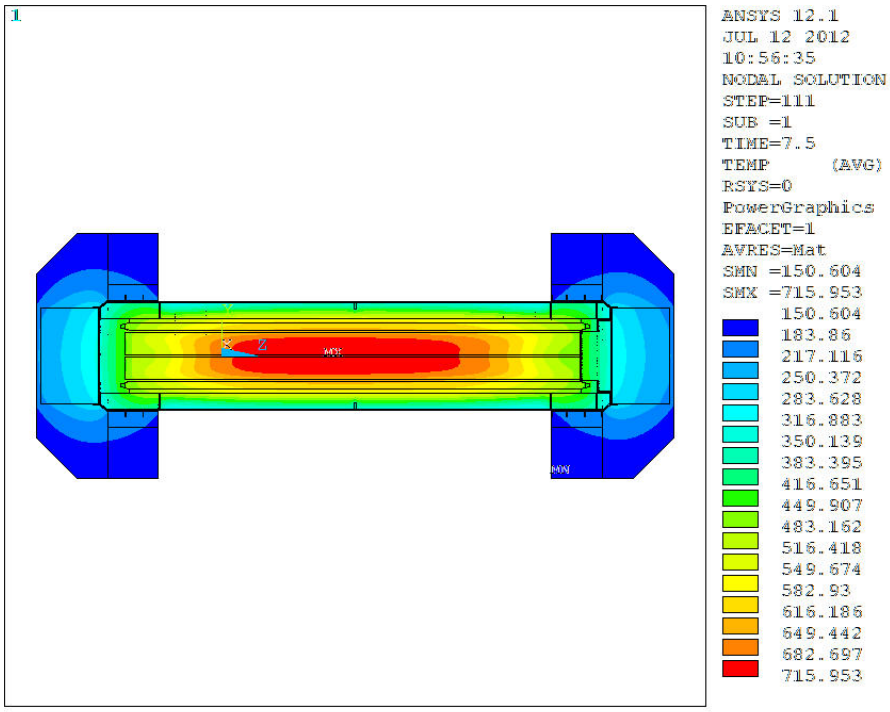

Figure C.56. NIST-02: (at 7 hours – 5 hours after end of fire on vehicle #23 – ambient temperature 126°F [52°C])

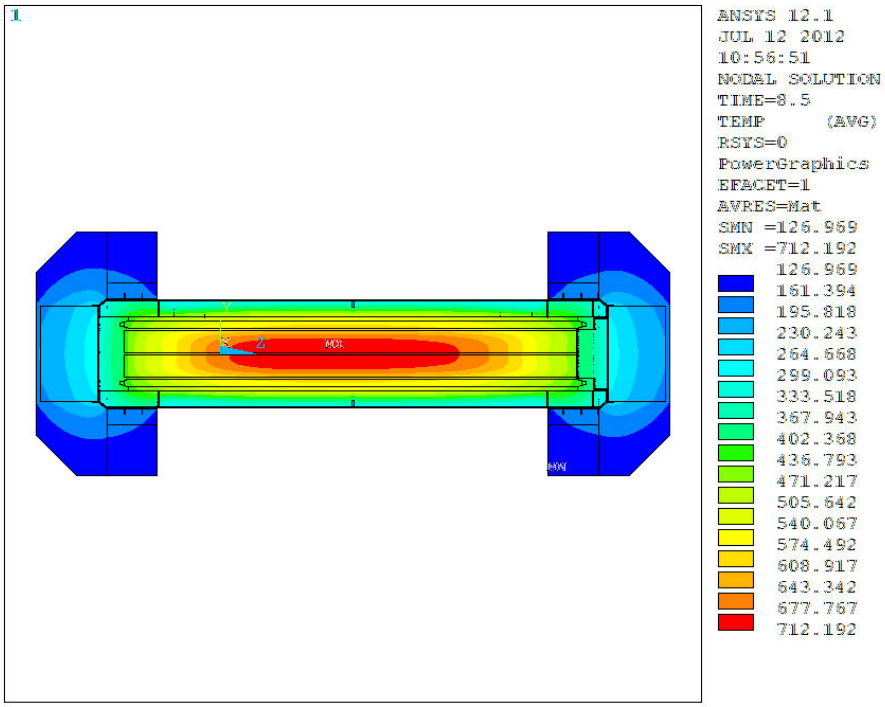

Figure C.57. NIST-02: (at 8 hours – 6 hours after end of fire on vehicle #23 – ambient temperature 100°F [38°C])

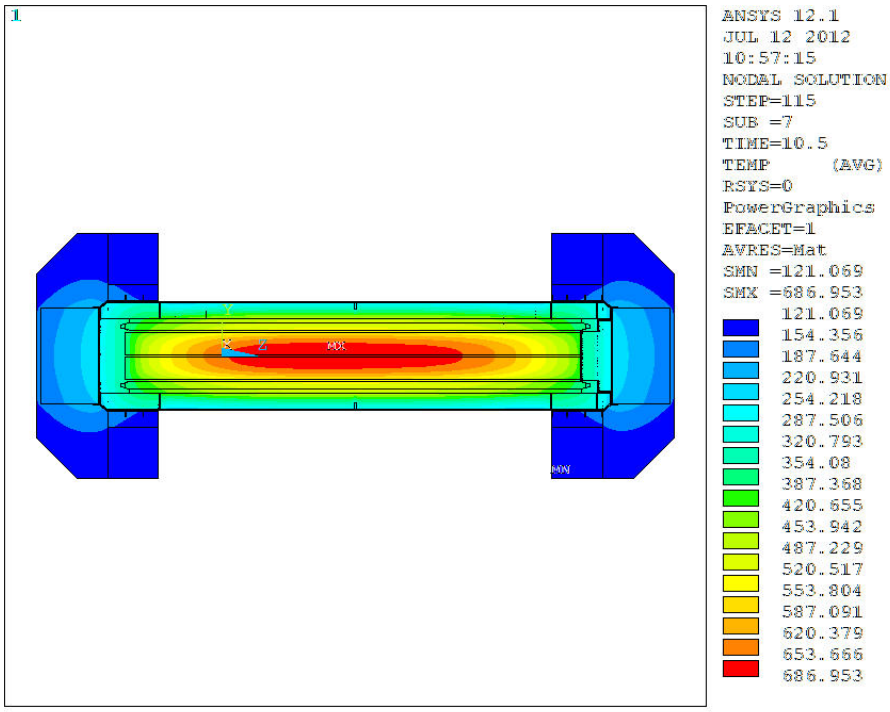

Figure C.58. NIST-02: (at 10 hours – 8 hours after end of fire on vehicle #23 – ambient temperature 100°F [38°C])

C.2.2 NIST-02: Package at Longest Fire Location

The longest fire location for this case is on vehicle #31, near the tunnel entrance. Due to the faster spread rate, the fire on this vehicle begins at approximately 2 hours into the fire scenario, compared to the 4-hour lag time at this location in NIST-01. Due to the faster spread rate assumed for this case, more vehicles are burning in the tunnel at the same time, and the ambient temperature is higher at locations the fire has not yet spread to. At the location of vehicle #31, the ambient temperature rises to nearly 800°F (427°C) in the first hour of the fire, and is held there for the remaining hour before the fire reaches this location.

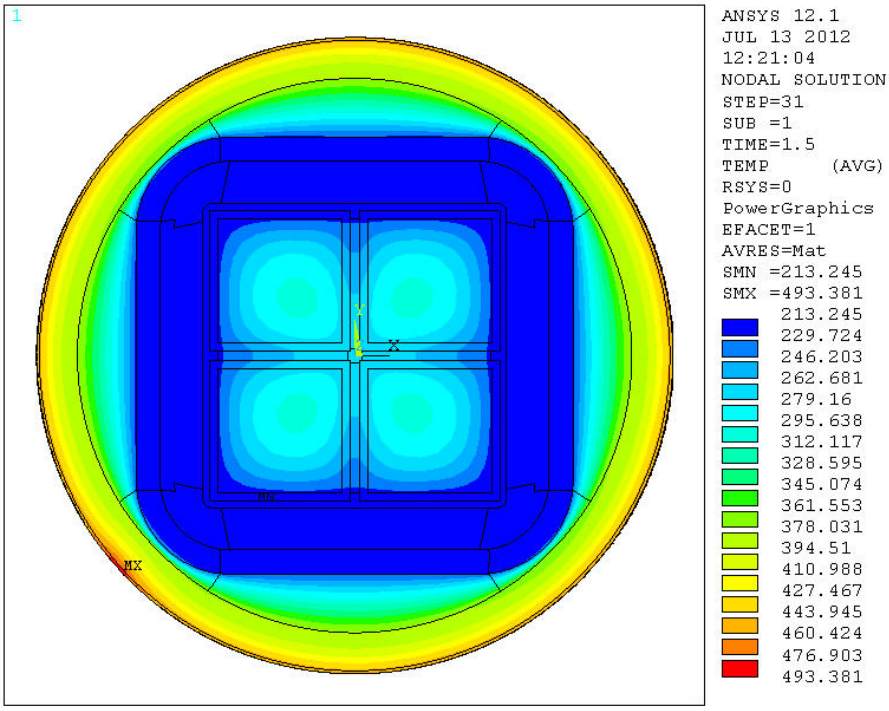

Figure C.59. NIST-02: (at 1 hour – 1 hour before beginning of fire on vehicle #31 – ambient temperature 709°F [376°C])

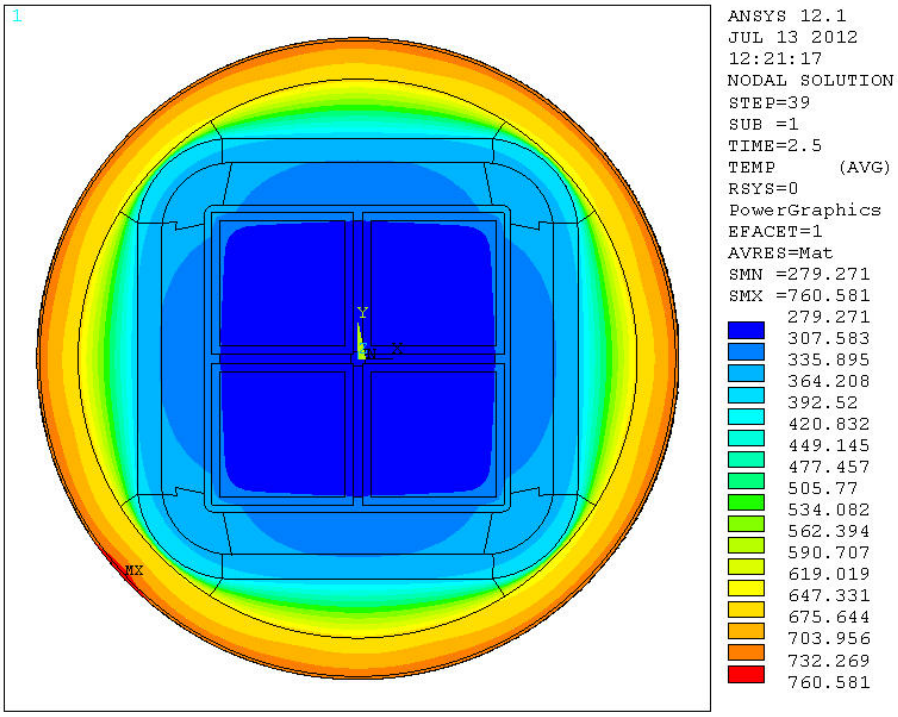

Figure C.60. NIST-02: (at 2 hours – beginning of fire on vehicle #31 (end of fire on vehicle #23) – ambient temperature 932°F [500°C])

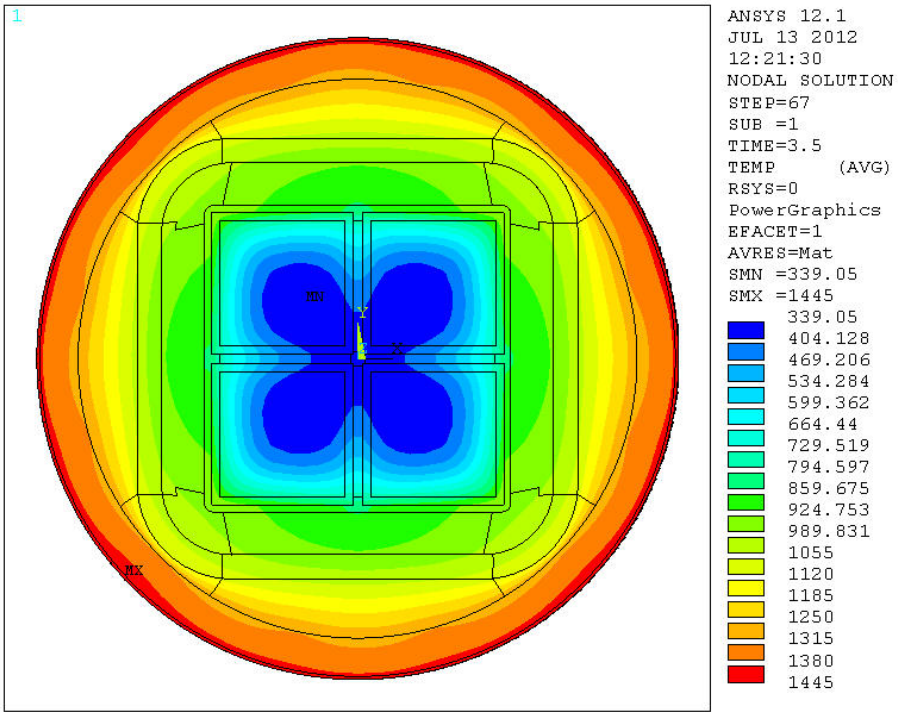

Figure C.61. NIST-02: (at 3 hours – 6 minutes before end of fire on vehicle #31 – ambient temperature 1543°F [840°C])

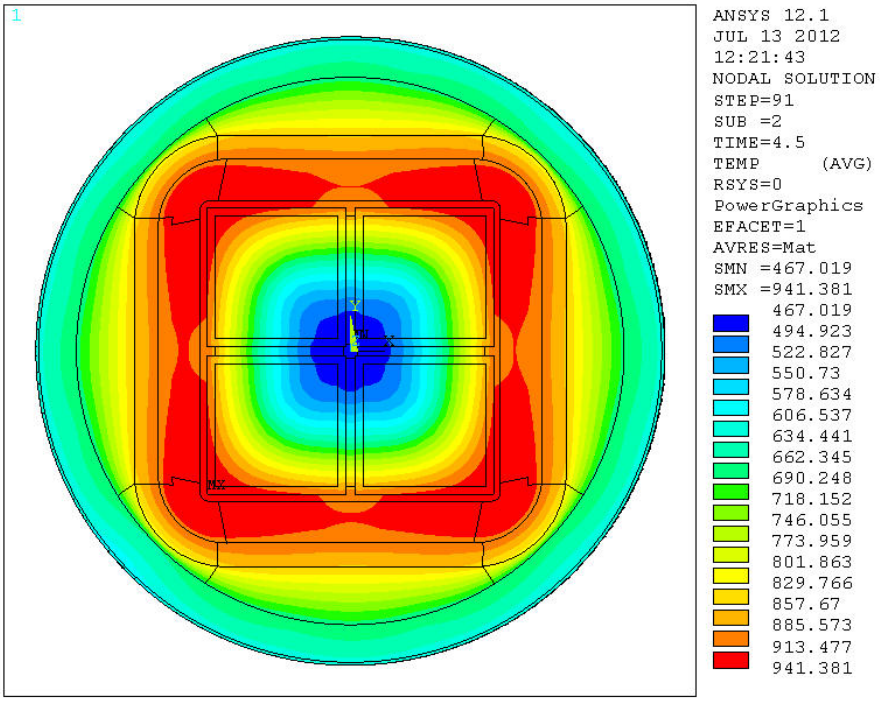

Figure C.62. NIST-02: (at 4 hours – 1 hour after end of fire on vehicle #31 – ambient temperature 314°F [157°C])

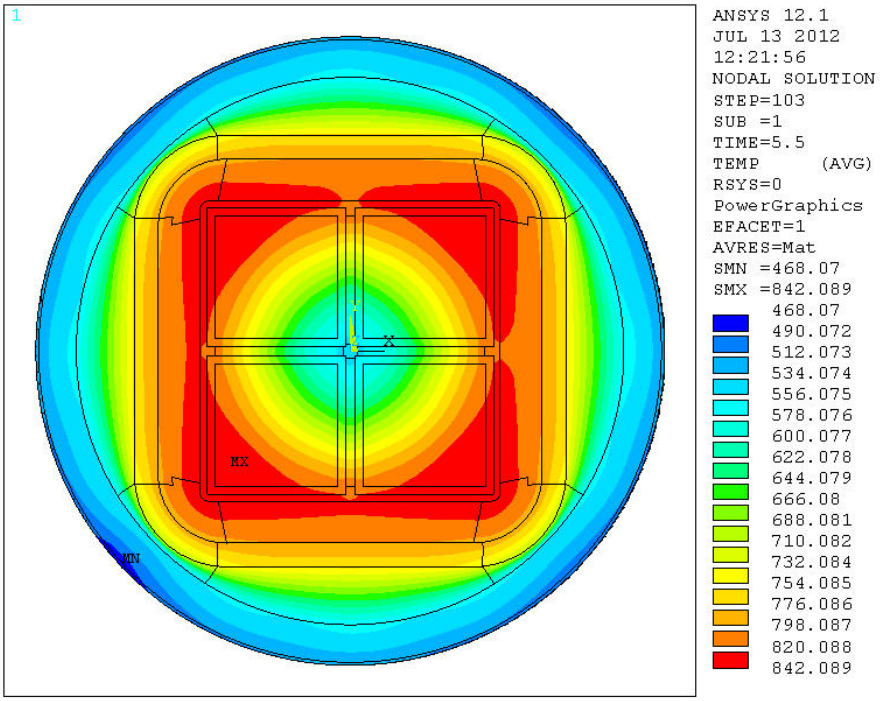

Figure C.63. NIST-02: (at 5 hours – 2 hours after end of fire on vehicle #31 – ambient temperature 224°F [107°C])

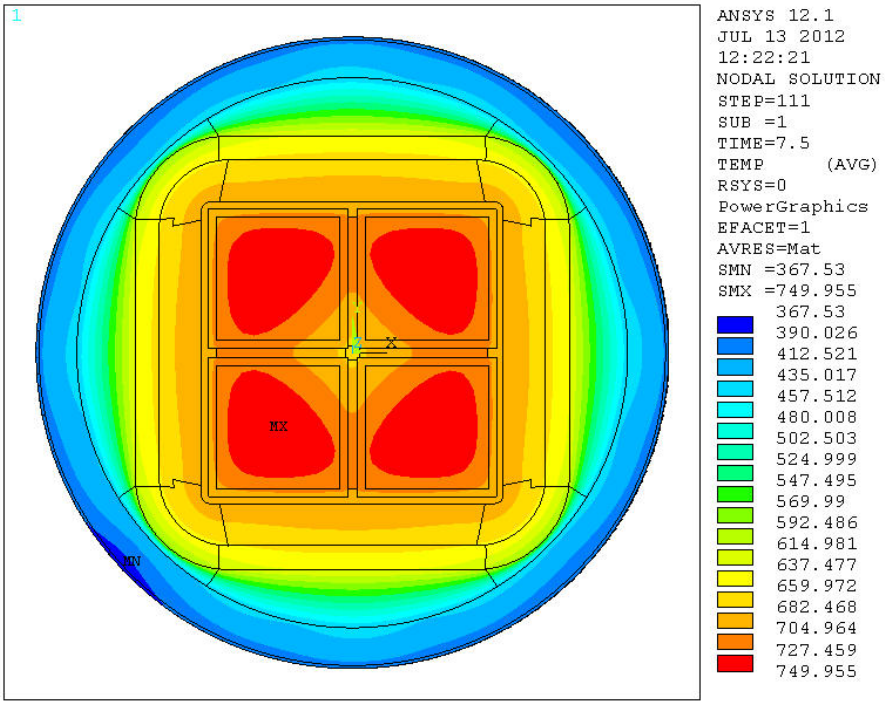

Figure C.64. NIST-02: (at 7 hours – 4 hours after end of fire on vehicle #31 – ambient temperature 158°F [70°C])

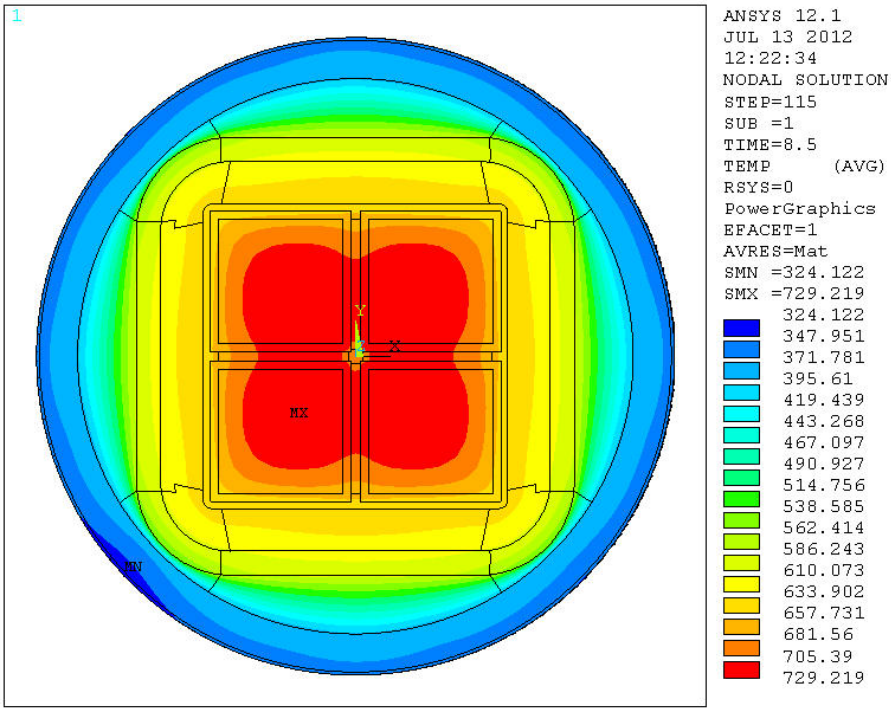

Figure C.65. NIST-02: (at 8 hours – 5 hours after end of fire on vehicle #31 – ambient temperature 120°F [49°C])

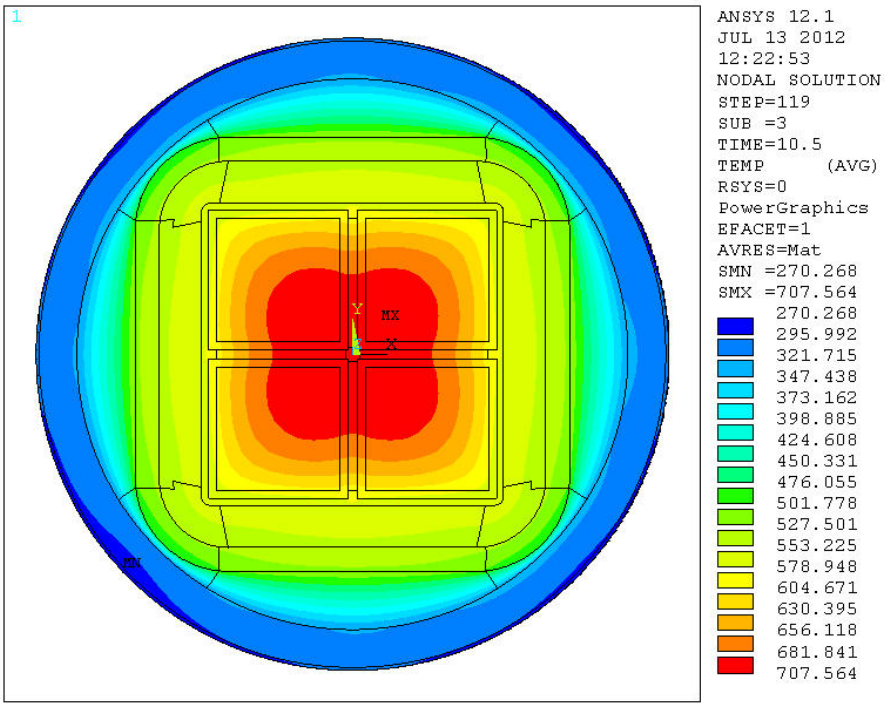

Figure C.66. NIST-02: (at 10 hours – 7 hours after end of fire on vehicle #31 – ambient temperature 100°F [38°C])

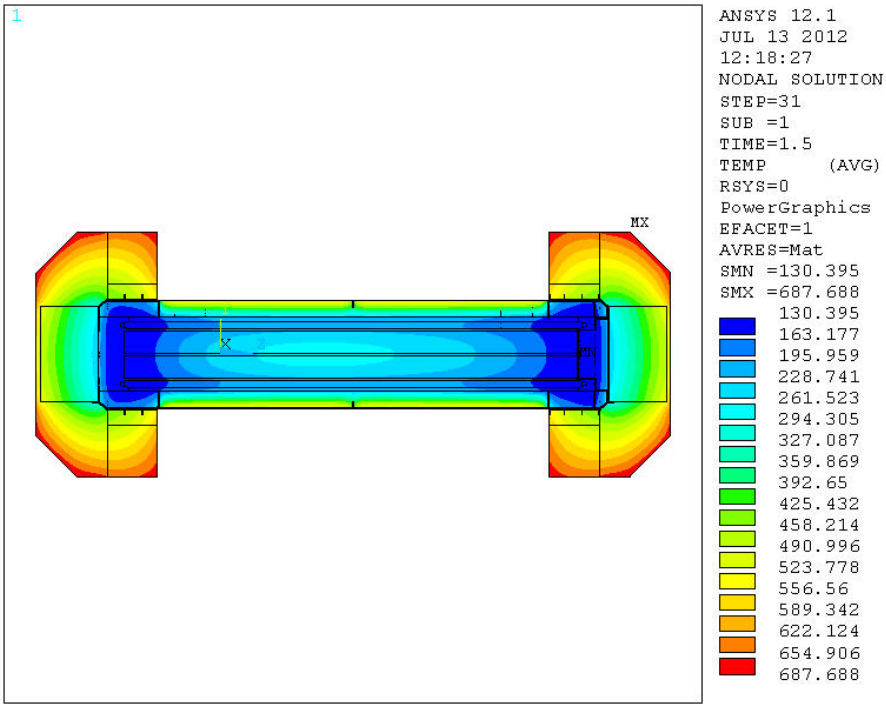

Figure C.67. NIST-02: (at 1 hour – 1 hour before beginning of fire on vehicle #31 – ambient temperature 709°F [376°C])

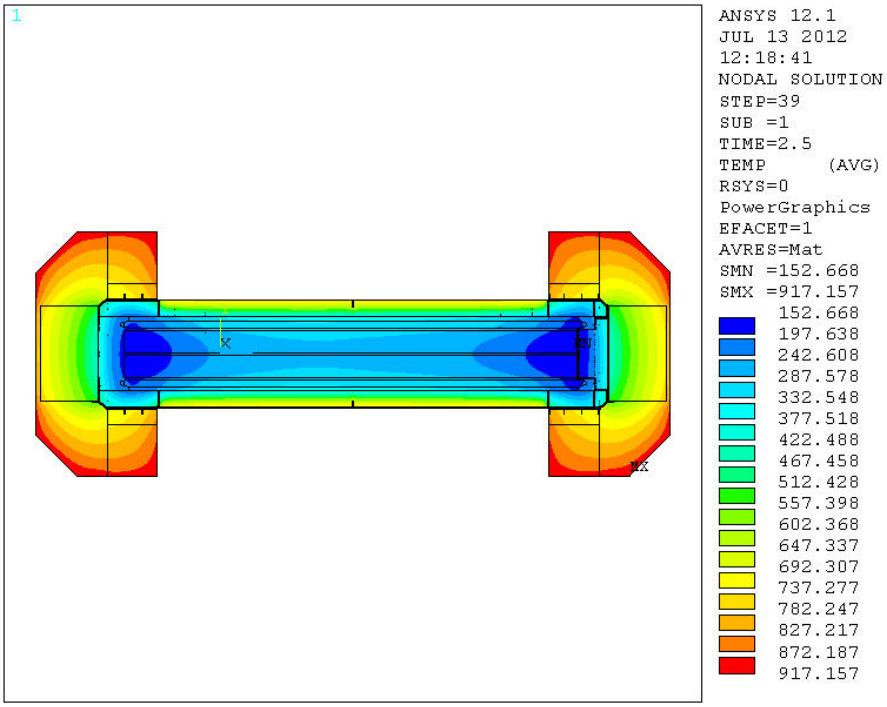

Figure C.68. NIST-02: (at 2 hours – beginning of fire on vehicle #31 (end of fire on vehicle #23) – ambient temperature 932°F [500°C])

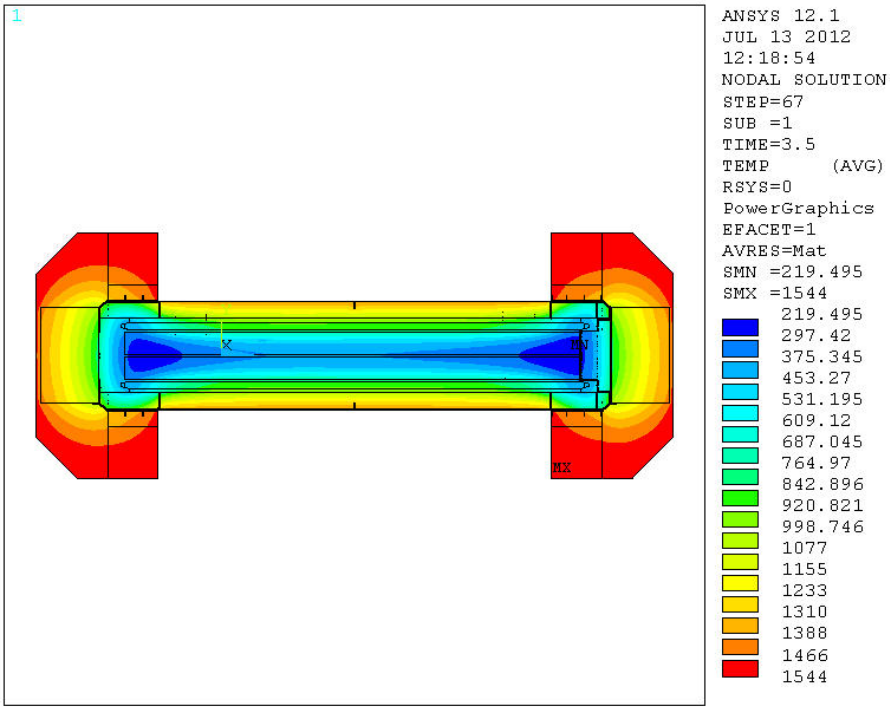

Figure C.69. NIST-02: (at 3 hours – 6 minutes before end of fire on vehicle #31 – ambient temperature 1543°F [840°C])

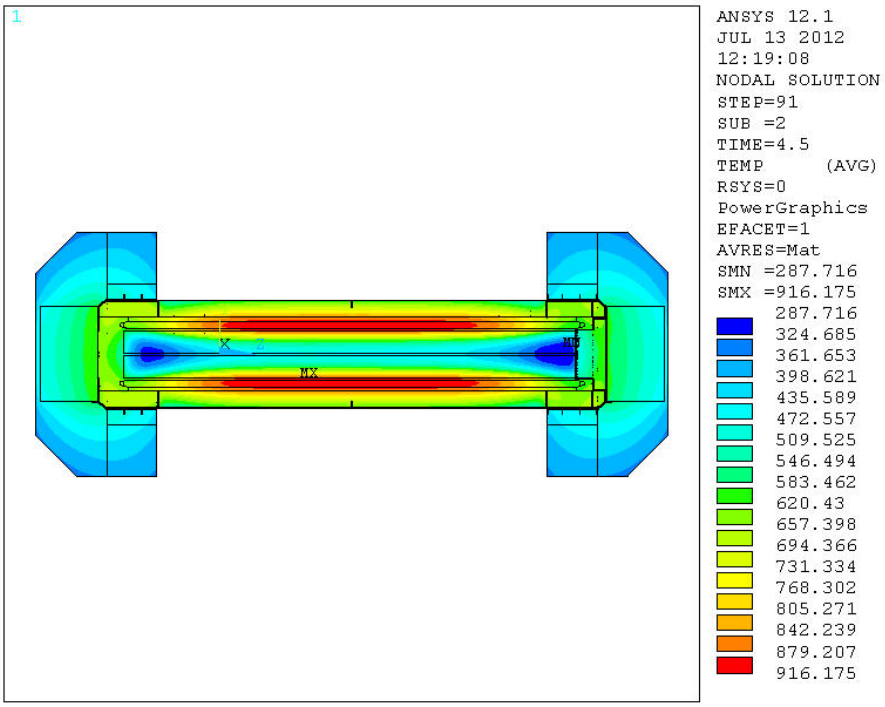

Figure C.70. NIST-02: (at 4 hours – 1 hour after end of fire on vehicle #31 – ambient temperature 314°F [157°C])

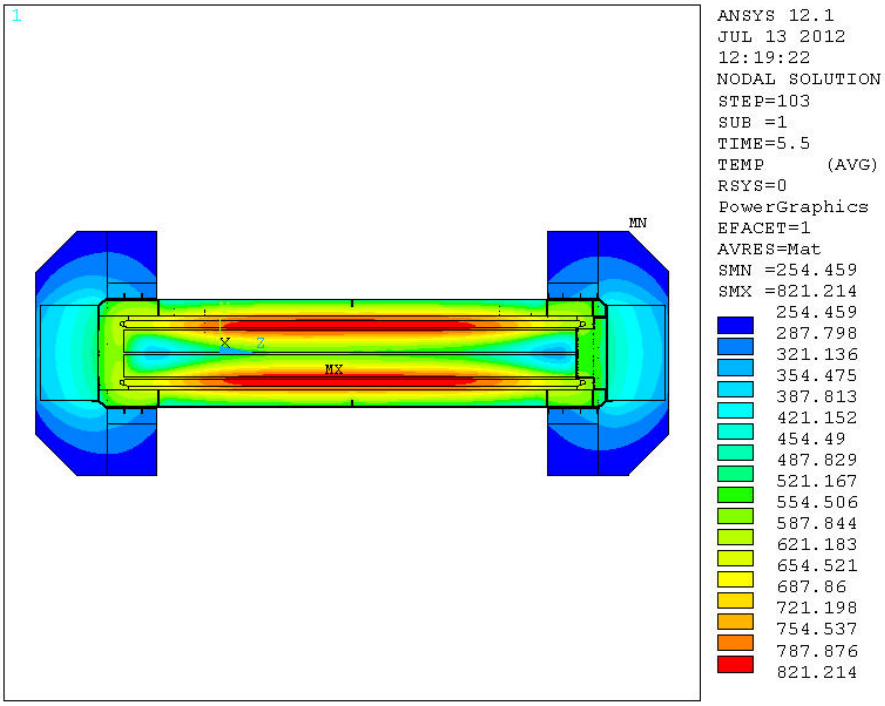

Figure C.71. NIST-02: (at 5 hours – 2 hours after end of fire on vehicle #31 – ambient temperature 224°F [107°C])

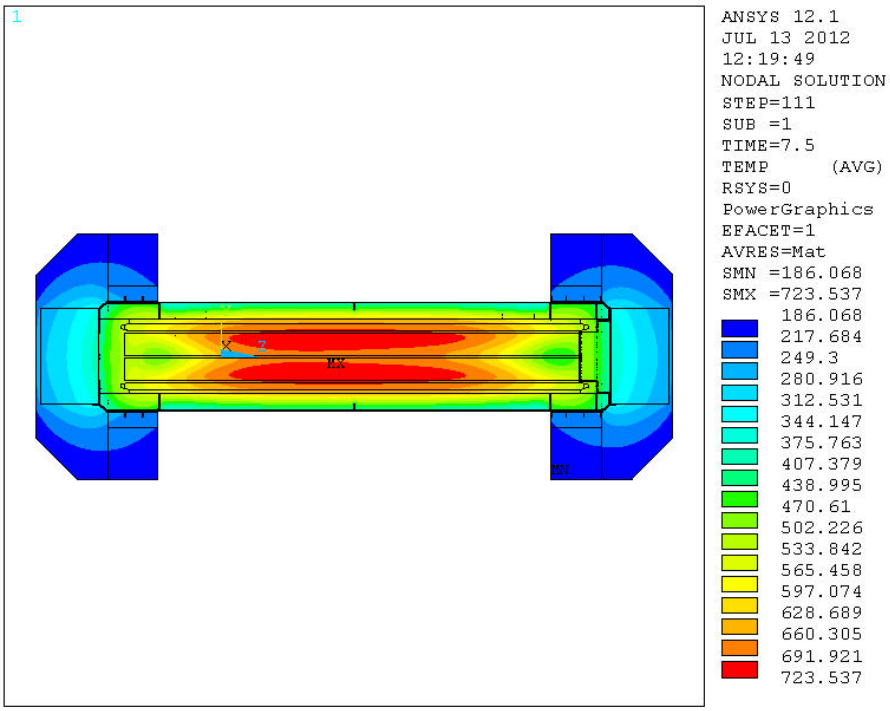

Figure C.72. NIST-02: (at 7 hours – 4 hours after end of fire on vehicle #31 – ambient temperature 158°F [70°C])

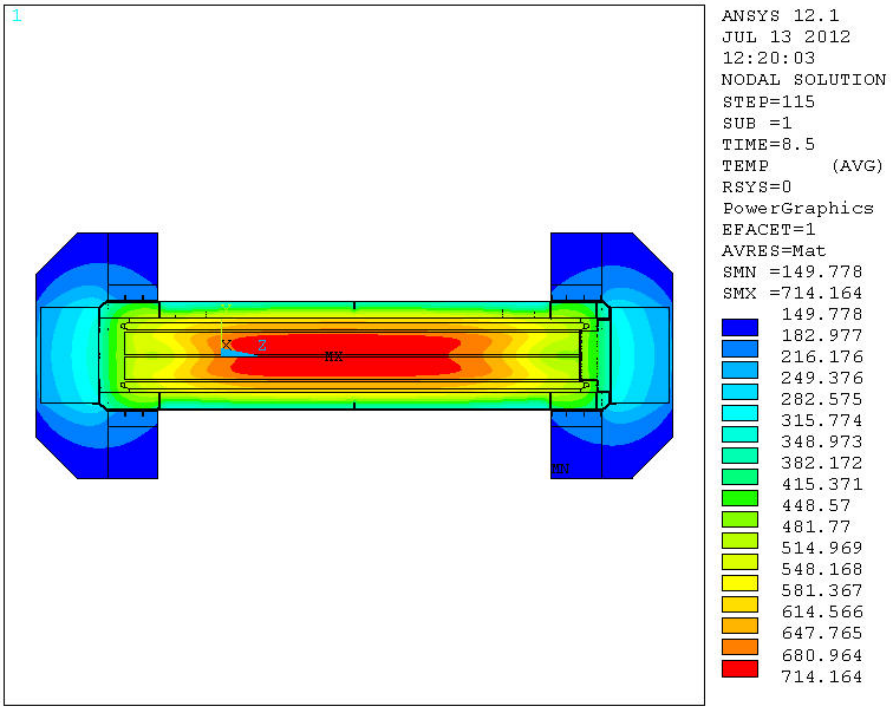

Figure C.73. NIST-02: (at 8 hours – 5 hours after end of fire on vehicle #31 – ambient temperature 120°F [49°C])

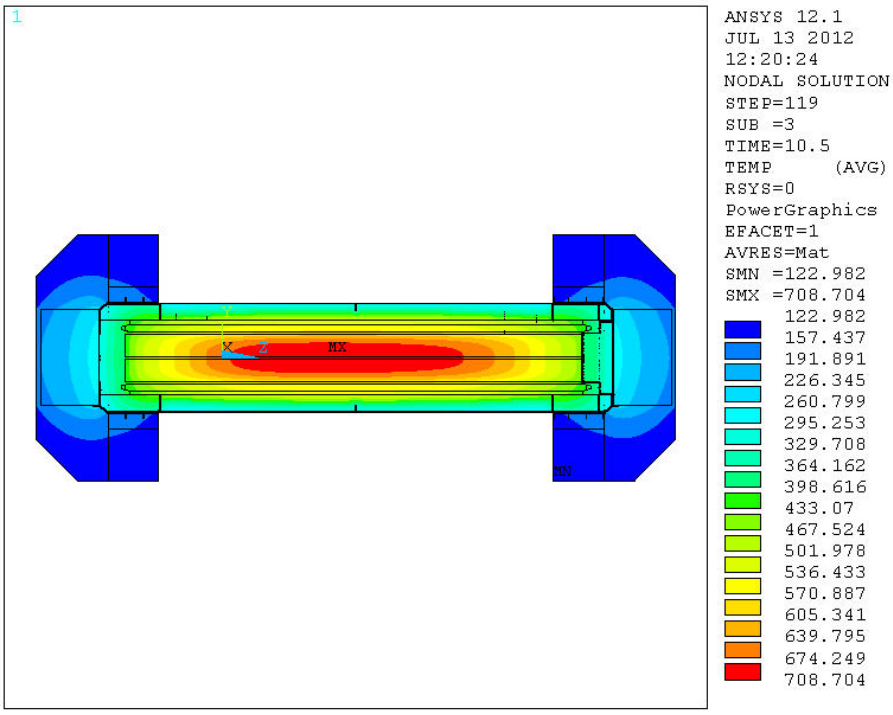

Figure C.74. NIST-02: (at 10 hours – 7 hours after end of fire on vehicle #31 – ambient temperature 100°F [38°C])

C.3 NIST-03

The fire conditions predicted with FDS for NIST-03 are determined for an assumed spread rate fast enough to result in the shortest possible total fire duration, based on the known fire time-line. This results in a total fire duration of approximately 2 hours, compared to the maximum estimated duration of 5 hours in NIST-01. As in NIST-01, the fuel available for the fire is based on an assumed typical cargo load for each vehicle (including those known to have been empty). The burn rate is also the same, with the fire on each vehicle lasting approximately 1 hour.

C.3.1 NIST-03: Package at Hottest Fire Location

The hottest fire location for this case is on vehicle #22, near the center of the tunnel. Due to the fast spread rate, the fire on this vehicle begins at approximately 30 minutes into the fire scenario, compared to the 2-hour lag time at this location in NIST-01. The rapid spread rate specified for this case brings the fire to the longest fire location, on vehicle #31, near the tunnel entrance, in approximately 1 hour. Figure C.75 illustrates this with the fire boundary temperatures for the local vehicle fires at these two locations. The fire on vehicle #31 starts before the fire on vehicle #22 is over, and since the vehicles between these two locations are also burning during this interval, this case essentially fills the entire tunnel with fire for approximately 2 hours.

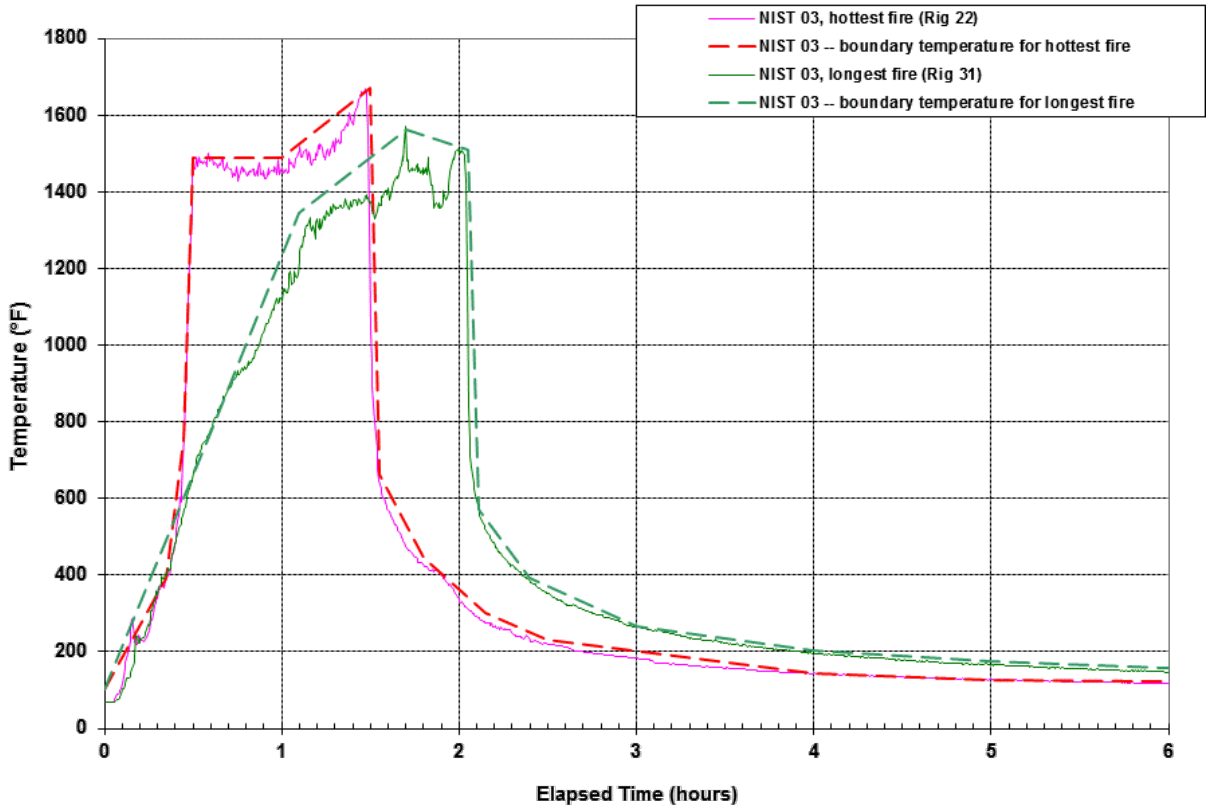

Figure C.75. Boundary Temperatures for Hottest Fire and Longest Fire Locations for Case NIST-03

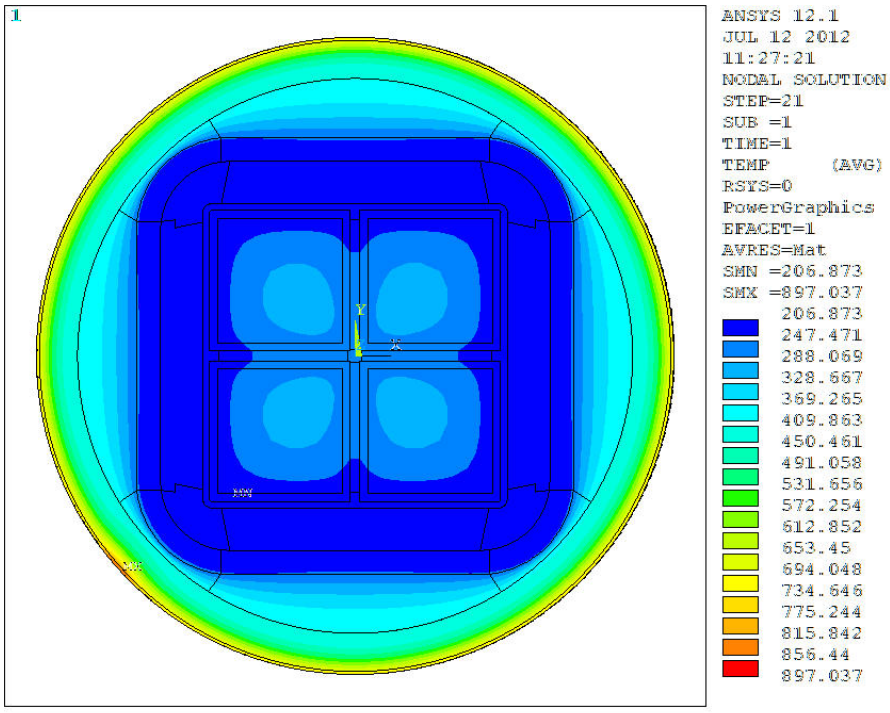

Figure C.76. NIST-03: (at 30 minutes – start of fire on vehicle #22 – ambient temperature 1490°F [810°C])

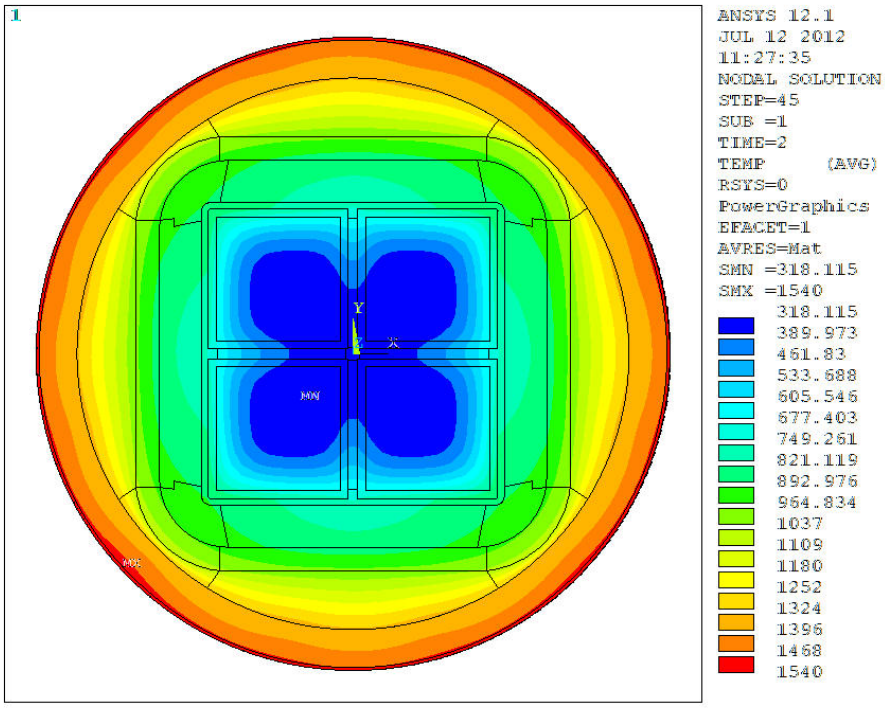

Figure C.77. NIST-03: (at 1.5 hours – ~3 minutes before end of fire on vehicle #22 – ambient temperature 1670°F [910°C])

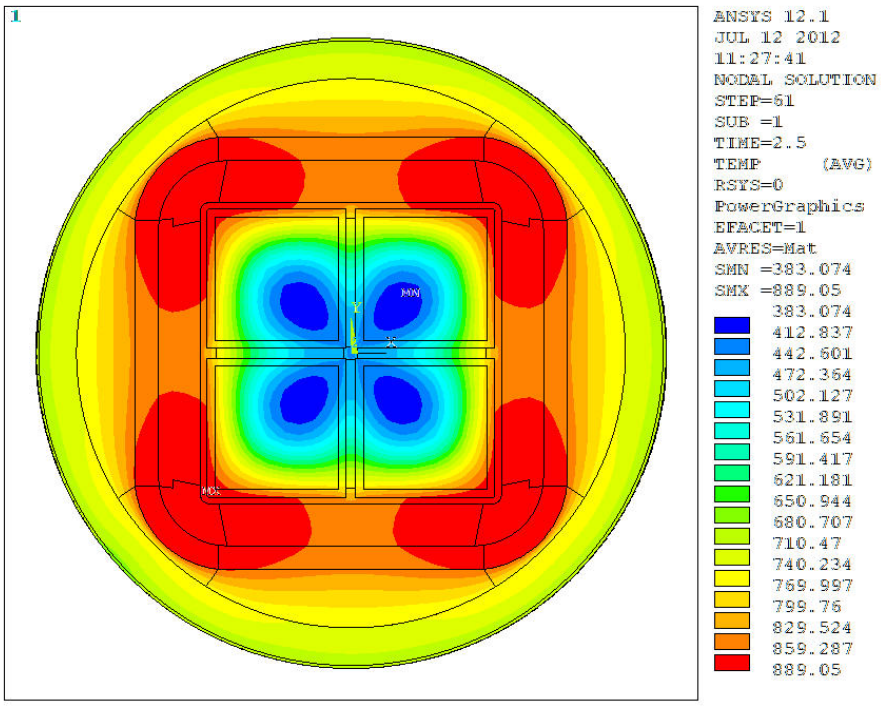

Figure C.78. NIST-03: (at 2 hours – 30 minutes after end of fire on vehicle #22 – ambient temperature 397°F [203°C])

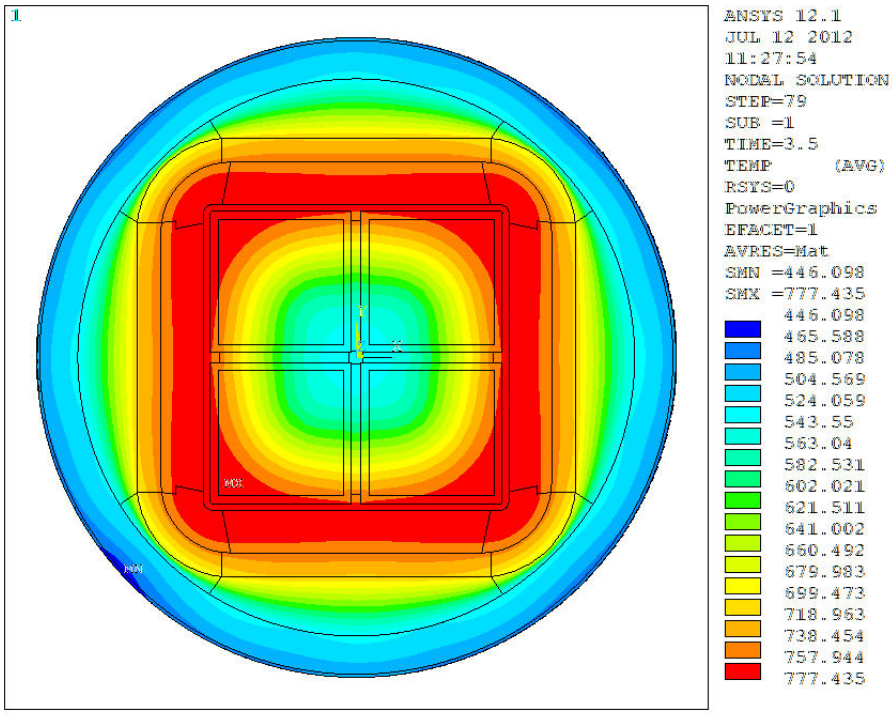

Figure C.79. NIST-03: (at 3 hours – 1.5 hours after end of fire on vehicle #22 – ambient temperature 210°F [99°C])

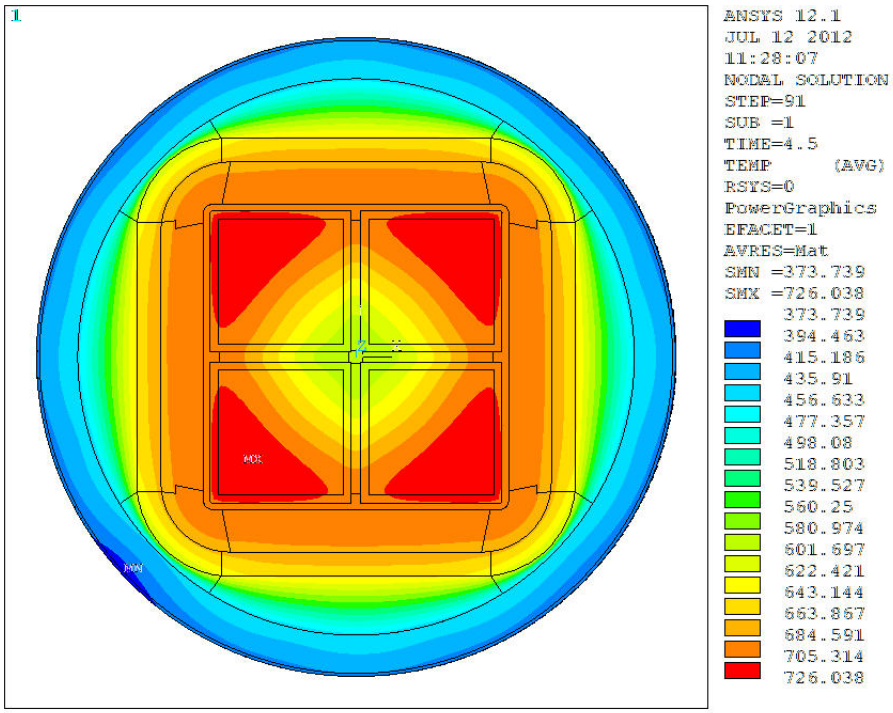

Figure C.80. NIST-03: (at 4 hours – 2.5 hours after end of fire on vehicle #22 – ambient temperature 153°F [67°C])

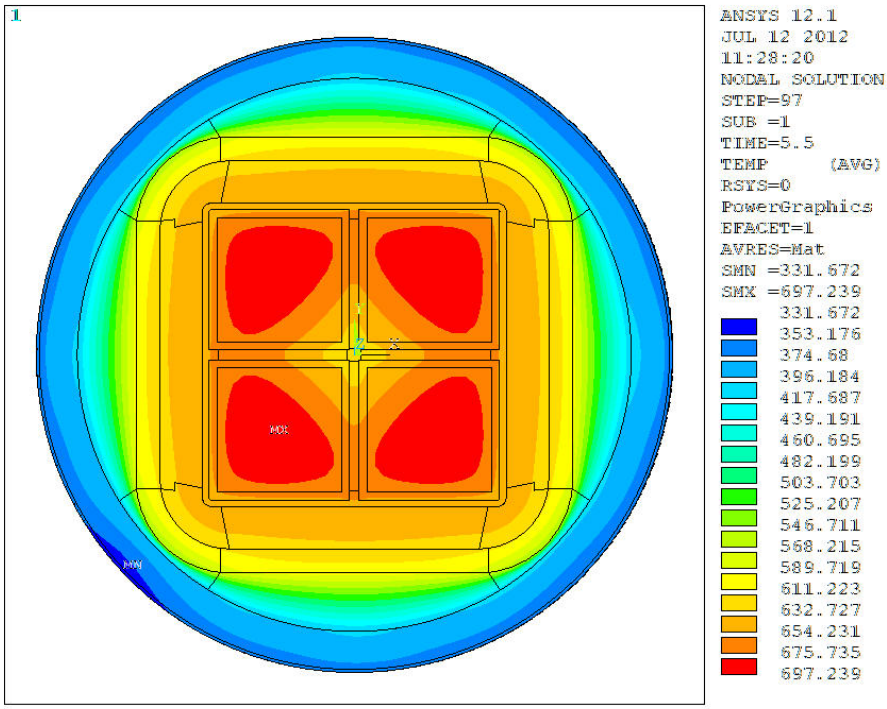

Figure C.81. NIST-03: (at 5 hours – 3.5 hours after end of fire on vehicle #22 – ambient temperature 132°F [56°C])

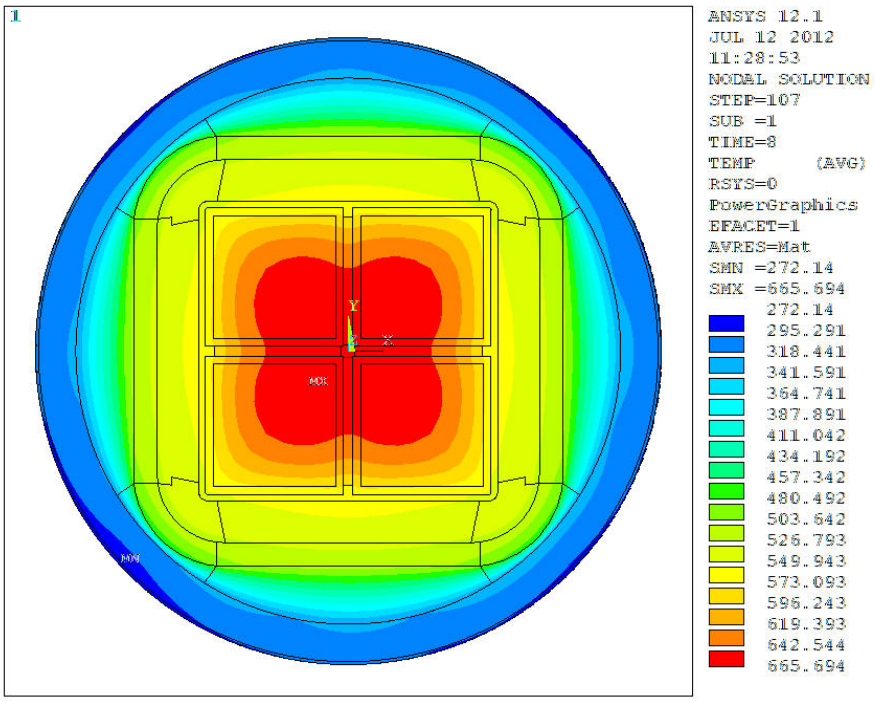

Figure C.82. NIST-03: (at 7.5 hours – 6 hours after end of fire on vehicle #22 – ambient temperature 132°F [56°C])

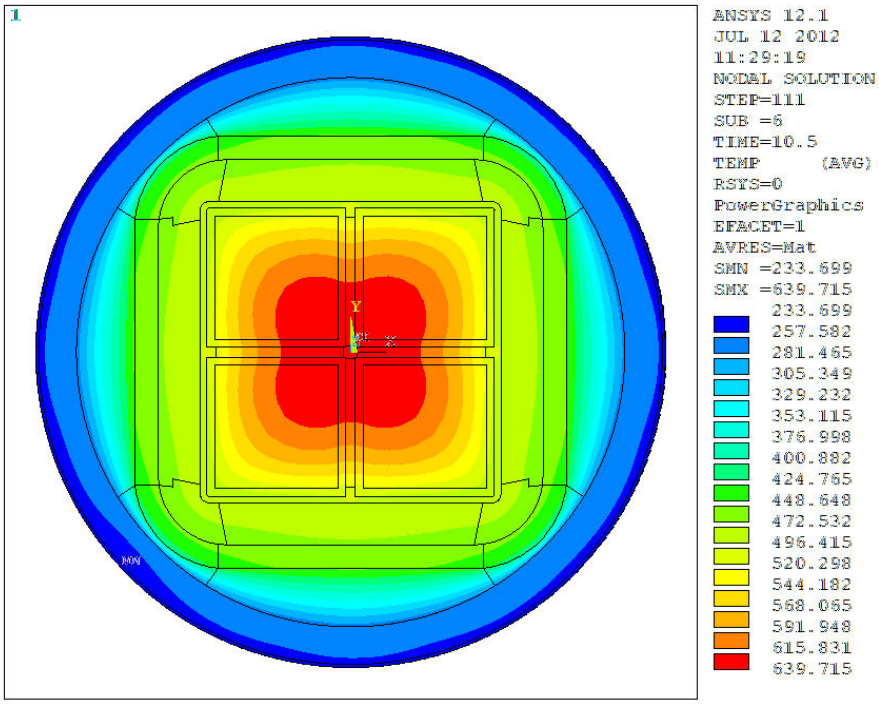

Figure C.83. NIST-03: (at 10 hours – 8.5 hours after end of fire on vehicle #22 – ambient temperature 100°F [38°C])

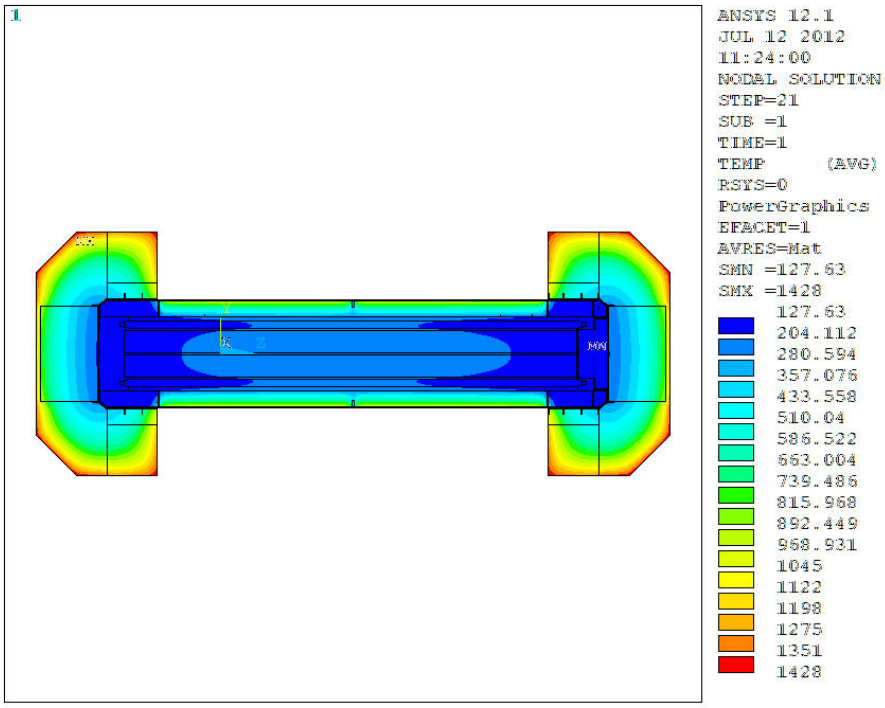

Figure C.84. NIST-03: (at 30 minutes – start of fire on vehicle #22 – ambient temperature 1490°F [810°C])

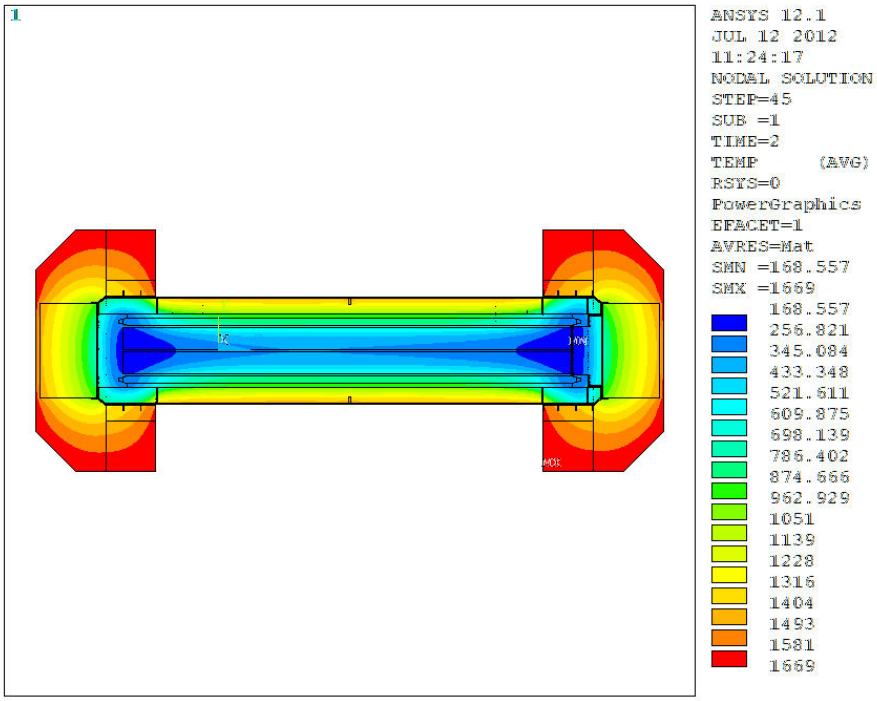

Figure C.85. NIST-03: (at 1.5 hours – ~3 minutes before end of fire on vehicle #22 – ambient temperature 1670°F [910°C])

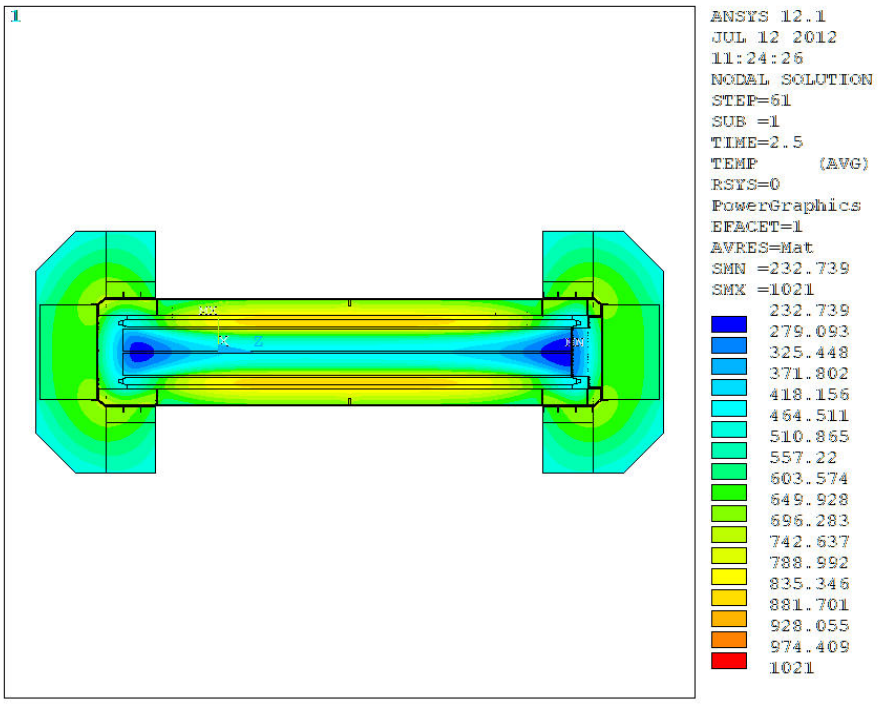

Figure C.86. NIST-03: (at 2 hours – 30 minutes after end of fire on vehicle #22 – ambient temperature 397°F [203°C])

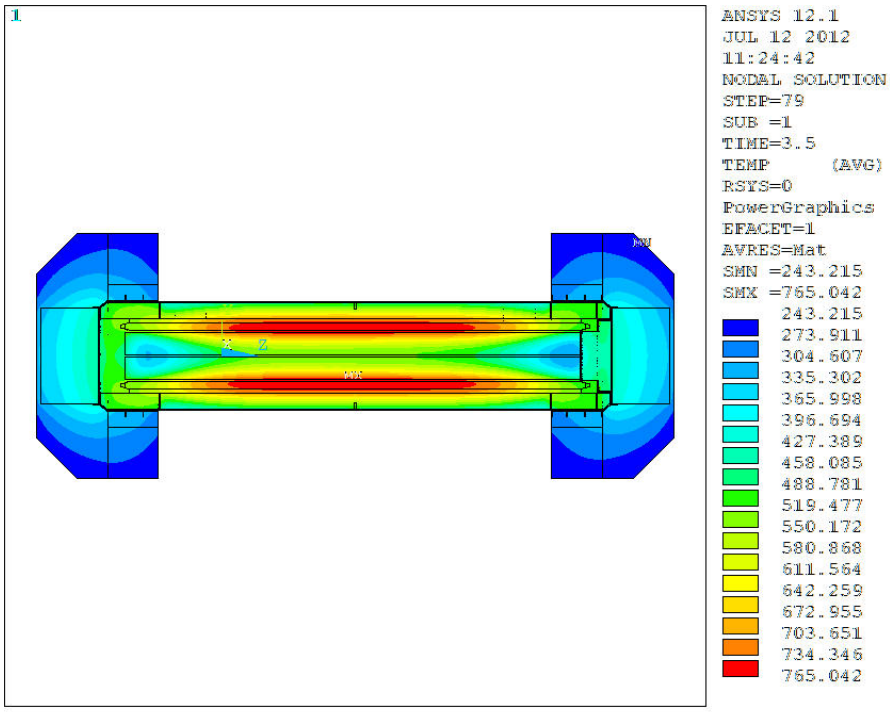

Figure C.87. NIST-03: (at 3 hours – 1.5 hours after end of fire on vehicle #22 – ambient temperature 210°F [99°C])

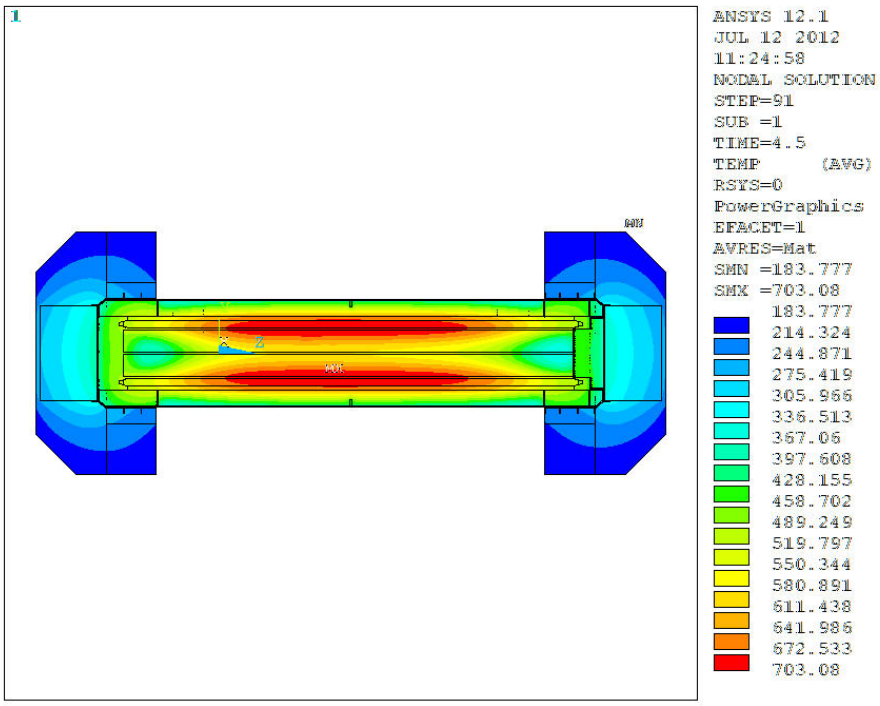

Figure C.88. NIST-03: (at 4 hours – 2.5 hours after end of fire on vehicle #22 – ambient temperature 153°F [67°C])

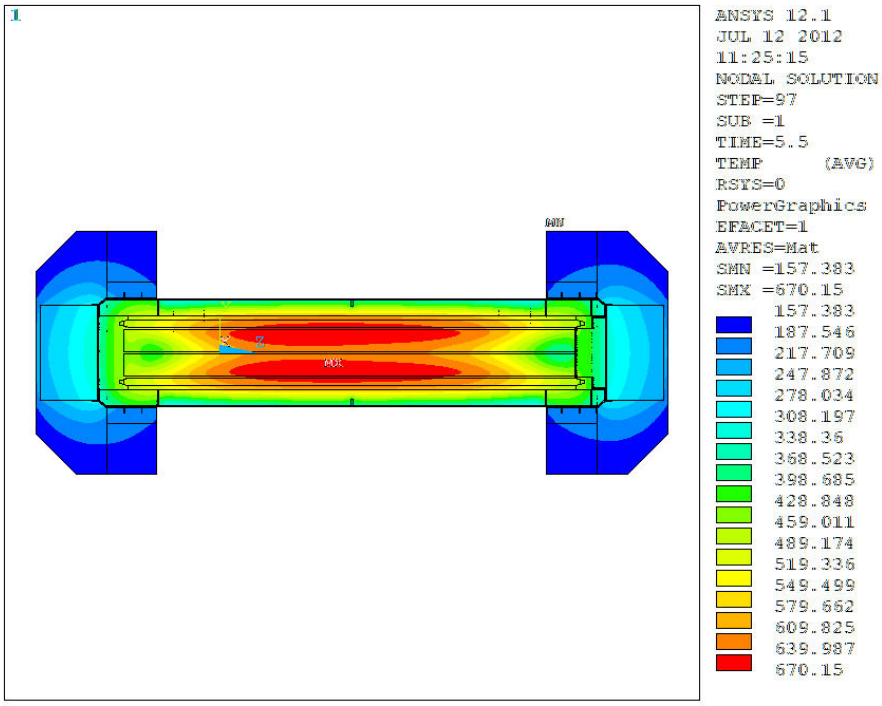

Figure C.89. NIST-03: (at 5 hours – 3.5 hours after end of fire on vehicle #22 – ambient temperature 132°F [56°C])

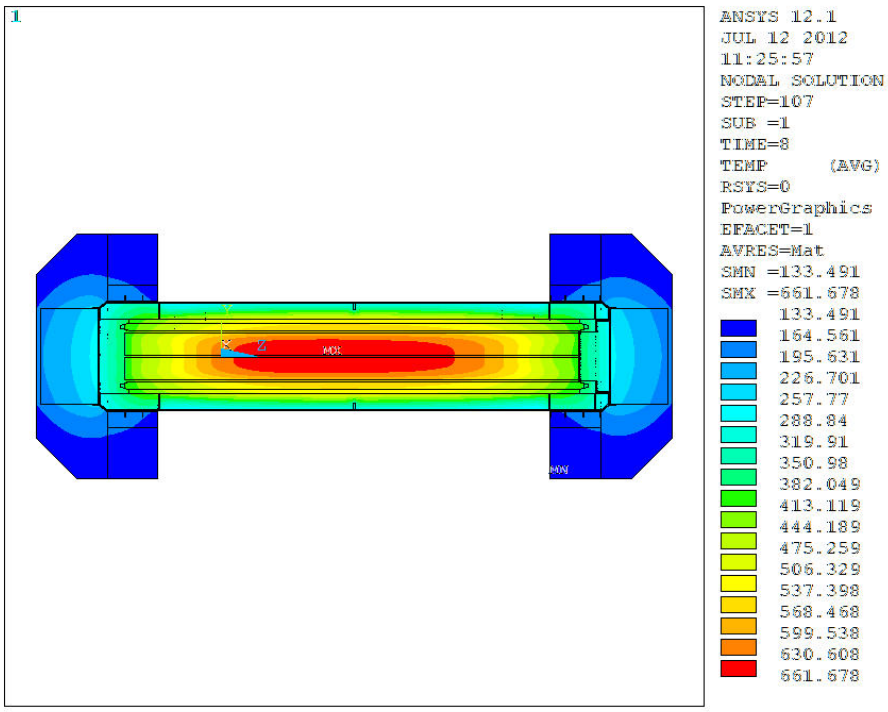

Figure C.90. NIST-03: (at 7.5 hours – 6 hours after end of fire on vehicle #22 – ambient temperature 132°F [56°C])

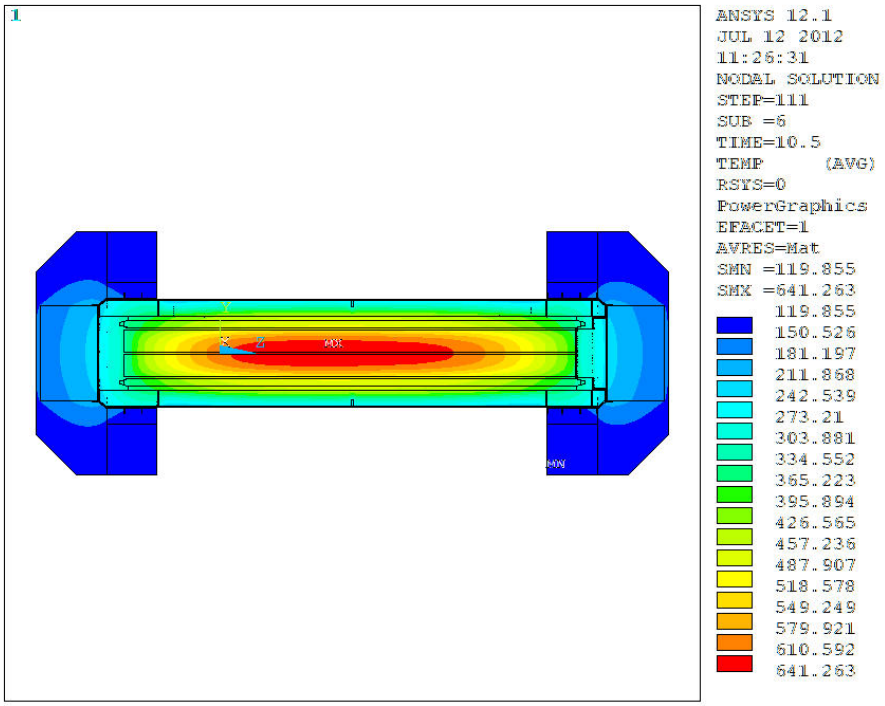

Figure C.91. NIST-03: (at 10 hours – 8.5 hours after end of fire on vehicle #22 – ambient temperature 100°F [38°C])

C.3.2 NIST-03: Package at Longest Fire Location

The longest fire location for this case is on vehicle #31, near the tunnel entrance. Due to the faster spread rate, the fire on this vehicle begins within 1 hour of the start of the fire scenario, compared to the 4-hour lag time at this location in NIST-01. The rapid spread rate assumed for this case results in the greatest overlap of the fire durations on individual vehicles. The fires near the tunnel exit are just ending when the fire begins on vehicle #31. As a result, this case has the hottest pre-fire ambient temperatures for vehicle #31. The ambient temperature shows a steady increase from the beginning of the transient, reaching nearly 1300°F (704°C) over the first hour, such that it is not entirely clear precisely when the local vehicle fire begins on vehicle #31 in this case.

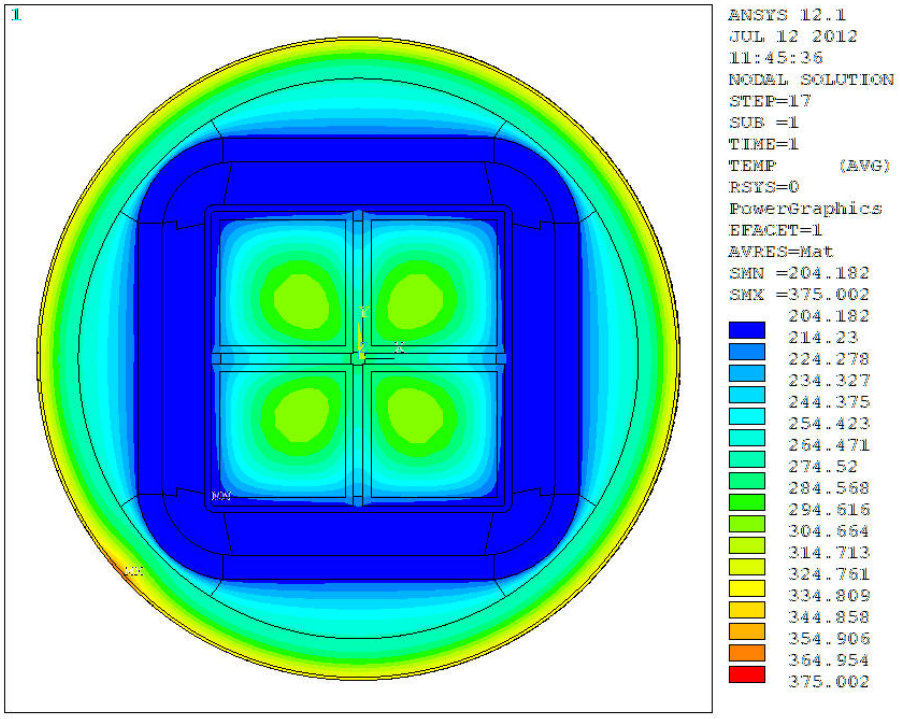

Figure C.92. NIST-03: (at 30 minutes – ~0.5 hour before start of fire on vehicle #31 – ambient temperature 658°F [348°C])

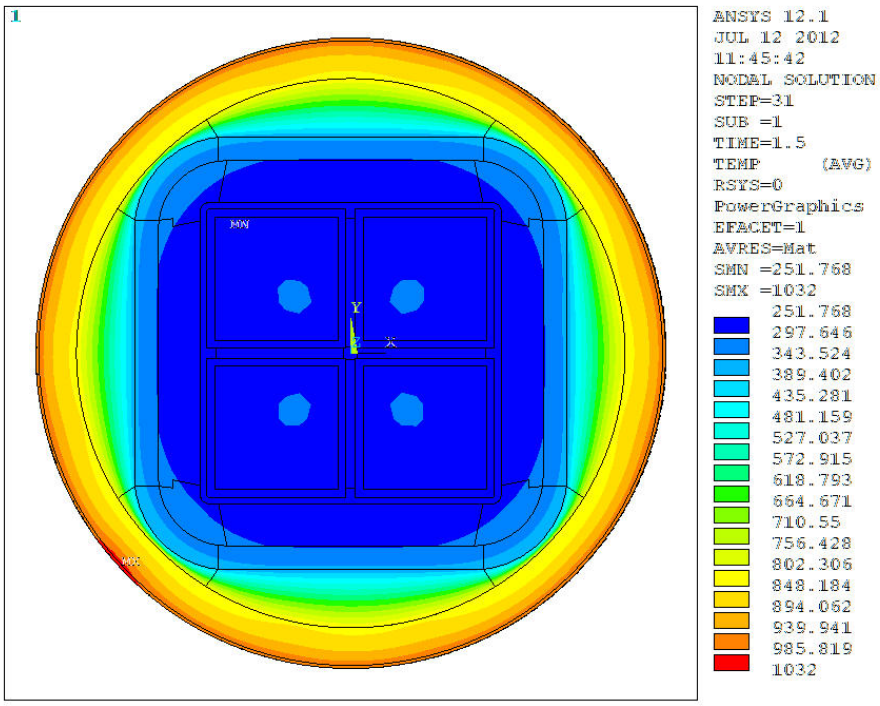

Figure C.93. NIST-03: (at 1 hour – estimated start of fire on vehicle #31 – ambient temperature 1231°F [666°C])

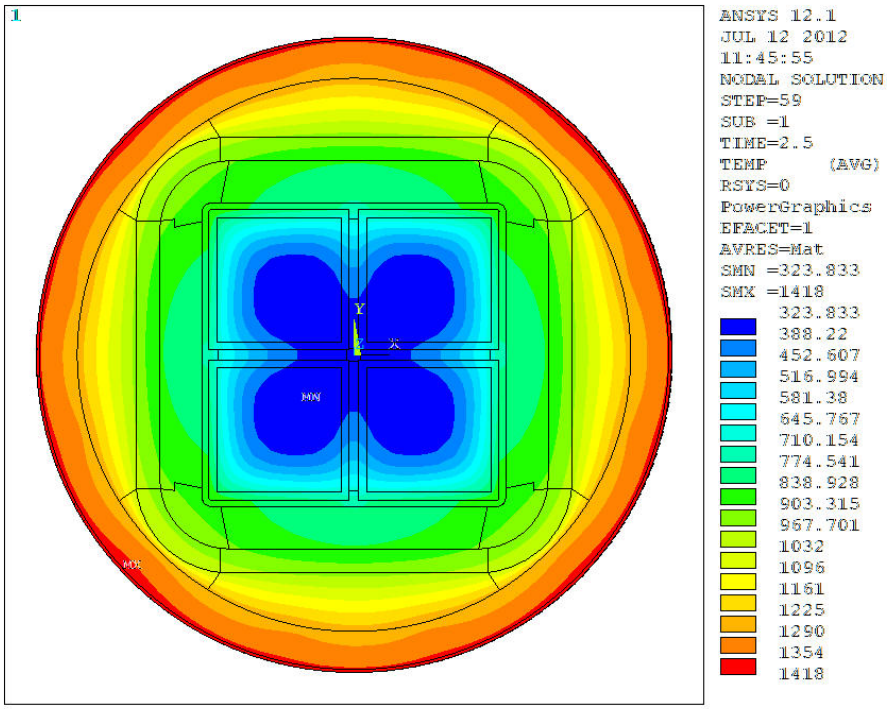

Figure C.94. NIST-03: (at 2 hours – ~5 minutes before end of fire on vehicle #31 – ambient temperature 1516°F [824°C])

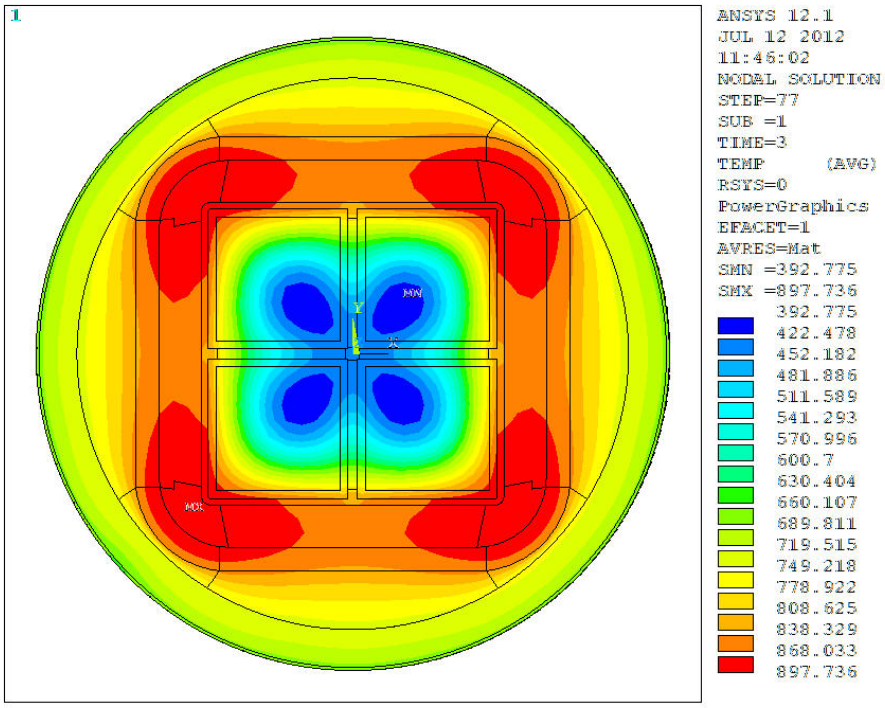

Figure C.95. NIST-03: (at 2.5 hours – 30 minutes after end of fire on vehicle #31 – ambient temperature 381°F [194°C])

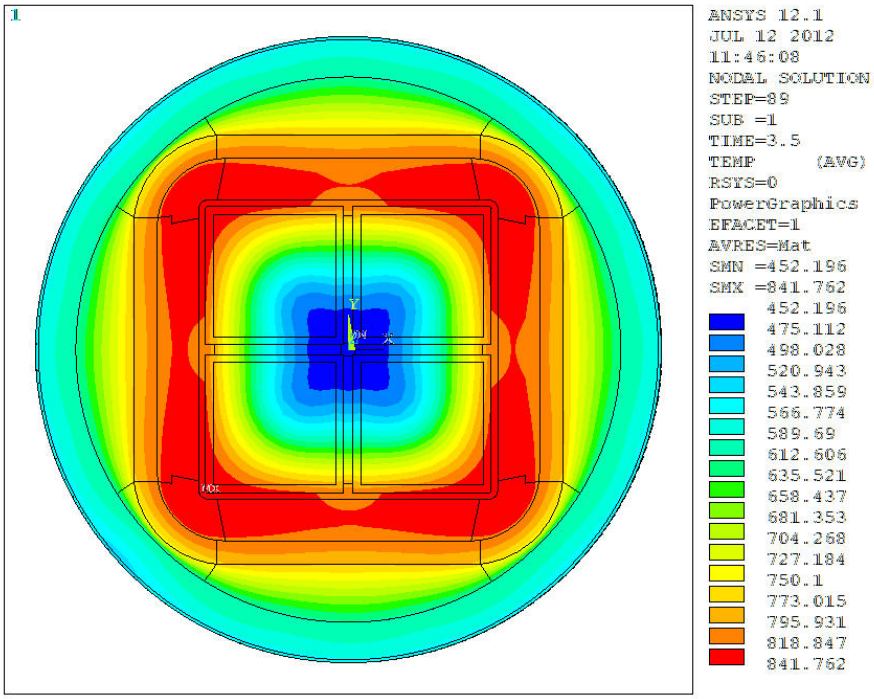

Figure C.96. NIST-03: (at 3 hours – 1 hour after end of fire on vehicle #31 – ambient temperature 283°F [140°C])

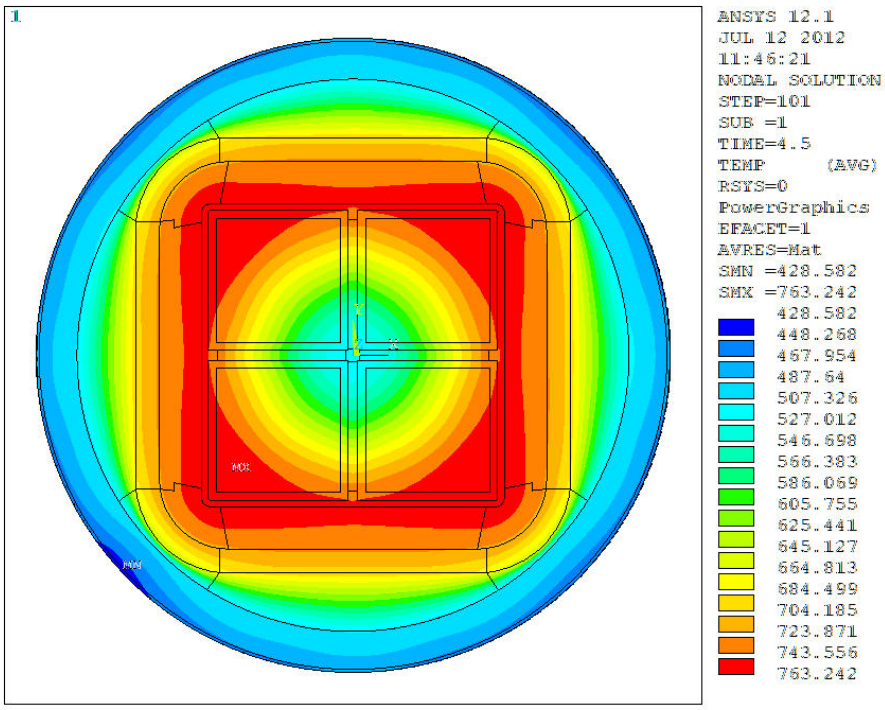

Figure C.97. NIST-03: (at 4 hours – 2 hours after end of fire on vehicle #31 – ambient temperature 213°F [101°C])

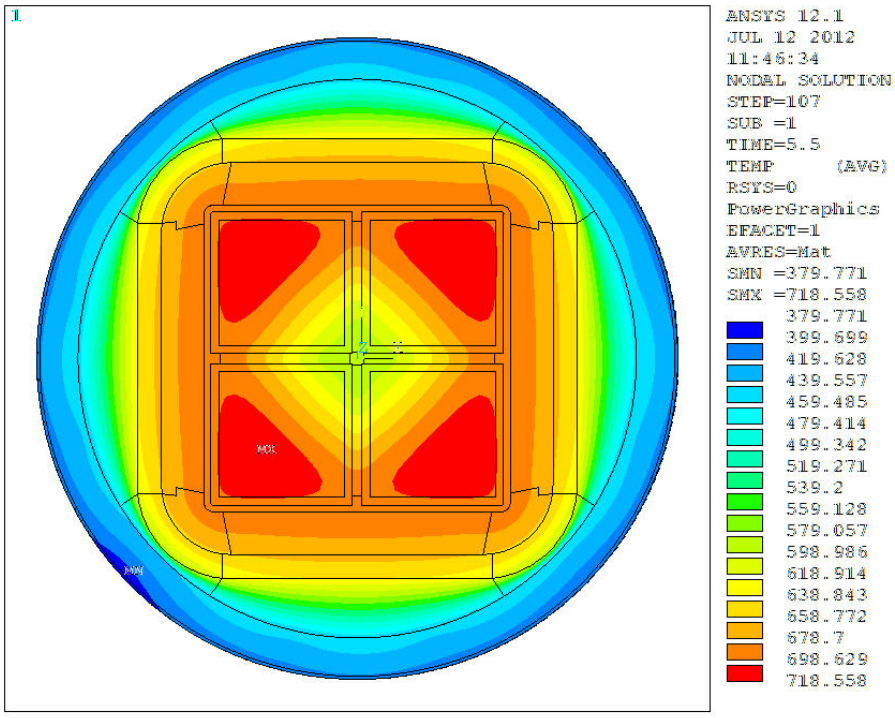

Figure C.98. NIST-03: (at 5 hours – 3 hours after end of fire on vehicle #31 – ambient temperature 185°F [85°C])

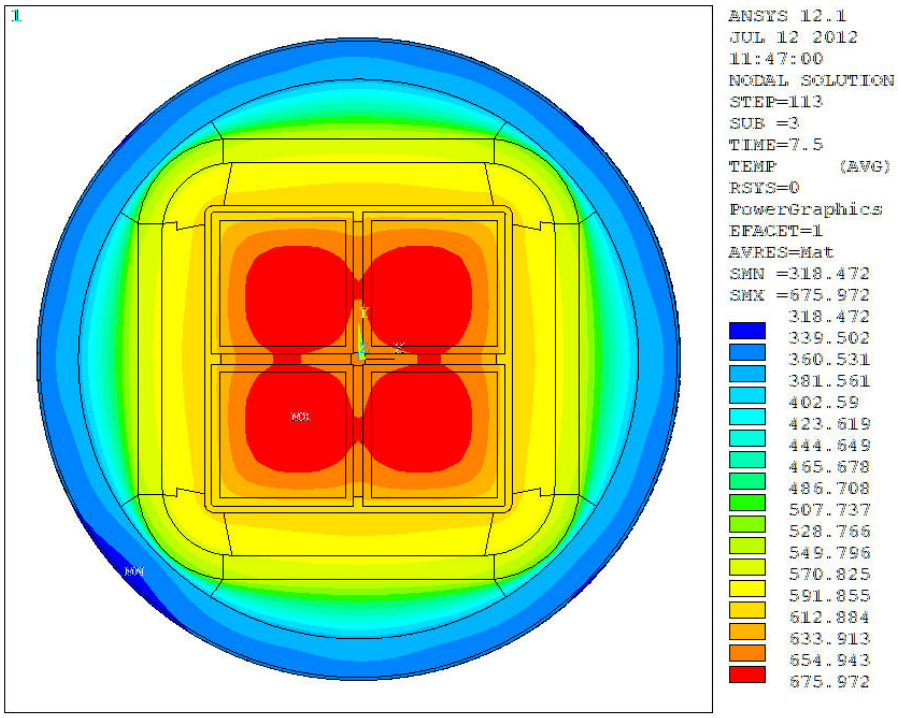

Figure C.99. NIST-03: (at 7 hours – 5 hours after end of fire on vehicle #23 – ambient temperature 158°F [70°C])

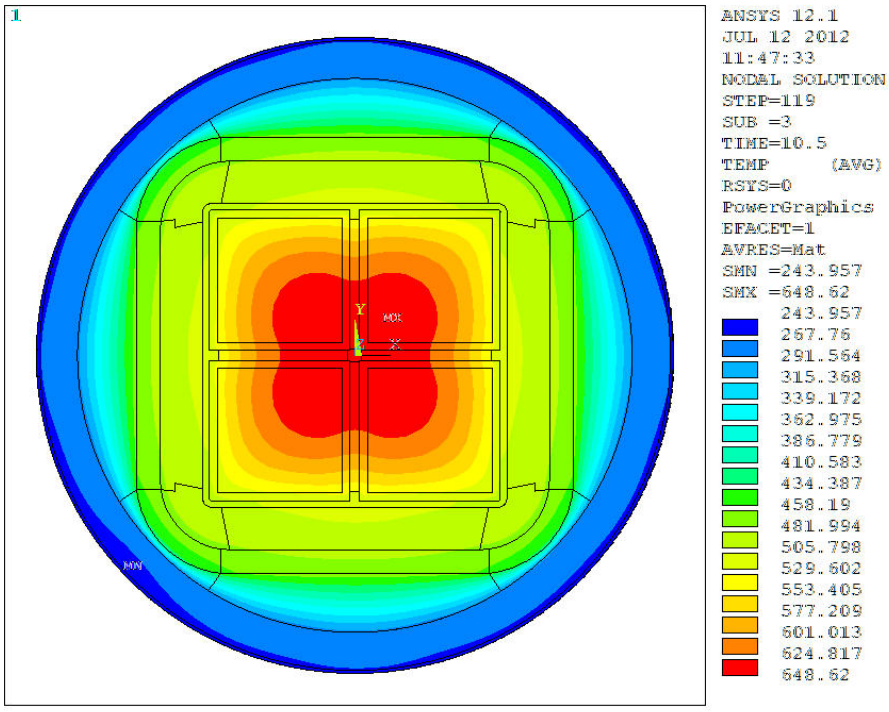

Figure C.100. NIST-03: (at 10 hours – 8 hours after end of fire on vehicle #23 – ambient temperature 100°F [38°C])

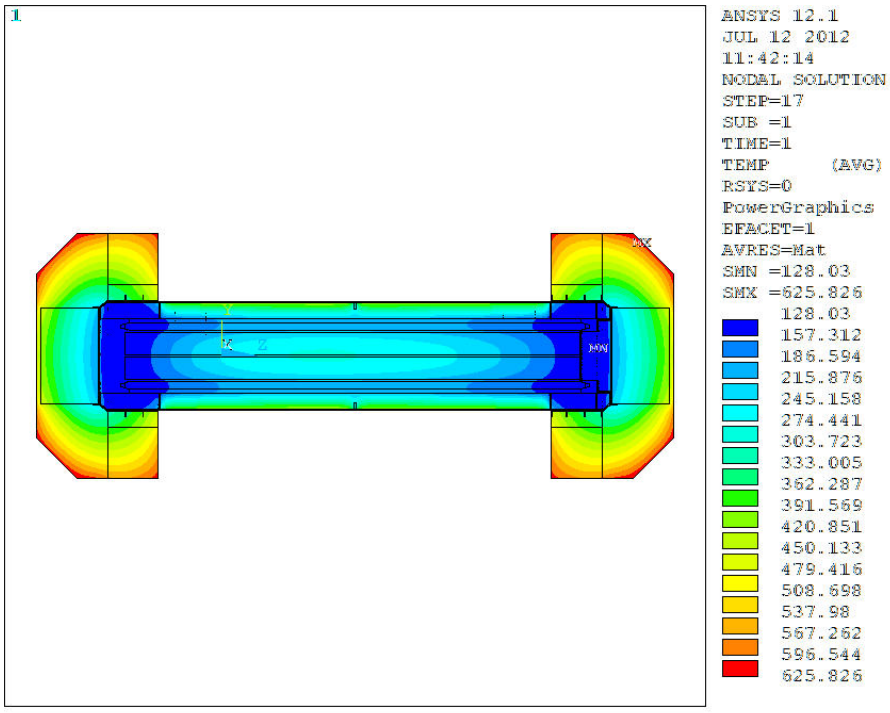

Figure C.101. NIST-03: (at 30 minutes – ~0.5 hour before start of fire on vehicle #31 – ambient temperature 658°F [348°C])

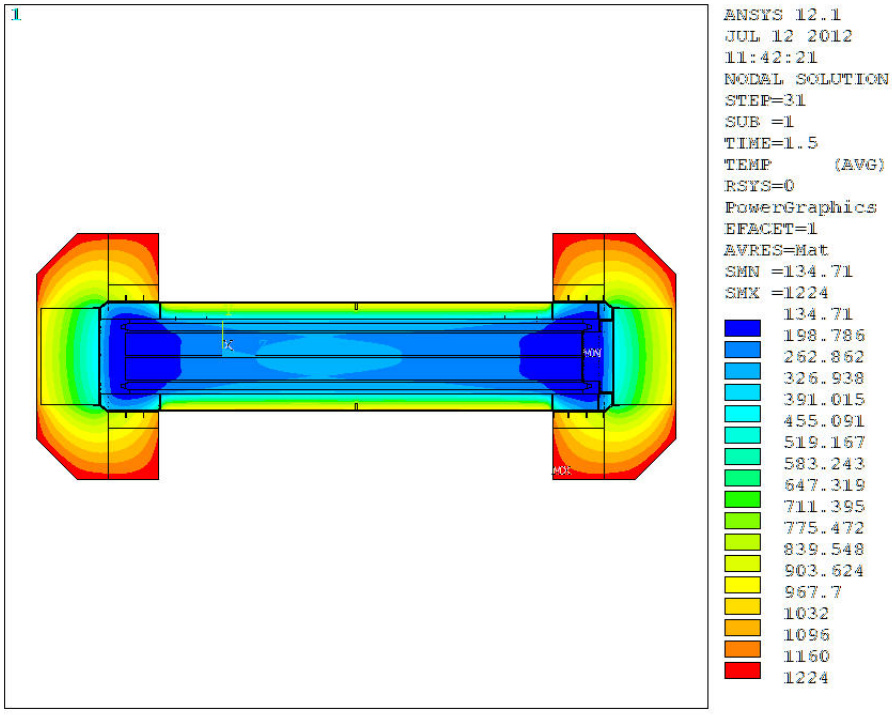

Figure C.102. NIST-03: (at 1 hour – estimated start of fire on vehicle #31 – ambient temperature 1231°F [666°C])

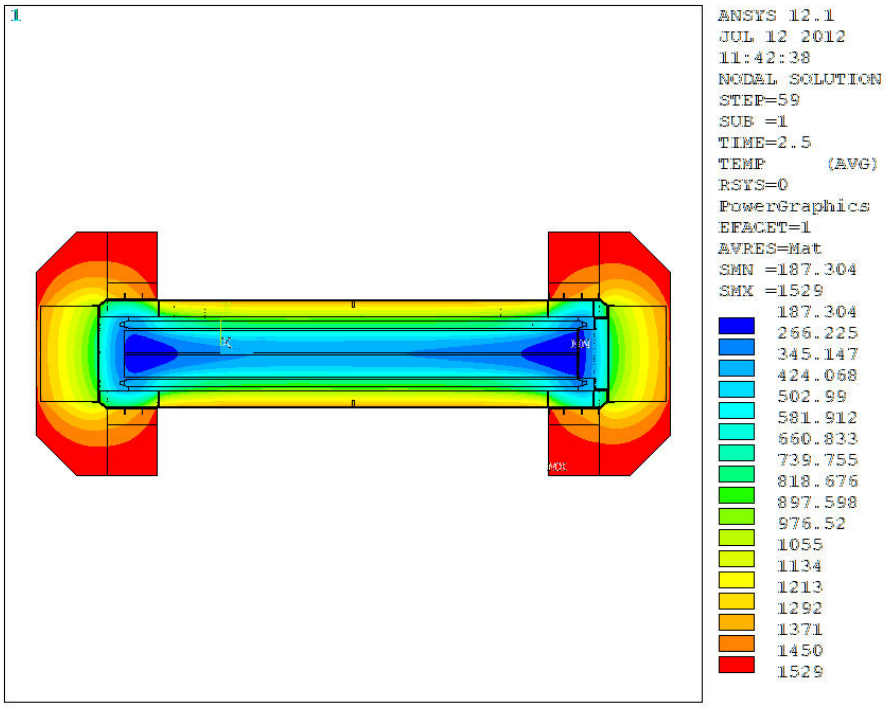

Figure C.103. NIST-03: (at 2 hours – ~5 minutes before end of fire on vehicle #31 – ambient temperature 1516°F [824°C])

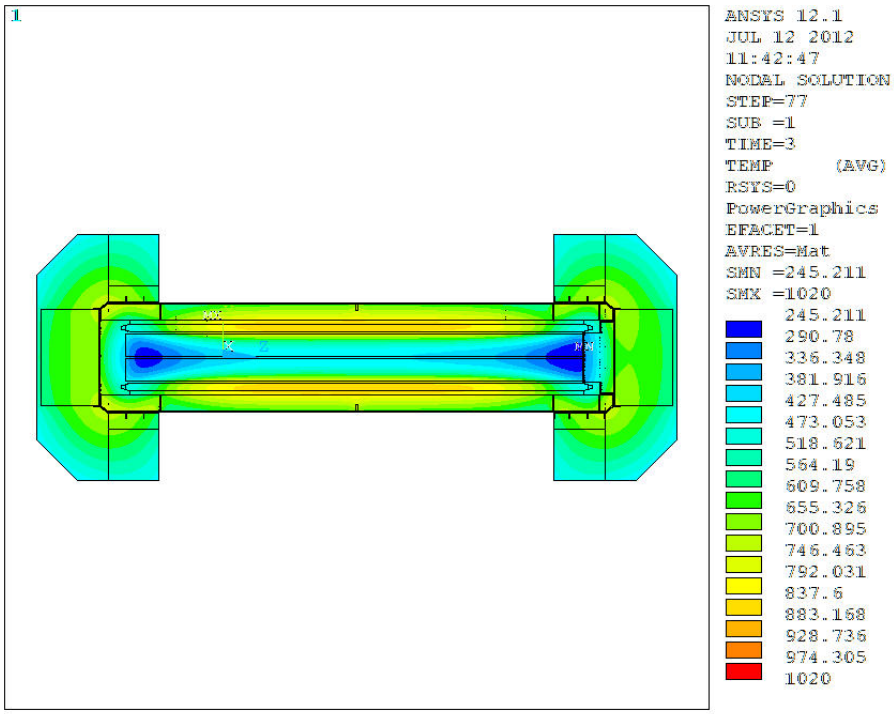

Figure C.104. NIST-03: (at 2.5 hours – 30 minutes after end of fire on vehicle #31 – ambient temperature 381°F [194°C])

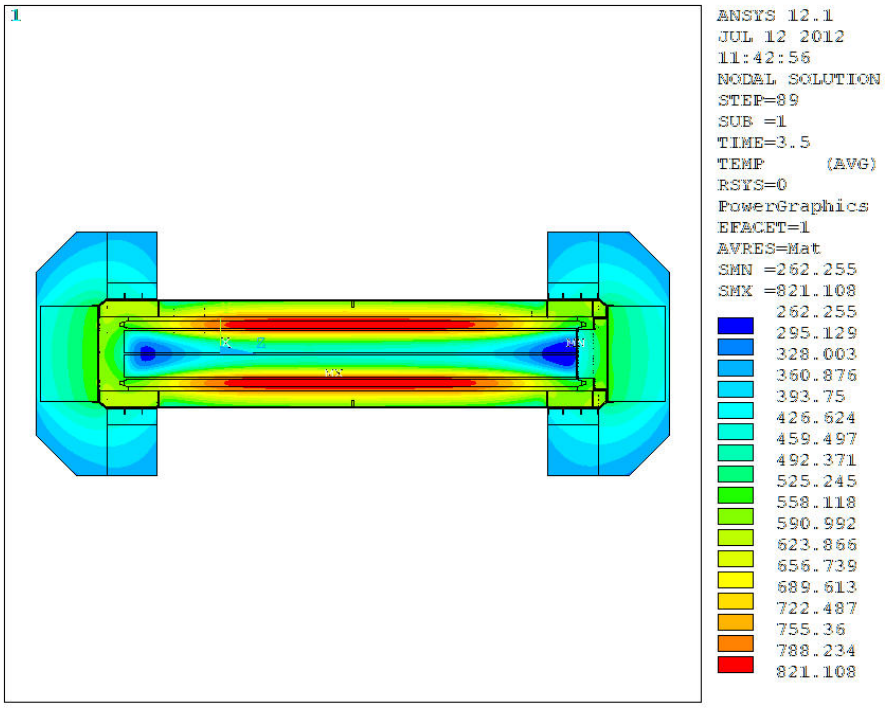

Figure C.105. NIST-03: (at 3 hours – 1 hour after end of fire on vehicle #31 – ambient temperature 283°F [140°C])

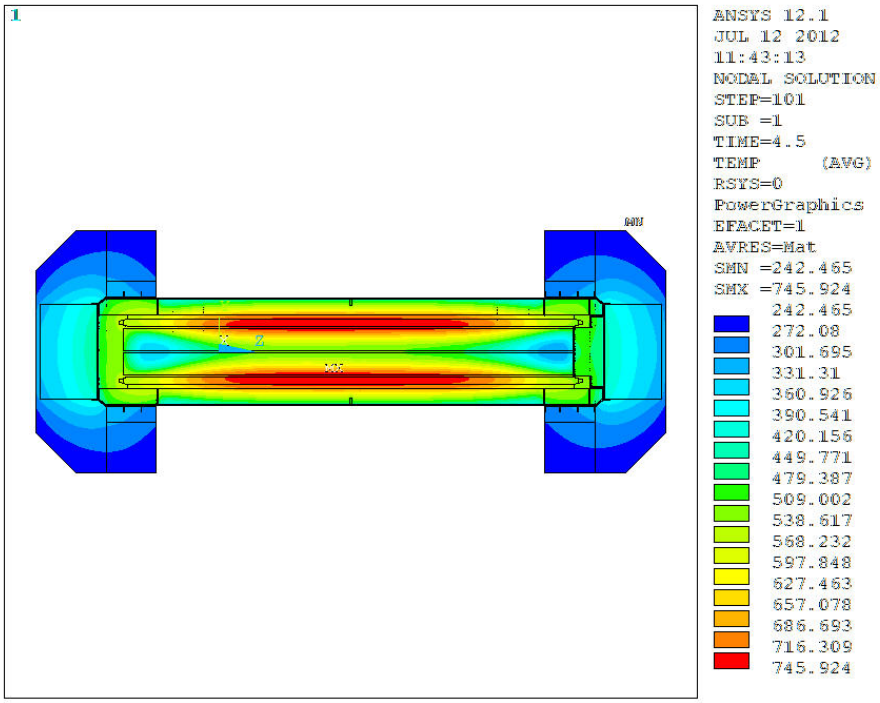

Figure C.106. NIST-03: (at 4 hours – 2 hours after end of fire on vehicle #31 – ambient temperature 213°F [101°C])

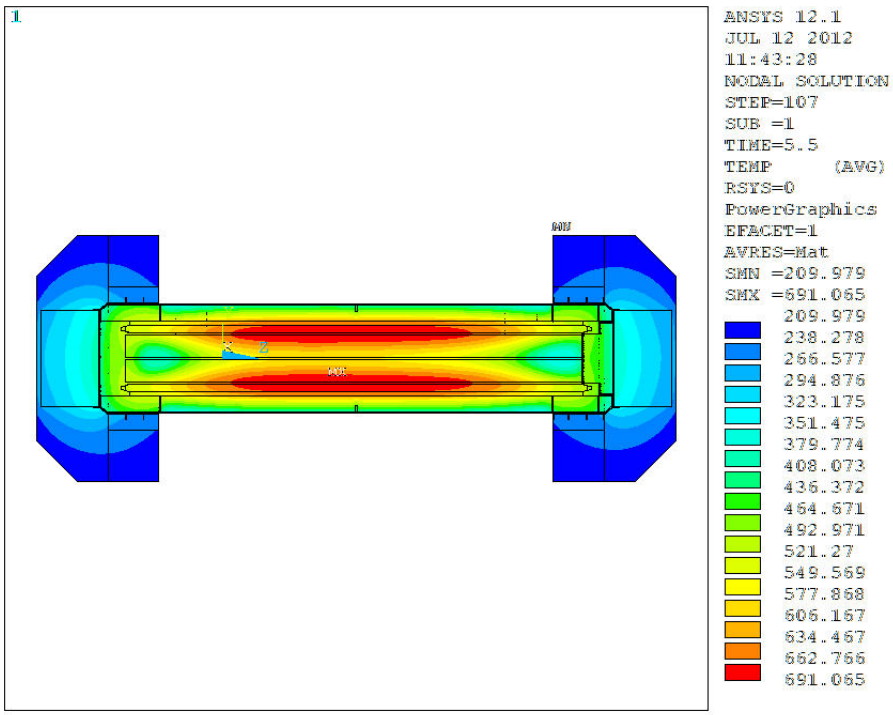

Figure C.107. NIST-03: (at 5 hours – 3 hours after end of fire on vehicle #31 – ambient temperature 185°F [85°C])

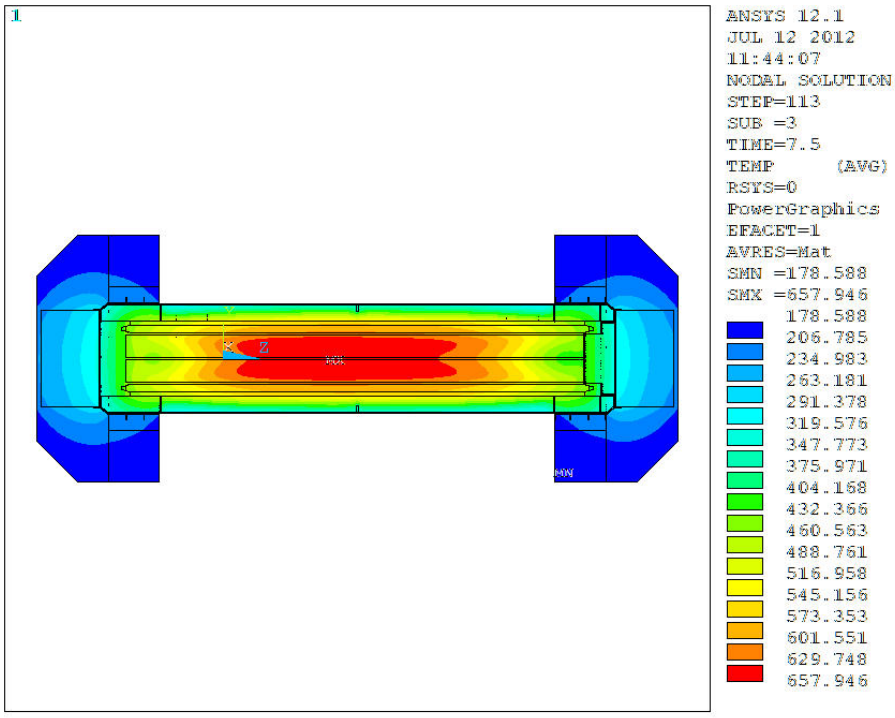

Figure C.108. NIST-03: (at 7 hours – 5 hours after end of fire on vehicle #23 – ambient temperature 158°F [70°C])

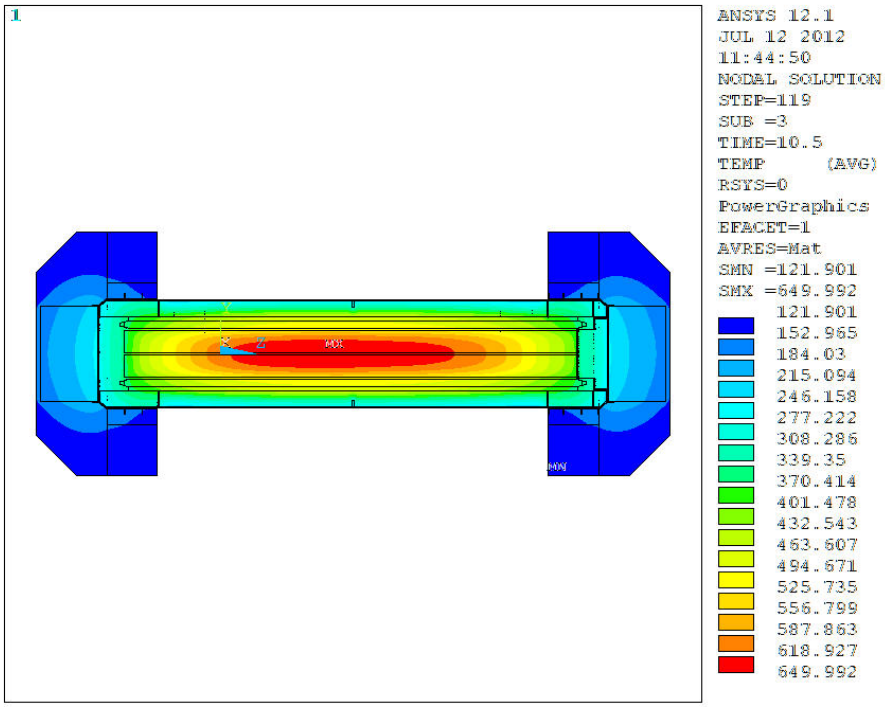

Figure C.109. NIST-03: (at 10 hours – 8 hours after end of fire on vehicle #23 – ambient temperature 100°F [38°C])

C.4 NIST-04

The fire conditions predicted with FDS for NIST-04 are determined for the same spread rate as assumed for the base case, resulting in a total fire duration of about 5 hours, approximately same length as in NIST-01. As in NIST-01, the fuel available for the fire is based on an assumed "typical" cargo load for each vehicle (including those known to have been empty), but the burn rate is doubled, to produce a hotter, more intense fire on each vehicle. As a result of the higher burn rate, the fuel is consumed more rapidly, and the local fire duration on each vehicle is only about 33 minutes.

C.4.1 NIST-04: Package at Hottest Fire Location

The hottest fire location for this case is on vehicle #22, near the center of the tunnel. The fire on this vehicle begins at approximately 1.8 hours into the fire scenario, essentially the same time lag as for the hottest fire location as in NIST-01. Similarly, the fire on vehicle #31, which is the longest fire location, begins after about 4 hours, since the fire spread rate is the same as in NIST-01. However, the burn rate of the individual fires is twice the value specified in the base case NIST-01, and therefore the fires burn more intensely, and for about half the time interval. Figure C.110 shows the engulfing fire boundary temperatures assumed for the two selected fire locations.

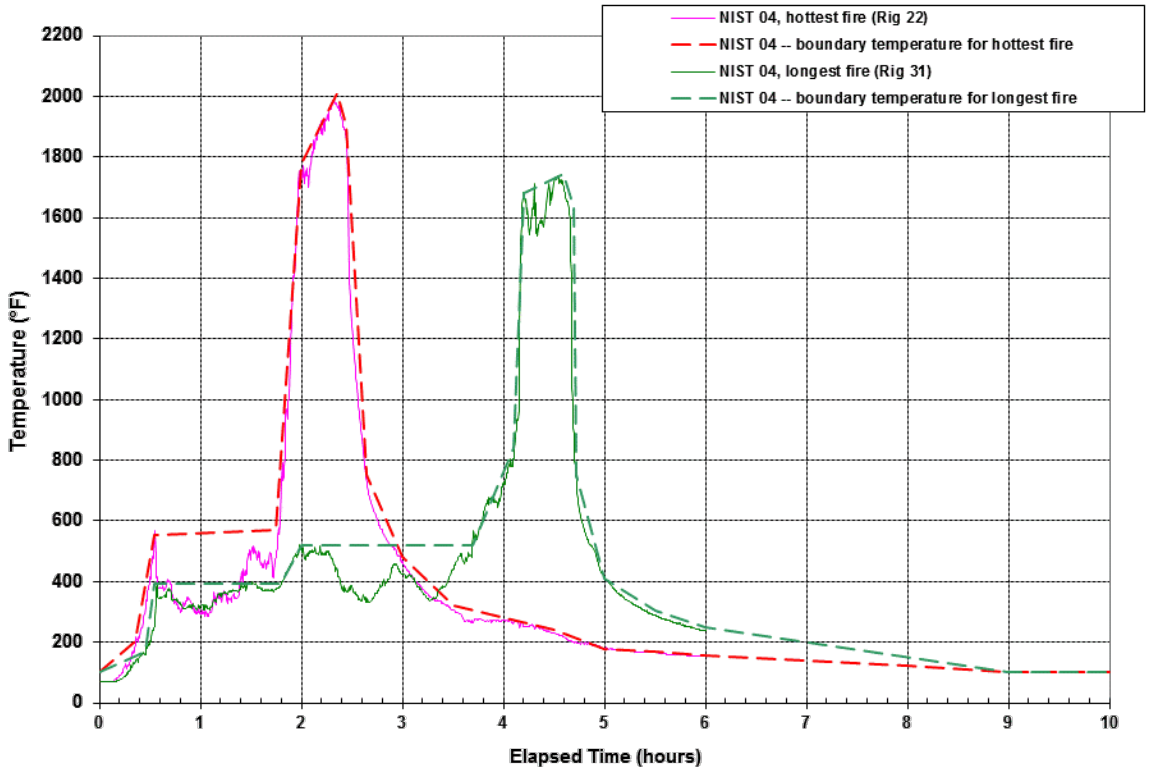

Figure C.110. Boundary Temperatures for Hottest Fire and Longest Fire Locations for Case NIST-04

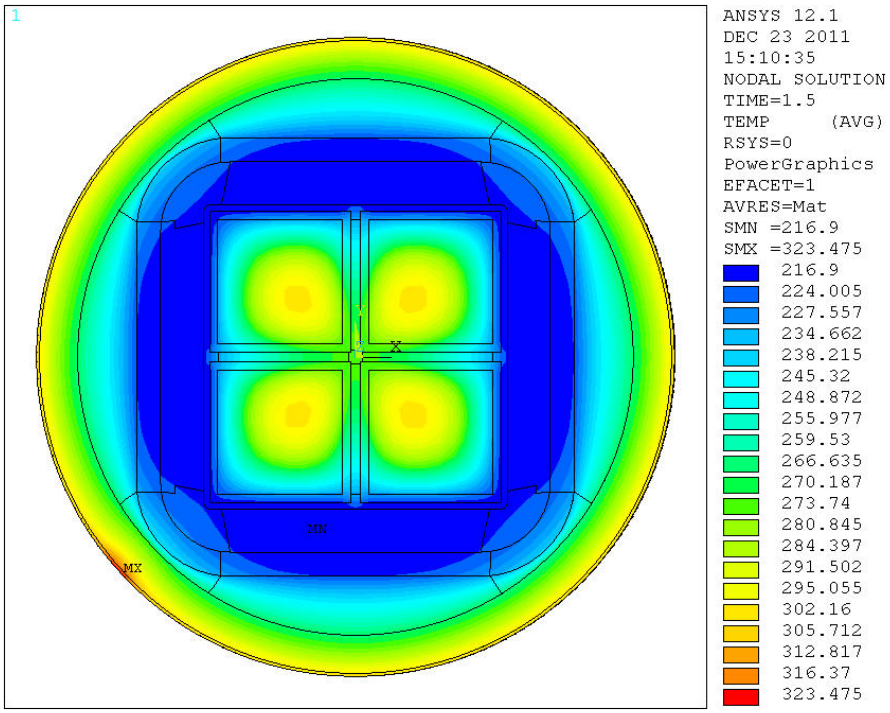

Figure C.111. NIST-04: (at 1 hour – ~1 hour before fire on vehicle #22 – ambient temperature 566°F [297°C])

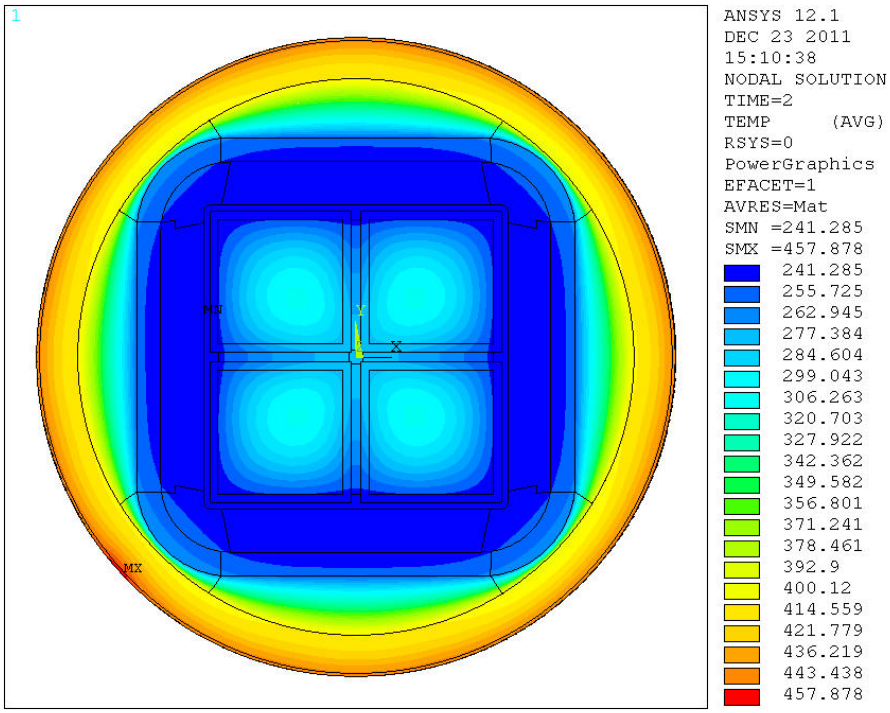

Figure C.112. NIST-04: (at 1.5 hours – ~15 minutes before fire on vehicle #22 – ambient temperature 572°F [300°C])

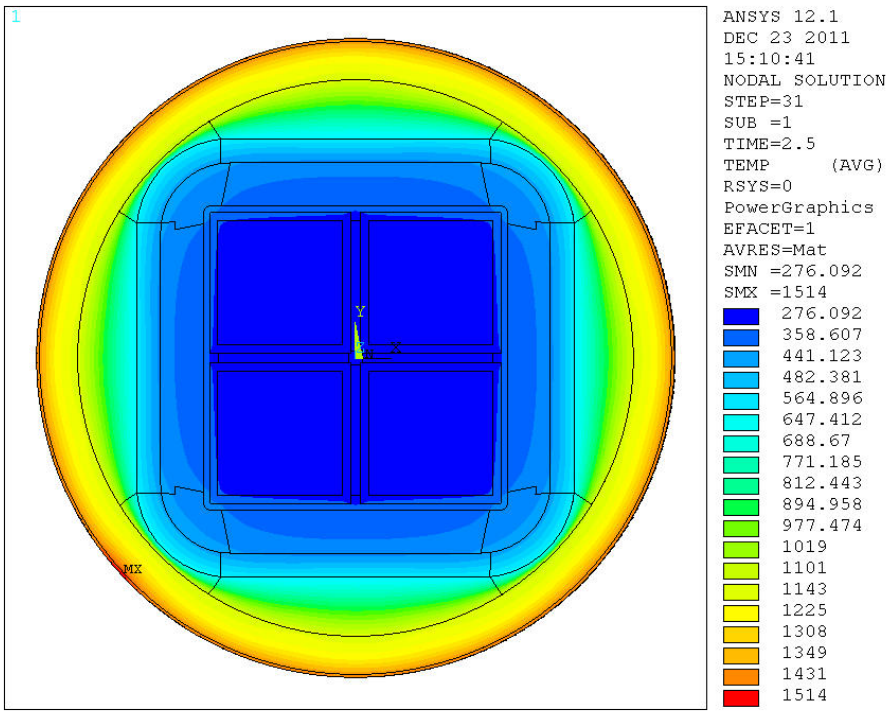

Figure C.113. NIST-04: (at 2 hours – start of fire on vehicle #22 – ambient temperature 1778°F [970°C])

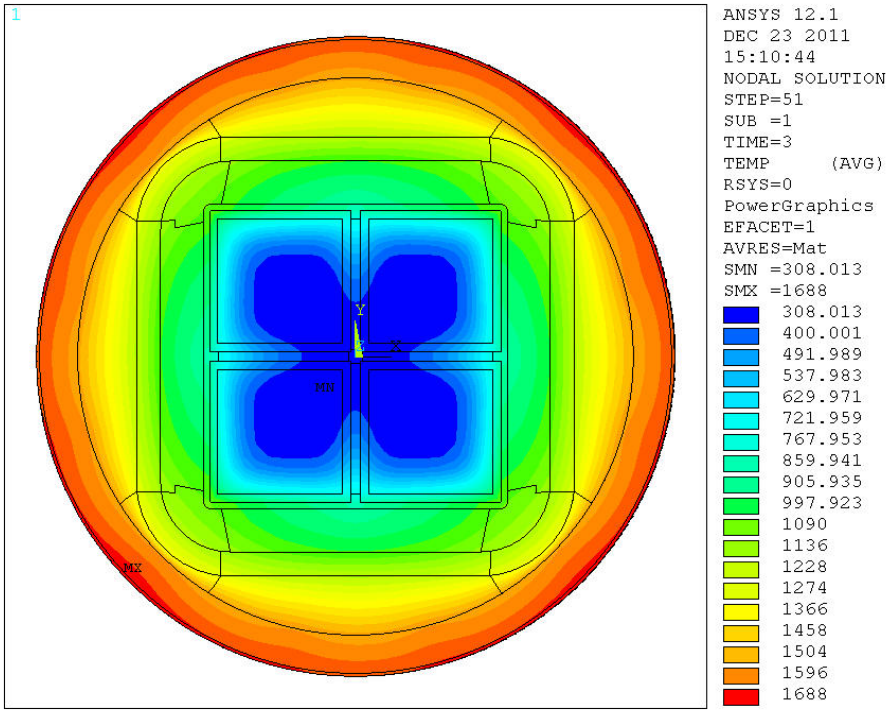

Figure C.114. NIST-04: (at 2.5 hours – ~5minutes before end of fire on vehicle #22 – ambient temperature 1750°F [954°C])

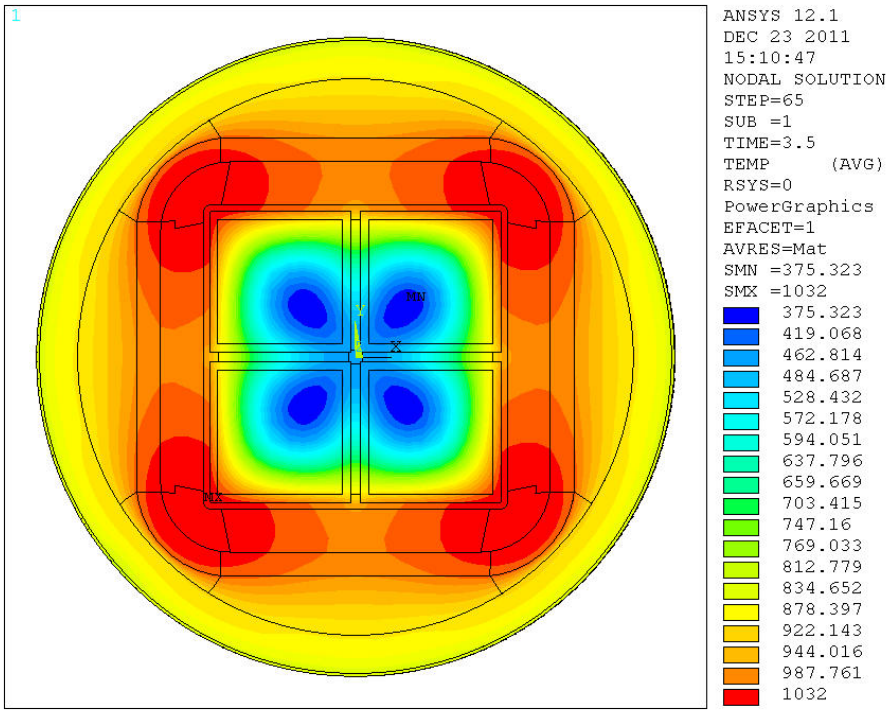

Figure C.115. NIST-04: (at 3 hours – 0.5 hour after end of fire on vehicle #22 – ambient temperature 545°F [285°C])

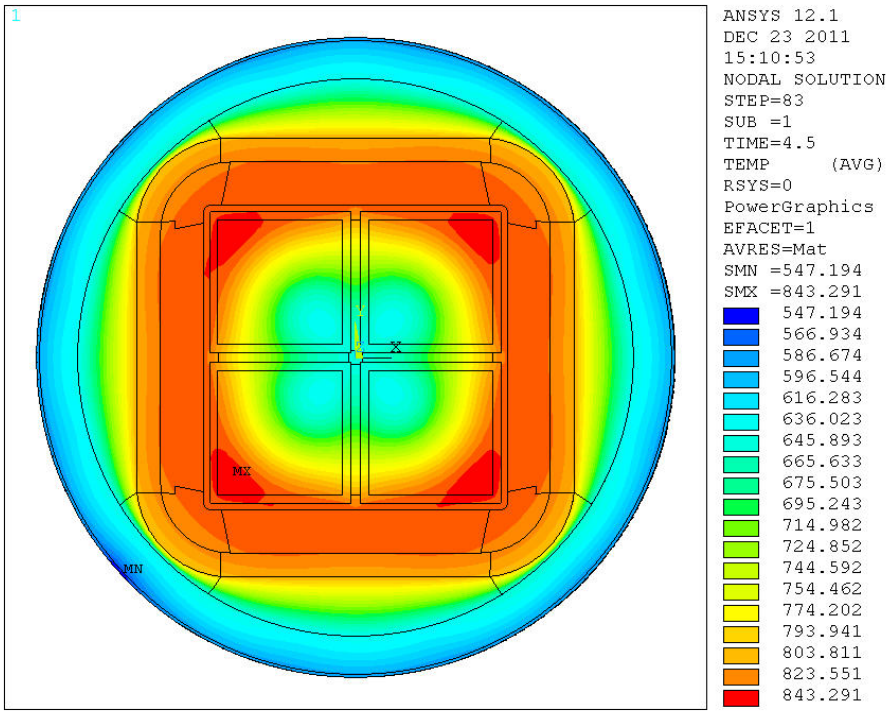

Figure C.116. NIST-04: (at 4 hours – 1.5 hour after end of fire on vehicle #22 – ambient temperature 293°F [145°C])

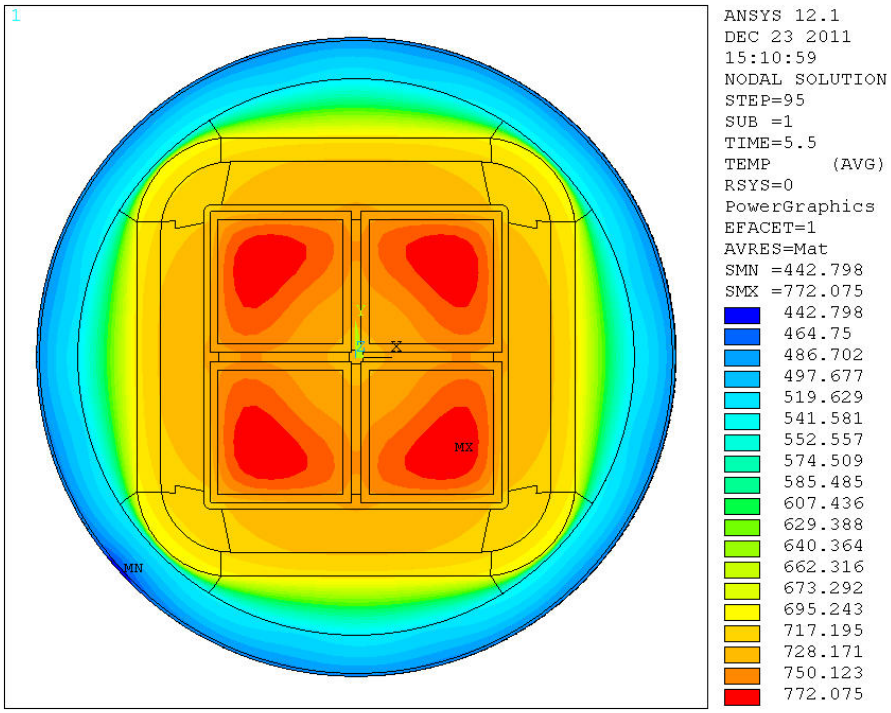

Figure C.117. NIST-04: (at 5 hours – 2.5 hour after end of fire on vehicle #22 – ambient temperature 198°F [92°C])

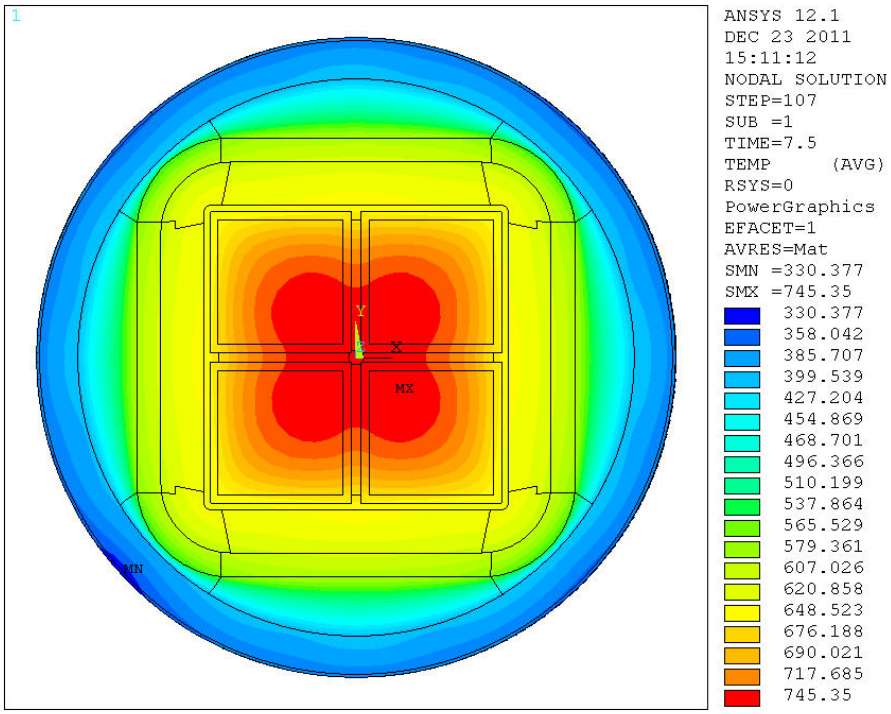

Figure C.118. NIST-04: (at 7 hours – 4.5 hour after end of fire on vehicle #22 – ambient temperature 145°F [63°C])

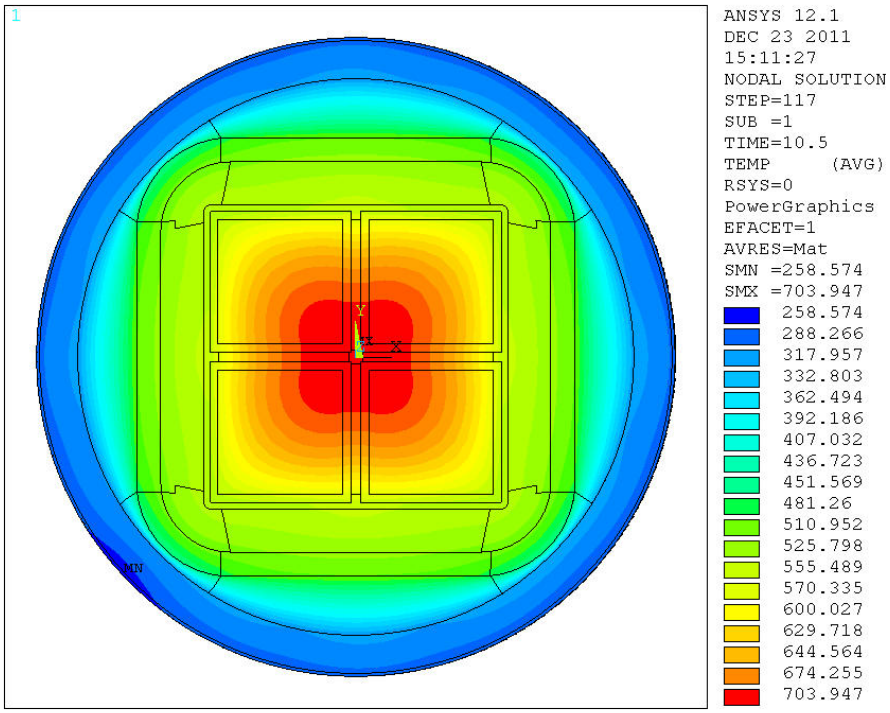

Figure C.119. NIST-04: (at 10 hours – 7.5 hour after end of fire on vehicle #22 – ambient temperature 100°F [38°C])

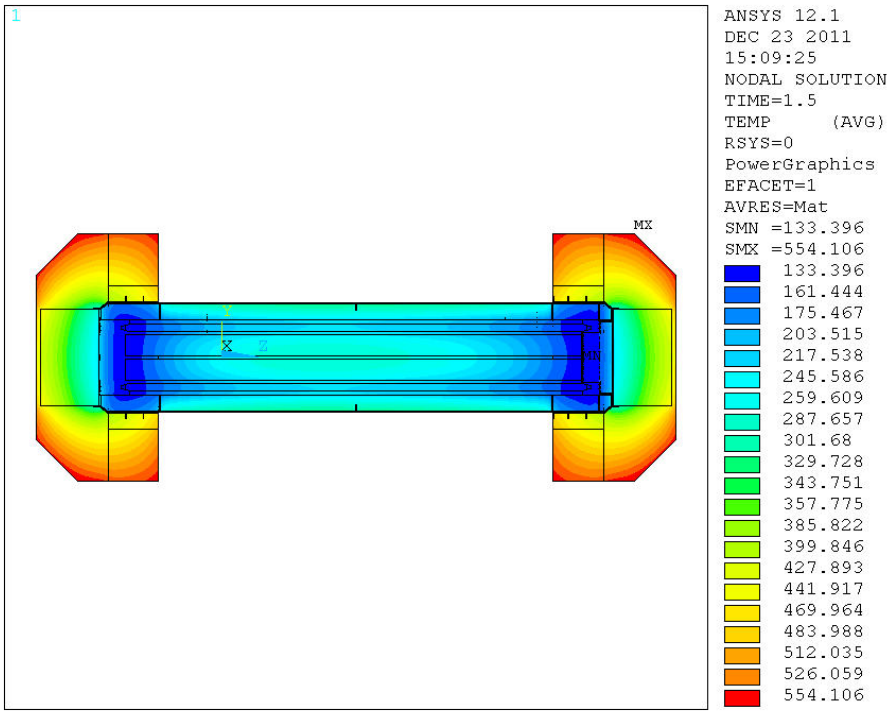

Figure C.120. NIST-04: (at 1 hour – ~1 hour before fire on vehicle #22 – ambient temperature 566°F [297°C])

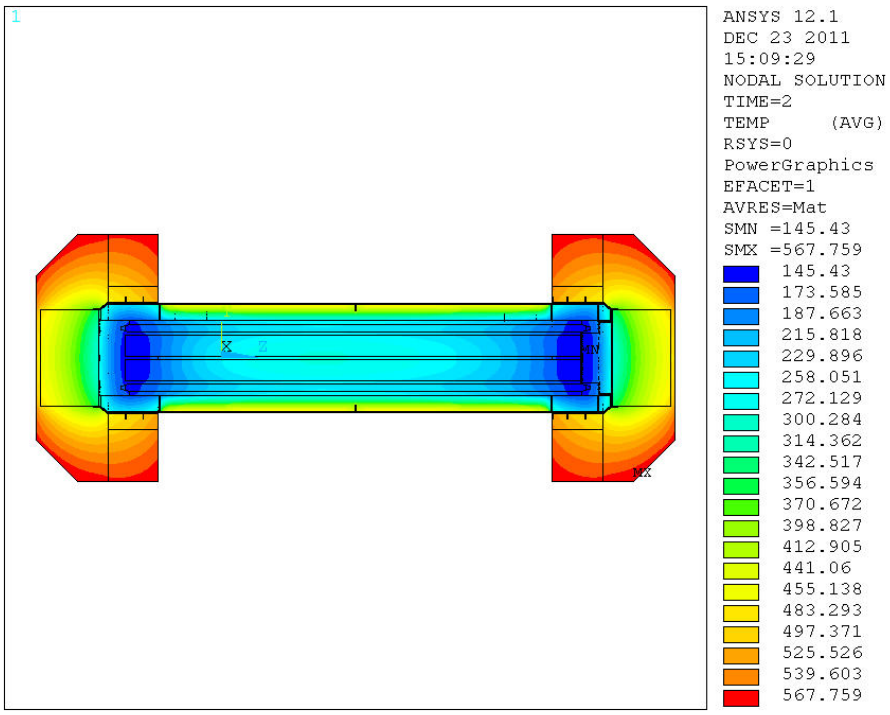

Figure C.121. NIST-04: (at 1.5 hours – ~15 minutes before fire on vehicle #22 – ambient temperature 572°F [300°C])

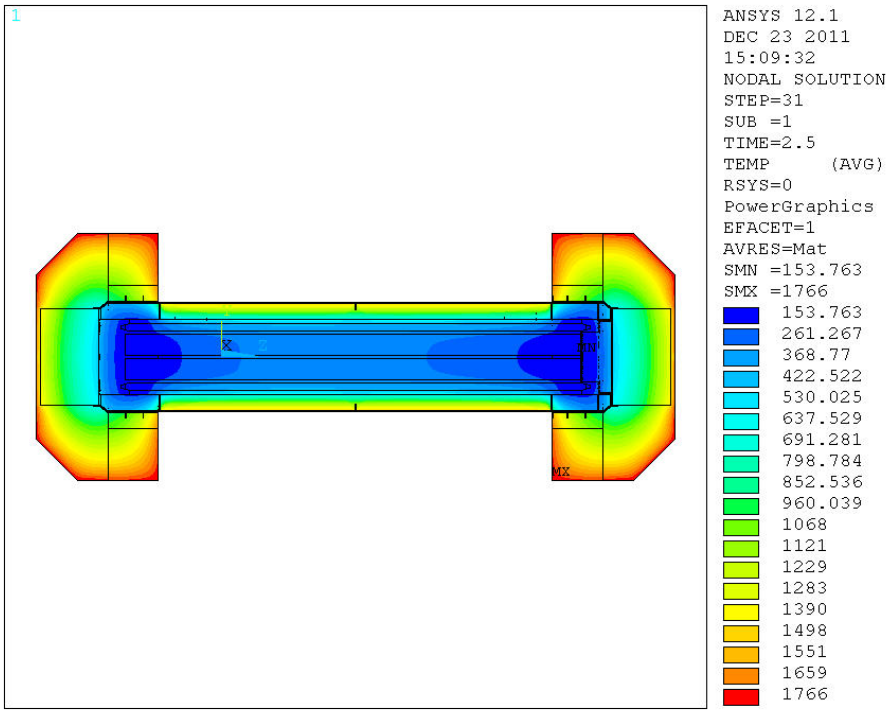

Figure C.122. NIST-04: (at 2 hours – start of fire on vehicle #22 – ambient temperature 1778°F [970°C])

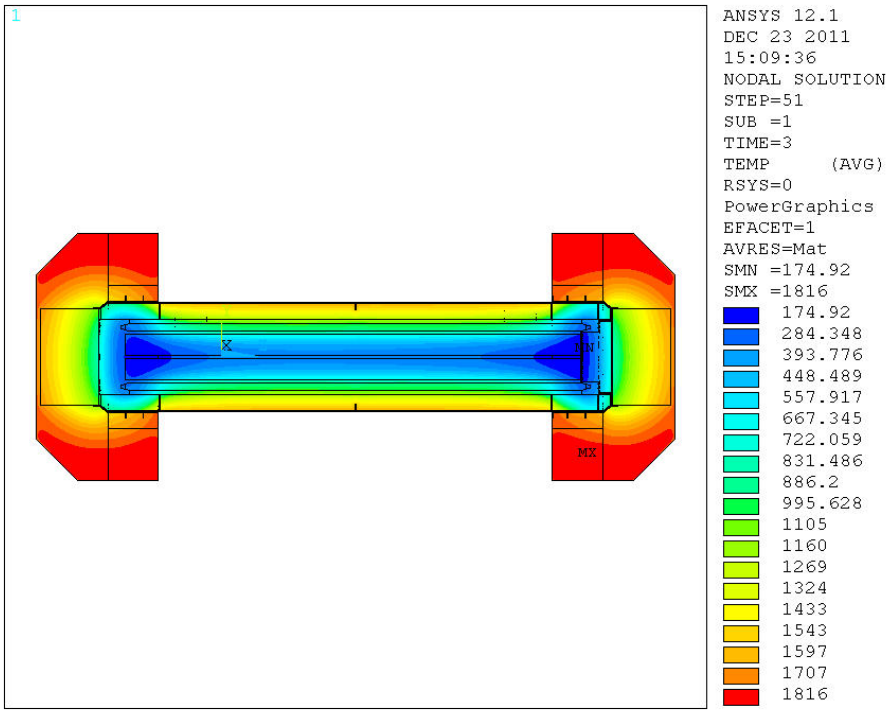

Figure C.123. NIST-04: (at 2.5 hours – ~5minutes before end of fire on vehicle #22 – ambient temperature 1750°F [954°C])

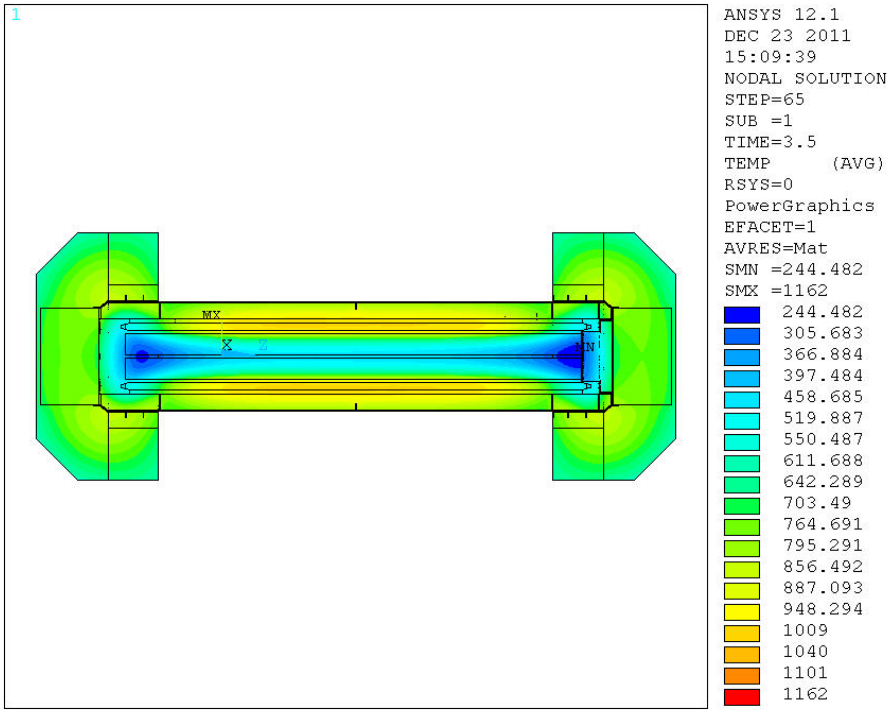

Figure C.124. NIST-04: (at 3 hours – 0.5 hour after end of fire on vehicle #22 – ambient temperature 545°F [285°C])

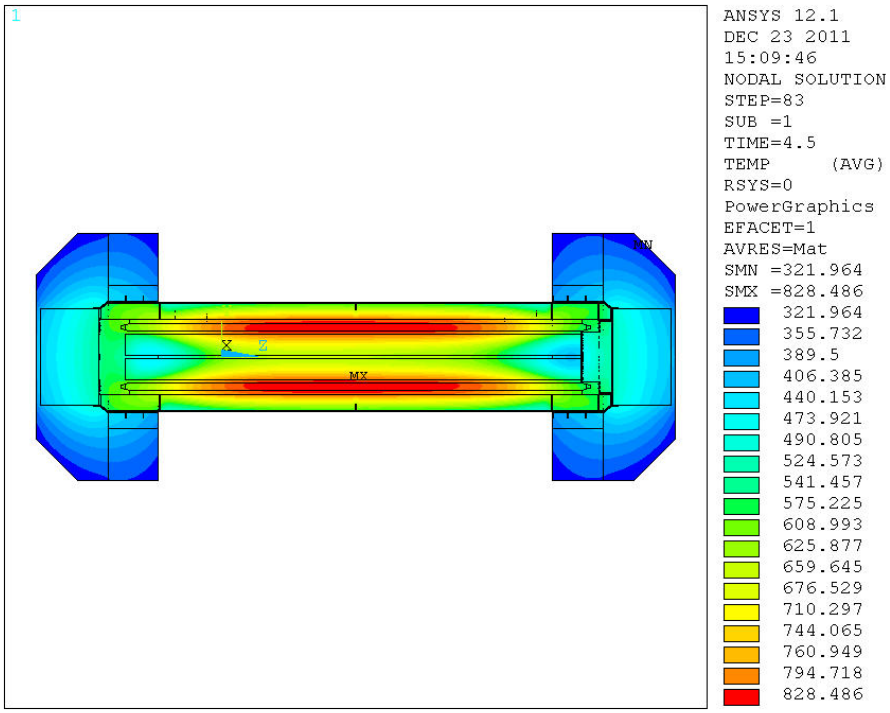

Figure C.125. NIST-04: (at 4 hours – 1.5 hour after end of fire on vehicle #22 – ambient temperature 293°F [145°C])

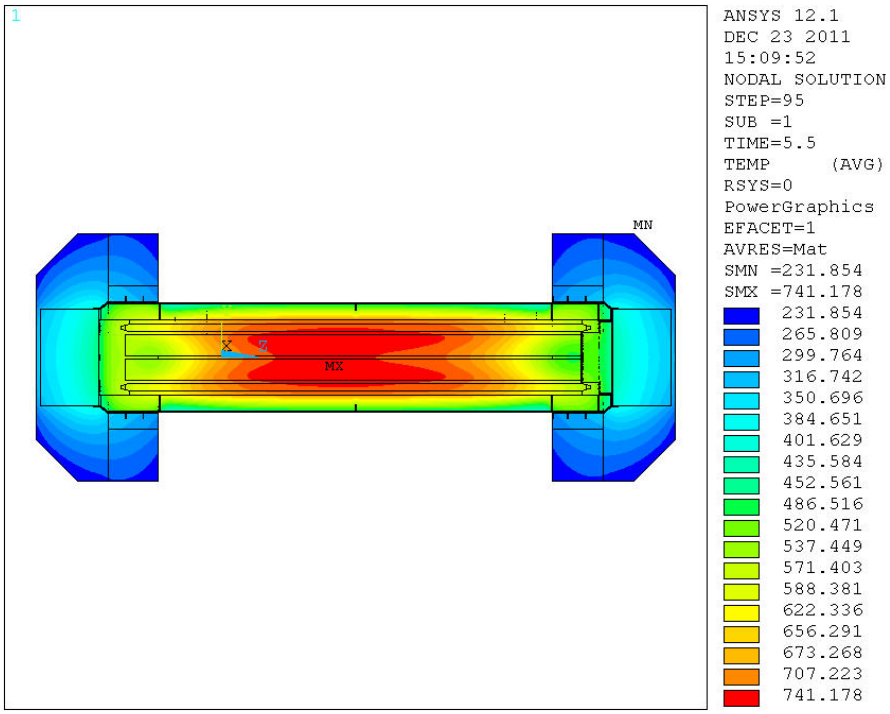

Figure C.126. NIST-04: (at 5 hours – 2.5 hour after end of fire on vehicle #22 – ambient temperature 198°F [92°C])

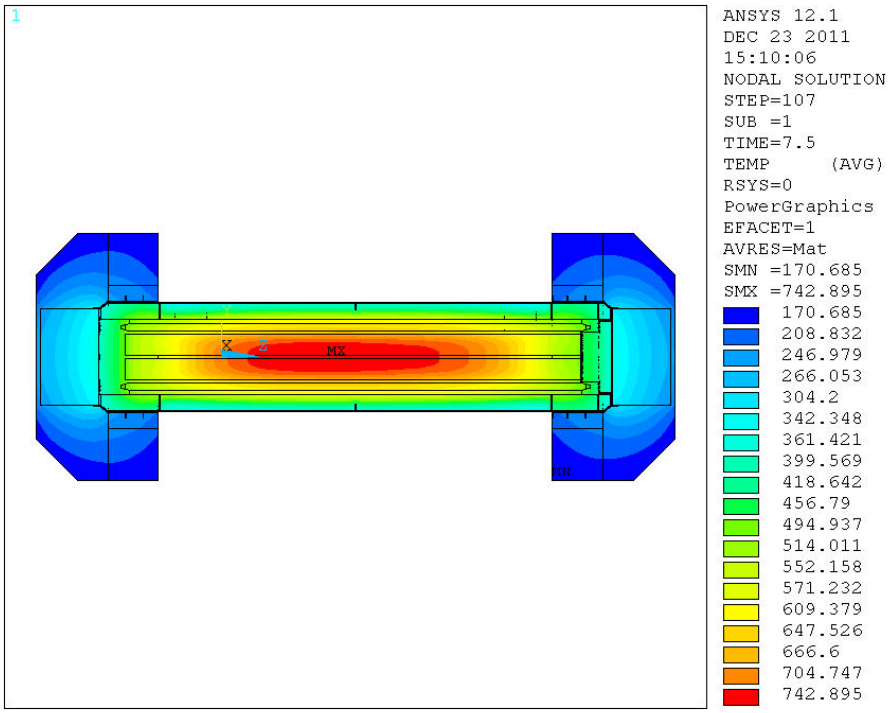

Figure C.127. NIST-04: (at 7 hours – 4.5 hour after end of fire on vehicle #22 – ambient temperature 145°F [63°C])

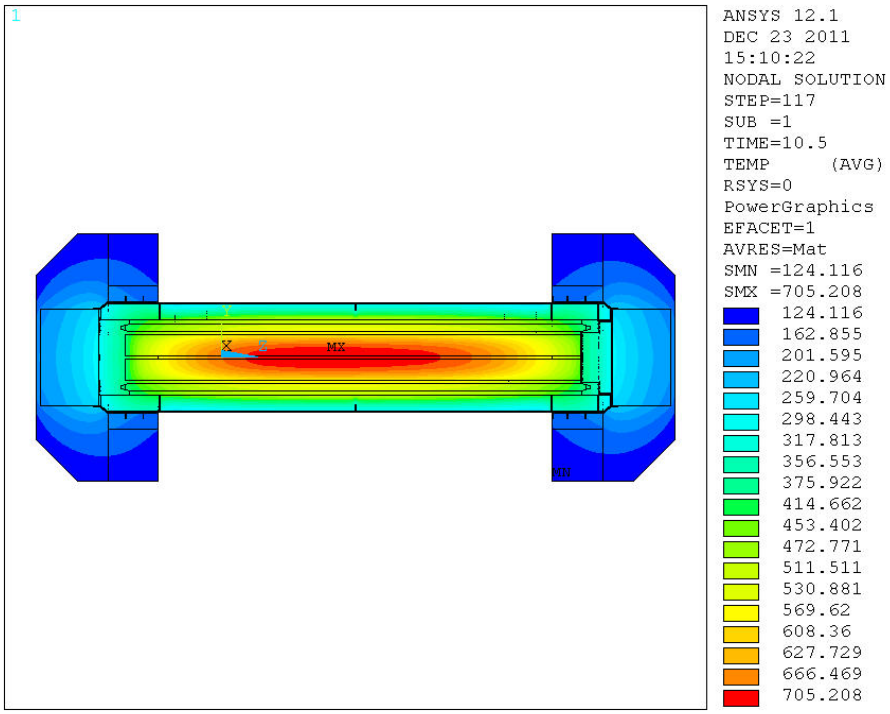

Figure C.128. NIST-04: (at 10 hours – 7.5 hour after end of fire on vehicle #22 – ambient temperature 100°F [38°C])

C.4.2 NIST-04: Package at Longest Fire Location

The longest fire location for this case is on vehicle #31, near the tunnel entrance. The fire on this vehicle begins within 4 hours of the start of the fire scenario, essentially the same lag time at this location as in NIST-01. The ambient temperature at this location rises more gradually than in case NIST-01, due to the shorter duration of the individual vehicle fires over the 5 hours of the transient. It reaches approximately 520°F (271°C) within about 2 hours, then holds fairly steadily near this value until the beginning of the local fire on vehicle #31.

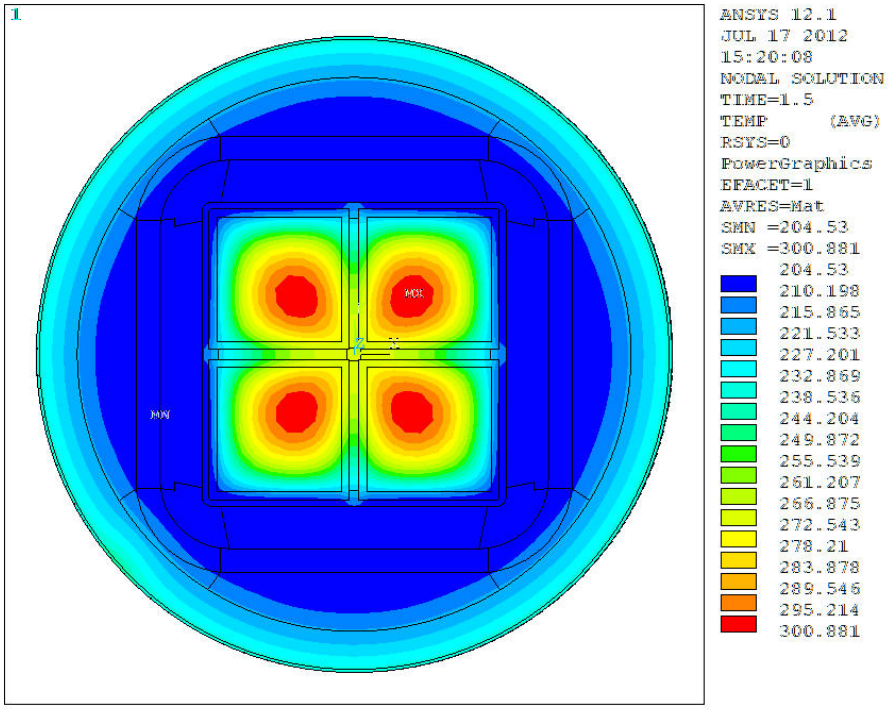

Figure C.129. NIST-04: (at 1 hour – 4 hours before start of fire on vehicle #31 – ambient temperature 392°F [200°C])

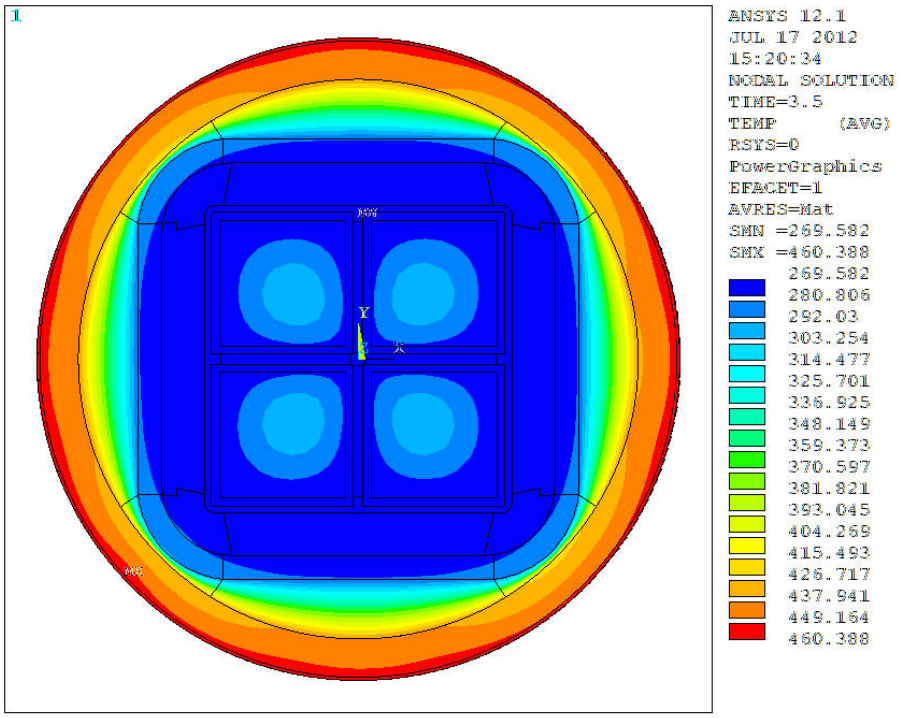

Figure C.130. NIST-04: (at 3 hours – 1 hour before start of fire on vehicle #31 – ambient temperature 518°F [270°C])

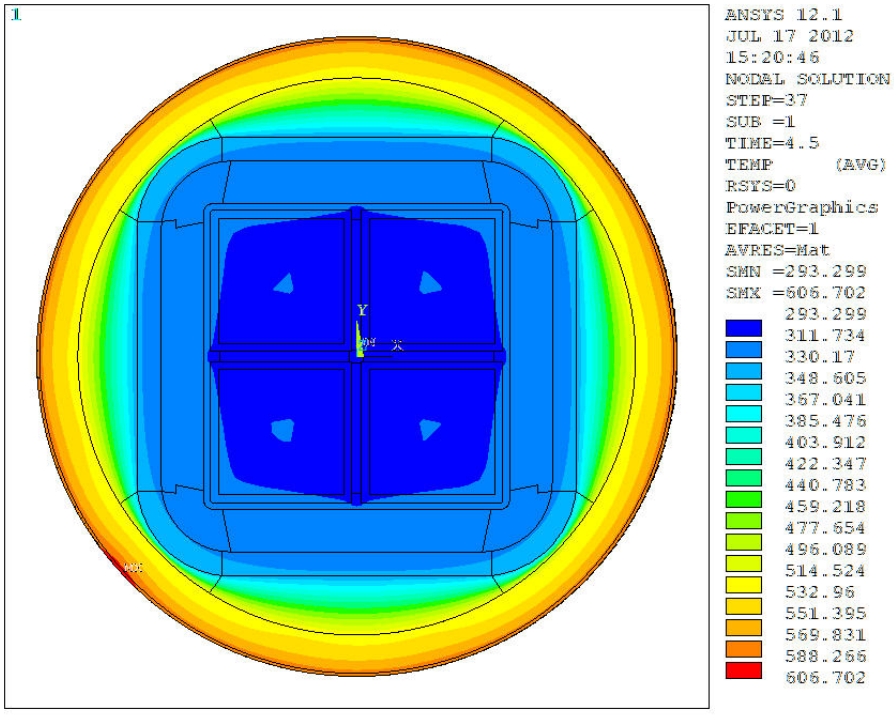

Figure C.131. NIST-04: (at 4 hours – start of fire on vehicle #31 – ambient temperature 761°F [405°C])

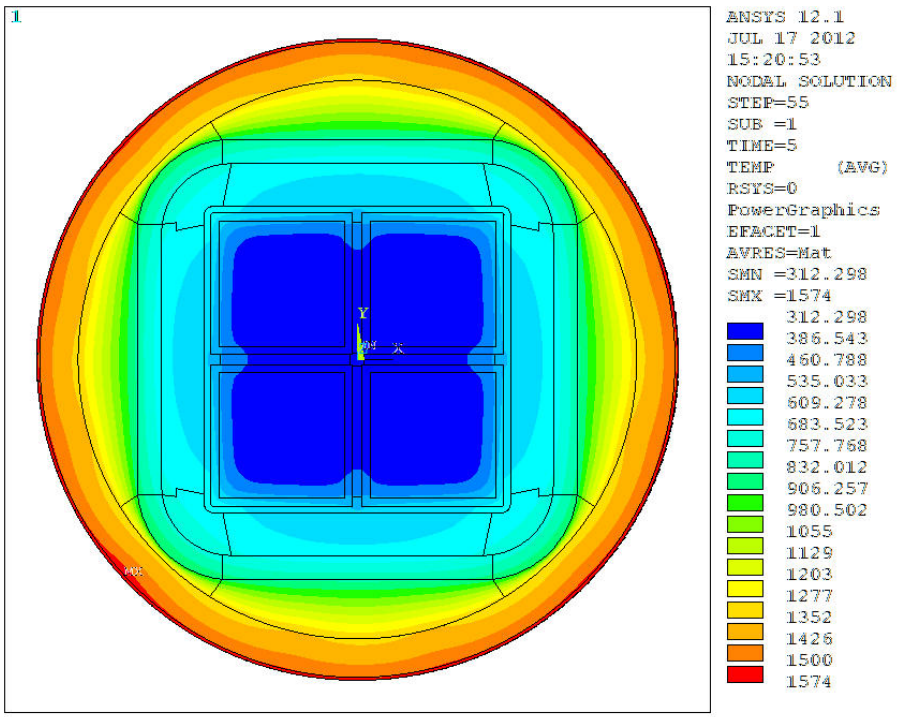

Figure C.132. NIST-04: (at 4.5 hours – 13 minutes before end of fire on vehicle #31 – ambient temperature 1726°F [941°C])

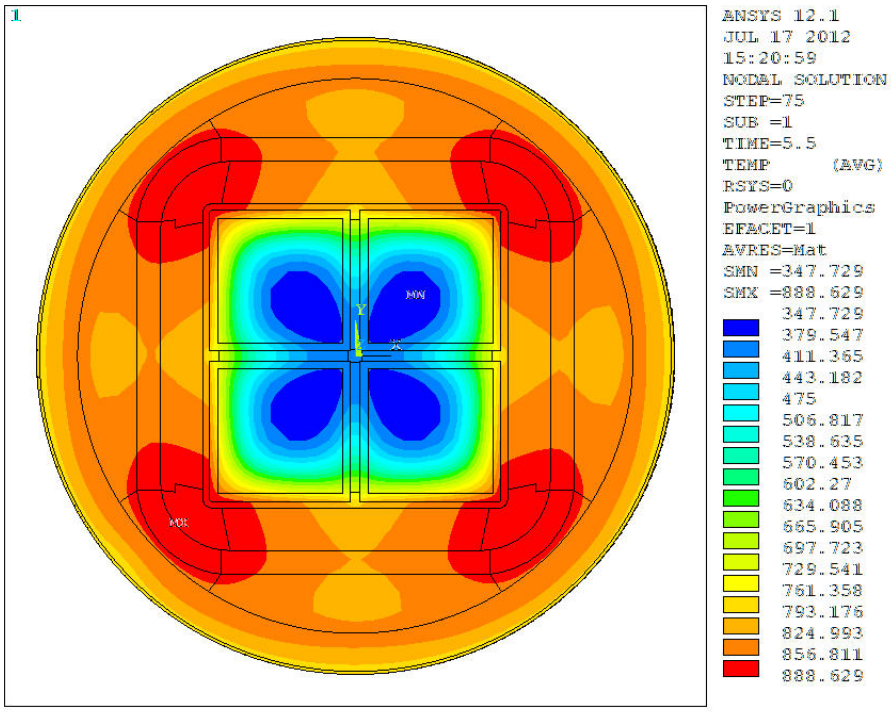

Figure C.133. NIST-04: (at 5 hours – 15 minutes after end of fire on vehicle #31 – ambient temperature 510°F [266°C])

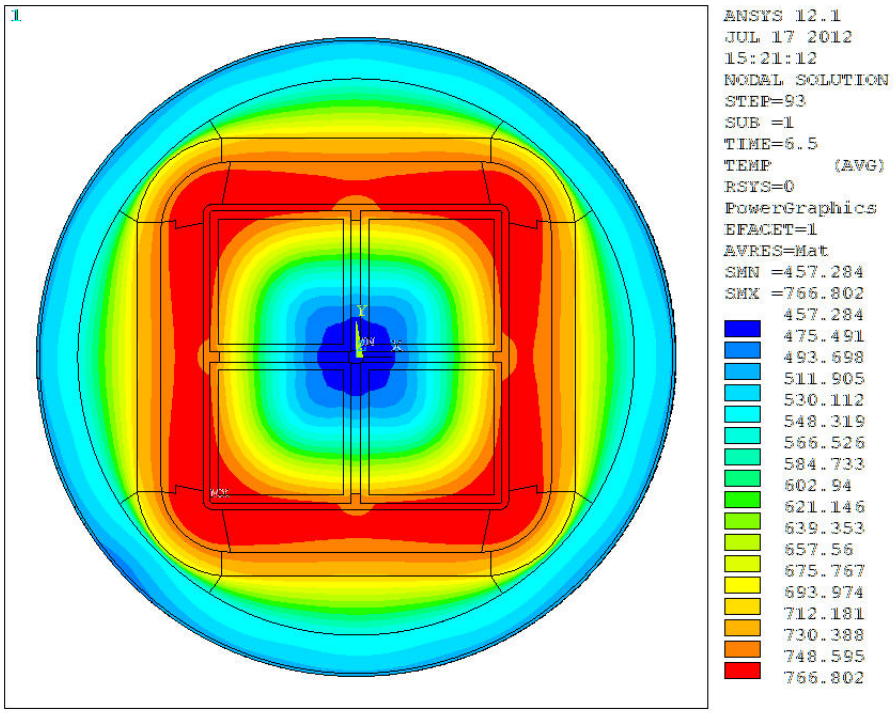

Figure C.134. NIST-04: (at 6 hours – 1.25 hour after end of fire on vehicle #31 – ambient temperature 266°F [130°C])

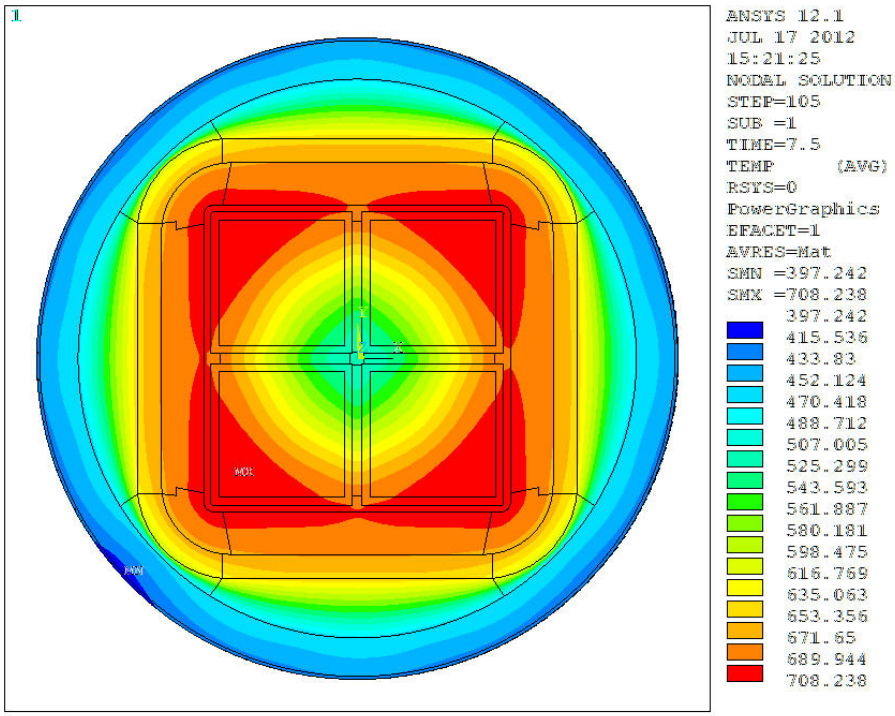

Figure C.135. NIST-04: (at 7 hours – 2.25 hour after end of fire on vehicle #31 – ambient temperature 207°F [97°C])

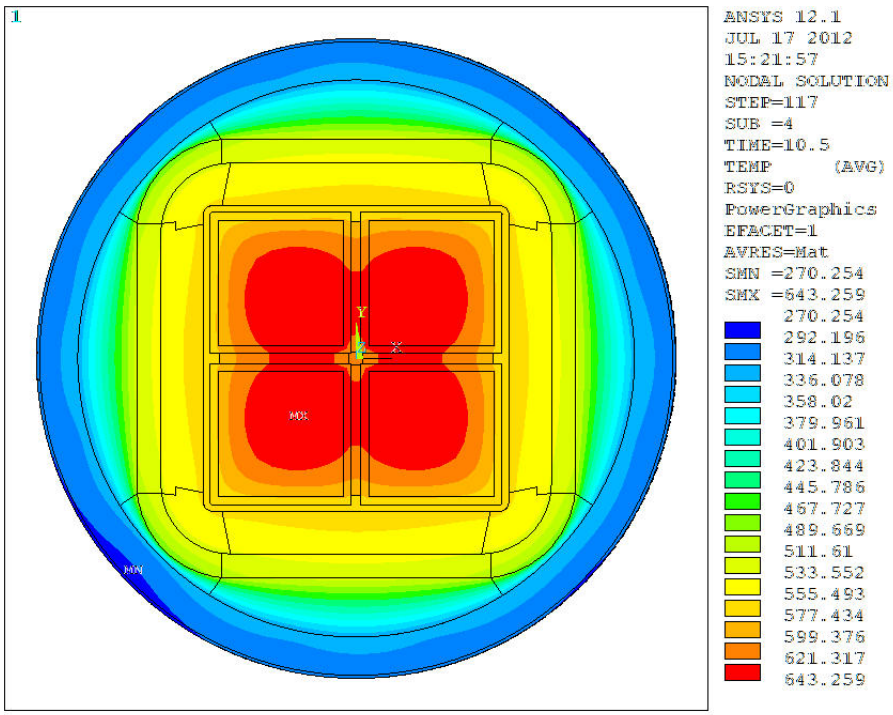

Figure C.136. NIST-04: (at 10 hours – 5.25 hour after end of fire on vehicle #31 – ambient temperature 100°F [38°C])

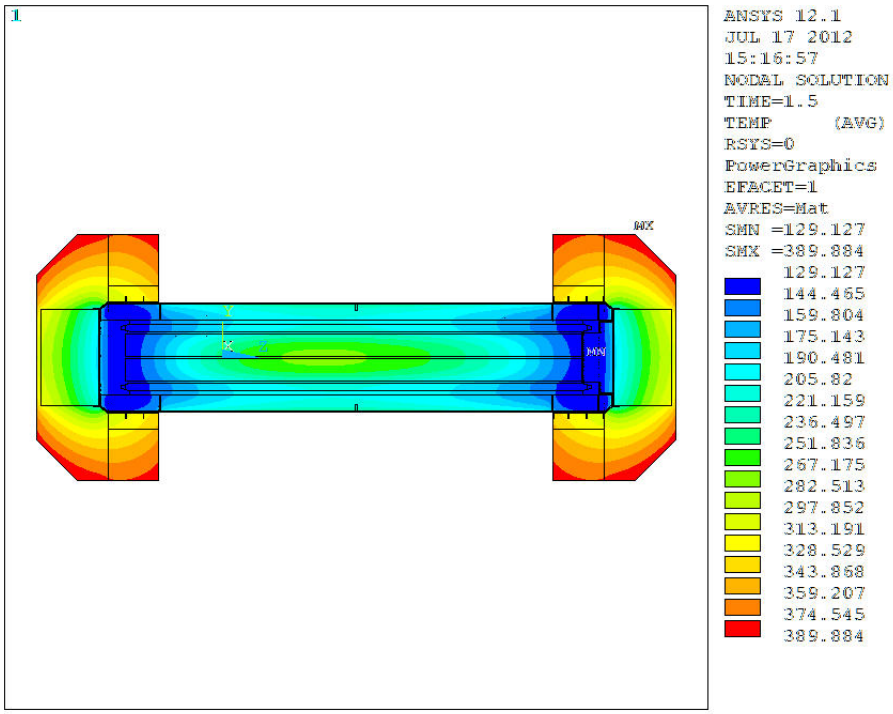

Figure C.137. NIST-04: (at 1 hour – 4 hours before start of fire on vehicle #31 – ambient temperature 392°F [200°C])

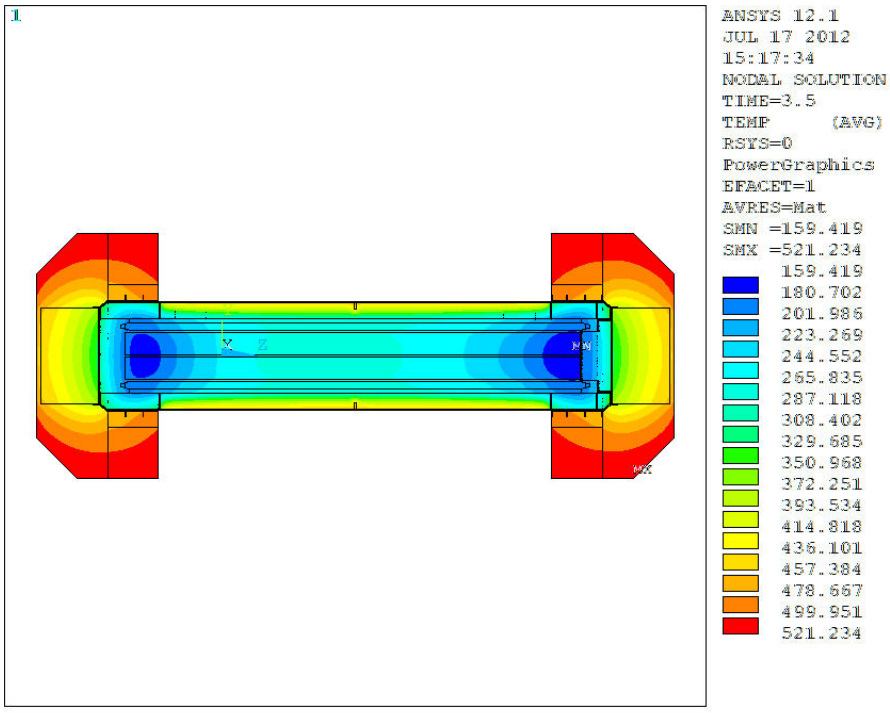

Figure C.138. NIST-04: (at 3 hours – 1 hour before start of fire on vehicle #31 – ambient temperature 518°F [270°C])

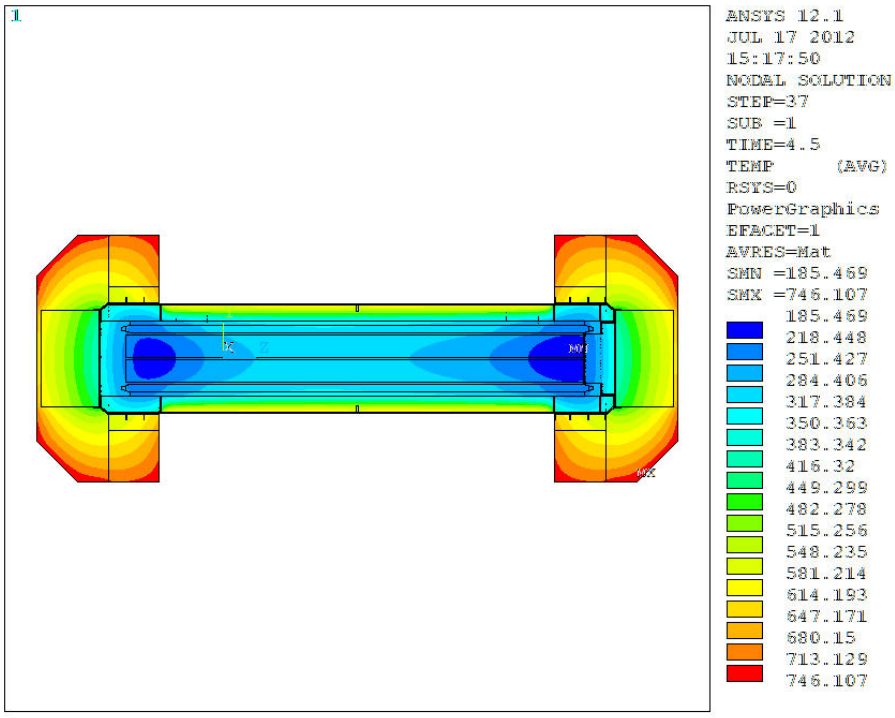

Figure C.139. NIST-04: (at 4 hours – start of fire on vehicle #31 – ambient temperature 761°F [405°C])

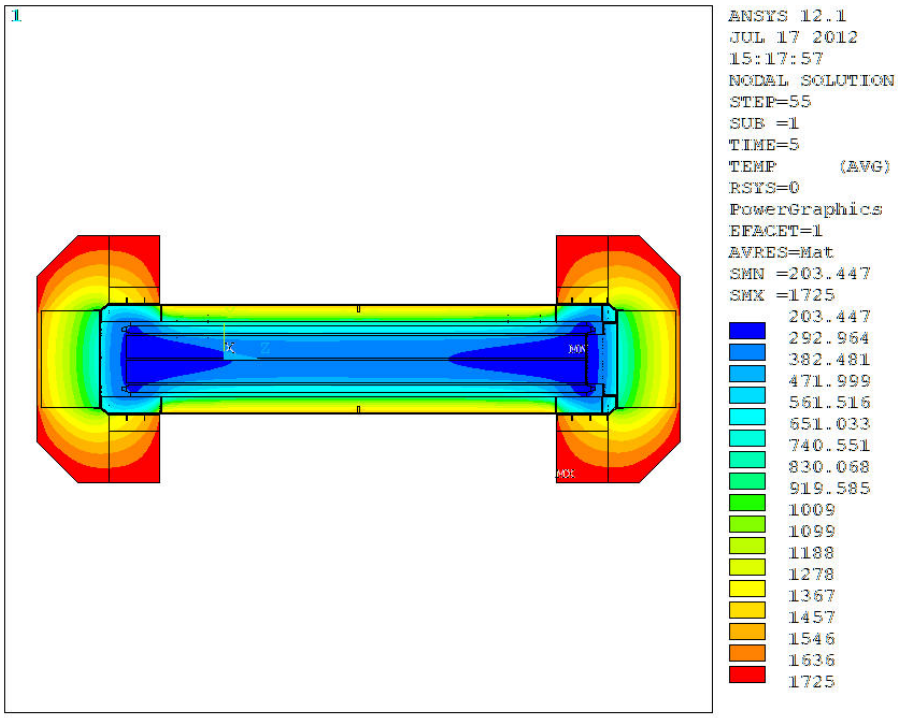

Figure C.140. NIST-04: (at 4.5 hours – 13 minutes before end of fire on vehicle #31 – ambient temperature 1726°F [941°C])

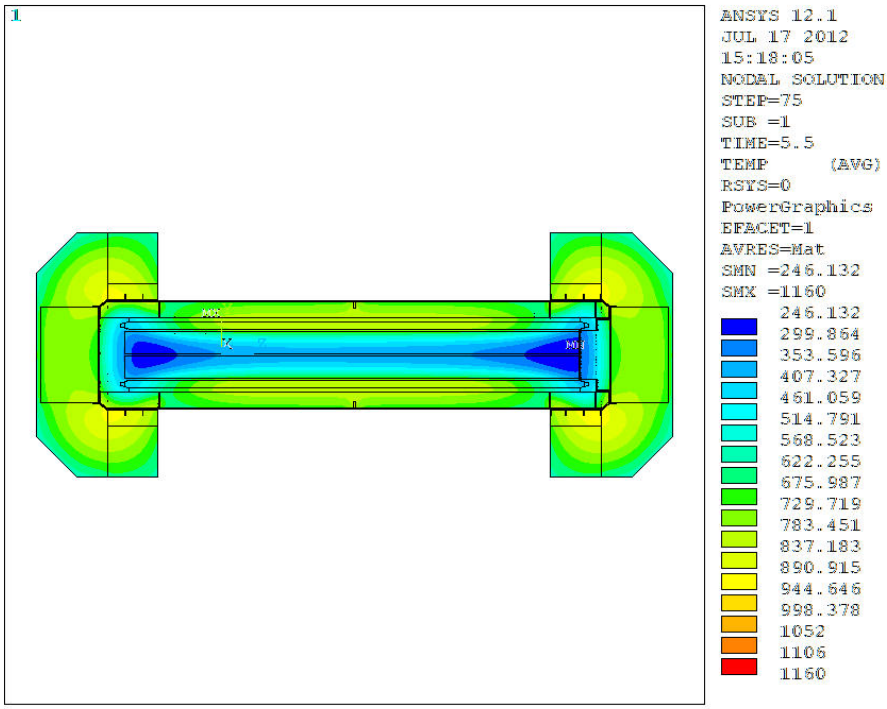

Figure C.141. NIST-04: (at 5 hours – 15 minutes after end of fire on vehicle #31 – ambient temperature 510°F [266°C])

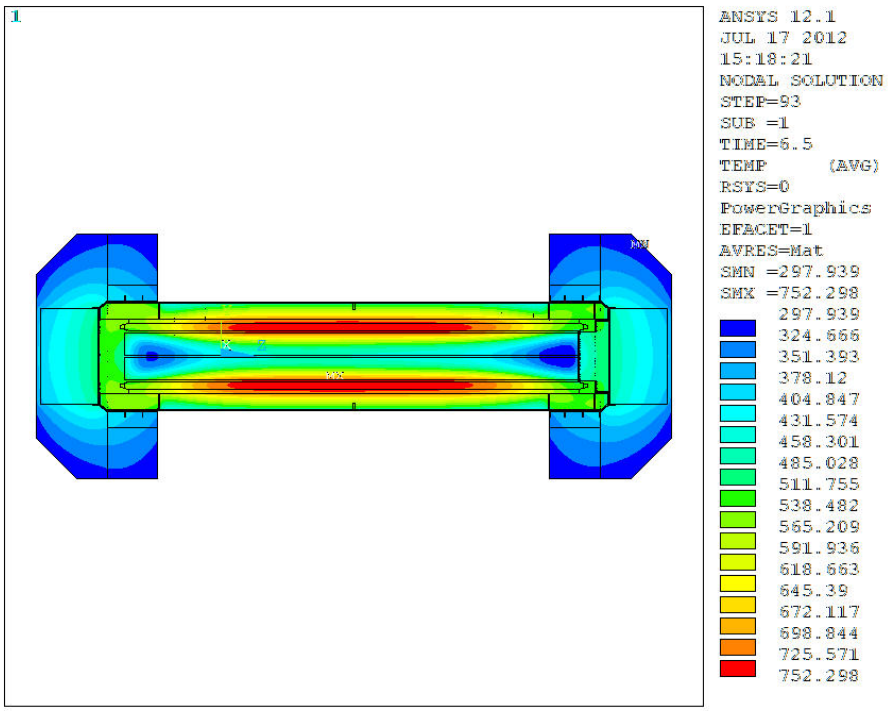

Figure C.142. NIST-04: (at 6 hours – 1.25 hour after end of fire on vehicle #31 – ambient temperature 266°F [130°C])

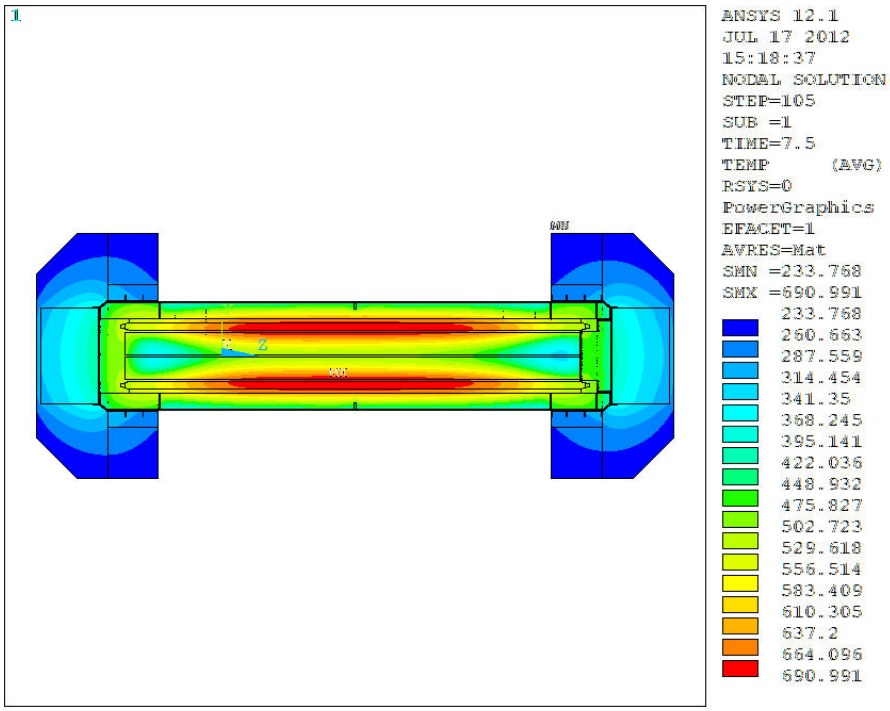

Figure C.143. NIST-04: (at 7 hours – 2.25 hour after end of fire on vehicle #31 – ambient temperature 207°F [97°C])

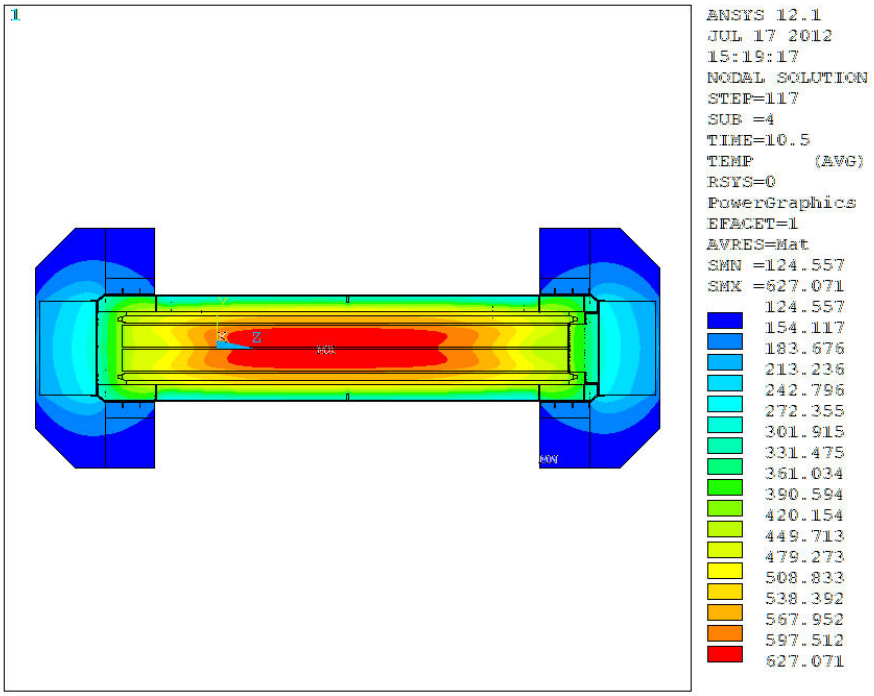

Figure C.144. NIST-04: (at 10 hours – 5.25 hour after end of fire on vehicle #31 – ambient temperature 100°F [38°C])

C.5 Conditions at Beginning of Local Vehicle Fires

This section shows comparisons of the package temperatures at the beginning of the local vehicle fire for the hottest fire location and longest fire location for cases NIST-01 through NIST-04. The range of assumed fire spread rates for cases NIST-01 through NIST-04 results in different durations of preheating for the package in the two locations. For the hottest fire location, near the center of the tunnel, the preheat period ranges from about 1.8 hours (for NIST-01 and -04), to 48 minutes (for NIST-02), to 30 minutes (for NIST-03). For the longest fire location, near the tunnel entrance, the preheat period ranges from about 4 hours (for NIST-01 and -04), to 2 hours (for NIST-02), to 1 hour (for NIST-03).

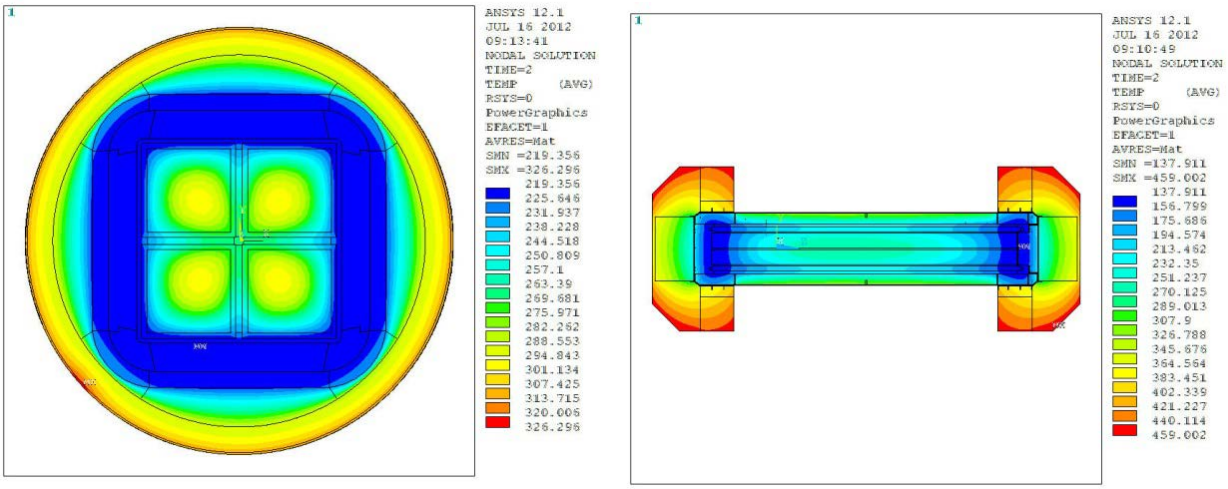

(NIST-01 [hottest fire location] at 1.5 hours – ~15 minutes before fire on vehicle #23 – ambient temperature ~465°F [241°C])

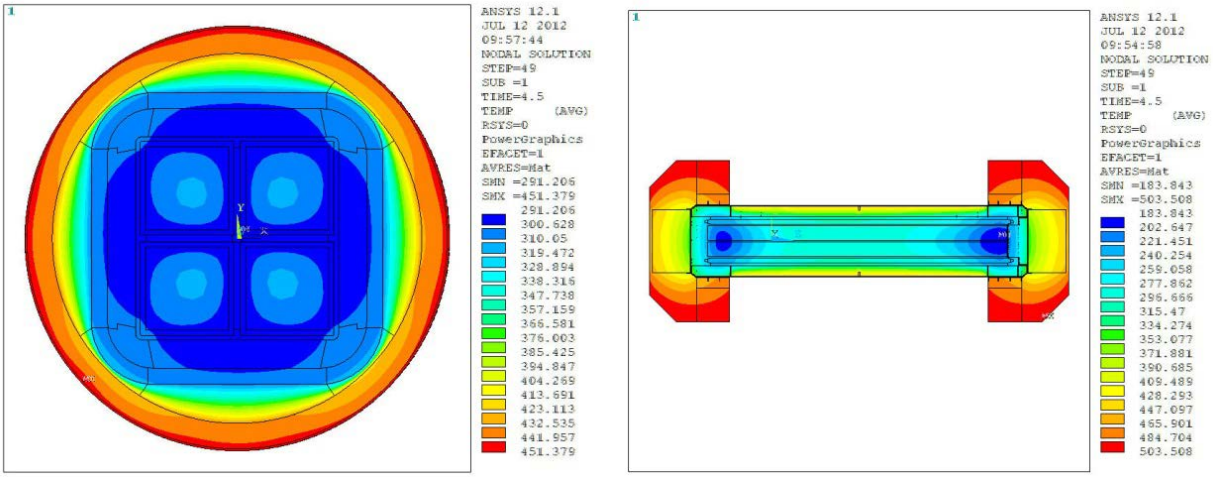

(NIST-01 [longest fire location) at 4 hours – just before beginning of fire on vehicle #31 – ambient temperature 500°F [260°C])

Figure C.145. ANSYS Model: Effect of Preheat Before Local Vehicle Fire at Hottest Fire Location and Longest Fire Location for Case NIST-01

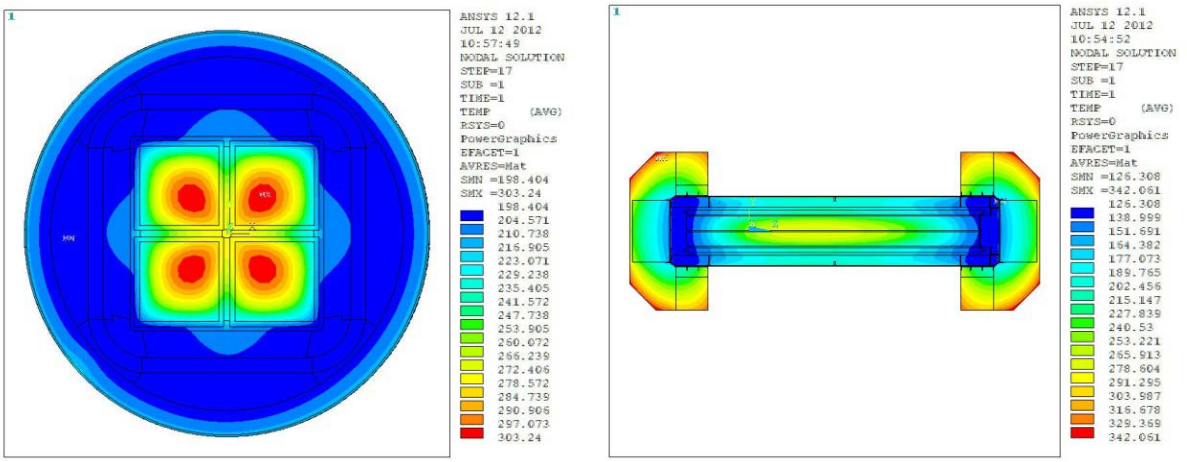

(NIST-02 [hottest fire location] at 30 minutes – 18 minutes before beginning of fire on vehicle #23 – ambient temperature 370°F [188°C])

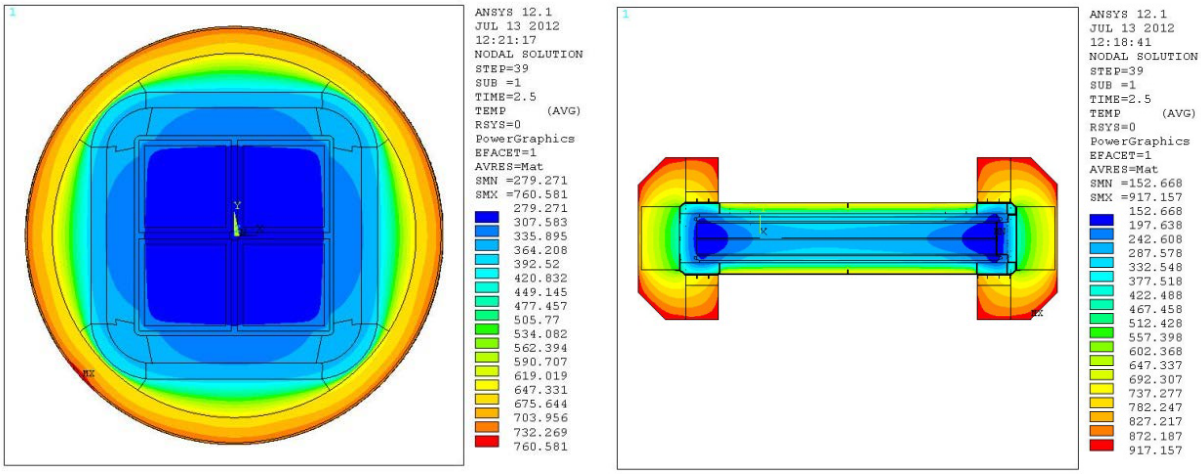

(NIST-02 [longest fire location) at 2 hours – beginning of fire on vehicle #31 – ambient temperature 932°F 500°C])

Figure C.146. ANSYS Model: Effect of Preheat before Local Vehicle Fire at Hottest Fire Location and Longest Fire Location for Case NIST-02

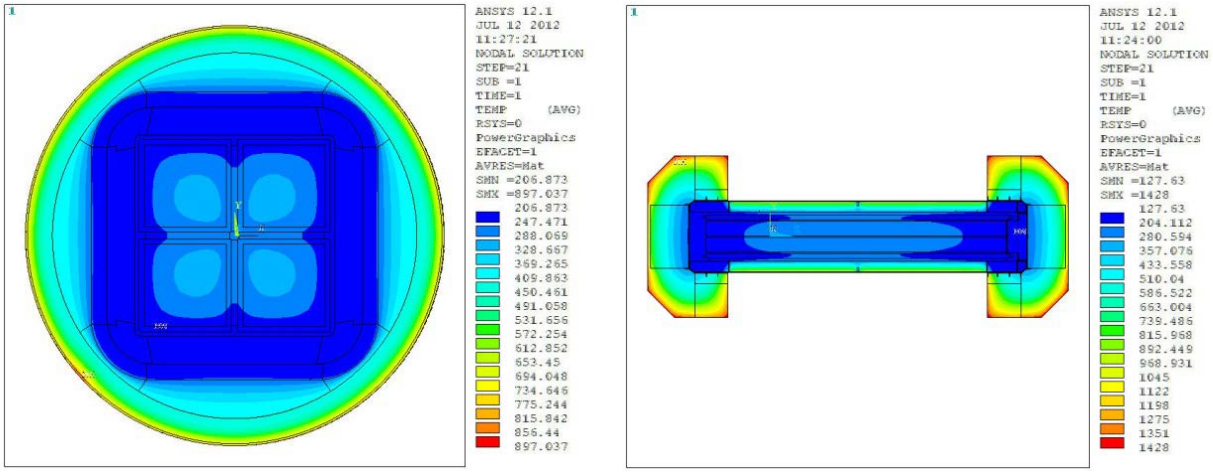

(NIST-03 [hottest fire location] at 30 minutes – start of fire on vehicle #22 – ambient temperature 1490°F [810°C])

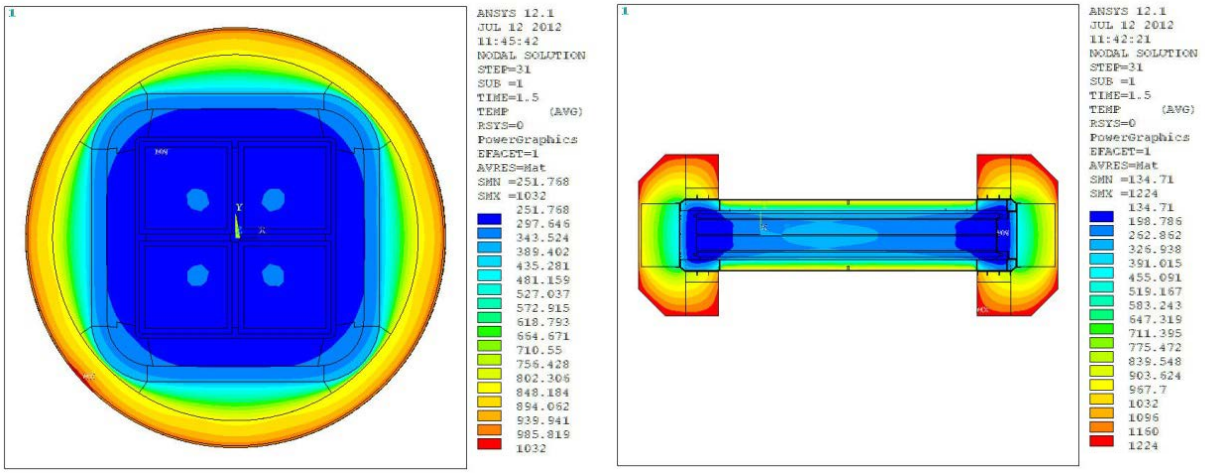

(NIST-03 [longest fire location] at 1 hour – estimated start of fire on vehicle #31 – ambient temperature 1231°F [666°C])

Figure C.147. ANSYS Model: Effect of Preheat before Local Vehicle Fire at Hottest Fire Location and Longest Fire Location for Case NIST-03

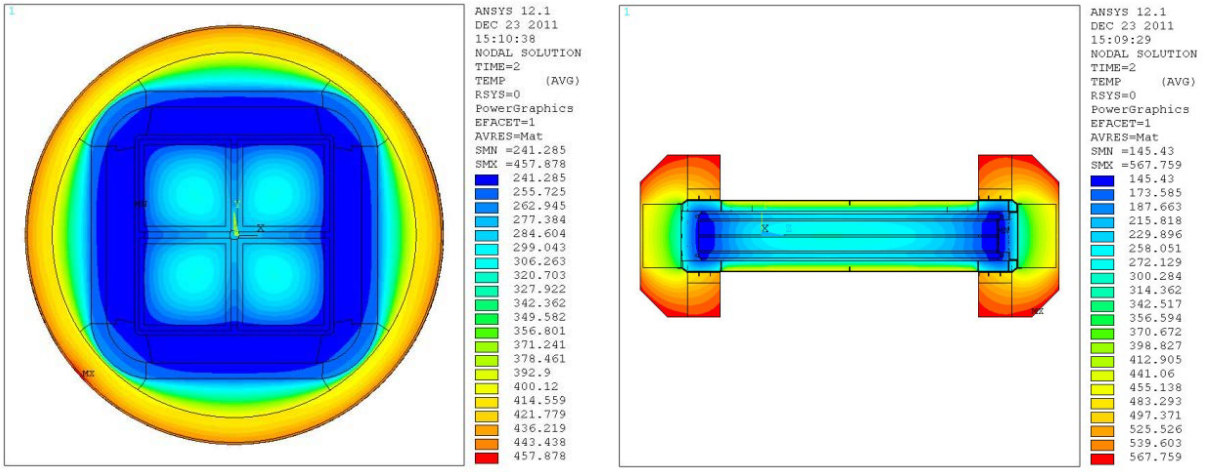

(NIST-04 [hottest fire location] at 1.5 hours – ~15 minutes before fire on vehicle #22 – ambient temperature 572°F [300°C])

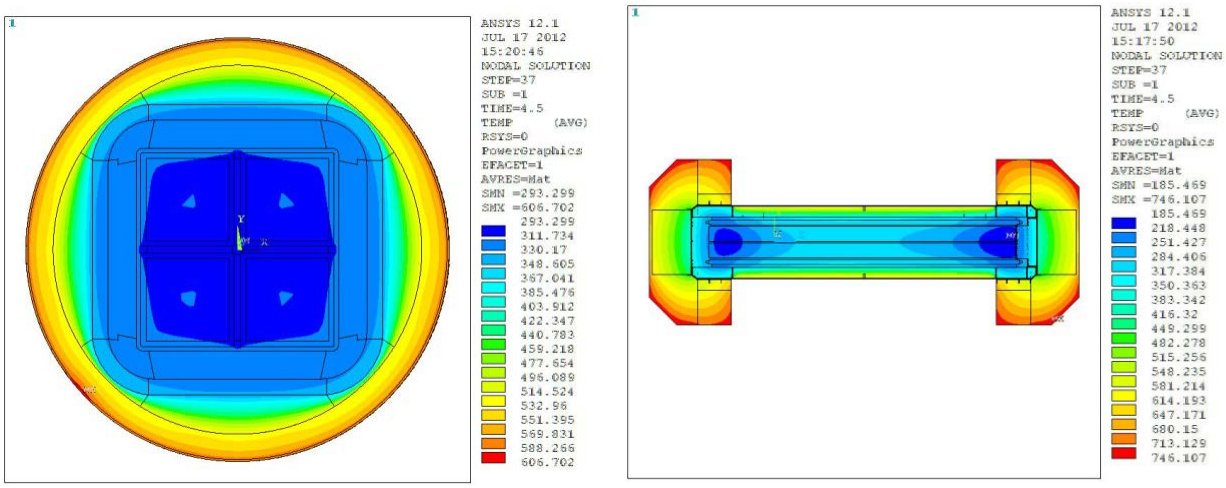

(NIST-04 [longest fire location) at 4 hours – start of fire on vehicle #31 – ambient temperature 761°F [405°C])

Figure C.148. ANSYS Model: Effect of Preheat before Local Vehicle Fire at Hottest Fire Location and Longest Fire Location for Case NIST-04

C.6 NIST-06

The fire conditions predicted with FDS for NIST-06 are determined for the same spread rate as assumed for the base case (NIST-01), resulting in a total fire duration of about 4.6 hours, only slightly shorter in total length than in NIST-01. In the case of NIST-06, the fuel available for the fire is estimated from (somewhat limited) available information on the actual cargo load for each vehicle, rather than the assumed typical cargo load for each vehicle used in all other cases. The assumed burn rate is the same as in the base case, but because of the variation in fuel available for each vehicle, the local fire duration on each vehicle varies significantly. Most of the individual vehicle fires last ~30 minutes or less (particularly for vehicles running empty or with a mainly non-combustible load); three last as long as 45 minutes, and two exceed an hour in length.

C.6.1 NIST-06: Package at Hottest Fire Location

The hottest fire location for this case is on vehicle #26, which was assigned one of the largest fuel loads[2] and is located near the center of the tunnel. The fire on this vehicle begins at approximately 2.5 hours into the fire scenario and lasts about 68 minutes. The longest fire location is defined to be on vehicle #30, carrying baked goods, since vehicle #31 is empty and has a very short fire with relatively low peak temperature, in this case. The fire on vehicle #30 is 42 minutes long. Figure C.149 shows the engulfing fire boundary temperatures assumed for the two selected fire locations.

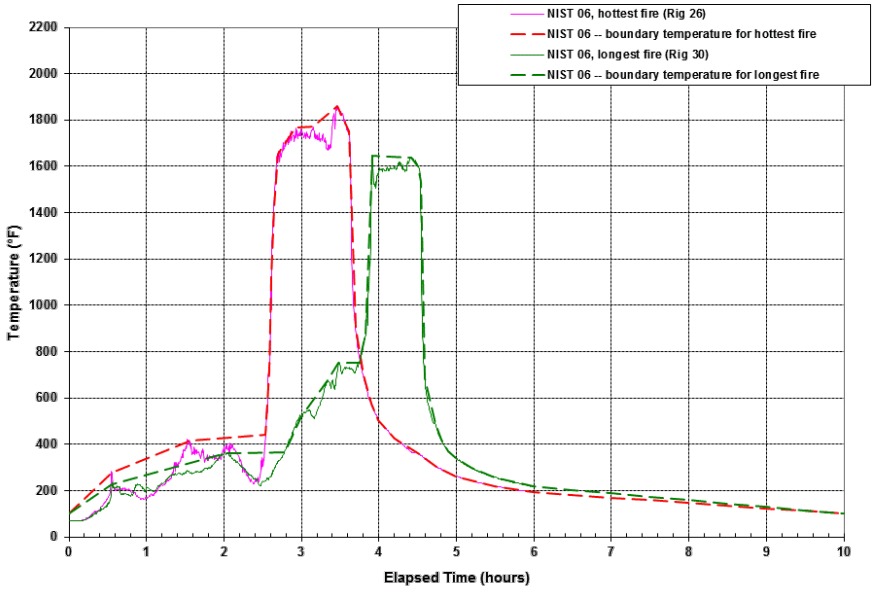

Figure C.149. Boundary Temperatures for Hottest Fire and Longest Fire Locations for Case NIST-06

[2] Vehicle #26 was running empty, but for modeling convenience, was assigned the cargo load from vehicle #25, consisting of 20,000 lb of coffee. Section 3 (and Table 3.3) for a complete description of the fuel load assigned to each vehicle in case NIST-06.

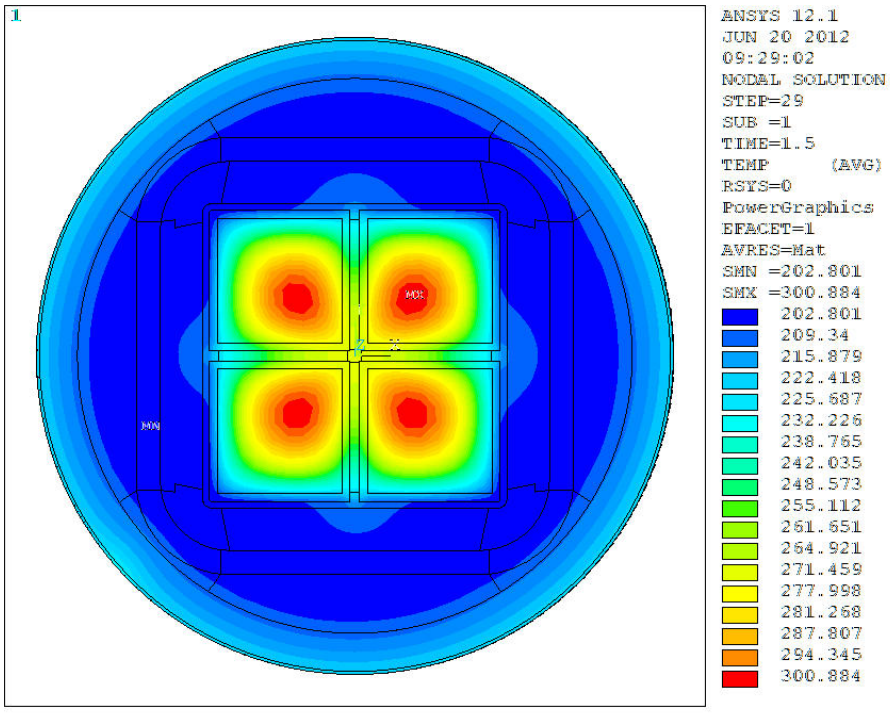

Figure C.150. NIST-06: (at 1 hour – 1.5 hours before start of fire on vehicle #26 – ambient temperature 338°F [798°C])

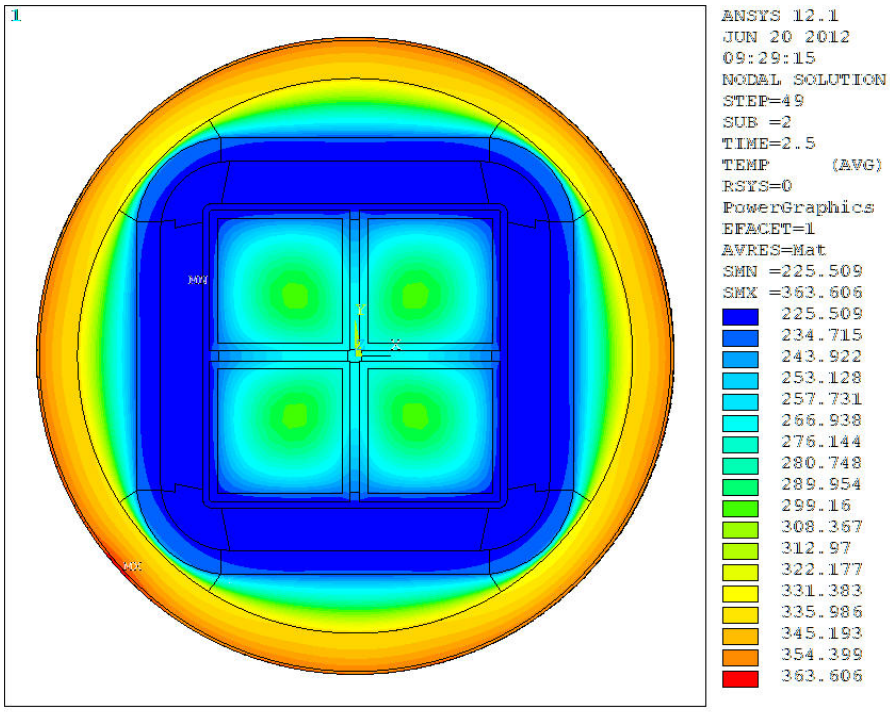

Figure C.151. NIST-06: (at 2 hours – ~30 minutes before start of fire on vehicle #26 – ambient temperature 428°F [220°C])

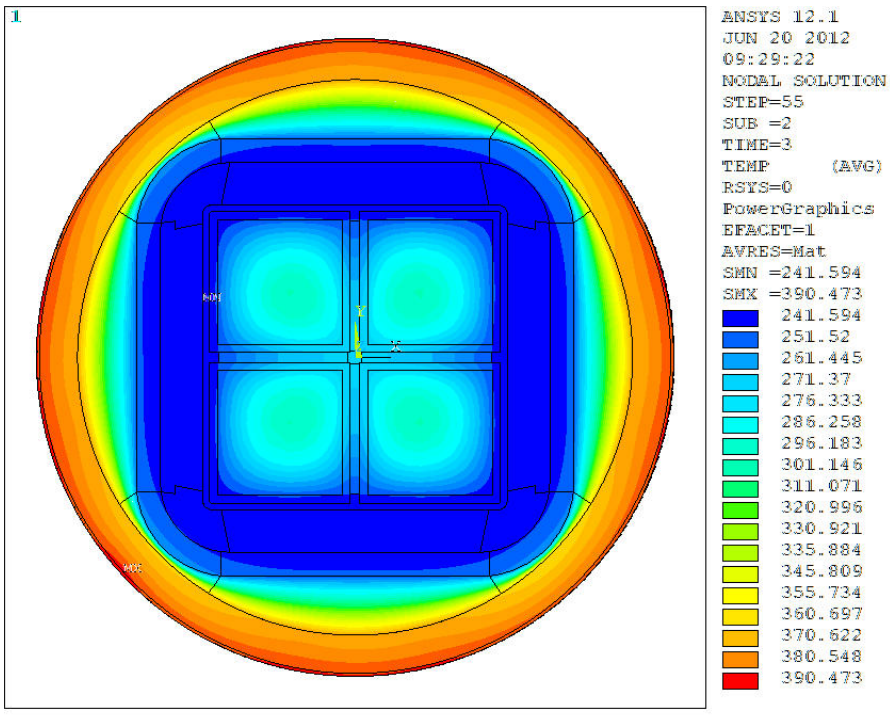

Figure C.152. NIST-06: (at 2.5 hours – start of fire on vehicle #26 – ambient temperature 440°F [227°C])

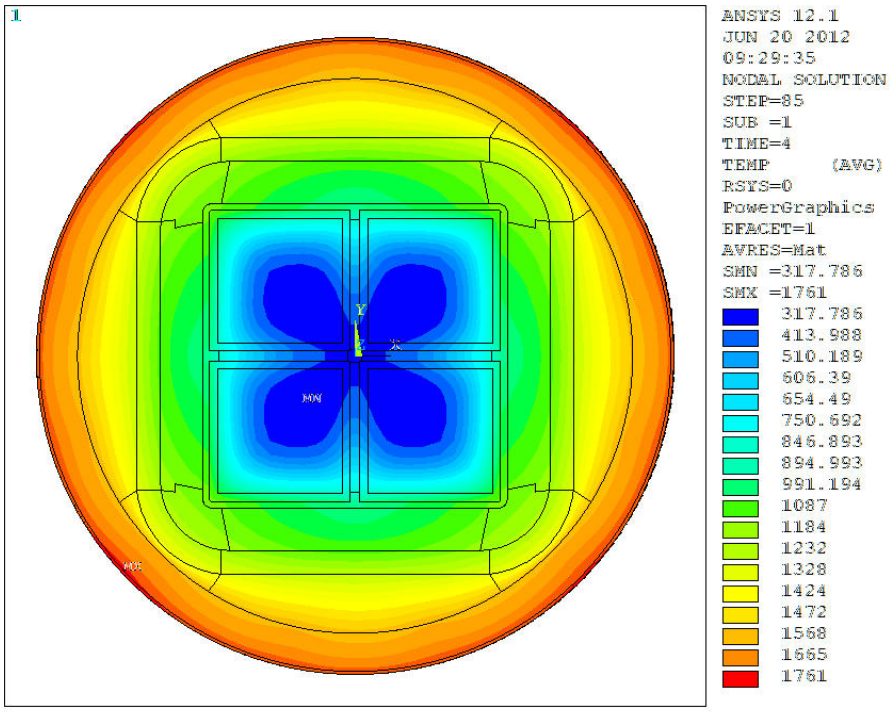

Figure C.153. NIST-06: (at 3.5 hours – ~10 minutes before end of fire on vehicle #26 – ambient temperature 1878°F [1026°C])

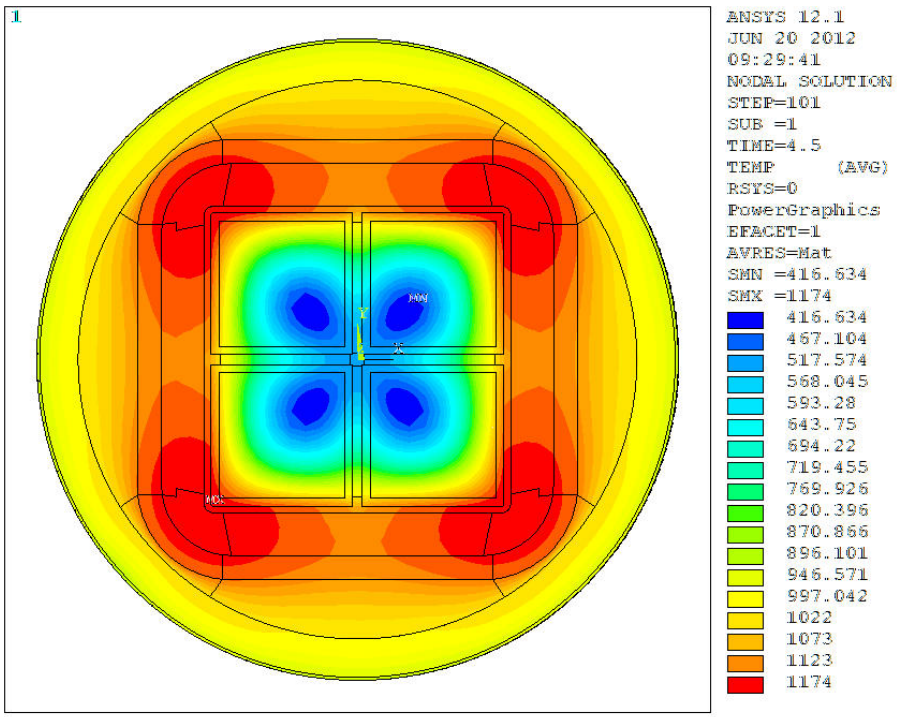

Figure C.154. NIST-06: (at 4 hours – ~20 minutes after end of fire on vehicle #26 – ambient temperature 585°F [307°C])

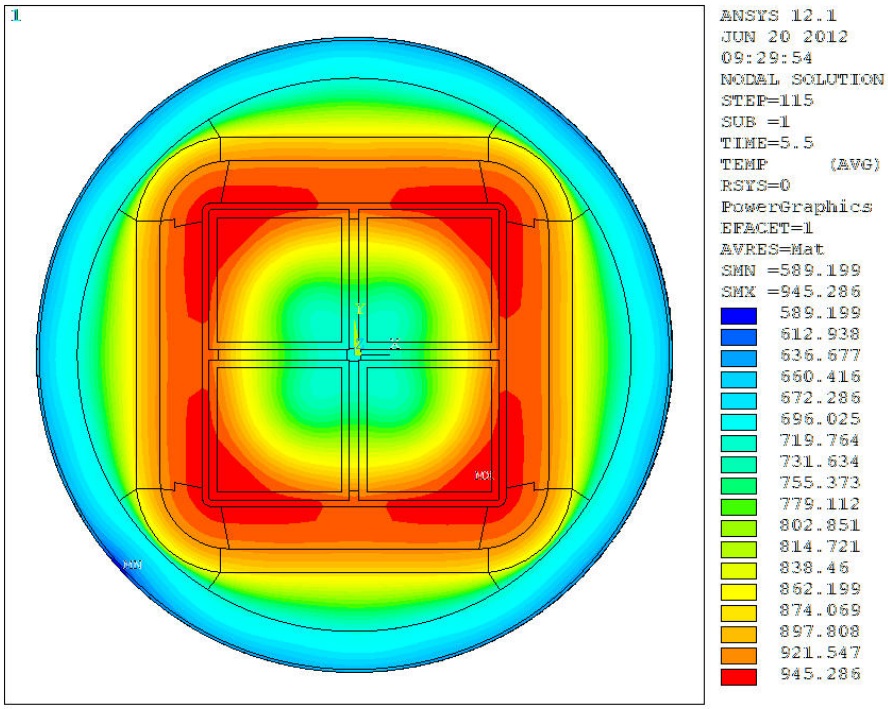

Figure C.155. NIST-06: (at 5 hours – ~1.5 hour after end of fire on vehicle #26 – ambient temperature 285°F [141°C])

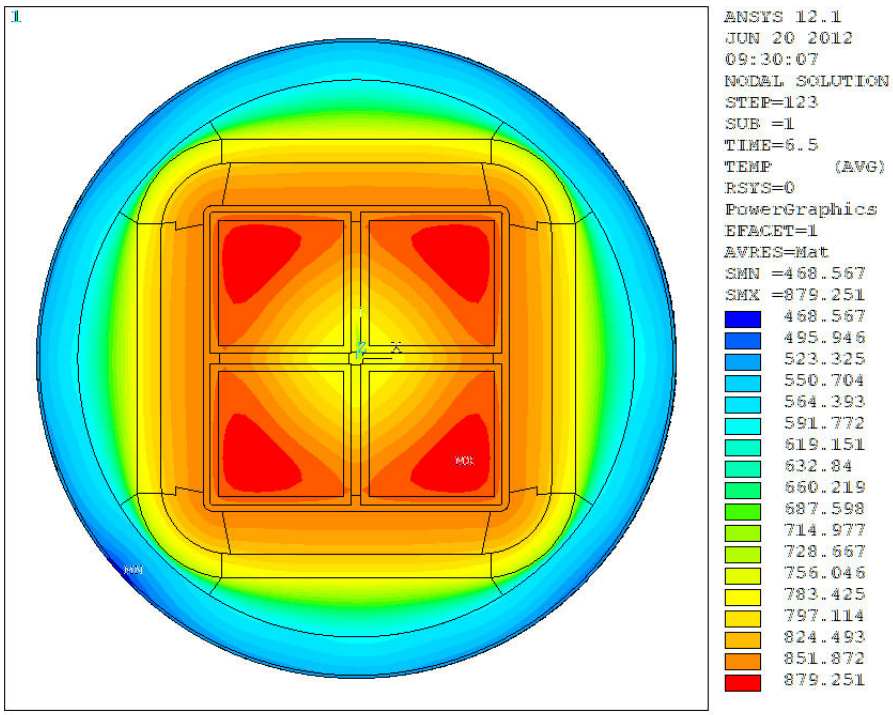

Figure C.156. NIST-06: (at 6 hours – ~2.5 hour after end of fire on vehicle #26 – ambient temperature 208°F [98°C])

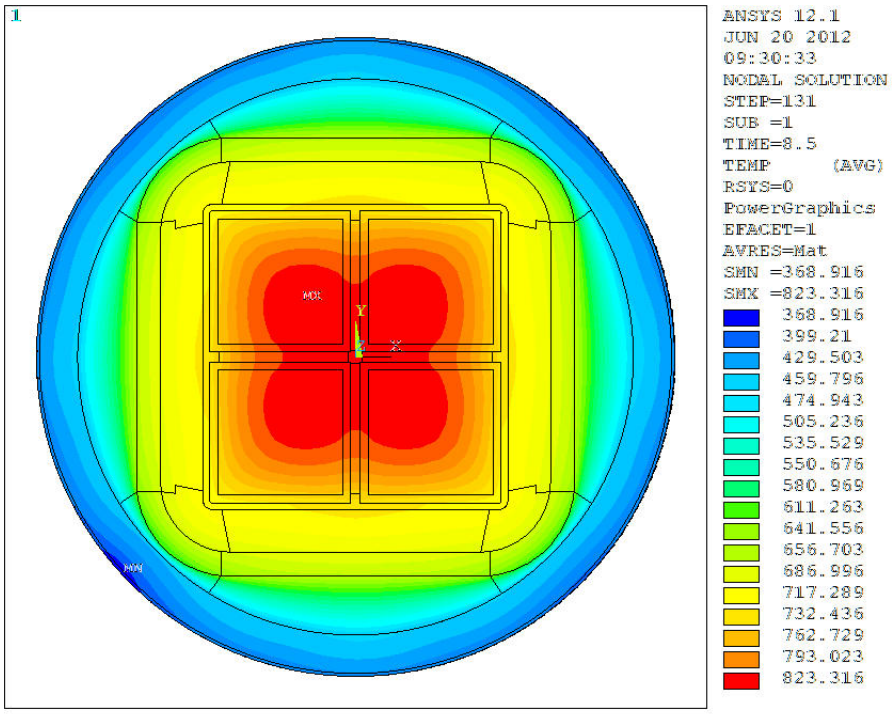

Figure C.157. NIST-06: (at 8 hours – ~4.5 hour after end of fire on vehicle #26 – ambient temperature 148°F [64°C])

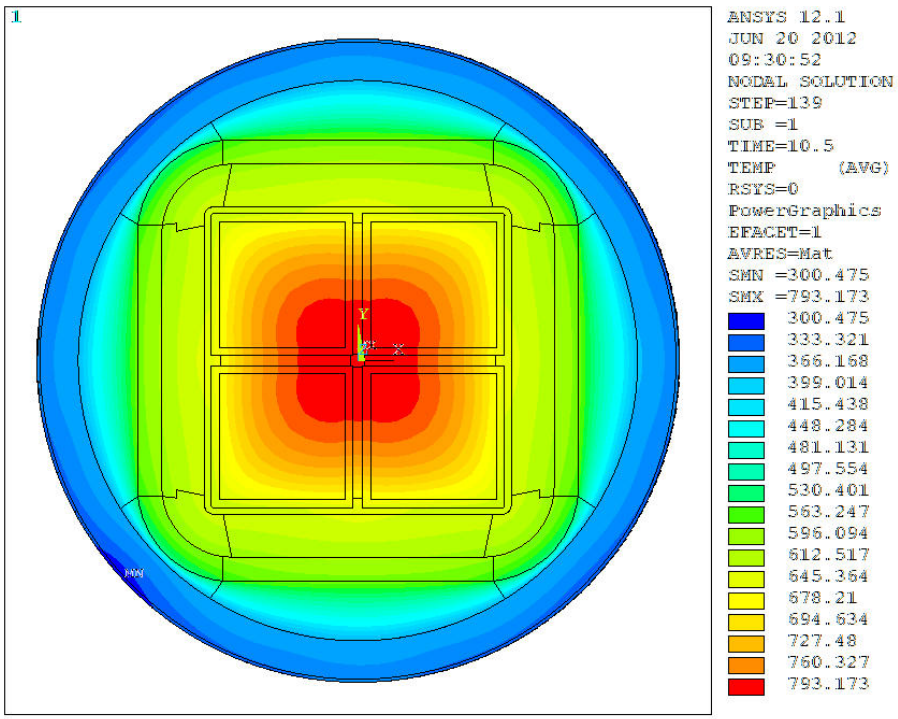

Figure C.158. NIST-06: (at 10 hours – ~6.5 hour after end of fire on vehicle #26 – ambient temperature 100°F [38°C])

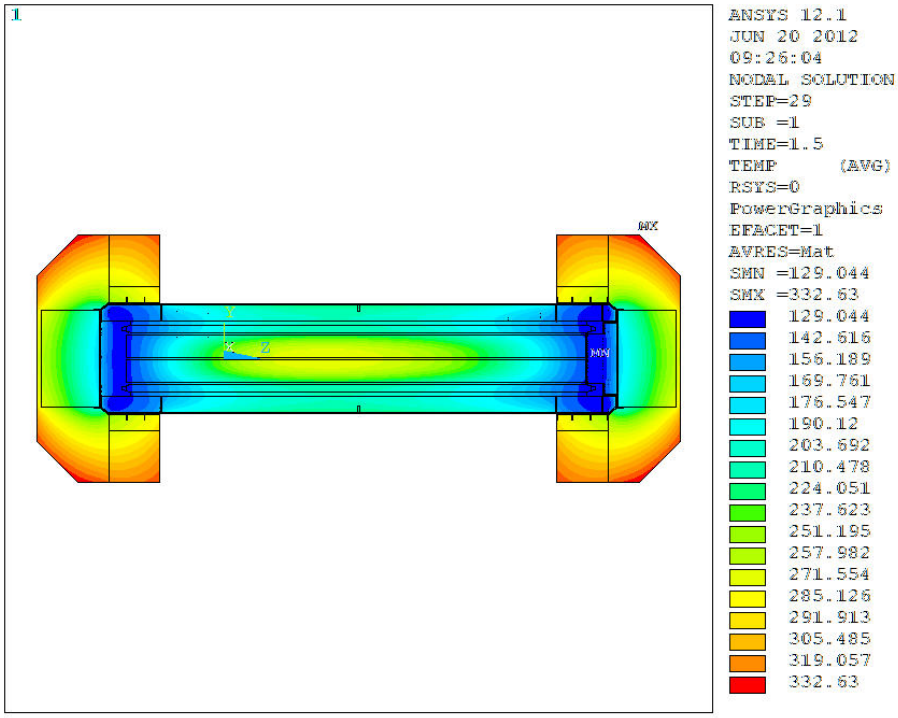

Figure C.159. NIST-06: (at 1 hour – 1.5 hours before start of fire on vehicle #26 – ambient temperature 338°F [798°C])

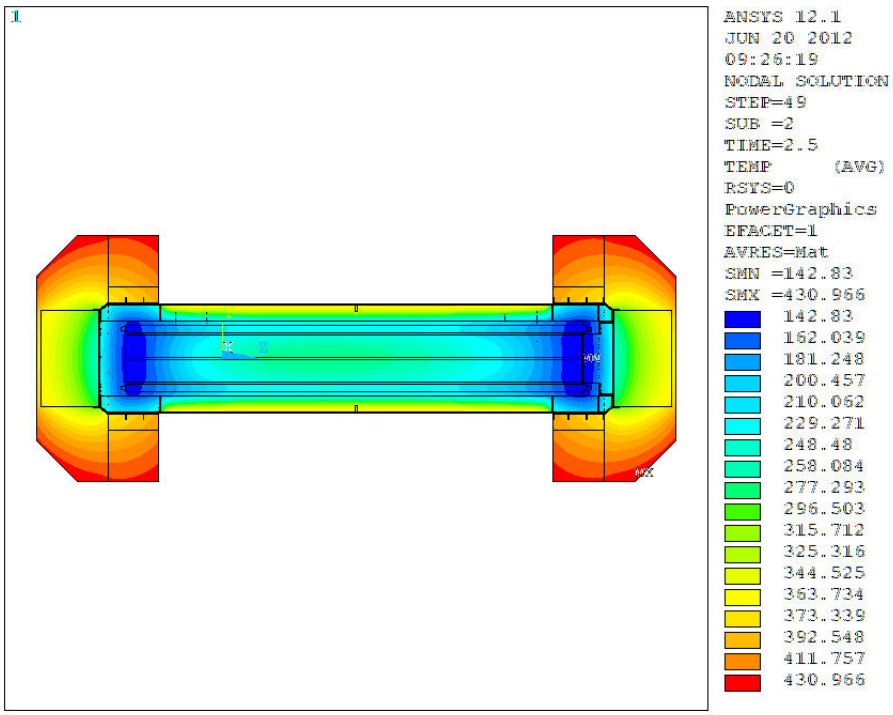

Figure C.160. NIST-06: (at 2 hours – ~30 minutes before start of fire on vehicle #26 – ambient temperature 428°F [220°C])

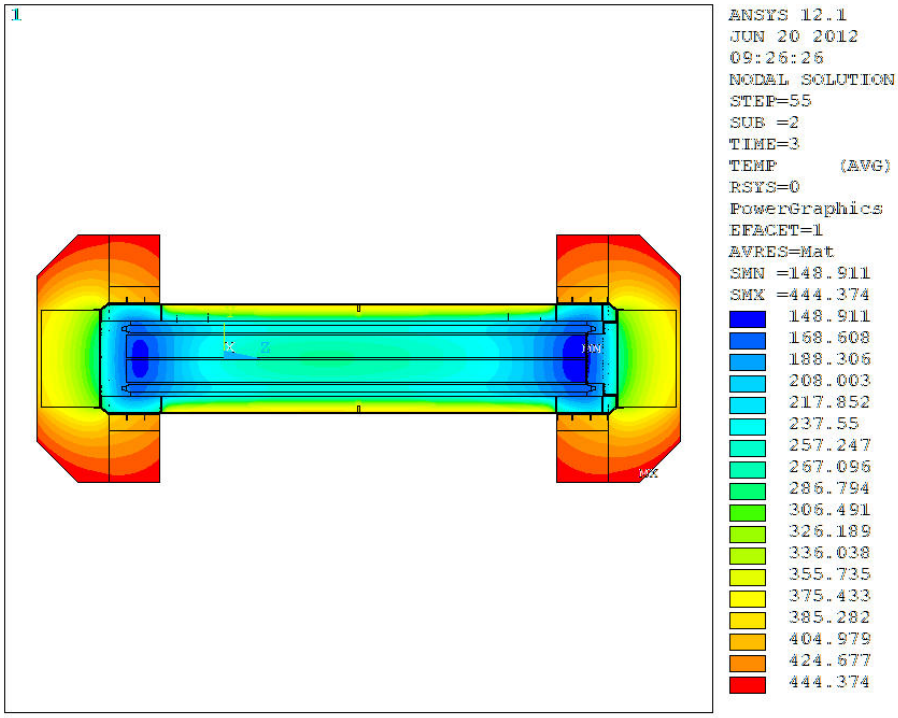

Figure C.161. NIST-06: (at 2.5 hours – start of fire on vehicle #26 – ambient temperature 440°F [227°C])

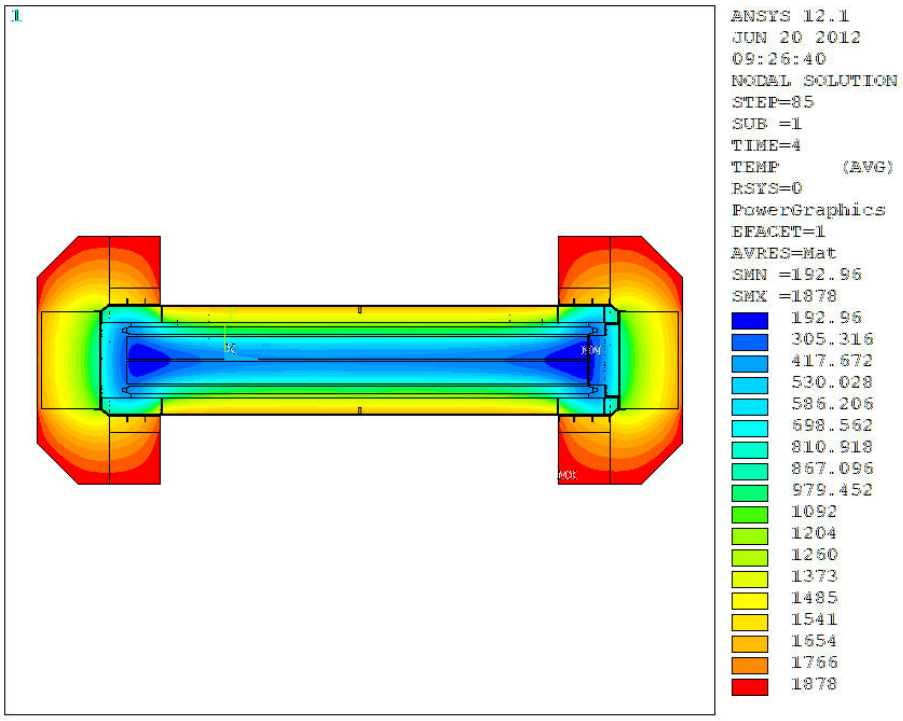

Figure C.162. NIST-06: (at 3.5 hours – ~10 minutes before end of fire on vehicle #26 – ambient temperature 1878°F [1026°C])

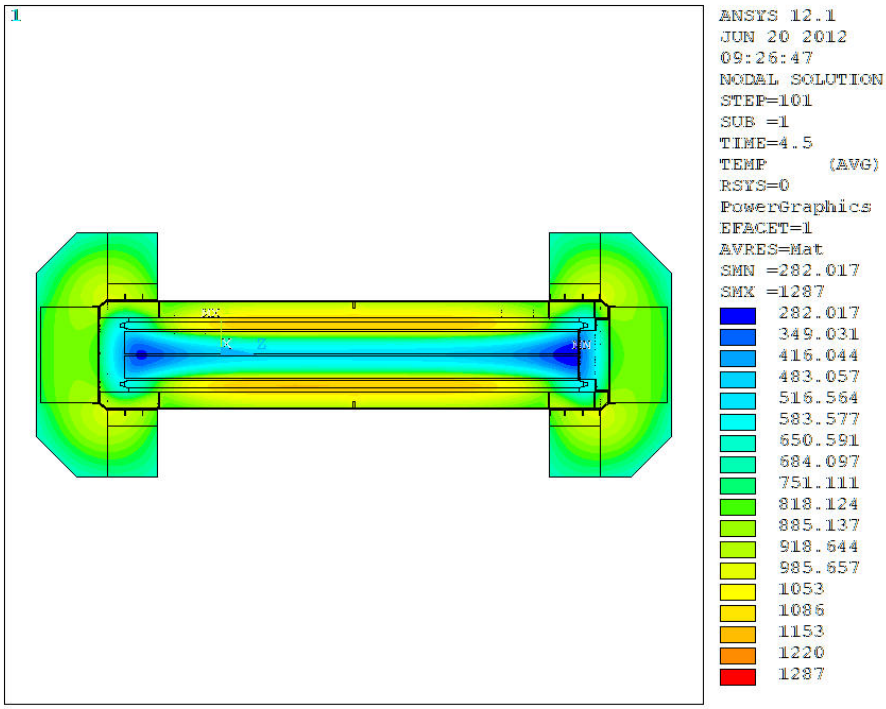

Figure C.163. NIST-06: (at 4 hours – ~20 minutes after end of fire on vehicle #26 – ambient temperature 585°F [307°C])

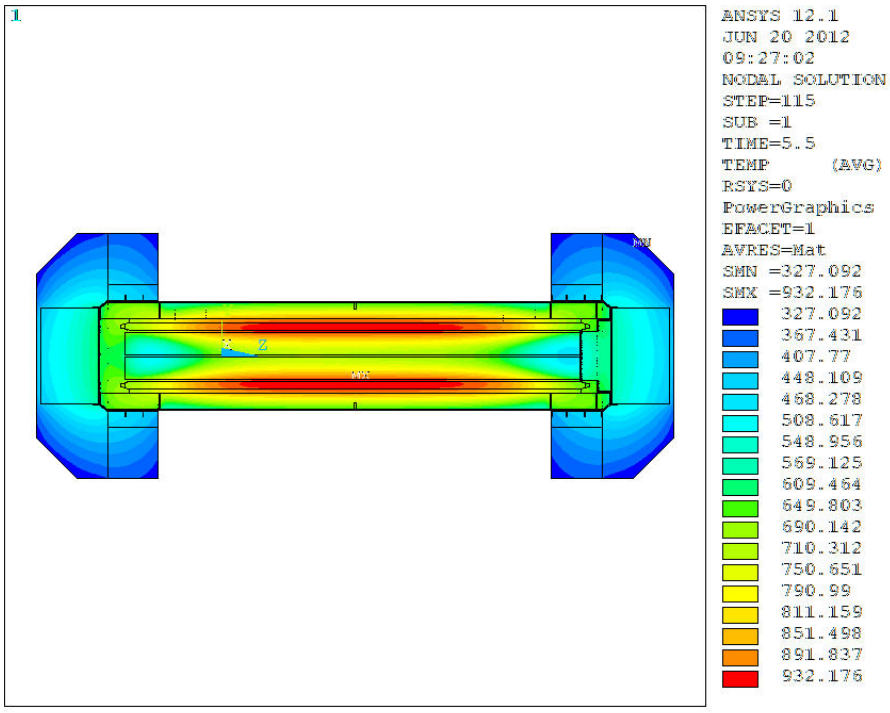

Figure C.164. NIST-06: (at 5 hours – ~1.5 hour after end of fire on vehicle #26 – ambient temperature 285°F [141°C])

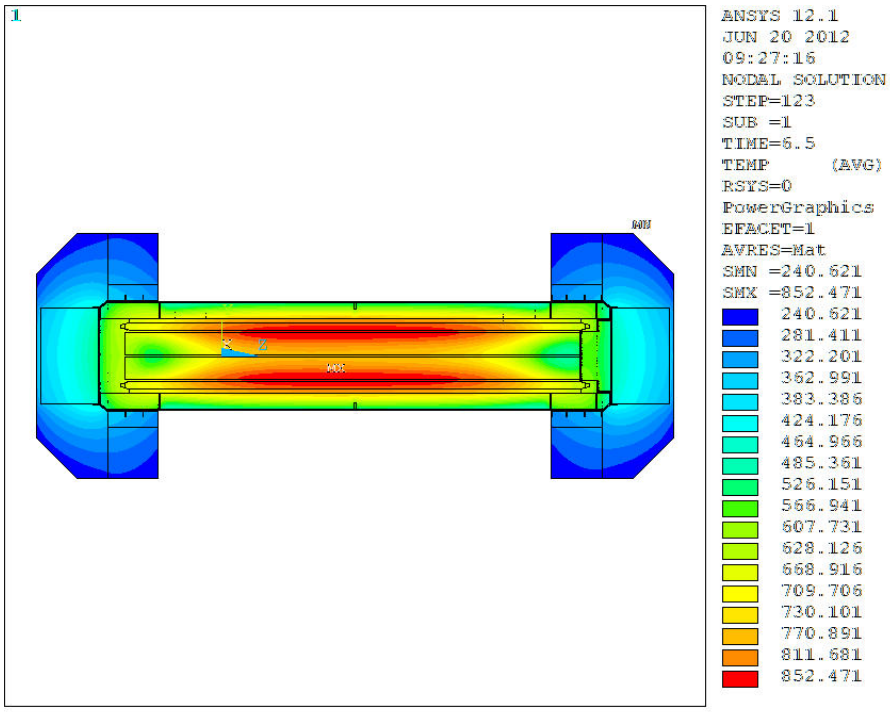

Figure C.165. NIST-06: (at 6 hours – ~2.5 hour after end of fire on vehicle #26 – ambient temperature 208°F [98°C])

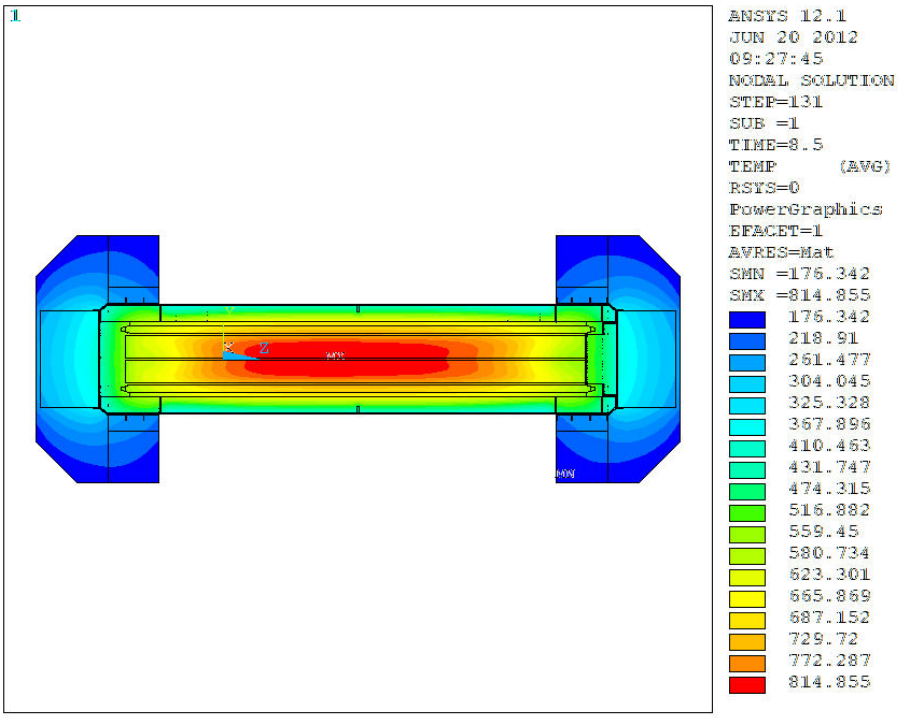

Figure C.166. NIST-06: (at 8 hours – ~4.5 hour after end of fire on vehicle #26 – ambient temperature 148°F [64°C])

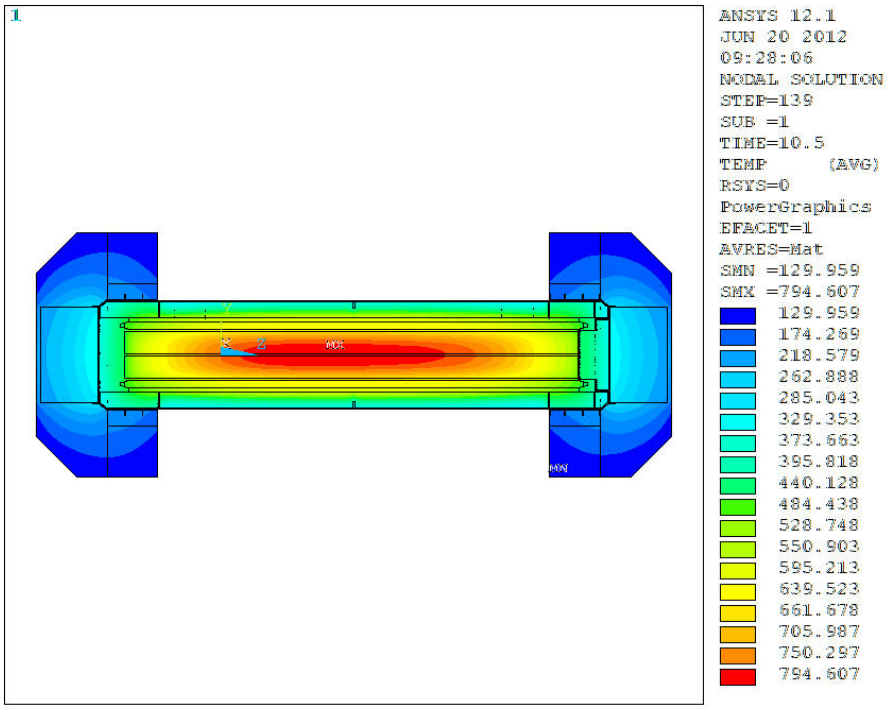

Figure C.167. NIST-06: (at 10 hours – ~6.5 hour after end of fire on vehicle #31 – ambient temperature 100°F [38°C])

C.6.2 NIST-06: Package at Longest Fire Location

The longest fire location for this case is assumed to occur on vehicle #30 (with a cargo of baked goods). Vehicle #31 is nearer to the tunnel entrance, but because this vehicle was running empty, it has a much less severe fire than vehicle #30. The fire on vehicle #30 begins about 4 hours after the start of the fire scenario and lasts approximately 42 minutes; the fire on vehicle #31 begins about 20 minutes later and lasts only about 26 minutes.

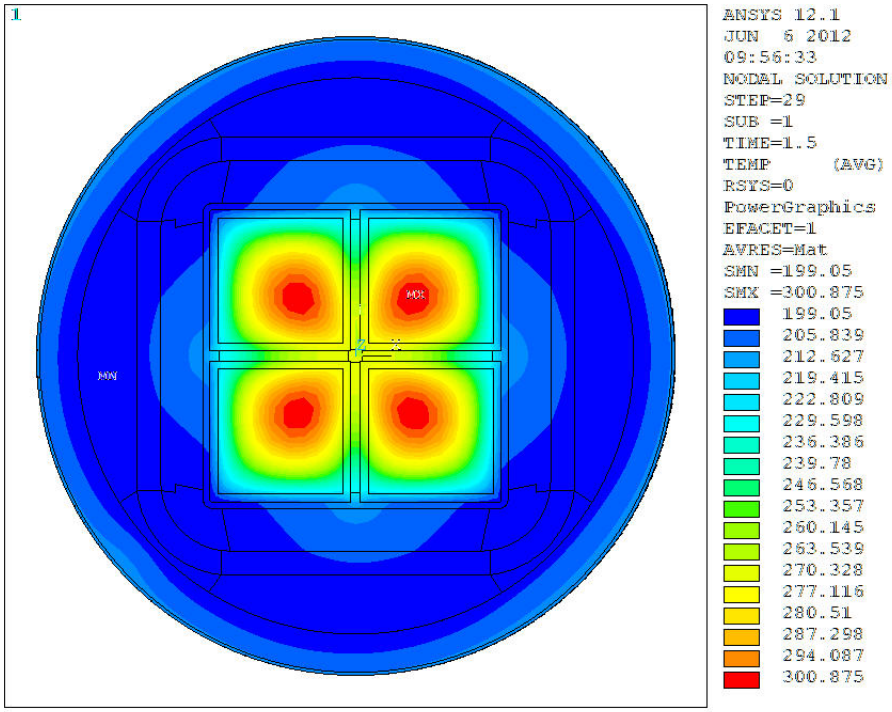

Figure C.168. NIST-06: (at 1 hour – ~3 hours before start of fire on vehicle #30 – ambient temperature 268°F [131°C])

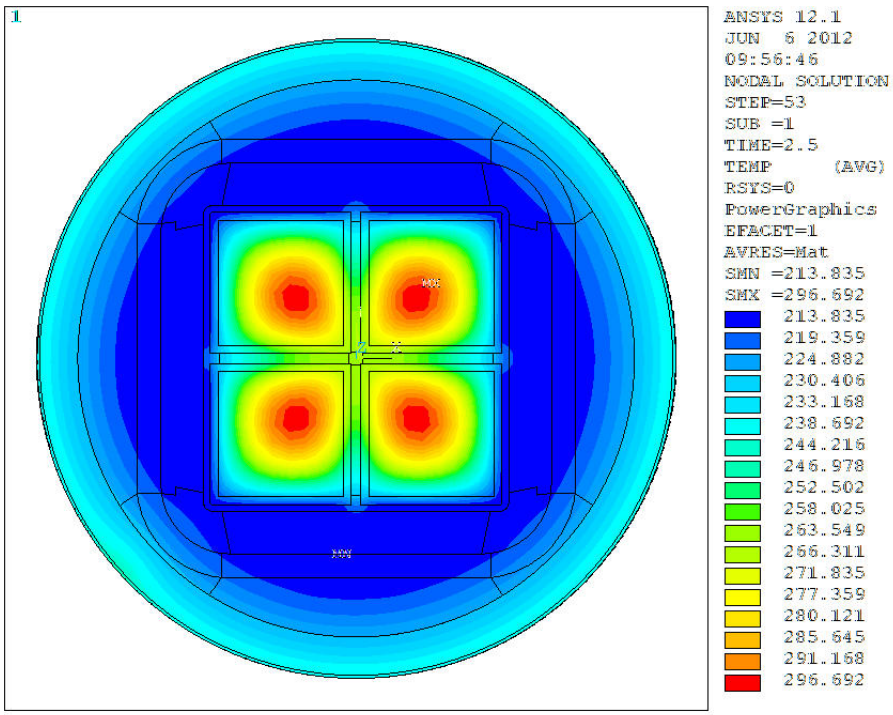

Figure C.169. NIST-06: (at 2 hours – ~2 hours before start of fire on vehicle #30 – ambient temperature 350°F [177°C])

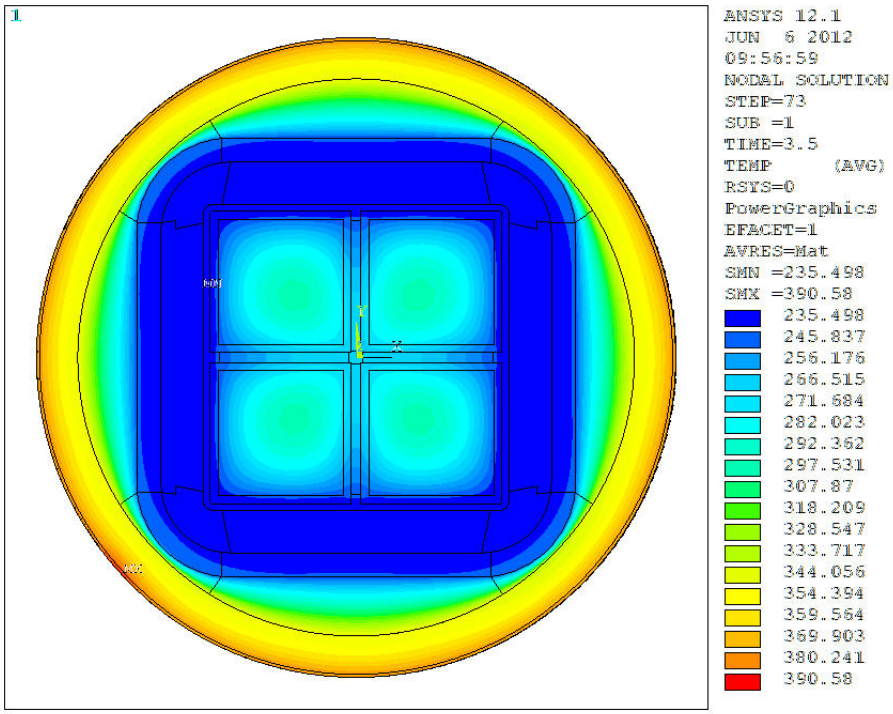

Figure C.170. NIST-06: (at 3 hours – ~45 minutes before start of fire on vehicle #30 – ambient temperature 514°F [268°C])

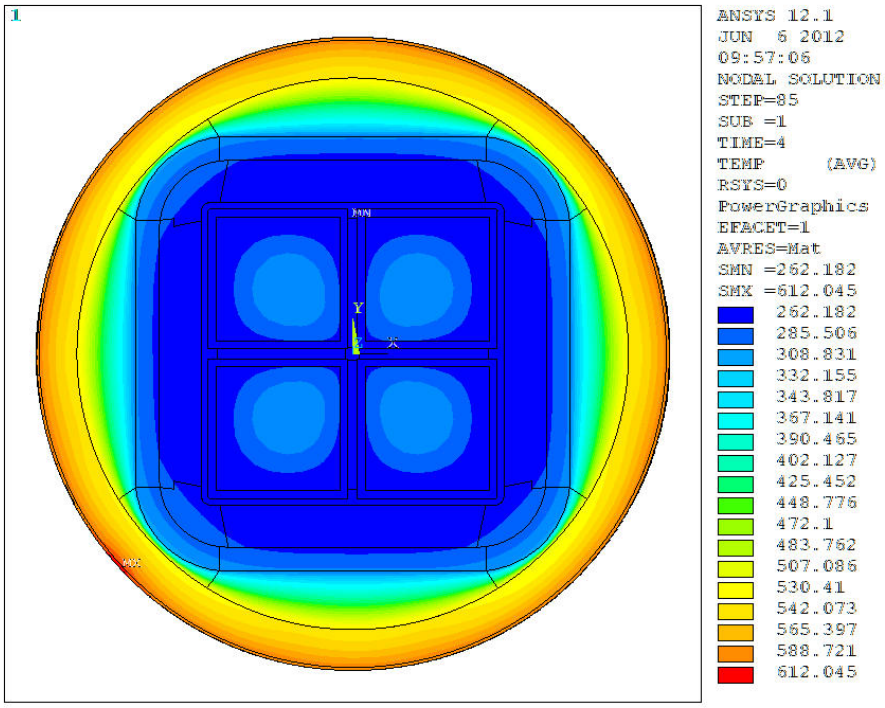

Figure C.171. NIST-06: (at 3.5 hours – ~15 minutes before start of fire on vehicle #30 – ambient temperature 756°F [402°C])

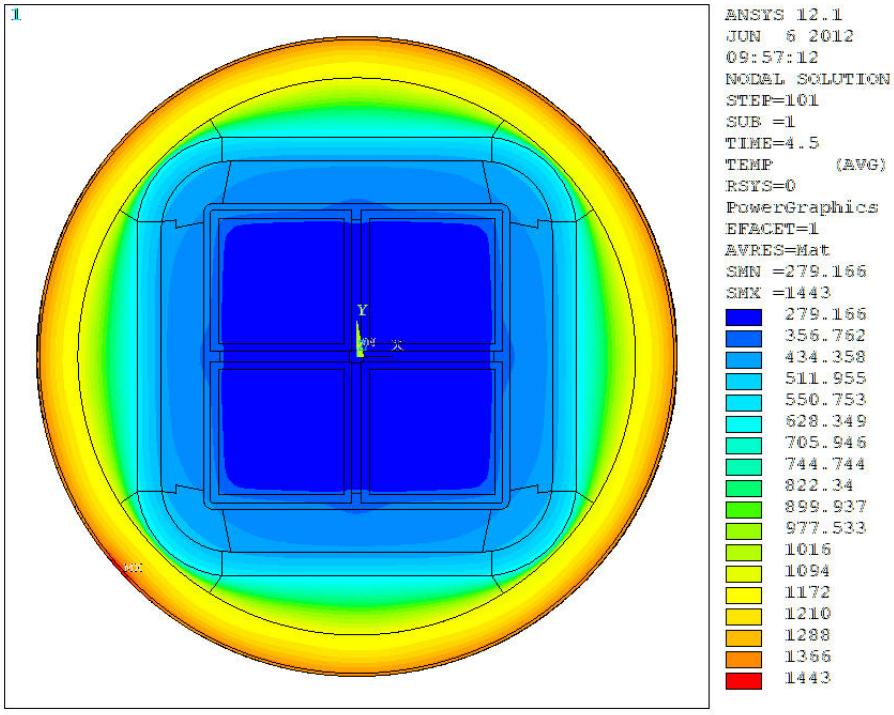

Figure C.172. NIST-06: (at 4 hours – ~15 minutes after start of fire on vehicle #30 – ambient temperature 1645°F [896°C])

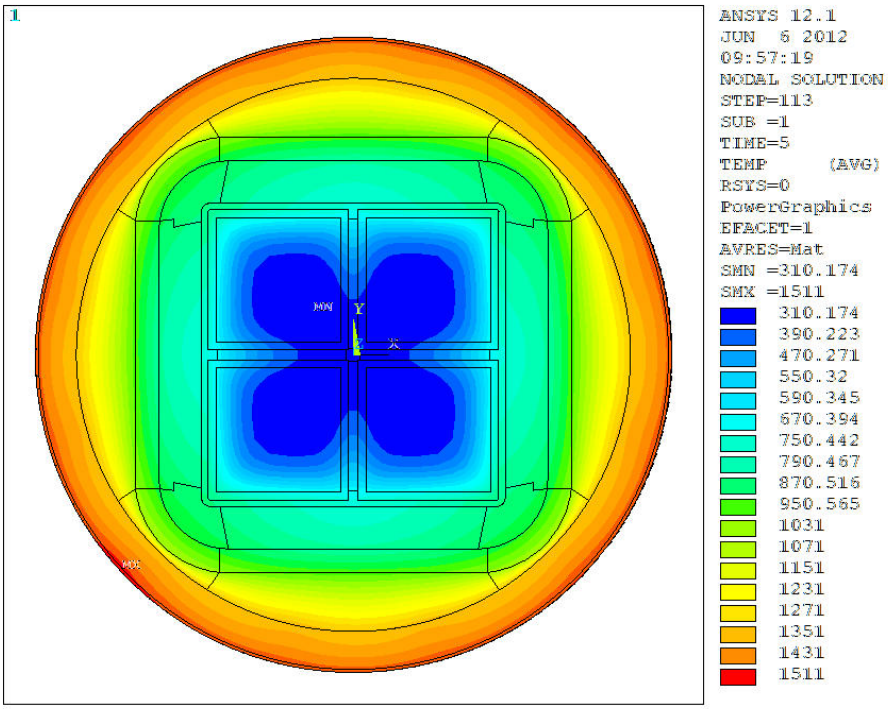

Figure C.173. NIST-06: (at 4.5 hours – ~6 minutes before end of fire on vehicle #30 – ambient temperature 1638°F [892°C])

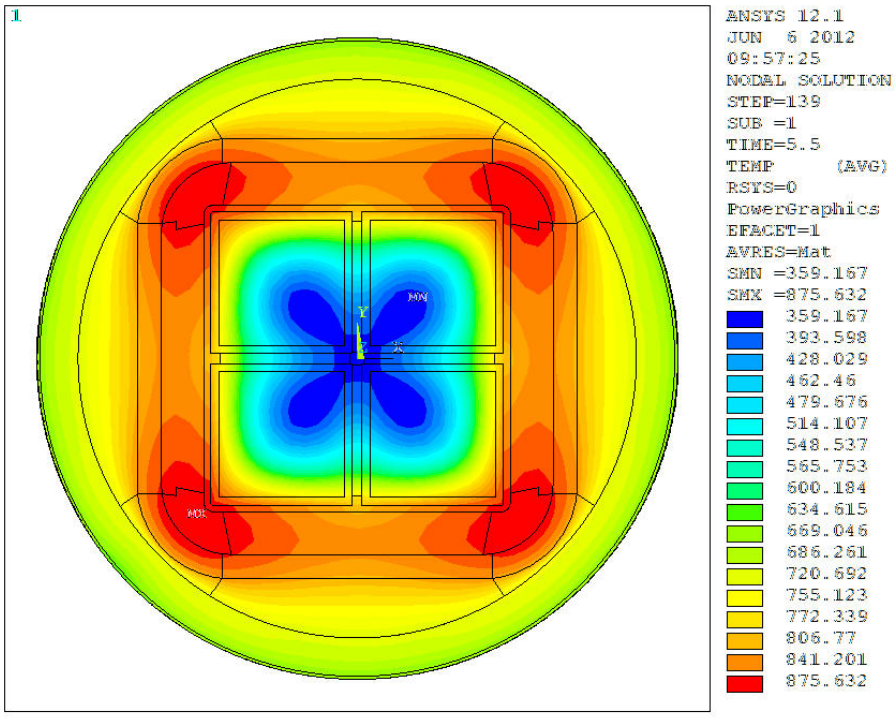

Figure C.174. NIST-06: (at 5 hours – ~24 minutes after end of fire on vehicle #30 – ambient temperature 377°F [192°C])

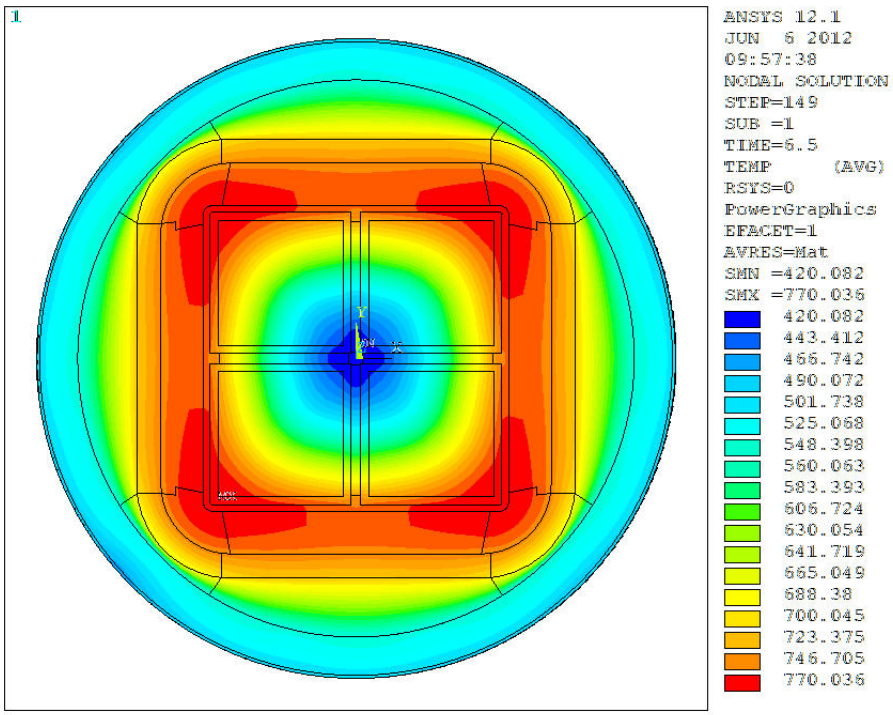

Figure C.175. NIST-06: (at 6 hours – ~1.5 hours after end of fire on vehicle #30 – ambient temperature 230°F [110°C])

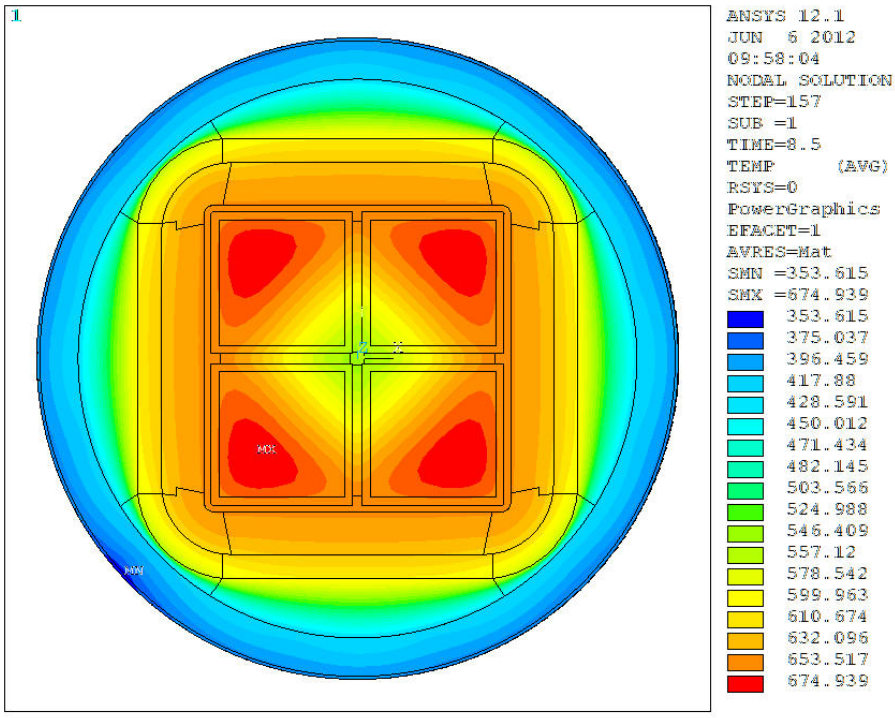

Figure C.176. NIST-06: (at 8 hours – ~3.5 hours after end of fire on vehicle #30 – ambient temperature 172°F [78°C])

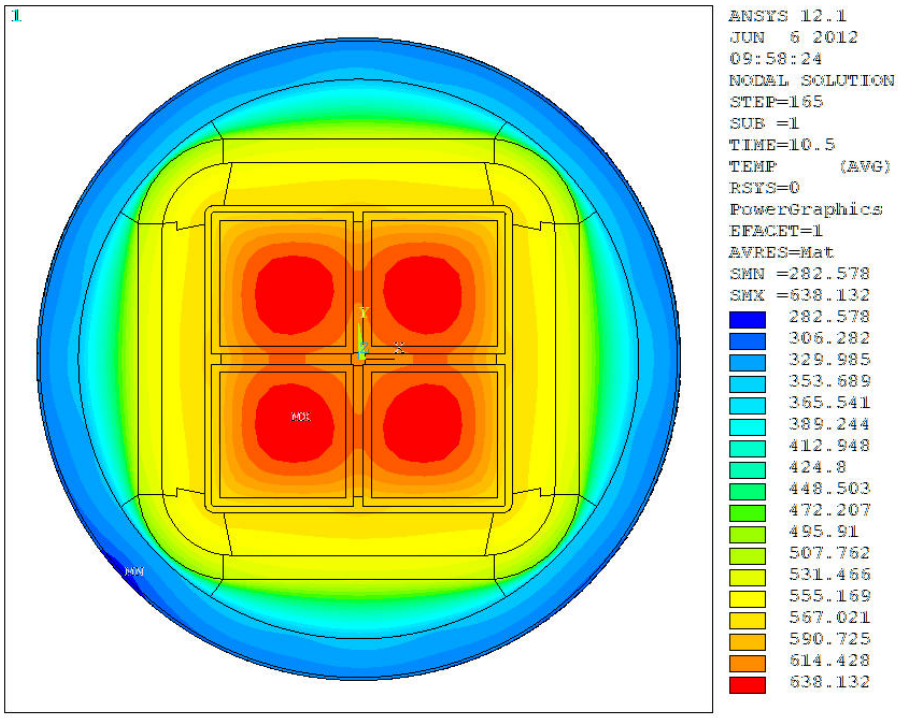

Figure C.177. NIST-06: (at 10 hours – ~5.5 hours after end of fire on vehicle #30 – ambient temperature 100°F [38°C])

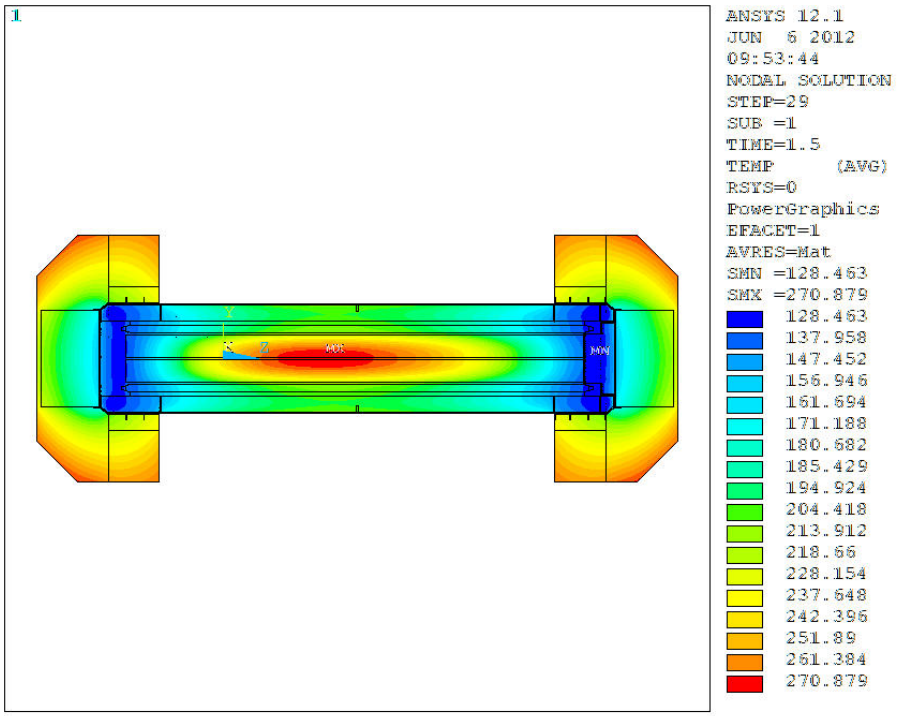

Figure C.178. NIST-06: (at 1 hour – ~3 hours before start of fire on vehicle #30 – ambient temperature 268°F [131°C])

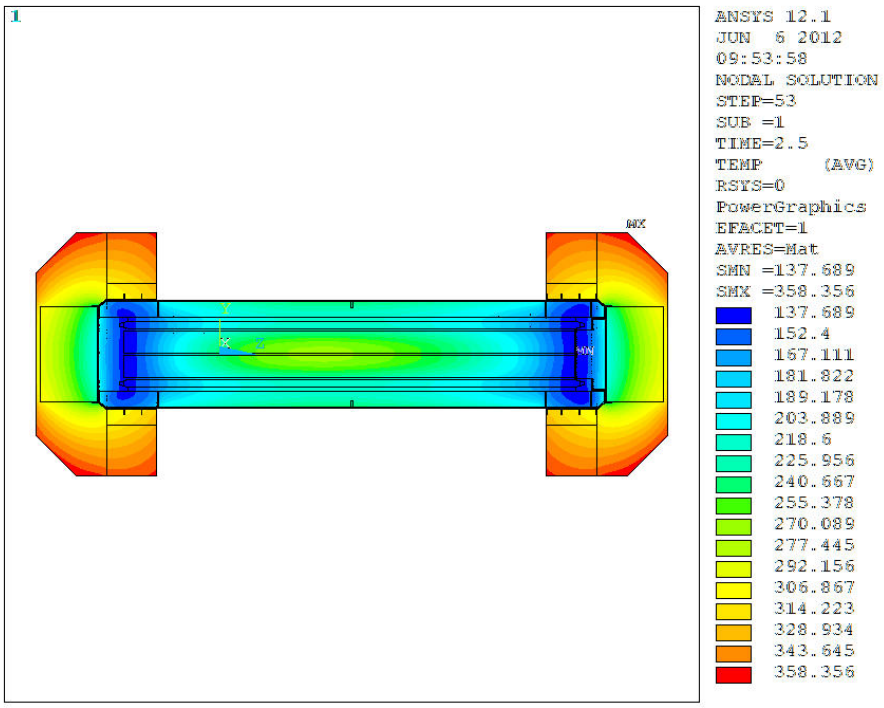

Figure C.179. NIST-06: (at 2 hours – ~2 hours before start of fire on vehicle #30 – ambient temperature 350°F [177°C])

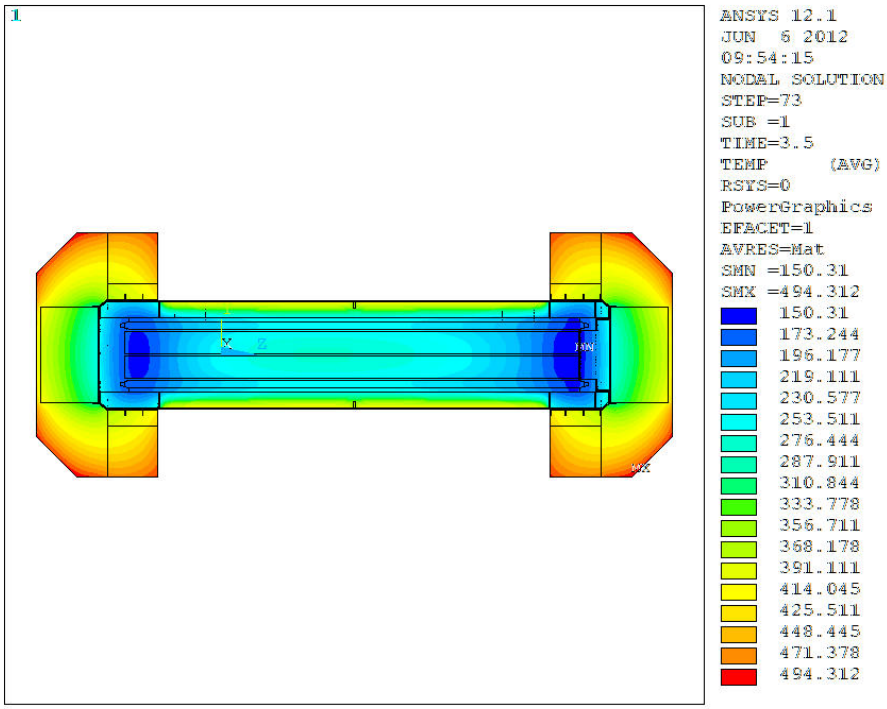

Figure C.180. NIST-06: (at 3 hours – ~45 minutes before start of fire on vehicle #30 – ambient temperature 514°F [268°C])

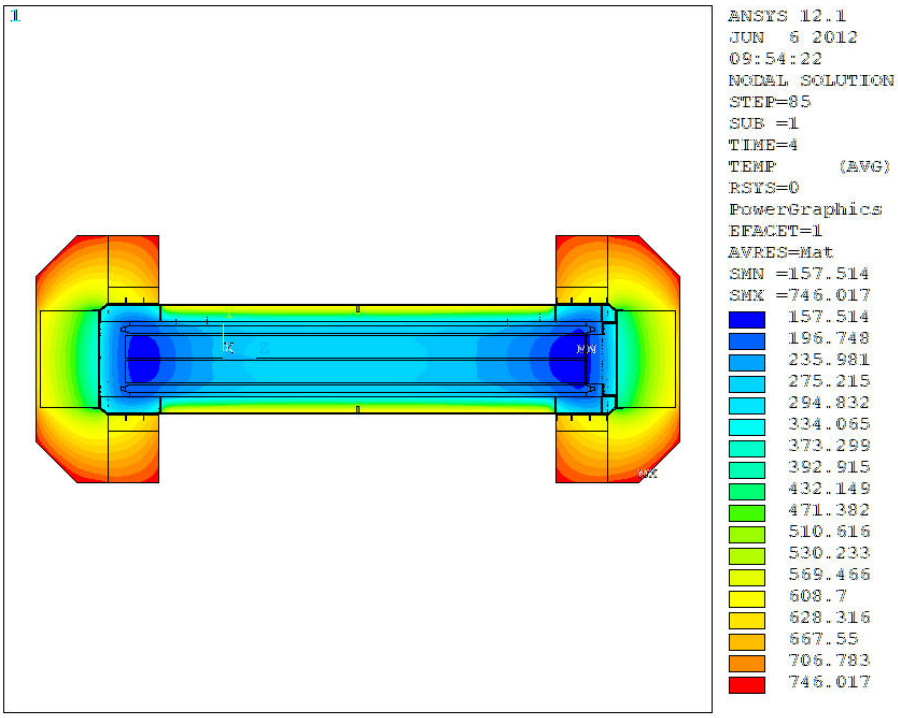

Figure C.181. NIST-06: (at 3.5 hours – ~15 minutes before start of fire on vehicle #30 – ambient temperature 756°F [402°C])

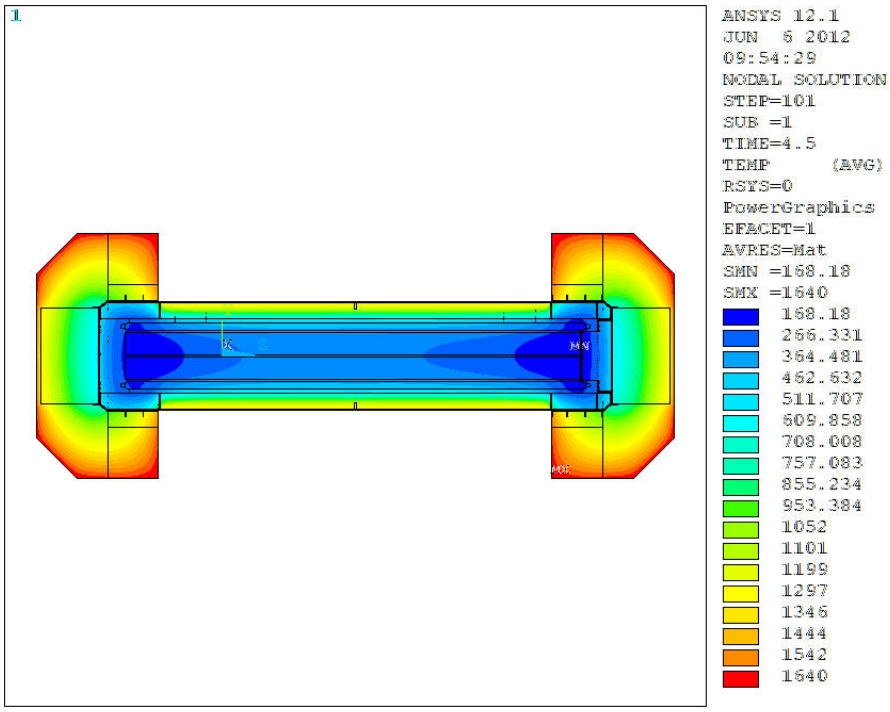

Figure C.182. NIST-06: (at 4 hours – ~15 minutes after start of fire on vehicle #30 – ambient temperature 1645°F [896°C])

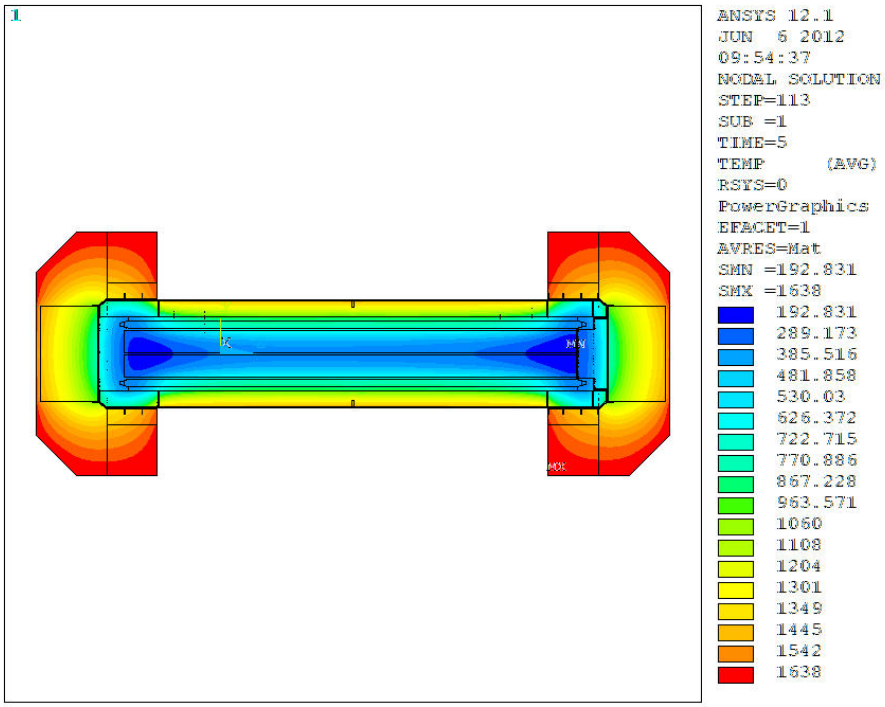

Figure C.183. NIST-06: (at 4.5 hours – ~6 minutes before end of fire on vehicle #30 – ambient temperature 1638°F [892°C])

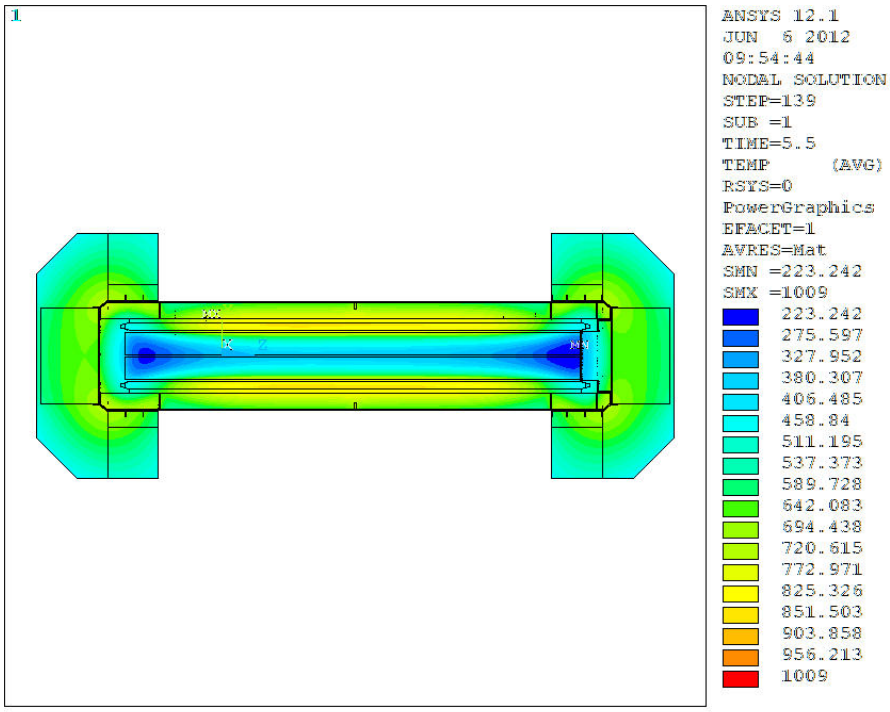

Figure C.184. NIST-06: (at 5 hours –~24 minutes after end of fire on vehicle #30 – ambient temperature 377°F [192°C])

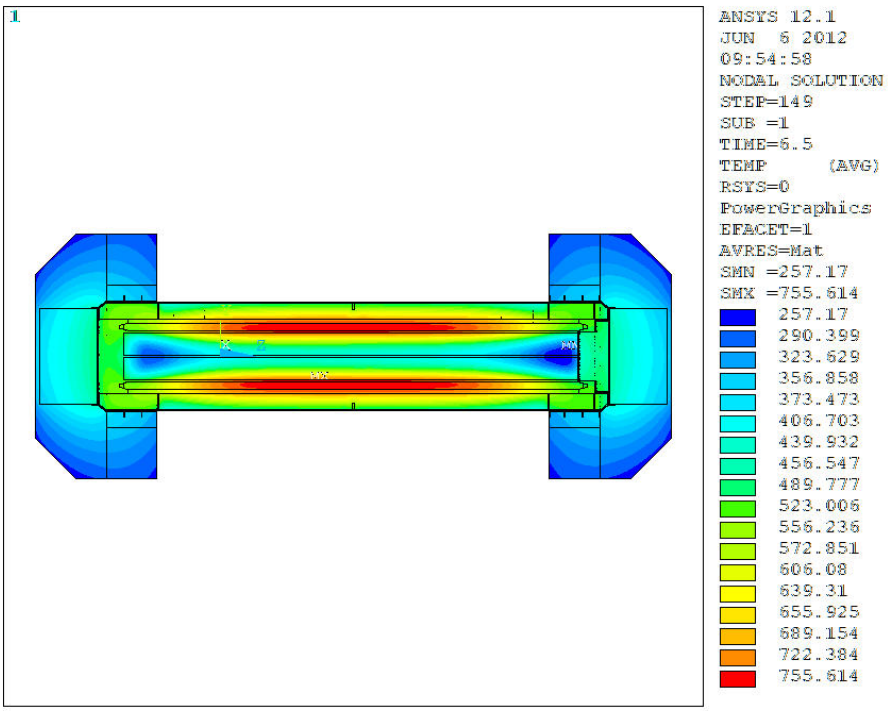

Figure C.185. NIST-06: (at 6 hours – ~1.5 hours after end of fire on vehicle #30 – ambient temperature 230°F [110°C])

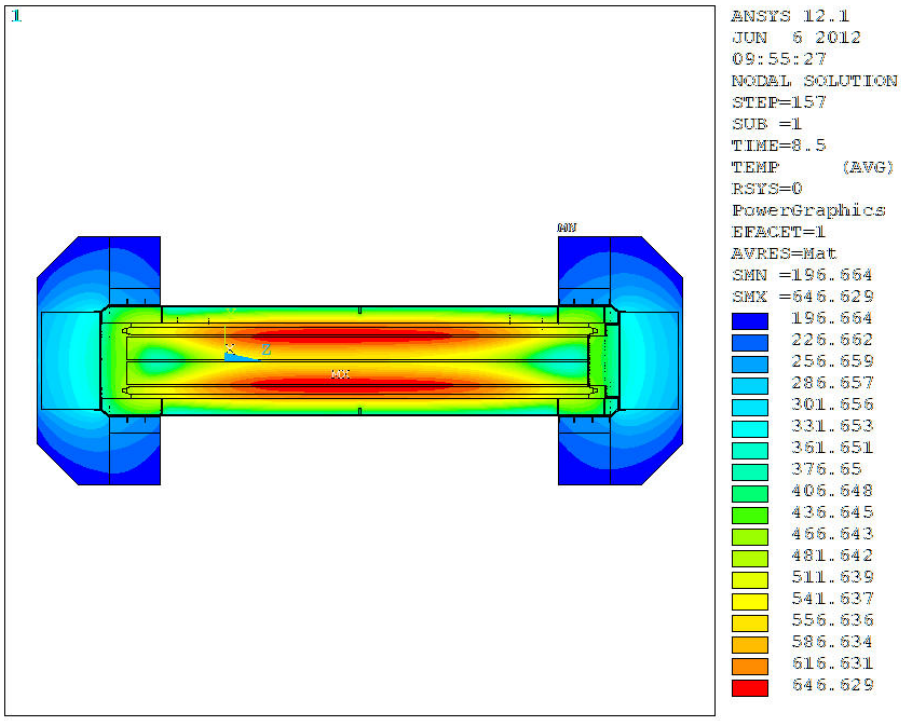

Figure C.186. NIST-06: (at 8 hours – ~3.5 hours after end of fire on vehicle #30 – ambient temperature 172°F [78°C])

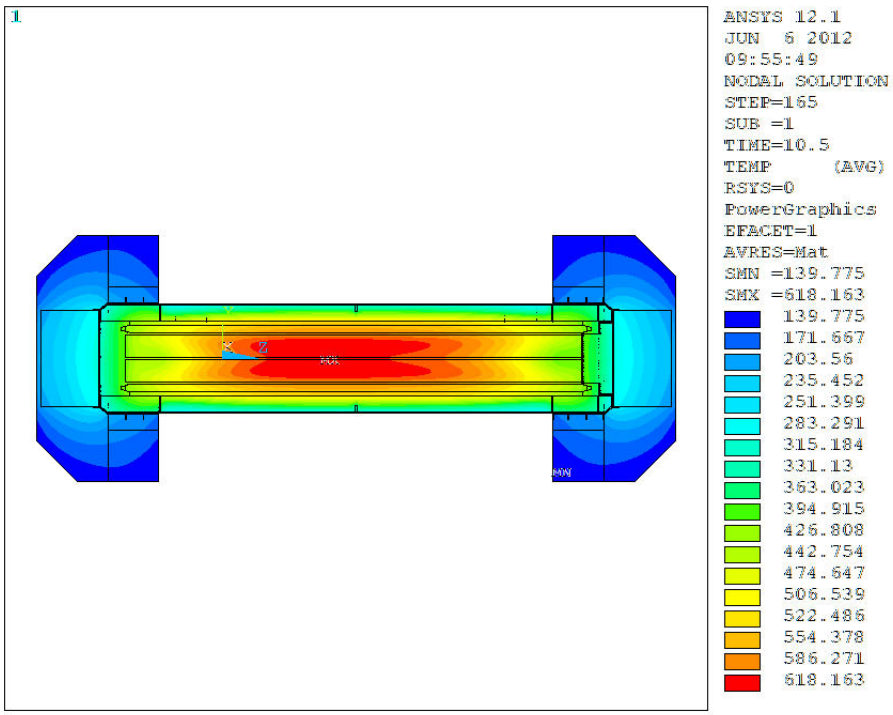

Figure C.187. NIST-06: (at 10 hours – ~5.5 hours after end of fire on vehicle #30 – ambient temperature 100°F [38°C])

NRC FORM 335 (12-2010) NRCMD 3.7

U.S. NUCLEAR REGULATORY COMMISSION

BIBLIOGRAPHIC DATA SHEET

(See instructions on the reverse)

1 REPORT NUMBER (Assigned by NRC, Add Vol., Supp., Rev., and Addendum Numbers, if any.)

NUREG/CR-7207
Final

2 TITLE AND SUBTITLE

Spent Fuel Transportation Package Response to the Newhall Pass Tunnel Fire Scenario

3 DATE REPORT PUBLISHED

MONTH	YEAR
October	2016

4 FIN OR GRANT NUMBER

5 AUTHOR(S)

H.E. Adkins, Jr., J.M. Cuta, N.A. Klymyshyn, S.R. Suffield, C.S. Bajwa, K.B. McGrattan, C.E. Beyer, A. Sotomayor-Rivera

6 TYPE OF REPORT

Technical

7 PERIOD COVERED (Inclusive Dates)

8 PERFORMING ORGANIZATION NAME AND ADDRESS (If NRC, provide Division, Office or Region, U. S Nuclear Regulatory Commission, and mailing address, if contractor, provide name and mailing address)

Pacific Northwest National Laboratory
P.O. Box 999
Richland, WA 99352

9. SPONSORING ORGANIZATION NAME AND ADDRESS (If NRC, type "Same as above" if contractor, provide NRC Division, Office or Region, U. S. Nuclear Regulatory Commission, and mailing address.)

Division of Spent Fuel Management
Office of Nuclear Material Safety and Safeguards
U.S. Nuclear Regulatory Commission
Washington, D.C. 20555-0001

10. SUPPLEMENTARY NOTES

J. Piotter, NRC Project Manager

11. ABSTRACT (200 words or less)

The U.S. Nuclear Regulatory Commission has undertaken the examination of specific transportation accidents (of non-nuclear materials) to determine what the potential consequences might be to a spent fuel transportation package. The Newhall Pass accident was selected as a fourth study in the evaluation series.

Analyses undertaken included FDS fire modeling, physical examination of material samples from the accident, ANSYS and COBRA-SFS code thermal modeling of a GA-4 package, and fuel performance modeling. The analyses suggest that although it is possible to obtain predictions of fuel failure for very conservative representations of the conditions of the Newhall Pass Tunnel fire, it is likely that realistic assessments of fire and modeling conditions would show that fuel would not be expected to fail. Nonetheless, the potential consequences for this accident, had it involved a SNF package, are determined from the evaluation of the potential consequences of the MacArthur Maze fire (NUREG/CR-7206), which is a more severe scenario and effectively bounds the maximum possible release from the package in the Newhall Pass Tunnel fire scenario. Using conservative and bounding modeling assumptions, the total possible release from the package, as a mixture of fission gases, CRUD and fuel particulate, is estimated as approximately one-fourth of the mixture A2 quantity Since the regulatory limit is specified as an A2 quantity per week for accident conditions, the estimated release from the hypothetical scenario is below the prescribed limit for safety

12. KEY WORDS/DESCRIPTORS (List words or phrases that will assist researchers locating the report)

Newhall Pass Tunnel
Spent Nuclear Fuel
Accident
Transportation Package
Fire

13 AVAILABILITY STATEMENT

unlimited

14 SECURITY CLASSIFICATION

(This Page)
unclassified

(This Report)
unclassified

15 NUMBER OF PAGES

16 PRICE

Federal Recycling Program

UNITED STATES
NUCLEAR REGULATORY COMMISSION
WASHINGTON, DC 20555-0001

OFFICIAL BUSINESS

NUREG/CR-7207
Final

Spent Fuel Transportation Package Response to the Newhall Pass Tunnel Fire Scenario

October 2016